Studies of Transition Metal Nitrite Complexes

by

Susan Georgina Oats B.Sc. (Hons)

Submitted in fulfilment of the requirements for the
Degree of Doctor of Philosophy

University of Tasmania (December, 2002)

Chemistry

This thesis may be made available for loan and limited copying in accordance with the *Copyright Act 1986*.

Susan Oats

2/12/02

To the best of my knowledge, this thesis does not contain material previously published by another person, except where due reference is given in the text, nor does it contain any material which has been accepted for the award of any other degree or diploma in any tertiary institution.

Susan Georgina Oats   2/12/02

ABSTRACT

A series of transition metal nitrite complexes have been prepared. These include tetranitrite complex ions of the formula $[M(NO_2)_4]^{2-}$, M = Zn(II), Cd(II) and Hg(II), a series of nickel(II) nitrite complexes with amines of varying degrees of substitution and the pentammine nitrite complexes $[Co(NH_3)_5NO_2]^{2+}$, $[Co(NH_3)_5ONO]^{2+}$ and $[Cr(NH_3)_5ONO]^{2+}$.

Single crystal optical spectra were measured for the Co(III), Cr(III) and Ni(II) complexes. The observed transition energies for these complexes are compared with those calculated using the Angular Overlap Model (AOM). Bonding parameters have been derived for the nitrite ligands, and the parameters are shown to be transferable to other complexes with the same transition metal ion and different nitrite coordination modes. An extended version of the AOM developed to include the effects of "bent bonding" was used to derive bonding parameters for O,O'-chelating and N,O,O'-bridging nitrite ligands.

The bonding parameter e_σ deduced for N-bonded and O-bonded nitrites implies that the N-bonded ligand is a marginally stronger σ-donor than the O-bonded ligand. The $e_{\pi y}$ parameters derived for the nitrito and nitro coordination modes suggest that the O-bonded nitrite is a moderate π-donor and the N-bonded nitrite a weak π-acceptor. The large difference in the overall field strength, and very different position in the spectrochemical series, is due mainly to the difference in the π-bonding of the two coordination modes.

The complexes $[Ni(NH_3)_4(NO_2)_2]$, $[Ni(en)_2(NO_2)_2]$ and $[Ni(N,N\text{-dimen})_2(ONO)_2]$, (N,N-dimen = N,N-dimethylethylenediamine) have been modelled using Density Functional Theory (DFT) calculations. The calculated energies for the nitro and nitrito isomers of the above complexes suggest that the nitro isomer is inherently slightly more stable than the nitrito isomer. This agreed with observation in the solid state for $[Ni(NH_3)_4(NO_2)_2]$ and $[Ni(en)_2(NO_2)_2]$, but not for the complex $[Ni(N,N\text{-dimen})_2(ONO)_2]$, though in chloroform solution the nitro isomer is slightly more stable for the last complex. In agreement with this trend, the difference in the

energies calculated for both isomers was the smallest for the complex with the substituted amines. The calculations confirm that the nitrite acts as π-donor when O-bonded, compared with the N-bonded form, and Δ values were derived that are comparable to those derived via the AOM, and estimated from the optical spectra.

Infrared and Raman spectra were measured for each complex prepared in the present work to unambiguously assign the fundamental nitrite vibrations (v_1, v_2 and v_3). Upon nitrito coordination, v_2 shifts significantly to lower energy compared with the ionic stretch. For nitro coordination, this vibration shifts to higher energy, decreasing the energy difference between v_2 and v_3. The energies of the nitrite stretching vibrations shift to slightly lower energy than those of the free ion upon O,O'-chelating coordination. The *cis*-N,O-bridging mode did not have a great effect on the vibrational energies of the nitrite, unlike the *trans* N,O-bridging mode, where v_2 shifts to lower energy and v_3 shifts to much higher energy relative to free nitrite.

Acknowledgements

I would like to thank:

Table of Contents

Ligand Abbreviations

The following ligand abbreviations are used throughout this thesis.

bdmppy	2,6-bis[(3,5-dimethyl)pyrazol-1-yl]pyridine
bipy	bipyridine
dmpn	2,2-dimethyldiaminopropane
dpt	bis(3-aminopropyl)amine
en	ethylenediamine
Hopn	1,3-diamino-2-propanol
isoquin	isoquinoline
medpt	bis(3-aminopropyl)methylamine
m-stien	*meso*-1,2-diphenylethylenediamine
N,N-dien	N,N-diethylenediamine
N,N'-dien	N,N'-diethylenediamine
N,N-dimen	N,N-dimethylethylenediamine
N,N'-dimen	N,N'-dimethylethylenediamine
o-cat	*o*-xylenebis(triphenylphosphonium)
oxpn	N,N-bis(3-aminopropyl)oxamide
py	pyridine
terpy	2,2':6',2"-terpyridine
trien	triethylenediamine
trimen	N,N,N'-trimethylethylenediamine
tn	1,3-diaminopropane

CHAPTER 1

Introduction

1.1 Historical Background

The first published description of a transition metal nitrite complex appeared in 1831[1]. The yellow potash salt, known as Fischer's salt after its discoverer, was rediscovered and analysed by Saint-Evre twenty years later, who introduced the bright yellow complex as a watercolour pigment[2]. Stromeyer erroneously determined its formula to be "$Co_2O_3.2NO_3+3KO,NO_3+2HO$"[3]. Today it is known as potassium cobaltinitrite, $K_3[Co(NO_2)_6]$.

Cobalt ammine nitrite complexes have been synthesised since the mid-nineteenth century. These early syntheses built on the discovery by Tassaert in 1798 that cobalt salts could combine with ammonia[4]. Originally, the complexes were formed by passing the gas obtained from the action of nitric acid on starch or sawdust through ammoniacal solutions of cobalt salts[5]. The authors claimed that the gas used was a "mixture of CO_2, NO_2, NO_3 and an excess of NO_4", but their physical descriptions of the complexes obtained and their analyses suggest that various cobalt ammonia nitrite complexes were produced. One of the complex ions synthesised in this manner, which is listed as the 'chlorid of xanthocobalt' with the structure '$NO_2.5NH_3.Co_2O$, $Cl+HO$', is of particular interest as it was to be featured in the later controversy over the nature of coordination compounds.

S.M. Jørgensen and Alfred Werner, two leaders in the field of coordination chemistry at the end of the nineteenth century, had conflicting opinions on the nature of bonding in coordination compounds. During the course of this disagreement, Jørgensen noticed that the pink colour of the unstable isomer of the xanthocobalt ion, $[Co(NH_3)_5NO_2]^{2+}$, was similar to the cobalt aquo complex, and the yellow colour of the stable isomer of this ion was similar to the cobalt ammine complex (Figure 1.1). He correctly deduced that this was an example of linkage isomerism, with the nitrite coordinating via oxygen in the pink isomer, and via nitrogen in the yellow isomer[6].

NITRO   NITRITO
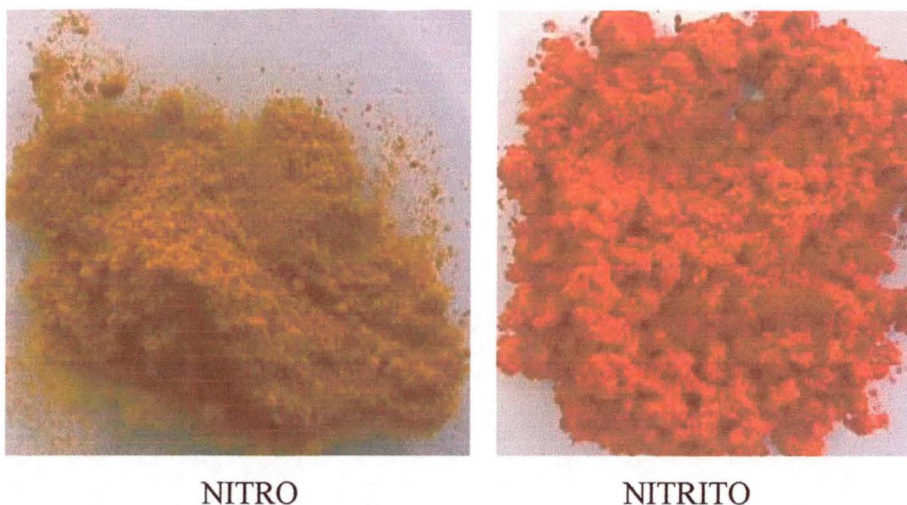
Figure 1.1: The two isomers of $[Co(NH_3)_5NO_2]^{2+}$.

Ultimately, he lost the more general argument, for although he was the first to explain linkage isomerism, the underlying basis of his theory of coordination was to be disproved by Werner[7]. Jørgensen's model describing bonding in these complexes was based on that of Blomstrand[8]. Blomstrand in turn used Odling's[9] suggestion, that metallic atoms can be substituted for hydrogen atoms in ammonia in a manner similar to that known for organic radicals, as the basis for his chain theory. Blomstrand formulated complexes such as cobalt(II) hexammine chloride as

$$
\begin{array}{c}
\qquad\qquad NH_3\text{-}NH_3\text{-}NH_3\text{-}Cl \\
Co \\
\qquad\qquad NH_3\text{-}NH_3\text{-}NH_3\text{-}Cl
\end{array}
$$
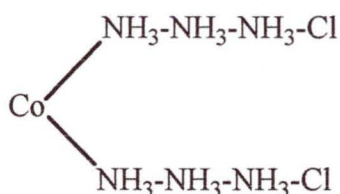
and said that the stability of the ammonia chain was not dependent on its length. Blomstrand and most other chemists also believed that cobalt(III) chloride and its ammine complexes were dimolecular, giving the purpureo salt $(Co_2Cl_6.10NH_3)$ and the luteo salt $(Co_2Cl_6.12NH_3)$ as

$$
Co_2 \left\{ \begin{array}{l}
NH_3\text{-}Cl \\
NH_3\text{-}NH_3\text{-}Cl \\
NH_3\text{-}NH_3\text{-}Cl \\
NH_3\text{-}NH_3\text{-}Cl \\
NH_3\text{-}NH_3\text{-}Cl \\
NH_3\text{-}Cl
\end{array} \right.
\qquad
Co_2 \left\{ \begin{array}{l}
NH_3\text{-}NH_3\text{-}Cl \\
NH_3\text{-}NH_3\text{-}Cl \\
NH_3\text{-}NH_3\text{-}Cl \\
NH_3\text{-}NH_3\text{-}Cl \\
NH_3\text{-}NH_3\text{-}Cl \\
NH_3\text{-}NH_3\text{-}Cl
\end{array} \right.
$$
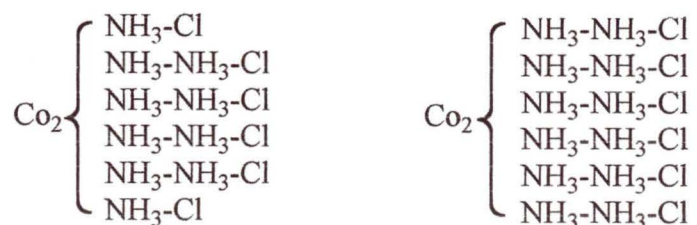
Jørgensen was able to show that there were two distinctly different chlorides present in the purpureo salt by comparing the rate of precipitation of silver chloride from a

solution of the cobalt complex and silver nitrate[10]. Two thirds of the chlorides precipitated at once, leaving the rest to slowly precipitate. Clearly, the above formulae didn't allow an explanation of these differing rates, so Jørgensen carried out analogous experiments on other similar complexes and concluded that chloride had coordinated directly to the metal

$$
Co_2 \left\{
\begin{array}{l}
Cl \\
NH_3\text{-}Cl \\
NH_3\text{-}NH_3\text{-}NH_3\text{-}NH_3\text{-}Cl \\
NH_3\text{-}NH_3\text{-}NH_3\text{-}NH_3\text{-}Cl \\
NH_3\text{-}Cl \\
Cl
\end{array}
\right.
$$
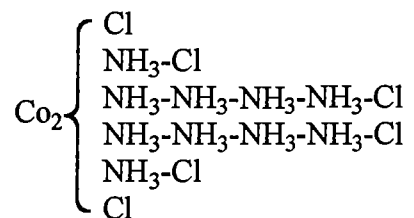
Jørgensen was also able to show that these complexes were unimolecular, resulting in the revised formula for the purpureo complex of

$$
Co \overset{\displaystyle Cl}{\underset{\displaystyle NH_3 NH_3\text{-}NH_3\text{-}NH_3\text{-}Cl}{-\!-NH_3\text{-}Cl}}
$$
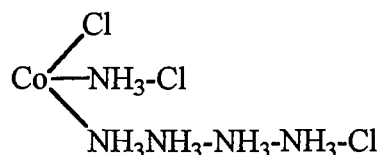
Using this model, he presented the formulae of the linkage isomers of $[Co(NH_3)_5NO_2]Cl_2$ as

$$
Co \overset{\displaystyle NO_2}{\underset{\displaystyle NH_3\text{-}Cl}{-\!-NH_3\text{-}NH_3\text{-}NH_3 NH_3\text{-}Cl}}
\qquad
Co \overset{\displaystyle ONO}{\underset{\displaystyle NH_3\text{-}Cl}{-\!-NH_3\text{-}NH_3\text{-}NH_3 NH_3\text{-}Cl}}
$$
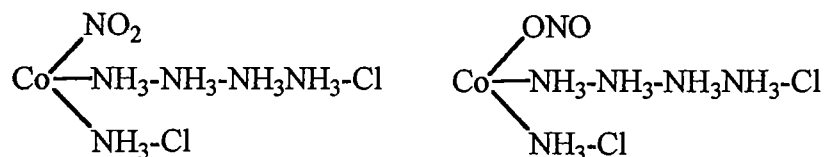
Werner did not think that the chain theory was correct, and so disagreed with Jørgensen's model. Instead, he devised new structural formulas, "coordination formulas", from his own theory of coordination. At the time, it was thought that every element had a constant valency. Werner pointed out that this was not the case. He also realised that valence alone could not be used to explain the formation and formula of complexes. He suggested that an atom, even when its combining properties were exhausted (primary valence), still possessed a form of affinity that enabled the formation of molecular compounds[7]. He proposed the term "auxiliary valence" for this affinity, and it is also known as the secondary valence. Originally, the distinction between auxiliary and secondary valence was not clear, and it was eventually realised that it was only a formal distinction.

Werner also proposed the term "coordination number", which he defined as the number of ligands attached to an atom via auxiliary valence. He found that only a few coordination numbers occurred, with six being by far the most common number. From this, he proposed spatial configurations for the complexes with each coordination number, thus explaining geometrical isomers and predicting optical isomers. Following this coordination model, the linkage isomers could be formulated as
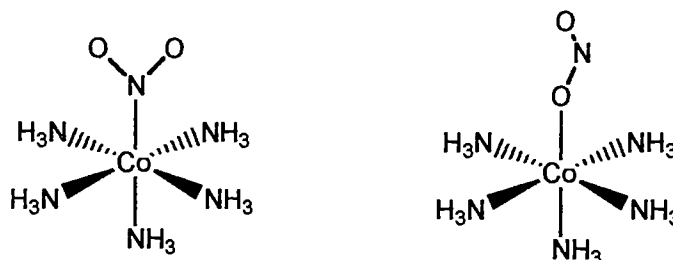
From these early beginnings, a greater appreciation of the versatility of the nitrite ligand has been reached. The ambidentate nature of the ligand arises from the number of lone pairs available for the formation of coordination bonds.
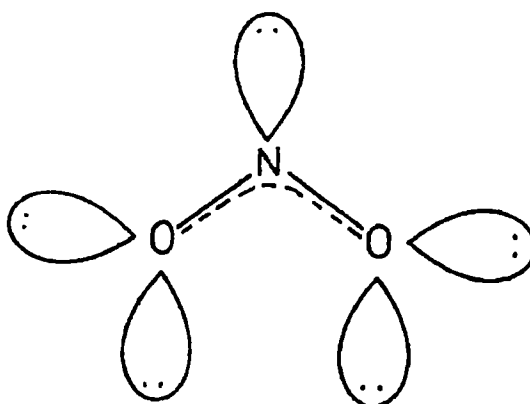
Figure 1.2: The lone pairs of the nitrite ion.

As shown in Figure 1.2, the lone pair on the nitrogen and two lone pairs on each oxygen are available for bonding. This allows monodentate bonding via nitrogen or oxygen and bi- and tridentate bonding modes in which the nitrite can either chelate or act as a bridge between two metal ions. The various modes of coordination that the nitrite ion is known to adopt are illustrated in Figure 1.3. Omitted from this diagram is an μ-O,O'-nitrito coordination mode which has both oxygen atoms bonding as a bridge between two metal centres, as it has not been seen experimentally.
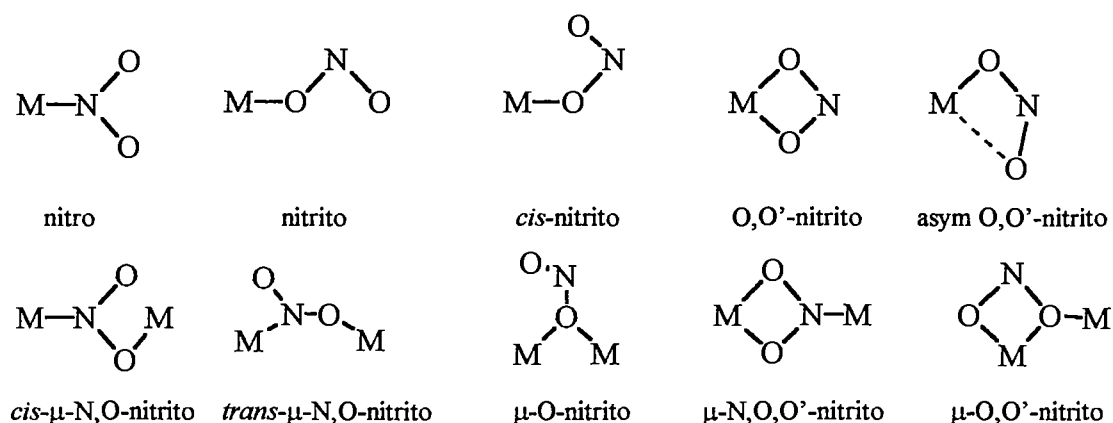
Figure 1.3: The modes of coordination of the nitrite ion.

In recent times, there has been a resurgence of interest in the nitrite ligand. This renewed interest can be seen in many fields of research, such as bioinorganic chemistry, biochemistry, catalysis and materials science. Although there are many reasons for this, one in particular is the increase in awareness of the vital roles played by small nitrogen containing molecules in biological settings. Another is that the versatility of the nitrite ligand allows the synthesis of many different complexes, some of which have novel physical and chemical properties.

1.2 Current Relevance of Nitrite Complexes

1.2.1 Biological Importance

It has been discovered that small nitrogen containing molecules play very important roles in biological systems. On a global scale, an understanding of the interactions of small nitrogen containing molecules, such as nitrate and nitrite, with metal ions is essential for the full comprehension of the global nitrogen cycle. Two steps in this cycle are nitrogen fixation and denitrification.

In nitrogen fixation, N_2 is reduced to ammonia in a reaction catalysed by an iron-molybdenum enzyme[11]. The process of denitrification, in which N_2 is released into the atmosphere by the activity of a broad family of soil-dwelling denitrifying bacteria, is also dependent on metal enzymes, known as nitrite reductases.

There are two types of bacterial nitrite (and nitrate) reductases. Assimilatory nitrite reductases catalyse the six-electron reduction of NO_2^- to NH_4^+ [12]. This enzyme has an active site containing iron and the reduction is thought to occur via the pathway:

$$NO_2^- \rightarrow Fe\text{-}NO \rightarrow hydroxylamine \rightarrow NH_4^+$$

Iron porphyrin nitrite complexes were considered suitable models for the active site of the enzyme, and this pathway was proposed after electrochemical studies of these complexes were carried out [13].

Dissimilatory nitrite reductases are involved in the denitrification process [12]. Denitrification occurs anaerobically, and is similar to the oxygen respiration of aerobic organisms. The reduction of nitrate and nitrite to gaseous nitric oxide (NO), nitrous oxide (N_2O) and nitrogen (N_2) provides an energy source for some anaerobic bacteria. Structural studies of the dissimilatory nitrite reductase of bacteria such as *Achromobacter cycloclastes* and *Bacillus halodenitrificans* have indicated that the enzyme is bimetallic with two copper ions in the active site, separated by a histidine-cysteine link [14,15]. It is thought that an electron transfer takes place from one of the copper ions to the other, possibly via the bridging histidine and cysteine. This electron is then transferred to the nitrite ion coordinated to the second copper cation. The reaction mechanism for the whole denitrification process is not fully understood. However, a mechanism for the conversion of nitrite to nitric oxide has been proposed, as it was assumed that it might be similar to that of the better-studied iron heme-containing nitrite reductases (Figure 1.4).
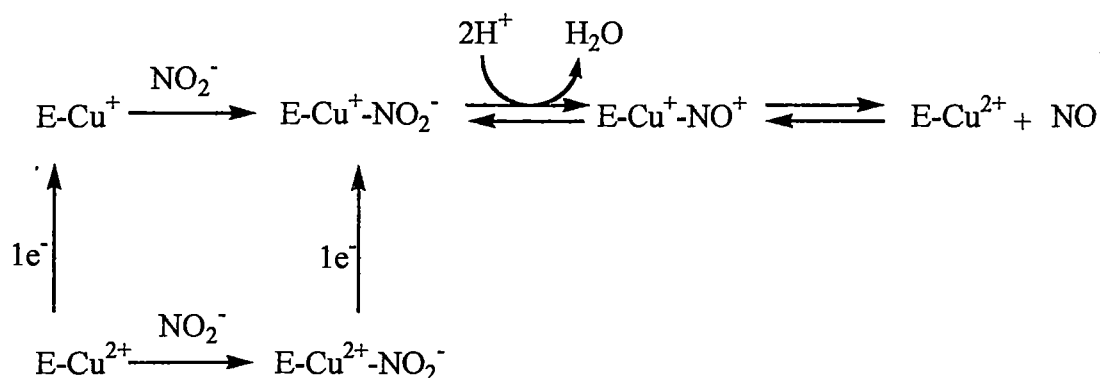
Figure 1.4: Proposed mechanism for the enzymatic reduction of nitrite to nitric oxide [16].

It was proposed that in this mechanism, the copper(I)-nitrite adduct was the key reaction intermediate, reached either through a reduction of a $Cu(II)$-NO_2^- precursor or directly, via substrate binding to the Cu(I) site. Dehydration to the nitrosyl complex, followed by the release of NO to regenerate the enzyme, completed the process.

When first proposed, this reaction mechanism was controversial, as there was little evidence for such a mechanism[17]. In fact, there were no synthetic examples of a copper (I) nitrite complex. However, in subsequent work, as well as synthesising novel model copper(II) nitrite complexes, researchers also synthesised the first copper(I) nitrite complexes to test the reactivity of such complexes[16]. Mechanistic studies provided further evidence for this mechanism[17].

Studies of copper(II) nitrite complexes also provided an interesting compound that illustrates the versatility of the nitrite ion as a ligand. The copper(II) nitrite complex, $[\{Cu(bdmppy)(NO_2)\}_2(\mu\text{-}NO_2)]_2[Cu(bdmppy)(NO_2)_2][Cu(NO_2)_4]\cdot MeCN$, where bdmppy = 2,6-bis[(3,5-dimethyl)pyrazol-1-yl]pyridine, was found to have two dimeric cationic, an anionic and two neutral Cu^{2+} molecules present in its unit cell[18]. The ambidentate nature of the nitrite made the formation of this unusual complex possible.

It must also be noted that as well as being of interest in itself, denitritification also has important environmental consequences. The loss of the agriculturally useful, but also polluting, nitrate and nitrite to form gaseous molecules has implications because these are implicated in ozone depletion, atmospheric warming and air pollution[17]. Studies of the basic process are thus clearly worthwhile from an environmental viewpoint, especially if ways in which the production of unwanted air pollutants could be trapped or removed from the cycle are revealed.

Small nitrogen containing molecules also play roles of great importance in mammalian biology[19]. In fact, these molecules, in particular nitric oxide (NO), are so important that the 1998 Nobel Prize for Medicine or Physiology was awarded to the three principal researchers who discovered the many roles that this molecule plays in the body. NO was found to be involved in neurotransmission, vascular dilation, cytotoxicity and immune responses and the activation of biochemical

processes[20]. Given that nitric oxide and the nitrite and nitrate ions are metabolically linked, knowledge of the interactions of these species with transition metal ions is again essential for understanding numerous biochemical reactions.

NO is produced *in vivo* in mammals by heme-containing nitric oxide synthases[20]. It has a short half-life and is rapidly broken down to nitrite and nitrate. To understand this process, and other biological processes involving NO, studies of iron nitrite complexes were carried out, as a proposed mechanism for the oxidation of NO to NO_3^- involved the bonding of NO to ferrous haemoglobin[21]. Nitrite is also thought to interact with ferrous haemoproteins, an example being the *in vivo* reaction of nitrite with oxyhaemoglobin to give the stoichiometric formation of nitrate and methemoglobin[22]. Another negative example of these interactions is the fact that nitrite is a direct causative agent for methemoglobinemia, a disease caused by the oxidation of the iron(II) centre of haemoglobin, destroying its ability to carry oxygen[21].

To understand these processes, a number of studies involving iron porphyrin model complexes have been carried out[20,23]. As there were few known examples of complexes of this type, the majority of this work has involved the synthesis and structural studies of iron porphyrins with nitrosyl and nitrite ligands. A further study has shown that the transfer of an oxygen atom from an iron-bonded nitrite to a substrate, for example nitrite, is feasible, thus providing evidence for the possible interaction of nitrite with ferrous haemoproteins to give nitrate[22]. Another recent experiment has provided the first unambiguous example of the conversion of an iron-nitrosyl complex to an iron-nitrite complex[24]. It is clear that further work must be done in this field, such as examining these reactions under biological conditions, and this will require an even deeper understanding of the chemical and physical properties of iron-nitrite and iron-nitrosyl complexes.

It is also of interest to note that the chemistry of iron-porphyrin nitrite complexes is of importance in the preservation of meat products. Sodium nitrite is used to cure certain meats as it is able to form an Fe-NO complex with the myoglobin present in the meat. This also preserves the colour of meat products. Nitrite is also thought to inhibit the growth of microbes such as *Clostridium botulinum* in meat by reacting with the Fe-S clusters in certain microbial proteins[21].

The importance of iron-porphyrin complexes has also sparked interest in analogous ruthenium complexes. This was helped by the discovery that ruthenium nitrosyl complexes may be useful antisepsis and antitumour agents[25]. However, a problem with this type of complex and other metalloporphyrin and nitrosyl-iron sulphur clusters is that they may be unstable in the aerobic aqueous environments encountered in biological systems[26]. Chromium complexes, for reasons that will be discussed in Chapter 4, are not as likely to generate such problems, and it is for this reason that renewed interest in their photochemistry has appeared. The aim of the research into chromium nitrite complexes is to determine whether they can act as delivering agents of nitric oxide to a target tissue. Ideally, an unreactive chromium nitrite complex would be introduced into the specific site, the area would be irradiated, preferably with a long wavelength to maximise tissue penetration, and this would result in the cleaving of NO from the complex, directly into the affected tissues:

$$Cr\text{-}ONO \rightarrow Cr\text{=}O + NO$$
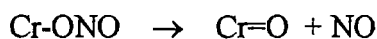
This would preferably occur at close to 100% yield, with minimal by-products. These requirements have meant that a number of photochemical studies of model chromium nitrite complexes have been carried out[27]. The results obtained from these studies are discussed in greater detail in Chapter 4.

1.2.2 Catalysis

Transition metal nitrite complexes undergo a wide range of stoichiometric and catalytic oxygen atom transfer reactions[28]. For this reason, they have been employed as catalysts for the mild oxidation of simple organic molecules[29-38]. This catalytic cycle occurs via the oxygen atom transfer reactions depicted in Figure 1.5, with the catalyst regenerating by the oxidation of a metal nitrosyl intermediate.
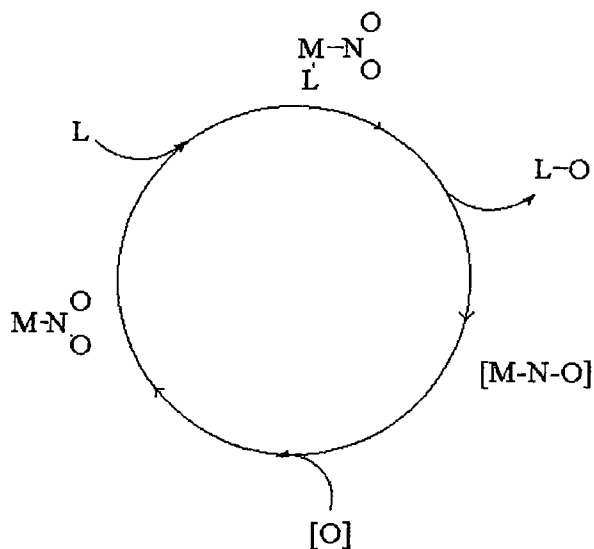
Figure 1.5: The catalytic cycle of metal-nitrite complexes.

This NO/NO_2^- redox couple has been used for numerous reactions, such as the catalytic air oxidation of alkenes to ketones, which has widespread industrial application[30]. Catalysts of this nature can also selectively oxidise alkenes to epoxides and glycol monoacetates, and have been employed in the oxidation of phosphines, carbon sulfide, nitric oxide, isonitriles and alcohols, and the oxidation of carbon monoxide to carbon dioxide[40].

Oxygen atom transfers have also been shown to occur via intramolecular mechanisms. This requires *cis*- nitro and nitrosyl groups, such as in $[Fe(NO)(NO_2)(S_2CN(Me)_2)_2]$[39,40]. The process has also been shown for the complex $CpCr(NO)_2(NO_2)$, which interestingly produces the linkage isomers $CpCr(NO)_2(NO_2)$ and $CpCr(NO)_2(ONO)$[41]. The reason that this is interesting is that it is the first published example of nitrite linkage isomerism for a chromium complex. Previously reported chromium nitrite complexes have displayed monodentate nitrito coordination only, and so the presence of a nitro group is rather unusual. Admittedly, it is difficult to determine the oxidation state of the chromium in this complex, as nitrosyl ligands can be thought of as carrying a single positive or negative charge or be neutral, so the formal oxidation state of chromium in this complex could range from (II) to (IV). As there are limited examples of nitrite complexes for Cr(II) and Cr(IV), it may be possible that nitro coordination may be more common for these ions than for Cr(III). However, with regard to this particular

example, it must be said that the evidence for this linkage isomerism is ambiguous and may have an explanation other than that given by the authors[41].

1.2.3 *Materials Science*

Transition metal nitrite complexes have attracted attention as possible precursors in the field of materials science. Preliminary work investigating the use of transition metal nitrite complexes in the formation of rare earth metal nickel oxides ($RNiO_3$, R= a rare earth metal) has been reported[42]. These compounds are of interest as they are among the few transition metal oxides that exhibit metallic or metal-to-insulator properties[43].

Oxides of this nature were originally prepared using traditional ceramic methods, but in recent years alternative syntheses have been increasingly used to improve the properties of the final metal oxides. These new syntheses have normally involved the use of organometallic precursors and have resulted in advantages such as allowing the synthesis of different oxides at the molecular level, shorter heating times at lower temperatures and the potential for significant modifications to the microstructure of the final products[44]. The ligands first employed in these syntheses were commonly carboxylate ions, but this resulted in the incorporation of large amounts of carbon, which had to be removed at a later stage[45]. To avoid this, Bolibar et al.[42] tested the usefulness of nickel nitrite complexes as a starting material. Complexes with the formula $K_2M[Ni(NO_2)_6]$, M= Ca, Sr, Ba, and $KLa[Ni(NO_2)_6]$, were decomposed to their respective oxides. This was not entirely successful, as $K_2Ca[Ni(NO_2)_6]$ did not form a mixed oxide. However, the other complexes did form the desired oxides, albeit sometimes with mixtures of others, so it appears to be a promising synthetic route to the desired metal oxide types.

A much less successful attempt to prepare potential semiconductors could have been avoided with a better understanding of the photochemistry of transition metal nitrite complexes. The development of alternative methods to prepare thin films of material for this purpose is of interest. These methods are currently based on the decomposition of inorganic and organometallic complexes by chemical, photochemical and photoassisted means onto a silicon wafer, thus producing the

desired thin film. Again, a problem faced in these methods is that the use of organometallic complexes leaves a large carbon deposit for removal. To circumvent this problem, Palmer and Hill used the starting complexes fac-Co(NH$_3$)$_3$(NO$_2$)$_3$ and mer-Co(NH$_3$)$_3$(N$_3$)$_3$[46]. Unfortunately, this nitro complex is not a suitable precursor for this method, as photochemical studies of Co(III) nitro complexes in the solid state have shown that light absorption causes the formation of nitrito complexes rather than a metal oxide[47], precluding the production of a thin metal film.

Transition metal complexes containing two or more metal centres are of interest as some show unusual magnetic behaviour. The properties of these polymers may be totally different from the sum of the magnetic properties of each metal ion surrounded by its nearest neighbours. These new properties depend on the nature and magnitude of the interaction between the metal ions through the bridging ligand and this can be altered through the selection of the interacting metal ions and the bridging and terminal ligands. This affects the symmetry and the delocalisation of the orbitals centred on the metal ions and those occupied by the unpaired electrons. For example, considering just two ions, each with an unpaired electron, the molecular state of lowest energy will be either a spin singlet or a spin triplet. A spin singlet state would result from an antiferromagnetic interaction, while a triplet results from a ferromagnetic interaction[48].

$$\uparrow\downarrow \qquad \uparrow\uparrow$$
$$S = 0 \qquad S = 1$$
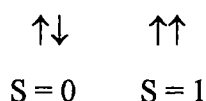
Figure 1.6: Spin states resulting from ferromagnetic and antiferromagnetic interactions.

The nitrite ligand has attracted attention as it is can bridge two metal centres. Particular interest in this aspect of transition metal nitrite complexes stems from the preparation of [Ni(en)$_2$NO$_2$]ClO$_4$, where en = ethylenediamine, in 1982[49]. This is a polymeric complex in which the nitrite coordinates as a μ-N,O-nitrito bridge between the Ni^{2+} ions. It was found to be a good example of a one dimensional Heisenberg S=1 antiferromagnet. This complex obtained additional importance, and the standard abbreviation of NENP in condensed matter journals, after Haldane's research of the following year[50].

Haldane suggested that a one-dimensional Heisenberg antiferromagnet should have an energy gap between the singlet ground state and the first excited triplet state for an integer spin quantum number, and that this gap should not exist for a half-integer spin quantum number (Figure 1.7).
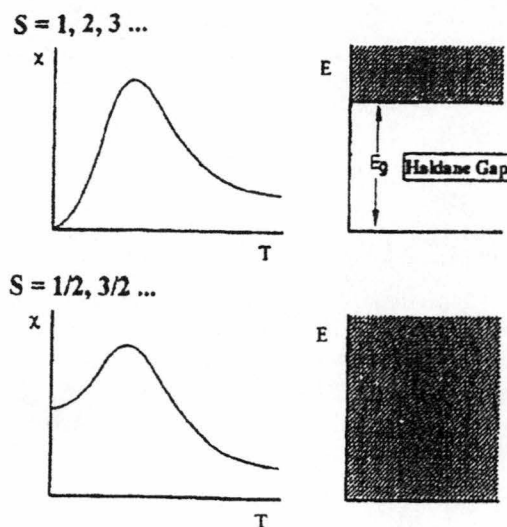
Figure 1.7: Magnetic susceptibilities of Haldane and non-Haldane gap systems (from Yamashita et al.[51]).

This means that the magnetic susceptibility approaches zero at T= 0 for a Haldane gap compound, while for a non-Haldane gap compound it would decrease to a finite value at this temperature. The behaviour of $[Ni(en)_2NO_2]ClO_4$ supported Haldane's theory[52]. It is now regarded as the archetypal Haldane gap compound, and further nitrite complexes have also shown this type of behaviour, $[Nitn_2NO_2]ClO_4$ (tn= 1,3-diaminopropane), $[Ni(dmpn)_2NO_2]PF_6.H_2O$ (dmpn = 2,2-dimethyldiaminopropane) and $(CH_3)_4N[Ni(NO_2)_3]$[51].

Transition metal nitrite complexes have also provided examples of ferromagnets, which are rather more difficult to synthesise. This is due to the fact that an achievement of a ferromagnetic interaction between two nearest neighbour transition metal ions goes against the trend favouring the pairing of electrons in molecular orbitals of low energy. To overcome this, the interaction must stabilise the state of highest spin multiplicity, which arises from orthogonality of the magnetic orbitals.
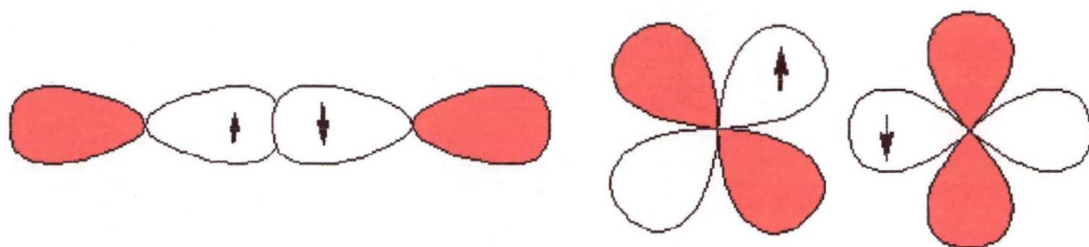
Figure 1.8: Orthogonal and non-orthogonal interactions of magnetic orbitals.

This is imposed strictly via symmetry requirements or accidentally, which is the case for some Cu(II)-Ni(II) dimers[53]. Such an interaction results in an increase in the product of the molar magnetic susceptibility and temperature as the complex is cooled down. This is the case for the mixed metal trinuclear complex $Mn(N_3)_4[Nien_2NO_2]_2$[54]. This has the nitrite coordination mode shown in Figure 1.9.
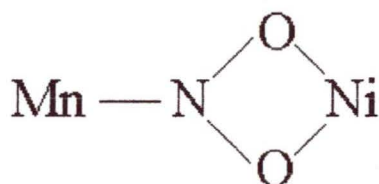
Figure 1.9: Nitrite coordination mode of $Mn(N_3)_4[Nien_2NO_2]_2$.

The electronic structures of these polymetallic complexes are not only of interest in the field of magnetic materials physics. They are also of interest to bioinorganic chemists studying polynuclear reaction sites in biological processes. For example, magnetic molecular clusters are interesting as they are relevant to biological systems such as photosystem (II) and ferritin[55]. Attempts have also been made to understand the mechanism of the transition from ferromagnetic to bulk magnetic behaviour[56]. The molecular cluster $[Ni_7(\mu-NO_2)_8(\mu-OH_2)_2(\mu-OH)_2(HOpn)_2(Opn)]_2 \cdot 7H_2O$, HOpn = 1,3-diamino-2-propanol, was prepared to try to isolate new superparamagnetic clusters of Ni(II)[55]. Again, the versatility of the nitrite ligand and its ability to allow unusual magnetic interactions made it a good choice to try to obtain such a material.

1.2.4 *Conglomerate Crystallisation*

Transition metal nitrite complexes have also been used in attempts to explain the phenomenon of conglomerate crystallisation. Conglomerate crystallisation occurs when a racemic solution produces a mechanical mixture of crystals consisting solely of a single enantiomer or diastereoisomer. The resolution occurs spontaneously, without the addition of an optically active auxiliary agent[57]. This type of crystallisation is rare, with relatively few known examples[58]. Some complexes that exhibit this are cobalt nitrite complexes, and in an effort to understand the phenomenon, a number of similar complexes have been prepared[59].

From studies of the series cis-α-[Co(trien)(NO$_2$)$_2$]X.H$_2$O X = Cl$^-$, Br$^-$ or I$^-$ and trien = triethylenetetramine, it was suggested that the conglomerate crystallisation mode for each complex is determined by specific intra- and intermolecular hydrogen bonded interactions. In particular, it was proposed that disturbing the intramolecular bonds between the oxygens of NO$_2^-$ with the axial NH$_2$ hydrogens, and the intermolecular H-bonds between the halides and the secondary NH hydrogens, would alter the final crystallisation. The studies confirmed these suggestions[60].

1.3 Factors Thought to Influence Nitrite Coordination

The widespread importance of nitrite complexes depends upon the fact that nitrite exhibits a wide range of coordination modes, with each having particular steric and electronic properties. However, it is often unclear why one nitrite coordination mode is adopted over another. Three main factors are thought to influence the coordination of the nitrite ligand. These are kinetic, steric and electronic factors.

1.3.1 *Kinetic Factors*

The formation and rearrangement of the thermodynamically unstable complex ion [Co(NH$_3$)$_5$ONO]$^{2+}$ to [Co(NH$_3$)$_5$NO$_2$]$^{2+}$ has been the subject of many studies[61-63]. It has been shown that the cobalt nitrito complex is formed following the initial attack of N$_2$O$_3$ on a hydroxo complex (Figure 1.10).

$$[Co(NH_3)_5OH]^{2+} + N_2O_3 \xrightarrow{\text{slow}} \left[\begin{array}{c} (H_3N)_5Co\text{-}O\cdots H \\ \vdots \\ O\text{-}N\text{-}ONO \end{array} \right]^{2+}$$

$$[(H_3N)_5Co\text{-}ONO]^{2+} + HNO_2 \xleftarrow{\text{fast}}$$
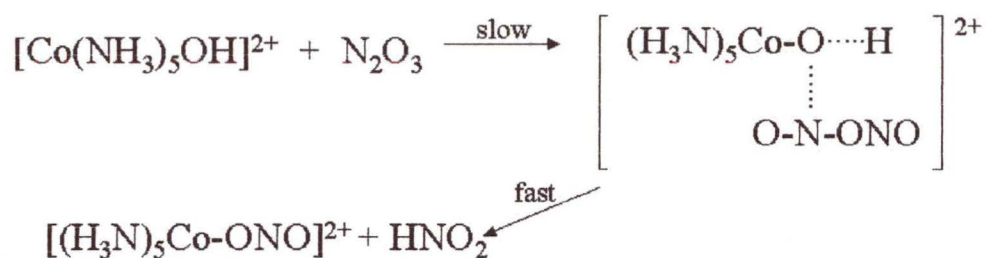
Figure 1.10: The formation of $[Co(NH_3)_5ONO]^{2+}$.

The subsequent reaction rate of the nitrito to nitro rearrangement was found to be independent of the concentration of excess nitrite added. This indicated that an intramolecular reaction was taking place[64]. Three possible intermediates for the rearrangement are illustrated in Figure 1.11.

I   II   III
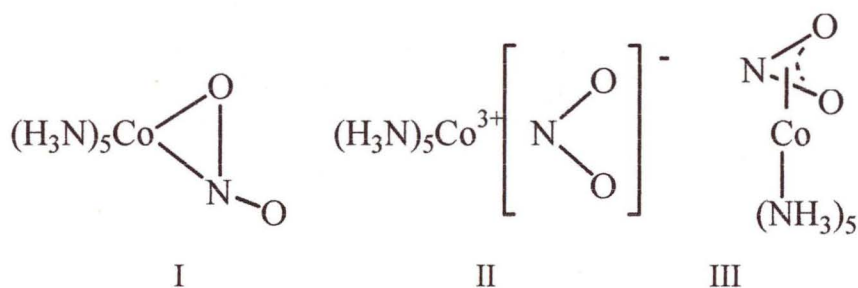
Figure 1.11: Three possible transition structures for the nitrito to nitro rearrangement.

The tight ion pair structure (II in Figure 1.11) has been discounted. The rearrangement has been carried out with excess ^{18}O-labelled nitrite and in solvents that readily dissociate ion pairs. No exchange of nitrite groups was detected, nor were the ionic strength effects consistent with an ion pair dissociation mechanism[65]. ^{18}O tracer experiments have been used to confirm that the isomerization is intramolecular, with no exchange of non-labelled coordinated nitrites with labelled nitrite groups added in excess to the solution[61]. ^{18}O has also been used to investigate the possibility of oxygen scrambling (Figure 1.12).
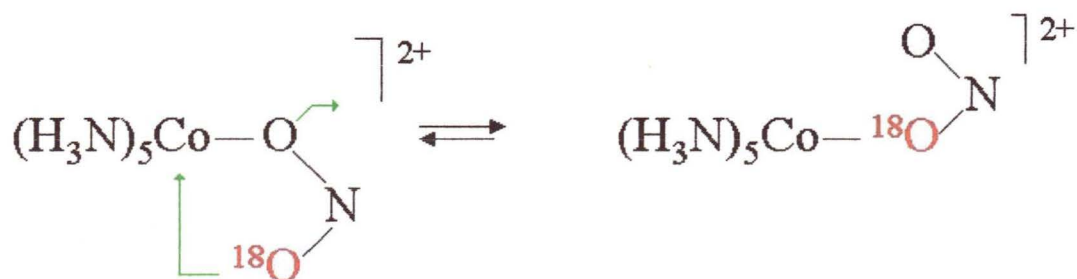
Figure 1.12: Oxygen scrambling of the $[Co(NH_3)_5ONO]^{2+}$ ion.

This scrambling occurs when the reaction is base catalysed, suggesting that in this case intermediate III in Figure 1.11 may be the likely intermediate[64].

The value for the change in volume for the rearrangement was negative, indicating that for a spontaneous isomerization, the volume of the intermediate was between that of the nitrito and nitro forms[65]. This is the case for a seven coordinate structure (I) (Figure 1.11). Density functional theory calculations studying the rearrangement from nitrito to nitro have also determined that this is the likely intermediate for the spontaneous rearrangement[66].

The kinetics of formation of cobalt(III) nitrito complexes with ethylenediamine have also been studied, as have the formation and rearrangement reactions of similar complexes of Cr(III), Ir(III), Rh(III) and Pt(IV) [62,67,68]. With the exception of chromium, for which only the nitrito complex is seen, these all show similar behaviour to that of the cobalt complexes. This suggests that the nitro complex is generally the more thermodynamically stable coordination mode for these metal ions, and so the metastable nitrito complex can only be isolated due to the relatively inert nature of Co(III), Ir(III), Rh(III) and Pt(IV) complexes.

1.3.2 Steric Factors

It has been suggested that steric crowding may influence the manner of coordination adopted by a number of ambidentate ligands[69]. Although it is difficult to prove such a suggestion, a comparison of the structures for a range of nitrite complexes of a particular metal with other ligands of varying bulk may provide some supporting evidence for the idea. The most comprehensive data of this kind involves complexes formed by nickel(II) nitrite and various amines.

Table 1.1 summarises the coordination modes seen for a number of nickel(II) nitrite complexes with substituted amine ligands. A comparison of these complexes reveals that there is a general tendency for the nitrite to adopt nitro coordination when the amine ligands are not substituted to a great degree, with it adopting nitrito coordination as the amine ligand becomes more bulky.

Complex	Coordination mode	State	Ref.
Ni(NH₃)₄(NO₂)₂	*trans* Nitro	Solid	70
Ni(en)₂(NO₂)₂	*trans* Nitro	Solid	71
[Ni(*NN*'-dimen)₂(NO₂)₂].H₂O	*trans* Nitrito	Solid	72
Ni(*NN*-dimen)₂(ONO)₂	*trans* Nitrito	Solid	72
Ni(*NN*-dimen)₂(NO₂)₂	Nitro/Nitrito	In CHCl₃ solution	73
Ni(*NN*'-dien)₂(NO₂)₂	Nitro	Solid	74
Ni(*NN*-dien)₂(ONO)₂	Nitrito	Solid	75
[Ni(*m*-stien)₂(O₂N)]X	Chelating	Solid	76
X= NO₂⁻, Cl⁻, ClO₄⁻			
[Ni(en)₂NO₂]ClO₄	Bridging	Solid	49

Table 1.1: Nitrite coordination modes for nickel(II) nitrite amine complexes.

The polynitrite complexes $M(NO_2)_4^{2-}$, M = Mn, Co, Zn, Cd and Hg, also provided some supporting evidence for the steric influence on nitrite coordination modes. In each of these ions, the nitrite coordinates via oxygen. The bonding in the Mn, Cd and Hg complexes occurs via symmetrical chelation[77-79], but for Zn and Co, this chelation is so asymmetric as to be essentially monodentate[69]. It is possible that in this case the nitrite ligands are very crowded around the smaller metal ions, Zn and Co, resulting in high interligand repulsions, thus forcing the length of one of the chelate bonds to increase. This would not be so much of a problem with the larger metal ions.

1.3.3 *Electronic Factors*

The electronic structure of the metal ion or other ligands in a complex may also affect the nature of the metal-nitrite bond. Although there is not widespread evidence for this, an example of the effect may be seen when comparing analogous cobalt(III) and chromium(III) complexes. For cobalt(III), the more thermodynamically stable form of monodentate nitrite coordination is via nitrogen, whereas for chromium(III) complexes, all synthesised complexes to date have been monodentate nitrito complexes. When the major difference between such complexes

is the identity of the metal, e.g. $[M(NH_3)_5NO_2]^{2+}$, it seems likely that electronic effects must be exerting an influence on the coordination mode.

Another possible example is provided by a comparison of analogous nickel(II) and zinc(II) compounds. $Ni(en)_2(NO_2)_2$ is a nitro complex, but the analogous zinc(II) complex $[Zn(en)_2(NO_2)]NO_2$ has a chelating nitrite and an ionic nitrite ion[71,80]. As the ionic radius of Zn(II) is slightly larger than the radius of Ni(II), it seems doubtful that ligand-ligand repulsions are causing this chelation. $[Ni(en)_2NO_2]ClO_4$ has a μ-N,O-nitrito bridging nitrite, but again the analogous Zn(II) complex contains a chelating nitrite[49,81]. As with chromium(III), all known nitrite complexes of Zn(II) have coordination via oxygen, thus implying that this is the preferred coordination mode to this metal ion.

The above factors may contribute to influencing the mode of coordination of the nitrite, so it is likely that in transition metal nitrite complexes the stereochemistry may be a balance between various factors. Sometimes these may be delicately balanced, for example, the complex $Ni(1-(2-aminoethylpiperidine)_2(NO_2)_2$ has been isolated both as a nitro and a monodentate nitrito complex[82]. $Ni(NN-dimen)_2(ONO)_2$ exhibits an equilibrium between the nitro and nitrito form in chloroform solutions[73].

1.4 Purpose of the Present Study

As mentioned in previous sections, the coordination chemistry of the nitrite ion is of current interest in a wide range of fields. However, the reason why one nitrite mode is adopted over another in a given complex often remains unclear. This study aims to investigate the influences on the coordination mode of the nitrite in a number of transition metal complexes. A second, related major interest is the nature of the bonding between the nitrite ligand and different metal ions, and how this changes with the manner of nitrite coordination.

The linkage isomers $[Co(NH_3)_5NO_2]^{2+}$ and $[Co(NH_3)_5ONO]^{2+}$ and the analogous $[Cr(NH_3)_5ONO]^{2+}$ complex have been prepared. These are used to provide an example in which the main factor influencing the nitrite would be an electronic factor, as the only difference between these complexes is the metal.

The polynitrite complexes with the formula $[M(NO_2)_4]^{2-}$ where M is cadmium, zinc and mercury are also examined, as in this case the major differences between nitrite coordination would possibly result from the size of the metal, hence steric effects would most likely influence the coordination mode.

The steric factor was also studied in a series of nickel nitrite complexes with amines of varying steric bulk. These complexes also afforded a comparison between the various coordination modes as the series provided examples of almost all known coordination modes.

A range of physical techniques and calculations were chosen to examine the nature of nitrite bonding in a range of transition metal complexes. These will be described in greater detail in Chapter 2.

1.5 References

1. Fischer N.W., *Pogg. Ann.*, **lxxxiv**, 115; and **lxxxviii**, 496, (1831).

2. Saint-Evre E., *Compt. Rend.*, **xxxiv**, 479 and *Ann. Chem. et Phys.*, **xxxviii**, 177, (1851).

3. Stromeyer F., *Journal fur Pract. Chemie*, **lxi**, 41, (1853) and *Ann. der Chemie und Pharmacie*, **xcvi**, 218, (1853).

4. Tassaert B.M., *Ann. Chem. Phys.*, **28(1)**, 92, (1798).

5. Gibbs W. and Genth F.A., *American Journal of Science*, **24**, 86-107, (1857).

6. Jørgensen S.M., *Z. Anorg. Chem.*, **5**, 169-180, (1894).

7. Werner A., *Neuere Anschauungen*, Vieweg, Braunschwieg, (1920).

8. Blomstrand C.W., *Ber.*, **4**, 40-45, (1871).

9. Odling W., *Chem. News.*, **21**, 289-293, (1870).

10. Jørgensen S.M., *J. Prakt. Chem.*, **2[18]**, 209-217, (1878).

11. Eady R.R. and Leigh G.J., *J. Chem. Soc. Dalton Trans.*, 2739-2747, (1994).

12. Suslick K.S. and Watson R.A., *Inorg. Chem.*, **30**, 912-919, (1991).

13. Wei Z. and Ryan M.R., *Book of Abstracts, 210th A.C.S. Nat. Meeting*, Chicago IL, August 20-24, (1995).

14. Godden J.W., Turley S., Teller P.L., Adman E.T., Liu M.Y., Payne W.J. and LeGall J., *Science*, **253**, 438-442, (1991).

15. Denariaz G., Payne W.J., LeGall J., *Biochem. Biophys. Acta*, **1056**, 255-262, (1991).

16. Halfen J.A. and Tolman W.B., *J. Am. Chem. Soc.*, **116**, 5475-5476, (1994).

17. Halfen J.A., Mahapatra S., Wilkinson E.C., Gengenbach A.J., Young Jr. V.G. Que Jr. L. and Tolman W.B., *J. Am. Chem. Soc.*, **118**, 763-776, (1996).

18. Blake A.J., Hill S.J. and Hubberstey P., *Chem. Comm.*, 1587-1588, (1998).

19. The Biology of Nitric Oxide; Moncada S., Marletta M.A., Hibbs J.B., Higgs E.A. (eds), Portland Press: London 1992 Vols I and II.

20. Nasri H., Ellison M.K., Chen S., Huynh B.H. and Scheidt W.R., *J. Am. Chem. Soc.*, **119**, 6274-6283, (1997).

21. Fanning J.C., *Coord. Chem. Rev.*, **110**, 235-273, (1991).

22. Munro O.Q. and Scheidt W.R., *Inorg. Chem.*, **37**, 2308-2316, (1998).

23. Ellison M.K., Schulz C.E. and Scheidt W.R., *Inorg. Chem.*, **38**, 100-108, (1999).

24. Cheng L., Powell D.R., Khan M.A. and Richter-Addo G.B., *Chem. Comm.*, 2301-2302, (2000).

25. Chen Y., Lin F.T. and Shepard R.E., *Inorg. Chem.*, **38**, 973-983, (1999).

26. De Leo M.A. and Ford P.C., *J. Am. Chem. Soc.*, **121**, 1980-1981, (1999).

27. De Leo M.A. and Ford P.C., *Coord. Chem. Rev.*, **208**, 47-59, (2000).

28. Feltham R.D. and Rajaseelan E., *Inorg. Chim. Acta.*, **218**, 195-197, (1994).

29. Tovrog B.S., Diamond S.E. and Mares F., *J. Am. Chem. Soc.*, **101**, 270-272, (1979).

30. Andrews M.A. and Kelly K.P., *J. Am. Chem. Soc.*, **103**, 2894-2896, (1981).

31. Andrews M.A. and Cheng C.W.F., *J. Am. Chem. Soc.*, **104**, 4268-4270, (1982).

32. Andrews M.A., Chang T.C.T., Cheng C.W.F., Emge J.J., Kelly K.P. and Koetzle T.F., *J. Am. Chem. Soc.*, **106**, 5913-5920, (1984).

33. Andrews M.A., Chang T.C.T., Cheng C.W.F. and Kelly K.P., *Organometallics*, **3**, 1777-1785, (1984).

34. Andrews M.A., Chang T.C.T. and Cheng C.W.F., *Organometallics*, **4**, 268-274, (1985).

35. Baeckvall J.E. and Heumann A., *J. Am. Chem. Soc.*, **108**, 7107-7108, (1986).

36. Leising R.A. and Takeuchi K.J., *J. Am. Chem. Soc.*, **110**, 4079-4080, (1988).

37. Muccigrosso D.A., Mares F., Diamond S.E. and Solar J.P., *Inorg. Chem.*, **22**, 960-965, (1983).

38. Mares F., Diamond S.E., Regina F.J. and Solar J.P., *J. Am. Chem. Soc.*, **107**, 3545-3552, (1985).

39. Ileperuma O.A. and Feltham R.D., *J. Am. Chem. Soc.*, **98**, 6039-6040, (1976).

40. Ileperuma O.A. and Feltham R.D., *Inorg. Chem.*, **16**, 1876-1883, (1977).

41. Hubbard J.L., Zoch C.R. and Elcesser W.L., *Inorg. Chem.*, **32**, 3333-3338, (1993).

42. Bolibar A., Insauti M., Lorene L., Pizarro J.L., Arriortua M.I. and Rojo T., *J. Mater. Chem.*, **7(11)**, 2259-2264, (1997).

43. Lacorre P., Torrance J.B., Pannetier J., Nazzal A.I., Wang P.W. and Huang T.C., *J. Solid State Chem.*, **91**, 225-237, (1991).

44. Insausti M., Pizarro J.L., Lezama L., Cortés R., Bocanegra E.H., Arriortua M.I. and Rojo T., *Chem. Mater.*, **6**, 707-713, (1994).

45. Horowitz H.S., McLain S.J., Sleight A.W., Druliner J.D., Gai L., Vankavelaar M.J., Wagner J.L., Biggs R.D. and Poon S.J., *Science*, **243**, 66-69, (1989).

46. Palmer B.J. and Hill R.H., *J. Photochem. Photobiol. A: Chem.*, **72**, 243-249, (1993).

47. Scandola F., Bartocci C. and Scandola M.A., *J. Phys. Chem.*, **78(6)**, 572-575, (1974).

48. Kahn O., *Angew. Chem. Int. Ed. Eng.*, **24**, 834-850, (1985).

49. Meyer A., Gleizes A., Girerd J.J., Verdaguer M. and Kahn O., *Inorg. Chem.*, **21**, 1729-1739, (1982).

50. Haldane F.D.M., *Phys. Rev. Letters*, **51**, 605-608, (1983) and *Phys. Lett. A.*, **93**, 464-468, (1983).

51. Yamashita M., Ishii T. and Matsuzaka H., *Coord. Chem. Rev.*, **198**, 347-366, (2000).

52. Renard J.P., Verdaguer M., Regnault L.P., Erkelens W.A.C., Mignod J.R. and Stirling W.G., *Europhys. Lett.*, **3**, 945-952, (1987).

53. Pei Y., Verdaguer M., Kahn O., Sletlen J. and Renard J.P., *Inorg. Chem.*, **26**, 138-143, (1987).

54. Rajendiran T.M., Mathonière C., Golhen S., Ouahab L. and Kahn O., *Inorg. Chem.*, **37**, 2651-2654, (1998).

55. El Fallah M.S., Rentschler E., Caneschi A., Sessoli R. and Gatteschi D., *Inorg. Chem.*, **35(13)**, 3723-3724, (1996).

56. Gatteschi D, Pardi L., Barra A-L., Müller A. and Döring J., *Nature*, **354**, 463-465, (1991).

57. Bernal I., *Inorg. Chim. Acta*, **96**, 99-110, (1985).

58. Bernal I., Cetrullo J., Myrczek J., Cai J. and Jordan W.T., *J. Chem. Soc. Dalton Trans.*, 1771-1776, (1993).

59. Cai J., Myrczek J., Chun H. and Bernal I., *J. Chem. Soc. Dalton Trans.*, 4155-4160, (1998).

60. Bernal I. and Cetrullo J., *Inorg. Chim. Acta*, **134**, 105-112, (1987).

61. Basolo F., Pearson R., Henry P.M. and Bergmann J.G., *J. Am. Chem. Soc.*, **76**, 5920-5923, (1954).

62. Murmann R.K. and Taube H., *J. Am. Chem. Soc.*, **78**, 4886-4890, (1956).

63. Wendlandt W.W. and Woodlock J.H., *J. Inorg. Nucl. Chem.*, **27**, 259-260, (1965).

64. Jackson W.G., Lawrance G.A., Lay P.A. and Sargeson A.M., *Inorg. Chem.*, **19**, 904-910, (1980).

65. Mares M., Palmer D.A. and Kelm H., *Inorg. Chim Acta*, **27**, 153-156, (1978).

66. Ciofini I. and Adamo C., *J. Phys. Chem. A*, **105**, 1086-1092, (2001).

67. Basolo F. and Hammaker G.S., *J. Am. Chem. Soc.*, **82**, 1001-1002, (1960).

68. Basolo F. and Hammaker G.S., *Inorg. Chem.*, **1**, 1-5, (1962).

69. Hitchman M.A. and Rowbottom G.L., *Coord. Chem. Rev.*, **42(1)**, 55-132, (1982).

70. Figgis B.N., Reynolds P.A., White A.H., Williams G.A. and Wright S., *J. Chem. Soc. Dalton Trans.*, 997-1003, (1981).

71. Porai-koshits M.A. and Minacheva L.Kh., *J. Struct. Chem.*, **5**, 595-597, (1964).

72. Finney A.J., Hitchman M.A., Raston C.L., Rowbottom G.L. and White A.H., *Aust. J. Chem.*, **34**, 2047-2060, (1981).

73. Goodgame D.M.L. and Hitchman M.A., *Inorg. Chem.*, **5**, 1303-1307, (1966).

74. Green R.W., *Aust. J. Chem.*, 1841-1845, (1973).

75. Walker I.M., Lever A.B.P. and McCarthy P.J., *Can. J. Chem.*, **58**, 823-832, (1980).

76. Finney A.J., Hitchman M.A., Raston C.L., Rowbottom G.L. and White A.H., *Aust. J. Chem.*, **34**, 2069-2084, (1981).

77. Goodgame D.M.L. and Hitchman M.A., *J. Chem. Soc. (A)*, 612-615, (1967).

78. Ohba S., Matsumoto F., Takazawa H. and Saito Y., *Acta Cryst.*, **C43**, 191-194, (1987).

79. Power L., King J. and Moore F., *J. Chem. Soc. Dalton Trans.*, 93-96, (1976).

80. Finney A.J., Hitchman M.A., Raston C.L., Rowbottom G.L. and White A.H., *Aust. J. Chem.*, **34**, 2061-2067, (1981).

81. Finney A.J., Hitchman M.A., Raston C.L., Rowbottom G.L. and White A.H., *Aust. J. Chem.*, **34**, 2159-2176, (1981).

82. Das D., Laskar I.R., Ghosh A., Mondal A., Okamoto K. and Chaudhuri N.R., *J. Chem. Soc. Dalton Trans.*, 3987-3990, (1998).

CHAPTER 2

Experimental Techniques and Calculations

Optical and vibrational spectroscopy were the two main physical techniques first used to determine the presence and coordination mode of nitrite in a given complex. These techniques looked at different properties of the complexes. Optical spectroscopy allows the measurement of electronic transitions, both d-d and charge transfer, within the complex, whereas vibrational spectroscopy measures the internal ligand and metal-ligand stretching and bending modes. It was also possible to observe vibrations occurring in excited states in some cases.

From this information, it was possible to determine the coordination mode of the nitrite ligand. The coordination of nitrite to a metal results in vibrational energy changes for the fundamental stretching modes of the nitrite. This is dependent on the mode of coordination adopted by the ligand, and these changes could be measured and interpreted with the use of vibrational spectroscopy. The electronic transitions also undergo energy shifts when the coordination mode changes, and again this could be measured using optical spectroscopy

As X-ray crystallography has become more widely used, more crystal structures for transition metal nitrite complexes have been published. This allowed the confirmation of previously assigned nitrite coordination modes, and also indicated errors in these assignments. It must be noted that as the coordination chemistry of the nitrite ligand is varied, there have been some times in which the only way to obtain an unequivocal assignment of the nitrite coordination mode is through the measurement of a crystal structure. This was the case for a number of polymeric complexes in which nitrite adopts various bridging modes. In this work, crystal structure measurements have been obtained for a few complexes in which it was not possible to determine the nitrite coordination in any other way.

The use of the parameterisation schemes such as the Angular Overlap Model (AOM) has enabled an understanding of the nature of the metal-nitrite bond. This model

requires the input of information obtained from the optical spectrum and allows the calculation of chemically meaningful parameters for the ligands as they adopt particular coordination modes. This is explained in greater detail in Section 2.3.

Ab initio and density functional theory calculations have also provided information about the electronic structure and molecular geometry of transition metal nitrite complexes. These calculations will be referred to and explained when discussing the relevant complexes in following chapters.

2.1 Vibrational Spectroscopy

Infrared spectroscopy (IR) was the first technique used to identify the coordination mode of nitrite in novel complexes, apart from the early identification of the linkage isomerism in $[Co(NH_3)_5NO_2]^{2+}$ by Jørgensen[1]. Although IR was very useful for this purpose, it was shown using Raman spectroscopy that a number of the papers relying on this technique were interpreting spectra incorrectly[2-5]. The reason why this was the case can be seen when considering the different mechanisms giving rise to observable peaks in the two techniques.

The symmetry of the free nitrite ion is C_{2v}, and it has three fundamental vibrations (Figure 2.1).
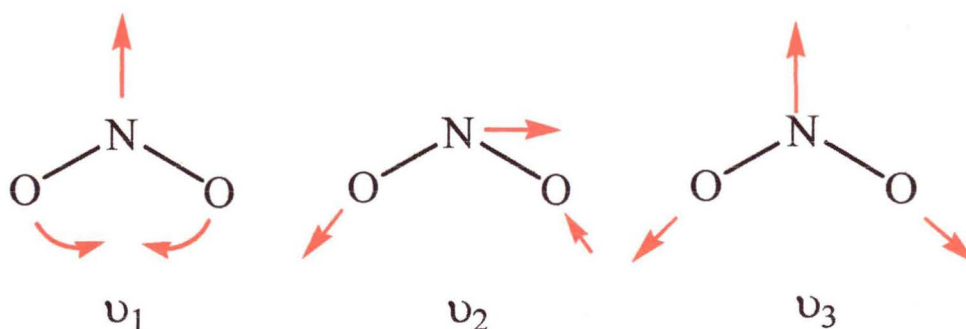
Figure 2.1: The three fundamental vibrational modes of the nitrite ion.

The selection rules for IR and Raman state that for a vibration to be IR active, the dipole moment must change, and for an active Raman vibration the polarisability must change. Considering the vibrations illustrated in Figure 2.1, a wagging (v_1) and an asymmetric stretch (v_2) cause a large change in the dipole moment, and are thus strongly IR active. The dipole moment would change only slightly for a symmetric

stretch (v_3), thus giving a weak peak in the IR spectrum. For Raman spectroscopy, there is a large polarisability change for the wagging mode and symmetric stretch, but not the asymmetric stretch. Overall, one would expect to see the wagging mode in both the IR and Raman spectra, a dominant asymmetric stretch in the IR spectrum and a dominant symmetric stretch in the Raman spectrum.

Experimentally, the IR spectrum of nitrite was characterised by three peaks: a medium intensity, sharp wagging mode v_1 peak at 828 ± 3 cm^{-1}, a broad, very strong asymmetric stretch (v_2) peak at 1 250 $\pm$ 30 cm^{-1} and a very weak, sharp peak due to the symmetric stretch (v_3) at 1 326 $\pm$ 2 cm^{-1} [6-9] (Figure 2.2).
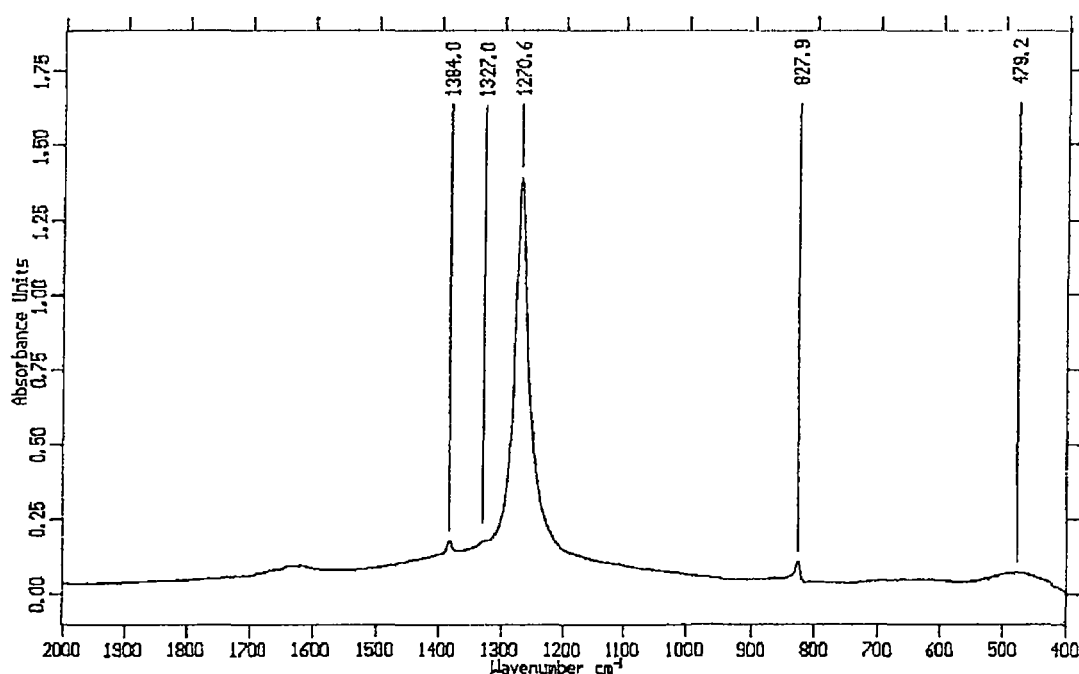
Figure 2.2: The infrared spectrum of sodium nitrite.

Usually, a symmetric stretch is of lower energy than the corresponding asymmetric stretch, but in the case of NO_2^-, the isoelectronic molecule ozone (O_3), and the isonuclear molecule nitrogen dioxide (NO_2), this is reversed. This has been explained by the presence of the two negatively charged oxygen atoms in the nitrite ion that results in a relatively large interaction constant[8]. Neglect of this unusual aspect was the reason why a number of quoted nitrite spectra have incorrectly assigned peaks[2-5]. The use of Raman spectroscopy indicated this error, as the intensity of the asymmetric and symmetric stretches are the reverse of that found in the infrared spectrum[10] (Figure 2.3).
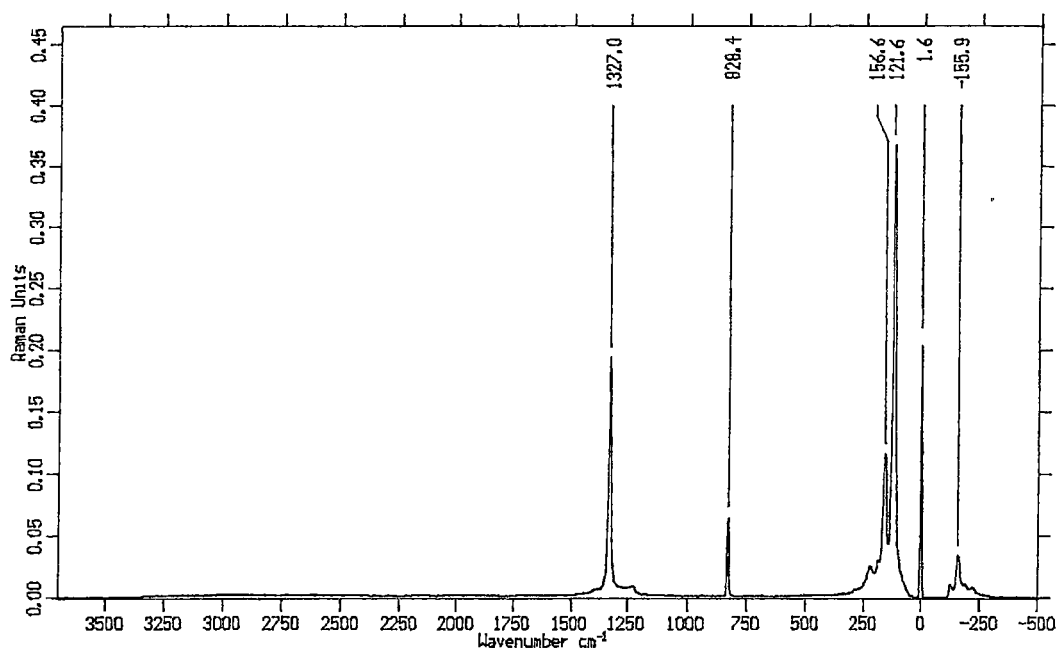
Figure 2.3: The Raman spectrum of sodium nitrite.

From their measurements of the Raman spectrum, Mathieu et al.[10] were able to show that the symmetric stretch was lower in energy than the asymmetric stretch. Unfortunately, as these were published in French journals, it took some time for English-speaking researchers to discover this work and thus amend their infrared assignments.

Infrared spectroscopy is of particular use as a relatively simple way in which to determine the mode of coordination of the nitrite in the complex, and to check the effect of these coordination modes on the internal vibrations of the nitrite. The positions of the v_2 and v_3 bands vary due to changes in symmetry upon the coordination of the nitrite ion to the metal. Each mode of coordination has a different influence on the NO bond strengths, and as such has a characteristic effect on the positions of the stretching bands. This is shown diagrammatically in Figure 2.4 for nitrite bound to a divalent metal ion such as Ni^{2+}.

MODE	NITRITE STRETCHING FREQUENCIES (cm^{-1} x 10^2)

Ionic

Nitro

Nitrito

Chelating

O Bridged

NO Bridged
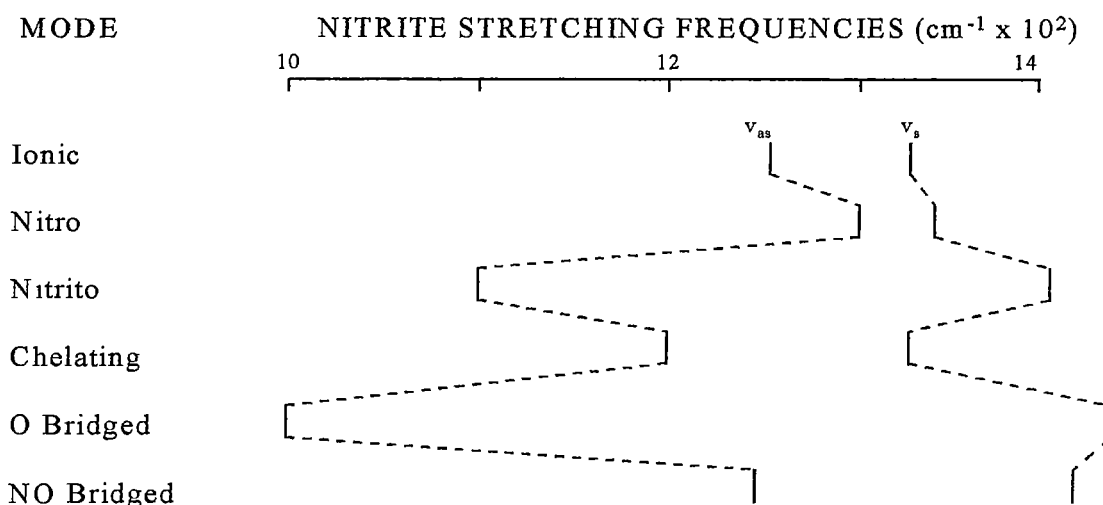
Figure 2.4: A comparison of v_2 and v_3 for the different nitrite coordination modes.

It must be noted that when a metal bonds to one of the oxygen atoms more strongly than the other, the two N-O bonds become inequivalent, and in the case of strong nitrito coordination, M-O-N=O, one tends toward a double bond and the other toward a single bond. The description 'symmetric' or 'asymmetric' stretch is then no longer appropriate. For this reason, the use of the symbols v_1, v_2 and v_3 have been adopted in this thesis.

Raman spectroscopy has rarely been employed in the study of nitrite complexes. This is most likely due to the high cost of the technique, and the problems encountered in the measurement of this type of spectrum. The Raman effect is very weak, as usually only about one in 10^{12} incident photons is scattered with a Raman shift. This signal is easily swamped by that due to the heating of the complex and this is usually a problem when the samples are darkly coloured. However, as the technique is now more readily accessible, it was employed in the present work because the information obtained complements that obtained from infrared techniques. This often enabled the unequivocal assignment of the nitrite peaks.

2.2 Optical Spectroscopy

The measurement of optical spectra and magnetic susceptibilities of complexes provided early coordination chemists with the approximate symmetry and

coordination number of the complex. There are two types of optical spectra, d-d and charge transfer spectra.

d-d spectra involve the transition of d-electrons from one metal d-orbital to another (Figure 2.5). These generally occur in the range 8 000 to 30 000cm^{-1} and the resulting bands are usually less intense than charge transfer bands.
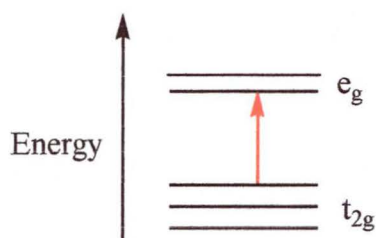
Figure 2.5: A simple illustration of a d-d transition from a t_{2g} orbital of a metal ion to an e_g orbital.

Charge transfer spectra result from the transfer of an electron from an orbital primarily on a metal to an orbital primarily on the ligand (metal to ligand charge transfer, MLCT) and vice versa (ligand to metal charge transfer, LMCT) (Figure 2.6). Charge transfer bands usually lie at the blue end of the visible spectrum and in the ultraviolet region. It is also possible to have lower energy charge transfers if the metal is easily reduced or oxidised or if the ligand is easily oxidised or reduced.
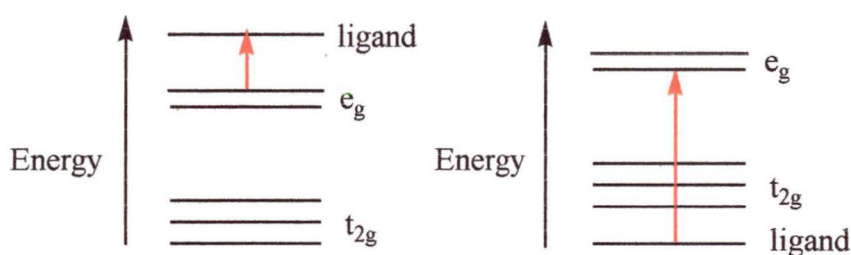
Figure 2.6: Metal to ligand and ligand to metal charge transfers.

"Intraligand" transfers may occur in the violet or near UV range for ligands with non-bonding electrons and empty π^* orbitals of low energy. Nitrite is in this category, and weak peaks in the violet and near UV for some nitrite complexes have been assigned as $n \rightarrow \pi^*$ transitions[11].

2.2.1 *d-d Transitions*

The optical spectrum provides important information about the mode of coordination of the nitrite ion. The optical spectra of the nitro and nitrito isomers of $[Co(NH_3)_5NO_2]^{2+}$ allowed a comparison of the relative field strengths of two known coordination modes. This showed that the energy of the d-d transitions for a nitro complex are considerably higher in energy than those of the analogous nitrito complex. This was incorporated with other data obtained for ligands to form the spectrochemical series, listed here in order of decreasing field strength (underline denotes donor atom)[12]:

$CN^- \gg \underline{N}O_2^- >$ bipy $>$ en $>$ py $\sim NH_3 >$ glycine $\sim$ edta $>$ SC$\underline{N} >$ H_2O $>$ O$\underline{N}$O $>$ ox $>$ RCOO $>$ OH$^- >$ F$^- >$ NC$\underline{S} >$ Br $>$ I
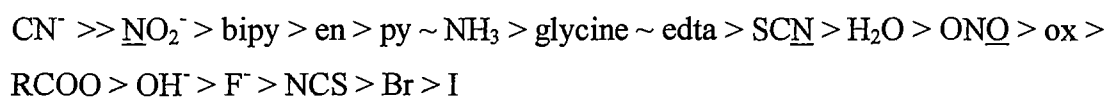
This series is followed for a number of complexes of different metal ions. It raises the important question as to why the nitrite ion is a much "stronger" ligand when it bonds via nitrogen compared with oxygen. A major aim of the present research is to answer this question.

As well as providing a method for identifying coordination modes in nitrite complexes, the use of electronic absorption spectroscopy enables the investigation of the electronic structure of a compound. Polarised absorption spectroscopy, in particular, gives a very clear view of electronic transitions in a transition metal complex, as it provides more information than other optical spectroscopic measurements, especially for a compound of known crystal structure. A summary of the benefits of this particular technique will be given after a description of the underlying theory, and an explanation of the intensities observed in a spectrum.

For an electronic transition to be observed, it must involve absorption of light. The intensity of light absorption, I, associated with an electronic transition from one state, ψ_1, to another, ψ_2, is proportional to the square of the transition moment integral, P,

$$I \propto |\langle\psi_2 | R | \psi_1\rangle|^2 = P^2 \qquad (2.1)$$

where R signifies an operator that represents the interaction of the electromagnetic radiation with the molecule.

To understand the basis of polarised absorption spectroscopy, it is first necessary to consider the nature of electromagnetic radiation. This consists of orthogonally oscillating electric (E) and magnetic (H) vectors as shown by Figure 2.7.
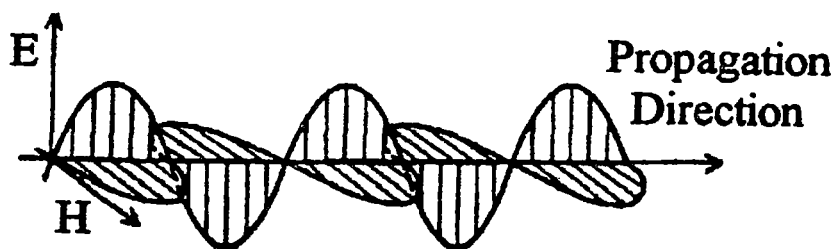
Figure 2.7: The electric and magnetic vectors of polarised light.

An electronic transition will have contributions from both the electric and magnetic dipole components, and also from the electric quadrupole and higher order terms. In practice, the electric dipole intensity is approximately 10^4 times greater in magnitude than the magnetic dipole intensity, and greater still than the other components. Therefore, electronic spectra mainly involve the electric dipole mechanism. This domination leads to the modification of Equation 2.1 to

$$P = <\psi_2 \mid r \mid \psi_1> \qquad (2.2)$$

The electric dipole operator is now represented by a unit vector, r, and in this case P varies in magnitude according to the direction of r within the molecule. This anisotropy of light absorption with respect to the orientation of the electric vector is the basis of polarised absorption spectroscopy.

The light absorption must conform to the symmetry of the crystal unit cell[13]. For cubic crystals, and uniaxial crystals when the electric vector is parallel to the unique crystal axis, it is not possible to measure a polarised spectrum because the light absorption is isotropic with respect to the direction of the electric vector of polarised light. Biaxial crystals, and other orientations of uniaxial crystals have two 'extinction' directions per face. These directions are the only directions in which polarised light does not become depolarised as it travels through the crystal.

The intensity of light absorption by the electric dipole mechanism obeys two "selection rules":

1. The spin quantum numbers of the ground and excited states must not change.

2. The parity of the two energy levels must be different.

These simple rules are based on two approximations. The first of these is from the Russell-Saunders coupling scheme, which allows the spin and orbital parts of the electronic wavefunction to be considered independently. This gives Equation 2.3:

$$P = <\Phi_2 \mid r \mid \Phi_1><\theta_{2,s} \mid \theta_{1,s}> \qquad (2.3)$$

where Φ_n and $\theta_{n,s}$ (n= 1 or 2) represent the orbital and spin components of the wavefunction, respectively.

For a 'spin-allowed' transition, the spin quantum numbers of the ground and excited states, $\theta_{1,s}$ and $\theta_{2,s}$, must be equal. For first row transition metal ions such as nickel, spin-allowed transitions are approximately one hundred times more intense than spin-forbidden transitions. However, spin-forbidden transitions may 'borrow' intensity from spin-allowed transitions and thus gain some intensity.

The orbital and spin components of the wavefunction should not be considered independently when interpreting the intensities of spin-forbidden transitions. A set of quantum numbers, J, is used to characterise states that are given by the spin-orbit coupling of the electrons. This coupling means that the wavefunctions must be described in terms of the spin-orbit irreducible representations, which have a double point group. Equation 2.4 may then be used to determine whether a transition is allowed for a particular polarisation, as an allowed transition $\Psi_{j1} \rightarrow \Psi_{j2}$ must contain, or equate to, the totally symmetric irreducible representation A_{1g} as shown by Equation 2.4.

$$\Gamma(\Psi_{j1}) \times \Gamma(r) \times \Gamma(\psi_{j2}) \subset A_{1g} \qquad (2.4)$$

The second rule, the Laporte rule, involves the parity of the ground and excited state wavefunctions Φ_1 and Φ_2. For the transition moment to be non-zero, thus allowing the electron to absorb a photon, the direct product of the irreducible representations of Φ_1 and Φ_2 with the irreducible representation of the electric dipole operator, r, must contain the totally symmetric representation $A_{1(g)}$ (Equation 2.5).

$$\Gamma(\Phi_1) \times \Gamma(r) \times \Gamma(\Phi_2) \subset A_{1(g)} \qquad (2.5)$$

When looking at a spectrum, it is possible to apply the Laporte rule to the different spectra measured when the polarised light is directed along different molecular axes.

In the case of a centrosymmetric complex, the irreducible representations are either *gerade* (*g*) or *ungerade* (*u*), depending on whether they are symmetric or asymmetric with respect to inversion across the symmetry centre. The direct product can only yield a totally symmetric representation if the ground and excited states are of a different parity, as the electric dipole vector is a *u*-function. It must be noted that the concept of parity has little significance when discussing non-centrosymmetric complexes, as the symmetry of these complexes leads to a relaxation of the Laporte rule.

For centrosymmetric complexes, the intensities observed for parity-forbidden transitions may be explained by considering the effects of vibronic coupling. As the name suggests, vibronic coupling refers to the coupling of the vibrational and electronic components of the wavefunction. If a molecule absorbs a quantum of vibrational energy corresponding to an *odd* vibration, the centre of symmetry will be lost[13]. The vibrationally excited molecule is thus no longer restricted by the Laporte rule, and can undergo an electronic transition.

As long as a molecule has at least one vibration of a symmetry type that equals

$$\Gamma(\Phi_{g2}) \times \Gamma(r) \times \Gamma(\Phi_{g1}) \qquad (2.6)$$

then the transition is vibronically allowed in r polarisation. Tabulated data are available for all direct products of normal modes for all molecular point groups[14] and this enables the derivation of simple vibronic selection rules for any molecule, aiding the assignment of electronic transitions.

It is therefore necessary to know the symmetry of both the ground and excited state wavefunctions. The ground state of a perfectly octahedral nickel(II) complex belonging to the point group O_h is $^3A_{2g}$. The superscript indicates that it is a triplet state and thus has two unpaired electrons, while the remainder are labels that indicate its symmetry species. However, as the symmetry descends from octahedral (O_h) through D_{4h}, D_{2h} to C_{2v}, the ground state symmetry also changes. Doubly and triply degenerate states, such as E_g and T_{2g} are split into non-degenerate states, as shown in Figure 2.8.

Energy

^3P $^3T_{1g}$ ^3E_g $^3B_{2g}$ $^3B_{3g}$ $^3B_1$ $^3B_2$
$^3B_{1g}$ $^3A_2$
$^3A_{2g}$

^1D $^1T_{2g}$ ^1E_g $^1B_{2g}$ $^1B_{3g}$ $^1A_2$ $^1B_1$
^1A_g
$^1B_{2g}$ $^1B_2$
$^1A_{1g}$ ^1A_g $^1A_1$

$^3T_{1g}$ ^3E_g $^3B_{2g}$ $^3B_{2g}$ $^3A_2$
$^3A_{2g}$ $^3B_1$
$^3B_{1g}$ $^3B_2$

^3F ^1E_g $^1B_{1g}$ $^1B_{1g}$ $^1B_1$

$^1A_{1g}$ ^1A_g $^3A_2$ $^1A_1$

$^3T_{2g}$ $^3B_{2g}$ $^3B_{2g}, ^3A_g$ $^3B_2$
^3E_g $^3B_{3g}$ $^3B_1$

$^3A_{2g}$ $^3B_{1g}$ $^3B_{1g}$ $^3B_1$

Free ion O_h D_{4h} D_{2h} C_{2v}
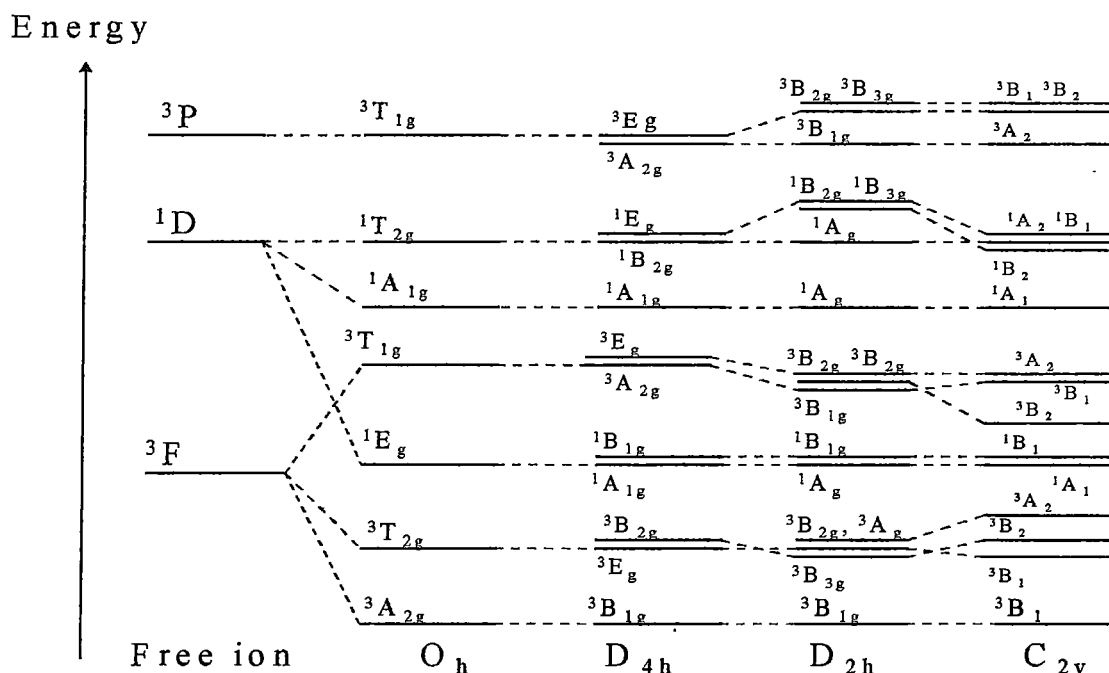
Figure 2.8: The effect of lowering complex symmetry on the symmetry species of a d^8 electron configuration (after Meredith et al.[15]).

Figure 2.8 contains the information required for most of the point groups encountered for the complexes studied. It shows that the ground state is a triplet in each point group, and so transitions to other triplet states are expected to be seen if vibronically allowed. It is also clear that at lower symmetry more transitions are possible due to the splitting of states.

To see these splitting patterns and resolve the peaks, low temperature, single crystal polarised spectra were measured for each complex where possible. The use of single crystals has a number of benefits, the most important of which is that the molecules within a crystal are held in a fixed position. This meant that the orientation of these molecules with regard to the direction of the polarised light's electric vector could be determined, allowing one to study the anisotropy of light absorption with regard to the molecular axes. This was achieved by calculating the projection of the electric vector onto the molecular axes by using the program G-TENSOR[16]. Another benefit is that molecular extinction coefficients may also be calculated from the density and thickness of the crystal.

The measurements were carried out at the lowest temperature possible, which in practice was about 15K. This reduced the number of transitions between the vibrational levels of the ground and excited states, improving resolution and in some cases leading to the observation of vibrational structure superimposed upon the electronic transitions.

To cool a crystal to this temperature, it first had to be mounted on a copper mask. This enabled a good thermal contact to be maintained, while a small hole that was completely overlapped by the crystal allowed the polarised light to shine through the crystal. The experimental arrangement is shown in Figure 2.9.
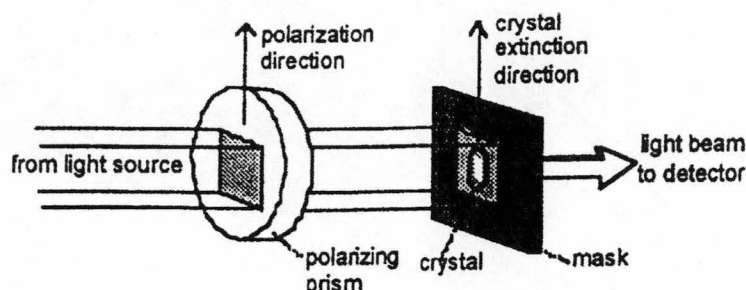
Figure 2.9: The experimental setup used for measuring single crystal spectra.

Although this technique has many benefits, some problems are also encountered that are unique to the measurement of single crystal optical spectra. The crystals used must be of good optical quality so as to obtain a useable spectrum. Twinned crystals are of no use, as it is impossible to obtain a polarised spectrum in this case. Crystal morphology may also be a limitation, as some morphologies create difficulties when trying to affix a crystal to the copper sheet with a face perpendicular to the incident light source. The size of the crystal is also limiting, in that a large crystal may be too optically dense to give a good spectrum, or may be too small for a commercial spectrophotometer to measure. It may be possible to grind a crystal to a desired thickness to overcome the problems faced when using a large crystal, but small crystals require specialised equipment, such as the custom built spectrophotometer of the Krausz group which was specially designed to cope with very small crystals[17].

2.2.2 Charge Transfer and Intraligand Transitions

Generally, charge transfer transitions occur at relatively high energies. However, complexes with empty low lying ligand antibonding orbitals may have low energy metal to ligand charge transfer transitions. In particular, unsaturated ligands with empty π^* antibonding orbitals such as pyridine and pyrazine can permit these transitions, as can the nitrite ligand. This has lead to some incorrect assignments of bands seen in the optical spectra of nickel(II) nitro complexes.

The spectrum of the hexanitro ion $[Ni(NO_2)_6]^{4-}$ has been measured a number of times. This consists of two bands centred at approximately 13 000 and 21 000cm^{-1} in the visible region, which have been assigned by a number of authors as the first two spin-allowed transitions of octahedrally coordinated nickel[18-20]. However, Reinen et al.[20] noted that although the band energy of the first transition varied according to the nature of the counter-cation, a corresponding movement was not seen for the second, higher energy transition. Instead, this band was seen to split into two peaks. It was concluded that the lower energy peak of the two was due to a d-d transition, but the higher energy peak was due to the superposition of a d-d and a charge transfer transition.

The superposition of a charge transfer and d-d transition can also been seen in nickel amine nitro complexes. The spectra of these complexes show two bands at about 12 500 and 20 000cm^{-1}. Low temperature studies indicated that the band at 20 000cm^{-1} had vibrational fine structure, which had an energy progression of approximately 600cm^{-1} [21]. It was doubtful that this was due to a metal-ligand mode, as it was too high in energy, but it was comparable to the progression observed in the spectrum of sodium nitrite. This had been assigned in the $NaNO_2$ spectrum to the v_1 nitrite wagging mode in an excited electronic state, in which an electron had been transferred to the nitrite π^* orbital[21]. Therefore, it was likely that the band in the nickel amine nitro spectrum was mainly due to a metal to ligand charge transfer and not a d-d transition as previously thought. The nature of this charge transfer is still contentious, and this is another area that has been examined in some detail in the present work.

Intraligand transitions have also been observed in the optical spectra of several nickel(II) nitrite complexes, and correlated with the presence of chelating nitrites by Lever[11]. These transitions have also been examined for the complex ions $[Cd(NO_2)_4]^{2-}$ and $[Hg(NO_2)_4]^{2-}$[11].

The measurement of the optical spectra of the complexes studied is essential to interpret the bonding in the complexes using the AOM. This procedure is described in Section 2.3.

2.3 The Angular Overlap Model

A number of theoretical models have been proposed to explain the spectral and magnetic properties of transition metal complexes in terms of their bonding properties. The first of these may be traced back to 1929, when Bethe described the electrostatic model and a group theoretical simplification of its application on the electronic levels of transition metal ions in crystals[22]. This model involved the use of a crystalline field, and so is a forerunner of what is now known as crystal field theory.

Crystal field theory treats a complex as if it consists of a positive metal ion surrounded by negatively charged ions or ligands. Although this theory could predict semi-empirically the number of d-d transitions and their relative energies[23], more sophisticated studies of optical spectra, paramagnetism and electron paramagnetic resonance (EPR) showed it to be lacking in both an experimental and theoretical sense. These shortcomings included:
1) parameters which were not transferable between similar molecules of different geometry, and with little correlation between them
2) parameters such as D_q, D_s and D_t were unable to provide any information about local, individual interactions between each ligand and the central metal ion as they were of a global nature and thus considered the complex as whole, and
3) it was useless for molecules of very low, or no, symmetry[24].

To overcome these problems, a different model was developed. Schäffer and Jørgensen referred to this model as the Angular Overlap Model in 1965[25], but it was similar to one first proposed by Yamatera[26], who applied a combination of the

electrostatic model and a molecular orbital approach to six coordinated orthoaxial ligands. However, Schäffer and Jørgensen, who formulated the more general model so that it could, in principle, apply to an l-electron system with σ-, π-, δ- and φ-bonding[27], worked from a molecular orbital basis, namely the Wolfsberg and Helmholz model[28].

Figure 2.10 shows the formation of molecular orbitals between a d-orbital and a ligand. This results in a lower energy bonding orbital and a higher energy antibonding orbital.

(a)   (b)
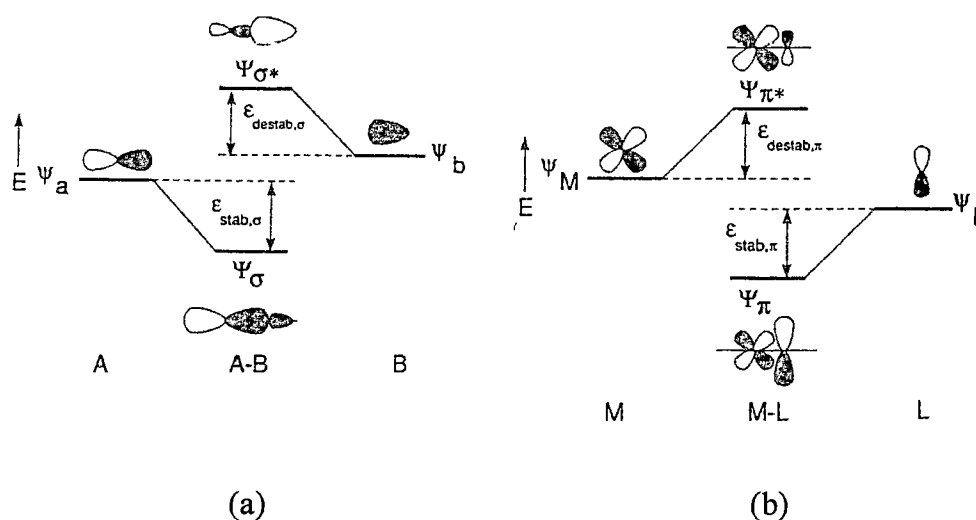
Figure 2.10: Molecular orbital diagrams for the interaction of two orbitals. (a) A p-orbital on A interacts with a σ orbital on B to form bonding and antibonding molecular orbitals. (b) A π interaction between a d_{xz} orbital and a ligand p-orbital (from Richardson[29]).

The energy changes are parameterised as part of the AOM. The model has two basic assumptions:

1. The energy change of a d-orbital when interacting with a ligand orbital depends on the square of the overlap integral, and

2. The energy change of a given d-orbital caused by the coordination of several ligands is the sum of the effects from each.

The second of these assumptions is important as it indicates that it is possible to consider each metal-ligand interaction in isolation. This is a great improvement over previous models in which these local effects were not parameterised.

The general equation for the energy change ΔE is

$$\Delta E = e_\lambda F^2 \qquad (2.7)$$

where F is the angular overlap factor; $e_\lambda = K_\lambda S_\lambda^2$ where K is a constant related to the difference in energy of the metal and ligand orbitals, $\lambda = \pi, \sigma, \delta$ or φ; and S is the overlap integral. The subscripts σ and π refer to the interactions shown in Figure 2.11.
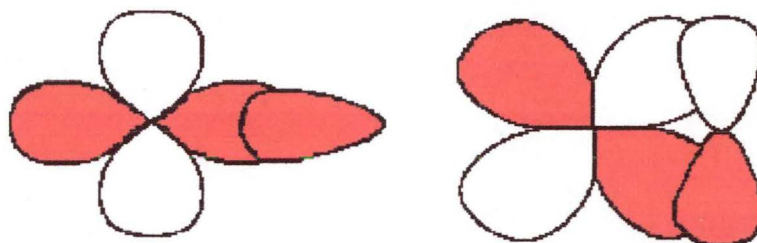

Figure 2.11: σ and π interactions.

An advantage of the AOM is that the parameters do have a "chemical meaning", as e_σ can be thought of as the σ-bonding strength of the ligand, and similarly for e_π. Therefore, a positive parameter value for e_π indicates a π-donor ligand, whereas a negative value indicates a π-acceptor.

The AOM is the basis for the computer program CAMMAG developed by Gerloch and coworkers[30]. This program requires the input of the crystal structure of the complex, and values for the parameters e_σ, $e_{\pi x}$ and $e_{\pi y}$ for each ligand, and the Racah parameters B and C. The output includes predicted energies for d-d transitions, which may be matched to the observed values by iteration.

A problem in applying the AOM is that there is often insufficient experimental data to allow the determination of a unique set of bonding parameters. A limited number of d-d transitions can be seen for a particular complex, and in principle these must be used to fit three parameters for each ligand. The use of single crystal polarised optical spectra of low symmetry complexes helps, but there is usually still insufficient information for the independent assignment of all parameters, especially in mixed ligand complexes. Therefore, a number of approximations must usually be made to derive the AOM parameters.

It is possible to transfer parameters derived for the same ligand from one complex to another. The overlap integral is sensitive to the length of the metal-ligand bond, and so this must be accounted for when transferring parameters in this way. It has been shown previously that a scaling factor of between r^{-5} and r^{-6} may be applied to adjust the parameters to take into account this change in bond length[12]. The relationship

$$e_\lambda(1) = e_\lambda(2)[r(1)/r(2)]^{-6} \qquad (2.8)$$

where $\lambda = \sigma$ or π and r = metal to ligand bondlength can be used to scale the model parameters.

In general, it is sometimes necessary to choose two mutually perpendicular π-parameters, $e_{\pi x}$ and $e_{\pi y}$, to describe the π-bonding of a ligand. A saturated N donor such as NH_3 or ethylenediamine (en) has a negligible covalent π-bonding capability along both x and y, that is, $e_{\pi x} = e_{\pi y} = 0 cm^{-1}$, whereas a pyridine ligand would have a π-interaction only perpendicular to the molecular plane, with $e_\pi = 0 cm^{-1}$. The nitrite ligand has a delocalised π-electron system similar to that of aromatic rings and pyridine, and so may also be assumed to have an in-plane π-interaction equal to zero. Studies of complexes for which sufficient data are available suggest that these approximations are quite good[12].

Further approximations have been used by a number of authors, though as studies progress, a number of these have been disproved. Reference will be made to these in following chapters, where these approximations become relevant in the interpretation of experimental results in this thesis.

Another question of interest is that of "misdirected valence", or "bent bonding". A simplified diagram illustrating this situation is shown in Figure 2.12. Here, the bonding within the ligand is taken to define the direction of the lone pair interacting with the metal d-orbital.
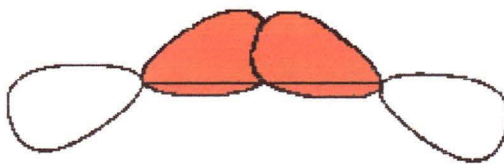

Figure 2.12: A simplified view of a bent bond.

Complexes with the chelating O,O'-nitrito coordination mode are expected to involve bent bonds. The bite angle ($\angle$ O-M-O') in these complexes is approximately 60°, which is much less than the "ideal" octahedral angle of 90° (Figure 2.13).
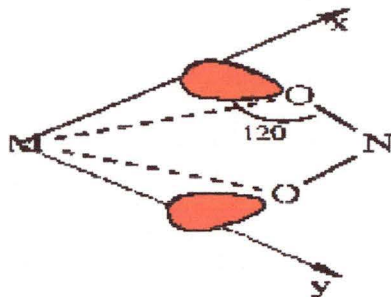

Figure 2.13: Oxygen orbital positions for a chelating nitrite.

In this situation, the ligand lone pair orbitals bend significantly away from the metal-oxygen bond vectors and the σ-orbital overlap is reduced. This lowers the σ interaction and introduces an interaction with the d orbitals of π symmetry. Both σ and π interactions are affected simultaneously, and this is represented by the additional parameter $e_{\sigma\pi}$. As mentioned previously, the model can have a tendency to become over parameterised, and this is often a problem for complexes with bent bonds.

An important aspect of the present work is to test the extension of the AOM to include bent bonding. As the bite angles of chelating O,O'-nitrito ligands are so much less than 90°, it is possible that the effect of bent bonding is quite large for these complexes, making them ideal candidates to study this extension of the AOM.

2.4 *Ab Initio* and Density Functional Theory Calculations

The development of increasingly powerful computers has made it possible to use *ab initio* and density functional theory (DFT) based computer programs to study many chemical properties of main group element compounds. These properties include such things as the molecular geometry, reactivity, spectra and electronic structure. However, the same properties of transition metal atoms and complexes have been much more difficult to calculate. This is due to the presence of unpaired electrons

and the many nearly degenerate electronic states that occur for the compounds of these metals[31].

The self-consistent field (SCF) calculations that are used in *ab initio* methods were originally based on closed shell molecules ie those with no unpaired electrons. This resulted in convergence problems when dealing with transition metal complexes[32]. Another problem was associated with the local nature of d-orbitals. These remain largely associated with the transition metals in their molecular complexes and this caused problems for the molecular orbital theory upon which many of the *ab initio* programs were based. Classical coordination complexes involve the metal in an ionic state (to a good approximation) and this aspect is not treated well in *ab initio* treatments, which solve molecular structures by determining the positions of the nuclei and then assigning electrons based on the *aufbau* principle. Again, the theory upon which the original methods were based had to be modified to take into account this ionic aspect, which was achieved through the use of pertubation theory, coupled cluster theory and configuration interactions[32].

Once these limitations were overcome, it was possible to use *ab initio* methods for transition metal complexes. A large number of papers exist in which these methods have been used to successfully model the geometry of transition metal complexes and transition states for certain catalytic systems[33]. However, one of the few examples which directly relates to the present study is the work of Ciofini and Adamo[34] in which *ab initio* methods have been used to determine a possible transition state structure for the rearrangement of the thermodynamically unstable nitrito isomer $[Co(NH_3)_5ONO]^{2+}$ to the more stable nitro isomer $[Co(NH_3)_5NO_2]^{2+}$. Other studies involving small nitrogen containing molecules have been confined to studies of the metal-ligand interaction of nitrogen dioxide (NO_2) with a metal ion, such as Ag^+ and Cu^+, and an examination of the adsorption of NO_2 onto a metal surface[35-37].

Density functional techniques are becoming more commonly applied to transition metal complexes, especially for calculations involving transition metal clusters, dimers and other complexes that are difficult to deal with using more conventional *ab initio* techniques[31]. Early studies of nitrogen containing molecules were confined to studies involving simple organic molecules such as methyl nitrite, but recent

studies have included an investigation of the ground and excited states of metal-nitrosyl complexes[38,39].

Adamo and Lelj[40,41] used the linkage isomers of $[Co(NH_3)_5NO_2]^{2+}$ as test complexes when studying the incorporation of solvent effects into the framework of density functional theory. This work was carried out in 1994, and while the basis sets used were the best available at the time, these have since been superseded. This was the only previous work carried out which directly related to the use of density functional theory calculations in the study of transition metal nitrite complexes. Density functional theory thus has the potential to provide information on the electronic factors associated with the different types of nitrite coordination. The present work explored this aspect, and particular attention was paid to the comparison with the results from the AOM analyses.

Molecular modelling is a method of studying the influence of non-bonding interactions on geometry. This has the potential to allow the investigation of steric factors on nitrite coordination. This aspect is also investigated in the present research.

2.5 References

1. Jørgensen S.M., *Z. Anorg. Chem.*, **5**, 169-180, (1894).

2. Goodgame D.M.L. and Hitchman M.A., *Inorg. Chem.*, **3**, 1389-1394, (1964).

3. Goodgame D.M.L. and Hitchman M.A., *Inorg. Chem.*, **4**, 721-725, (1965).

4. Nakamoto K., Fujita J. and Murata H., *J. Am. Chem. Soc.*, **80**, 4817-4823, (1958).

5. Chatt J., Duncanson L.A., Gatehouse B.M., Lewis J., Nyholm R.S., Tobe M.L., Todd P.F. and Venazi I.M., *J. Chem. Soc.*, 4073-4828, (1959).

6. Langseth A. and Walles E., *Z. Phys. Chem.*, **27**, 209-218, (1934).

7. Newman A.R., *J. Chem. Phys.*, **20**, 444-448, (1952).

8. Weston R.E. and Brodasky T.F., *J. Chem. Phys.*, **27**, 683-689, (1957).

9. Sidman J.W., *J. Am. Chem. Soc.*, **79**, 2675-2678, (1957).

10. le Postollec M., Mathieu J.P. and Poulet H., *J. Chim. Phys.*, **60**, 1319-1333, (1963).

11. Lever A.B.P., *Inorganic Electronic Spectroscopy (2nd Edition)*, Elsevier Science Publishers, Amsterdam, (1984).

12. Figgis B.N. and Hitchman M.A., *Ligand Field Theory and its Applications*, Wiley-VCH, New York, (2000).

13. Hitchman M.A. and Riley M.J., in *Inorganic Electronic Structure and Spectroscopy*, Volume 1, Chapter 5., Lever A.B.P and Solomon E.I (eds), Wiley, (1999).

14. Wilson E.B., Decius J.C. and Cross P.C., *Molecular Vibrations*, McGraw-Hill Book Company Inc, New York, (1955).

15. Meredith P. and Palmer R.A., *Inorg. Chem.*, **10**, 1049-1056, (1971).

16. McDonald R.G & Stratemeier H.A., GTENSOR, a FORTRAN Program, (1989).

17. Krausz E., *Aust. J. Chem.*, **46(7)**, 1041-1054, (1993).

18. Elliot H., Hathaway B.J. and Slade R.C., *Inorg. Chem.*, **5**, 669-677, (1966).

19. Goodgame D.M.L. and Hitchman M.A., *Inorg. Chem.*, **6**, 813-816, (1967).

20. Reinen D., Friebel C. and Reetz K.P., *J. Solid State Chem.*, **4**, 103-114, (1972).

21. Hitchman M.A. and Rowbottom G.L., *Coord. Chem. Rev.*, **42**, 55-132, (1982).

22. Bethe H., *Ann. Physik. (5)*, **3**, 133-208, (1929).

23. Ballhausen C.J., *J. Chem. Ed.*, **56**, 215-218, (1979).

24. Gerloch M., Harding J.H. & Woolley R.G., *Structure and Bonding*, **46**, 1-46, (1981).

25. Schäffer C.E. and Jørgensen C.K., *Mol. Phys.*, **9**, 401-412, (1965).

26. Yamatera H., *Bull. Chem. Soc. Japan*, **31**, 95-108, (1958).

27. Schäffer C.E., *Pure Appl. Chem.*, **24**, 361-392, (1970).

28. Wolfsberg M., and Helmholz L., *J. Chem. Phys.*, **10(5)**, 837-843, (1952).

29. Richardson D.E., *J. Chem. Education*, **70(5)**, 372-380, (1993).

30. Cruse D.A., Davies J.E., Gerloch M., Harding J.H., Mackey D., McMeeking R.F., CAMMAG, a Fortran Package, University of Cambridge, (1979).

31. Li J., Noodleman L. and Case D.A., in *Inorganic Electronic Structure and Spectroscopy*, Volume 1, Chapter 11, Lever A.B.P and Solomon E.I (eds), Wiley, (1999).

32. Martin C.H. and Zerner M.C., in *Inorganic Electronic Structure and Spectroscopy*, Volume 1, Chapter 10, Lever A.B.P and Solomon E.I (eds), Wiley, (1999).

33. see, for example, Chermette H., *Coord. Chem. Rev.*, **178-180**, 699-721, (1998).

34. Ciofini I. and Adamo C., *J. Phys. Chem. A*, **105**, 1086-1092, (2001).

35. Rodríguez-Santiago L., Branchadell V. and Sodupe M., *J. Chem. Phys.*, **103(22)**, 9738-9743, (1995).

36. Rodríguez-Santiago L., Sodupe M. and Branchadell V., *J. Chem. Phys.*, **105(22)**, 9966-9971, (1996).

37. Lu X., Xu X., Wang N. and Zhang Q., *J. Phys. Chem. A*, **103**, 10969-10974, (1999).

38. Boulet P., Buchs M., Chermette H., Daul C., Gilardoni F., Rogemond F., Schläpfer C.W. and Weber J., *J. Phys. Chem. A.*, **105**, 8991-8998, (2001).

39. Boulet P., Buchs M., Chermette H., Daul C., Furet E., Gilardoni F., Rogemond F., Schläpfer C.W. and Weber J., *J. Phys. Chem. A.*, **105**, 8999-9003, (2001).

40. Adamo C. and Lelj F., *Chem. Phys. Lett.*, **223**, 54-60, (1994).

41. Lelj F. and Adamo C., *Theor. Chim. Acta*, **91**, 199-214, (1995).

CHAPTER 3

Tetranitrite Complexes

The first known tetranitrite complexes were the planar complex ions in $K_2[Pd(NO_2)_4]$ and $K_2[Pt(NO_2)_4]$[1,2]. Further non-planar transition metal tetranitrite complexes have been synthesised by a number of authors, including Lang[3], Fock[4] and Goodgame and Hitchman[5]. Some of the complexes prepared by the latter authors had the formulae $K_2[M(NO_2)_4]$, where M = Hg and Cd, $Cs_2[M(NO_2)_4]$ with M = Zn and Mn, and a series of cobalt, zinc, copper and manganese complexes that were stabilised by the presence of bulky cations.

Upon measuring the infrared spectra of the above non-planar complexes, Goodgame and Hitchman showed that they could be divided into two groups[5]. The infrared spectra of the cobalt, zinc and copper complexes had a strong band at $1165\text{-}1195 \text{cm}^{-1}$, and a medium intensity band at $1370\text{-}1400 \text{cm}^{-1}$. This was suggestive of monodentate nitrito coordination. The infrared spectra of the manganese, mercury and cadmium complexes had a strong, broad band centred in the range from $1210\text{-}1270 \text{cm}^{-1}$. For $Cs_2[Mn(NO_2)_4]$, a weak shoulder was also resolved at 1300cm^{-1}. This indicated an O,O'-nitrito chelating mode, which has since been confirmed for the cadmium and mercury tetranitrites via crystal structure measurements[6-8].

The optical spectrum measured by Goodgame and Hitchman for the cobalt complex (o-cat)[Co(NO$_2$)$_3$], o-cat = [o-xylenebis(triphenylphosphonium)], was interesting in that the band intensities were midway between those expected for an octahedral and a tetrahedral complex. It was very similar to the optical spectrum seen for the cobalt tetranitrate complex [(CH$_3$)$_4$N]$_2$Co(NO$_3$)$_4$[9]. The optical spectrum of the nitrate complex had been explained as being caused by its novel structure in which it has four oxygen-bonded nitrate groups with a very asymmetric chelating mode (Figure 3.1a).
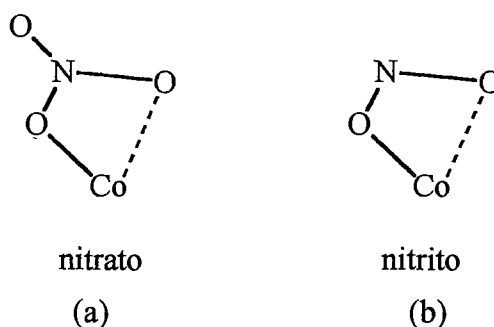
O
N——O
O
Co

N——O
O
Co

nitrato   nitrito

(a)   (b)

Figure 3.1: The asymmetric chelation mode present in (a) $[N(CH_3)_4]_2Co(NO_3)_4$ and (b) thought to be present in $(o\text{-cat})[Co(NO_2)_3]$.

From this spectral evidence, it was thought that the cobalt tetranitrite had a similar coordination mode for the nitrite ligands to the nitrato complex (Figure 3.1b). Furthermore, it was proposed on the basis of infrared spectral evidence that the zinc and copper tetranitrites also had these very asymmetric chelating nitrito groups.

From this work, it is interesting to speculate as to why the coordination mode of the nitrite changes when moving from M = Zn(II), Co(II) and Cu(II) to M = Mn(II), Cd(II) and Hg(II). Given that Zn(II), Cd(II) and Hg(II) are all d^{10} transition metal ions so that effects due to a partly filled d-shell are absent, it is possible that the size of the metal ion is influencing the nitrite coordination mode. Zinc(II) is much smaller that cadmium(II) and mercury(II), and it may be that there is simply not enough space for the nitrite groups to chelate symmetrically. If this is the case, then these complexes provide an example in which steric factors are the dominant influence on the nitrite coordination mode.

The present study has extended previous work in three ways. Raman spectra have been recorded, to characterise the vibrational spectra of the different coordination methods more fully. A study of the crystal structure of $Cs_2[Zn(NO_2)_4]$ was undertaken, to determine whether the ligand coordination conforms to the predictions made on the basis of vibrational spectroscopy. Finally, density functional theory calculations were carried out for the complexes $[M(NO_2)_4]^{2-}$, M = Zn(II), Cd(II) and Hg(II). It was hoped that these would indicate the relative stabilities of the different coordination geometries for the complexes, and also show whether it was possible to move easily from one coordination mode to another. It was found that the stereochemistry of these complexes is more flexible than initially thought, and this is

discussed in terms of the ligand-ligand repulsion model of the geometry of a complex developed by Kepert[10].

3.1 Experimental

Goodgame and Hitchman prepared $Cs_2[Zn(NO_2)_4]$ via a metathetic reaction of zinc(II) nitrate with silver nitrite in methanolic solution[5]. Using this method, it was found in the present work that it was difficult to prevent nitrate from incorporating into the final product, so a modified method was used. Silver nitrite was prepared via the reaction of aqueous silver nitrate with aqueous sodium nitrite. The resulting yellow precipitate (silver nitrite) was filtered from the aqueous solution, dried under vacuum and stored in light proof sample tubes. The freshly prepared silver nitrite (0.0035mol) was added to an aqueous solution of caesium bromide (0.003mol in 5ml water). The precipitate, silver bromide, was filtered from the caesium nitrite solution. This caesium nitrite solution was mixed with an aqueous solution of zinc nitrite, which had been prepared by adding silver nitrite (0.003mol) to a solution of zinc bromide (0.001mol) and removing the silver bromide precipitate by filtration. The combined zinc nitrite and caesium nitrite solutions were left to slowly evaporate at room temperature. Large yellow crystals formed after one week. These were filtered from solution and stored away from light under paraffin oil, as the surfaces appeared to decompose when exposed to air. Crystallographic details will be given in Section 3.3. Multiple elemental analyses were inconsistent with the expected compound and not reproducible, but the Raman spectrum indicated that it was the desired complex, and this was confirmed via crystallographic measurements.

$K_2[Cd(NO_2)_4]$ was prepared via the method of Ohba et al[6]. Again, elemental analyses were inconsistent, but the vibrational spectra indicating that the desired complex had been prepared.

All physical measurements, with the exception of the X-ray crystal structure, were carried out at the Central Science Laboratory, University of Tasmania. Elemental analyses were carried out using a Carlo Erba EA1108 elemental analyser. Inductively-coupled plasma mass spectroscopy (ICP-MS) metal analyses were obtained using an ELEMENT High Resolution ICP-MS (Finnigan-MAT, Bremen,

Germany). Manganese and zinc analyses were carried out at a medium resolution, while cadmium and caesium measurements were at a low resolution. The samples were prepared by dissolution in 1% nitric acid. The internal standard used was indium at a concentration of 100ppb, standards were also prepared for external calibration.

Potassium bromide discs of the complexes were prepared for infrared (IR) measurements. These were measured on a Bruker IFS66 FTIR. The complexes were crushed to a powder for Raman measurements, which were done using a Bruker FRA106 instrument, with a 450mV 105μ Adlas 300 infrared laser.

Prof. A.H. White and Dr B.W. Skelton at the Department of Chemistry, University of Western Australia, carried out X-Ray data collection and structure determination. Full spheres of low temperature CCD area-detector diffractometer data were measured (Bruker AXS instrument, ω-scans, $2\theta_{max} = 58.6°$; monochromatic Mo Kα radiation, $\lambda = 0.71073$ Å; T ca 150K). N_{total} (3163) reflections were merged after 'empirical'/ multiscan absorption correction to N (696) unique ($R_{int} = 0.0259$), N_0 with F > 4σ(F) considered "observed" and used in the full matrix least squares refinement, refining anisotropic thermal parameter forms for non-hydrogen atoms. Conventional residuals, R, R_w (weights: $(\sigma^2(F) + 0.0004F^2)^{-1}$) on $|F|$ are quoted at convergence, neutral atom complex scattering factors being employed within the context of the Xtal 3.0 program system[11]. Atoms are shown with 50% probability amplitude displacement ellipsoids (Figure 3.6).

3.2 Physical Measurements

3.2.1 *Vibrational Spectra*

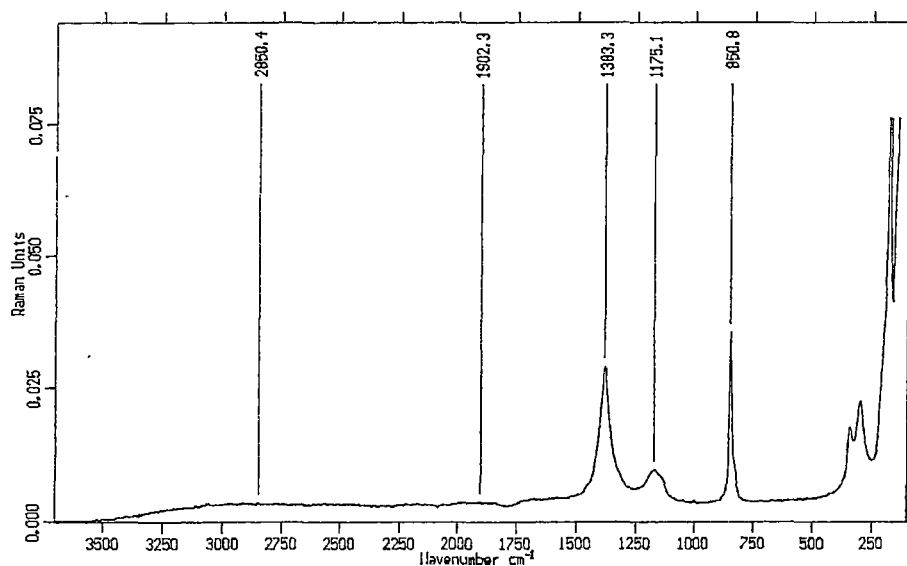The Raman spectrum of $Cs_2[Zn(NO_2)_4]$ is shown in Figure 3.2.

Figure 3.2: The Raman spectrum of $Cs_2[Zn(NO_2)_4]$.

This complex has a very sharp, intense peak at 1 383cm^{-1} which, from its prominence, may be assigned to the symmetric stretching vibration, and a weak, wider peak at 1 175cm^{-1} due to the asymmetric stretch. A sharp wagging peak is also seen at 850cm^{-1}.

The infrared spectrum of $Cs_2[Zn(NO_2)_4]$ has been measured previously by Goodgame and Hitchman[5]. This is reproduced in Figure 3.3. A sharp peak due to the wagging mode occurs at 847cm^{-1}, a strong asymmetric stretch at 1 167cm^{-1} and a less intense symmetric stretch (v_s) of higher energy at 1 381cm^{-1}; as expected, the intensities of the stretches have changed in proportion to each other in the infrared spectrum compared with the Raman (see Chapter 2, Section 2.1).
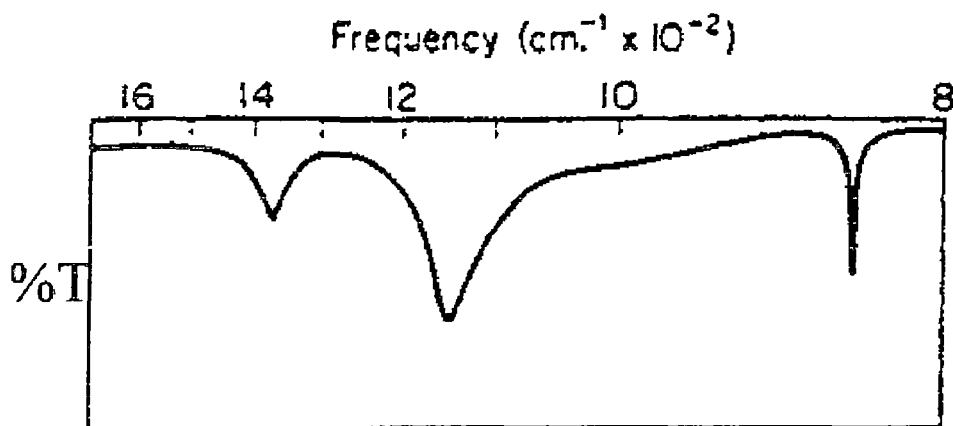

Figure 3.3: The infrared spectrum of $Cs_2[Zn(NO_2)_4]$ (from 5).

The spectra for the present complex are similar to that reported for Zn(N,N-dimethylethylenediamine)$_2$(ONO)$_2$[12]. This complex has $v_2 = 1\ 145$cm^{-1} and $v_3 = 1\ 380$cm^{-1}. However, it is different to that of Zn(N,N'-diethylenediamine)$_2$(ONO)$_2$ where $v_2 = 1\ 220$cm^{-1} and $v_3 = 1\ 380$cm^{-1}. The smaller difference between the energies suggests that the latter complex may have more symmetrically chelating nitrites, which the authors confirm by indicating that the crystal structure of this complex is similar to that of the nickel nitrito complex, which does have symmetrically chelating nitrite ligands[13].

The changes in intensity of v_2 and v_3 when measuring both Raman and IR spectra generally allow the unequivocal assignment of these vibrations for transition metal nitrite complexes. A particularly clear example of this can be seen when examining the spectra of K$_2$[Cd(NO$_2$)$_4$]. The IR of this complex, which is similar to that reported earlier[5], has a very broad peak due to the asymmetric stretch at $1\ 270$cm^{-1} (Figure 3.4). This obscures the weaker peak due to the symmetric stretch in this spectrum.
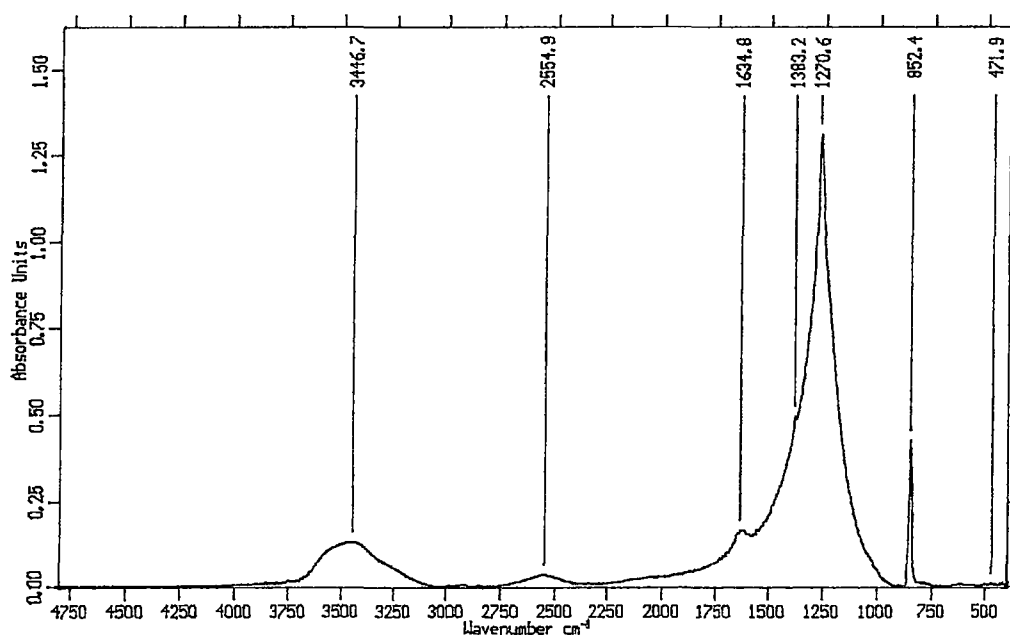

Figure 3.4: The infrared spectrum of K$_2$[Cd(NO$_2$)$_4$].

However, the reduced intensity of the v_2 peak in the Raman spectrum allows for the observation of the peak due to the symmetric stretch. This can be seen in Figure 3.5, and the vibration has an energy of $1\ 316$cm^{-1}. The peak due to the asymmetric

stretch is too weak to be observed in the Raman spectrum, but again, the wagging peak is clearly visible in both the infrared and Raman spectra.
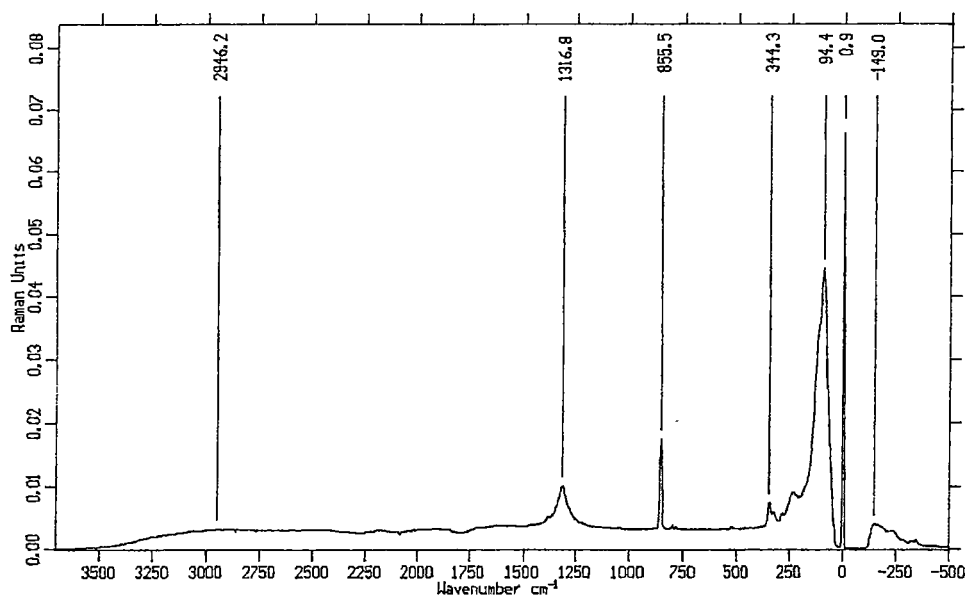

Figure 3.5: The Raman spectrum of $K_2[Cd(NO_2)_4]$.

The Raman spectrum of $K_2[Cd(NO_2)_4]$ has also been measured by Irish and Thorpe[14]. Peaks corresponding to those in Figure 3.5 were found by these authors, but they also saw a number of other peaks. These corresponded to those that would be expected for a nitrate complex, and so it may be possible that the sample that they measured was slightly contaminated by nitrate. The authors themselves commented on this when assigning their Raman spectrum[14], and it was also found to be a problem as samples aged in the present study.

The infrared and Raman spectra of $K_3[Hg(NO_2)_4](NO_3)$ have been measured previously[5,15]. These spectra are consistent with those seen for the Cd(II) complex, with a strong, broad asymmetric stretching peak at $1258cm^{-1}$ obscuring the peak due to the symmetric stretch in the infrared spectrum, which may be assigned an energy of $1308cm^{-1}$ from the Raman spectrum.

3.2.2 Crystal Structure of Cs₂Zn(NO₂)₄

A summary of the important crystal structure data of $Cs_2[Zn(NO_2)_4]$ is given in Table 3.1.

Molecular formula	$Cs_2N_4O_8Zn$
Molecular weight	515.20
Crystal system	Orthorhombic
Space group	Fddd
A	6.205(1)Å
B	13.089(3)Å
C	26.214(6)Å
V	2129Å^3
Z	8
F(000)	1856
T	150K
R_{int}	0.0259
R	0.021
R_w	0.034
Crystal dimensions	0.15 x 0.12 x 0.10mm

Table 3.1: Summary of crystallographic data for $Cs_2[Zn(NO_2)_4]$.

An ORTEP[16] diagram of the complex is shown in Figure 3.6. Table 3.2 summarises the important bond lengths and bond angles. A diagram of the unit cell is shown in Figure 3.7 overleaf. Further crystallographic data may be found in Appendix A.
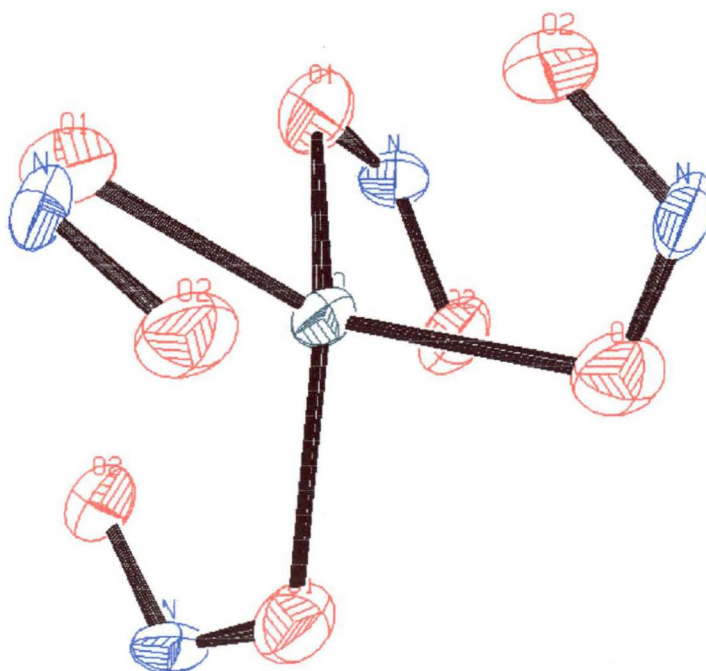

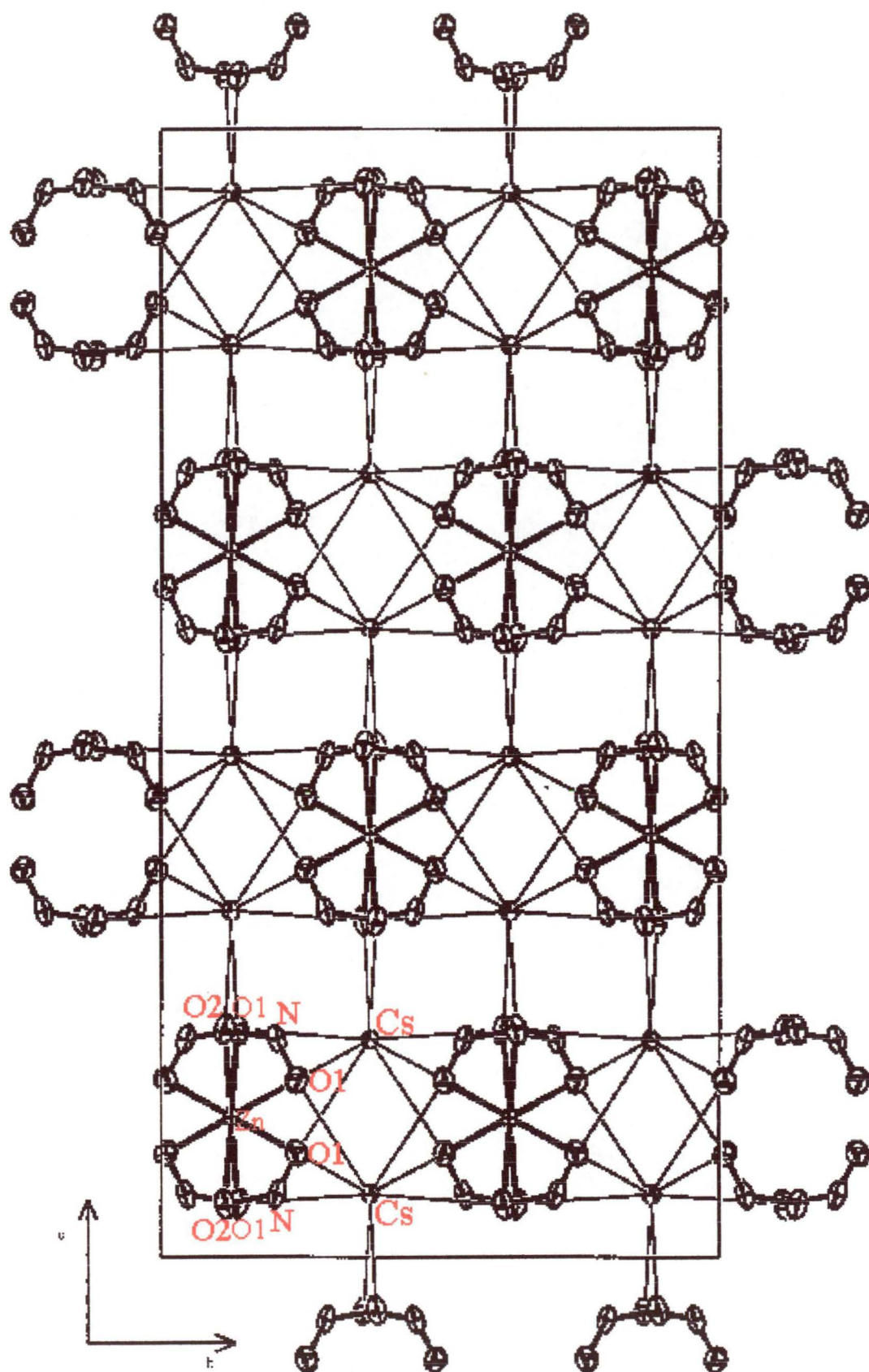**Figure 3.6**: The molecular geometry of the $[Zn(NO_2)_4]^{2-}$ ion in $Cs_2[Zn(NO_2)_4]$.

Figure 3.7: The unit cell contents of $Cs_2[Zn(NO_2)_4]$.

	BOND LENGTH (Å)	BOND ANGLE (°)
Zn-O(1)	2.080	
-O(2)	2.516	
N-O(1)	1.211	
N-O(2)	1.251	
O(1)-Zn-O(2)		52.8
Zn-O(1)-N(1)		107.3
O(1)-N(1)-O(2)		115.4

Table 3.2: $Cs_2[Zn(NO_2)_4]$ bond lengths and angles.

The large difference in the zinc-oxygen distances may be seen clearly in Figure 3.6. The metal-oxygen bond lengths are 2.08Å and 2.516Å, which may be contrasted with the much more equivalent bonds in, for example, $Ca[Cd(NO_2)_4]$, which are 2.313Å and 2.532Å.

It is possible to think of this coordination as either highly asymmetric chelation, or as *cis*-monodentate coordination (see Chapter 1, Figure 1.3), but it is really mid-way between these two extremes. The Zn-O-N angle for a sp^2 hybridised bond would be about 120°, and this is seen for the monodentate complex, Zn(N,N-dimethylethylenediamine)$_2$(ONO)$_2$, with a Zn-O-N angle of 118.0°[12]. This angle would decrease to 90° for a symmetrically chelating nitrite (because the sum of the angles of a quadrilateral equals 360°). For this complex, $\angle$Zn-O(1)-N(1) is 107.3°, which is slightly closer to that for the monodentate nitrite coordination mode.

However, if the bonding interaction of the shorter Zn-O(1) bond is taken as 100%, the interaction of the longer bond, Zn-O(2) can be estimated as approximately one third of that of the shorter bond. This takes the interaction to be proportional to about the inverse fifth or sixth power of the bond distance, as assumed in the angular overlap model (see Chapter 2, Section 2.3)[17]. Then:

$$(r1/r2)^{-5}$$

where r1 = Zn-O(2) and r2 = Zn-O(1). This interaction is too large to ignore, meaning that the coordination mode cannot be thought of as purely monodentate, but rather "in between" a highly asymmetric chelation and monodentate coordination mode.

3.3 Comparison of the Structure of [Zn(NO$_2$)$_4$]$^{2-}$ with those of [Cd(NO$_2$)$_4$]$^{2-}$ and [Hg(NO$_2$)$_4$]$^{2-}$

Important bond lengths and angles for [Zn(NO$_2$)$_4$]$^{2-}$ are compared with those of [Hg(NO$_2$)$_4$]$^{2-}$ and [Cd(NO$_2$)$_4$]$^{2-}$ with various counterions in Tables 3.3 and 3.4. Omitted from this table are the values for the complex Sr[Cd(NO$_2$)$_4$].4H$_2$O, in which the [Cd(NO$_2$)$_4$]$^{2-}$ ion has an essentially identical structure to that in Ca[Cd(NO$_2$)$_4$][6].

BOND	K$_2$Cd(NO$_2$)$_4$	MgCd(NO$_2$)$_4$	CaCd(NO$_2$)$_4$	K$_3$[Hg(NO$_2$)$_4$]NO$_3$	Cs$_2$Zn(NO$_2$)$_4$
M-O11	2.377	2.362	2.313	2.494	2.080
M-O12	2.525	2.542	2.532	2.414	2.516
M-O21	2.414	2.366	2.381	2.548	-
M-O22	2.414	2.482	2.439	2.566	-
M-O31	2.435	-	-	2.394	-
N1-O11	1.234	1.242	1.279	1.231	1.211
N1-O12	1.239	1.269	1.248	1.248	1.251
N2-O21	1.246	1.250	1.281	1.235	-
N2-O22	1.246	1.266	1.252	1 235	-
N3-O31	1.254	-	-	1.250	-
N3-O32	1.254	-	-	1.232	-

Table 3.3: Important bond lengths (Å) for [Cd(NO$_2$)$_4$]$^{2-}$, [Hg(NO$_2$)$_4$]$^{2-}$ and [Zn(NO$_2$)$_4$]$^{2-}$ in various lattices[6-8].

ANGLE	K$_2$Cd(NO$_2$)$_4$	MgCd(NO$_2$)$_4$	CaCd(NO$_2$)$_4$	[Hg(NO$_2$)$_4$]$^{2-}$	Cs$_2$Zn(NO$_2$)$_4$
M-O11-N1	101.6	103.4	102.6	96.0	107.3
M-O12-N1	94.1	94.0	92.8	99.5	84.5
O11-N1-O12	114.2	112.3	113.2	114.3	115.4
O11-M-O12	50.0	50.8	51.4	50.2	52.8
M-O21-N2	98 0	101.1	98.1	98.5	-
M-O22-N2	98.0	94.5	96.1	98.5	-
O21-N2-O22	112.8	113.2	113.6	114.7	-
O21-M-O22	50.9	51.2	52.1	48.2	-
M-O31-N3	98.1	-	-	101 7	-
M-O32-N3	98.1	-	-	93 7	-
O32-N3-O33	112.7	-	-	114.8	-
O32-M-O33	50 8	-	-	49.7	-

Table 3.4: Important bond angles (°) for [Cd(NO$_2$)$_4$]$^{2-}$, [Hg(NO$_2$)$_4$]$^{2-}$ and [Zn(NO$_2$)$_4$]$^{2-}$ in various lattices[6-8].

A comparison of the metal-oxygen bond lengths for the $[Cd(NO_2)_4]^{2-}$ and $[Hg(NO_2)_4]^{2-}$ ions (Table 3.3) with those of the $[Zn(NO_2)_4]^{2-}$ ion shows that the difference in bond length for each pair of metal-oxygen bonds in the nitrite ligands is far lower for the Cd(II) and Hg(II) complexes than the Zn(II) complex. This means that the chelation in these is much more symmetric than that of the Zn(II) nitrite ligands. Furthermore, a comparison of the two M-O-N bond angles for each nitrite of the complexes reveals that there is less difference between these values for the $[Cd(NO_2)_4]^{2-}$ and $[Hg(NO_2)_4]^{2-}$ than $[Zn(NO_2)_4]^{2-}$. Moreover, they are closer to 90°, which is the value anticipated for a symmetric chelation, than the angle of 107.3° for $[Zn(NO_2)_4]^{2-}$, which, as previously discussed in Section 3.2, lies between a highly asymmetric chelation and monodentate coordination mode.

The N-O bond lengths of the $[Zn(NO_2)_4]^{2-}$ ion are anomalous compared with those of other monodentate nitrito complexes[17]. One would expect the N-O bond involving the oxygen bound to the Zn(II) ion would be longer than the other nitrite N-O bond. This arrangement would be consistent with an increase in the double bond character of the shorter N-O bond. In the case of $[Zn(NO_2)_4]^{2-}$, the reverse is seen. However, for the $[Cd(NO_2)_4]^{2-}$ and $[Hg(NO_2)_4]^{2-}$ ions, these bond lengths are similar, which would be expected for the symmetric chelation modes adopted by the nitrite ligands in these examples.

3.3.1 *Disposition of the Nitrite Groups About the Metal*

In describing the geometry of the $[Zn(NO_2)_4]^{2-}$ ion, and the analogous Cd(II) and Hg(II) complexes, it might be thought that if the nitrite ions are considered as a single entity, then these would adopt a tetrahedral geometry about the central metal. However, a comparison of the bond angles between the ligands, the angles $\angle$N(1)-M-N(2), reveals that this is not the case. As seen in Table 3.5, these angles differ markedly from the tetrahedral angle, 109.5°. Figure 3.8 illustrates this, with the complexes being oriented so that the shortest bond is to the right of the metal, and the plane of this nitrite is parallel to the plane of the page.
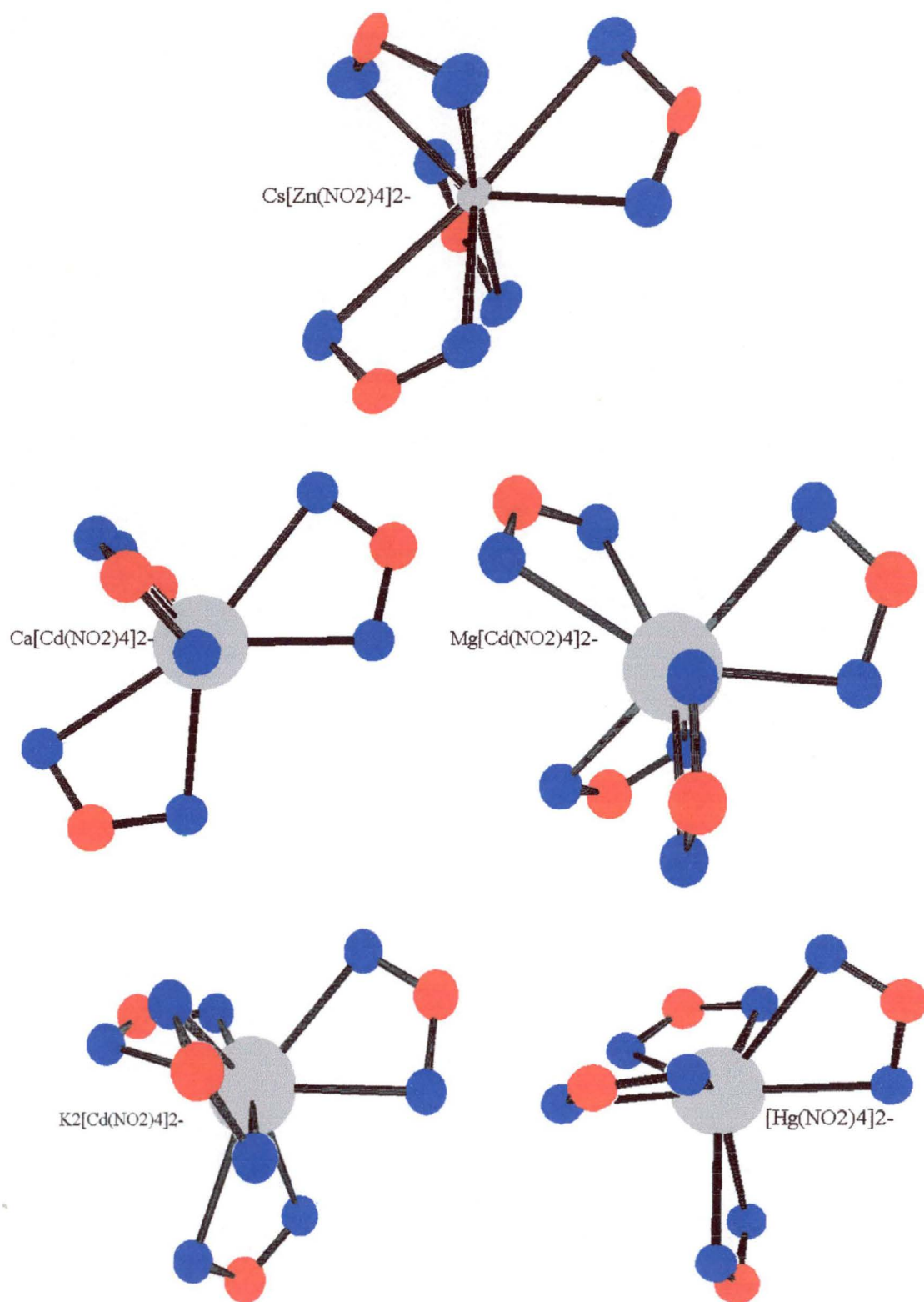
Figure 3.8: A comparison of the geometry of the complexes $K_2[Cd(NO_2)_4]$, $Mg[Cd(NO_2)_4]$ and $Ca[Cd(NO_2)_4]$ with $[Zn(NO_2)_4]^{2-}$ and $[Hg(NO_2)_4]^{2-}$.

ANGLE	$K_2Cd(NO_2)_4$	$MgCd(NO_2)_4$	$CaCd(NO_2)_4$	$Cs_2Zn(NO_2)_4$	$K_3[Hg(NO_2)_4]NO_3$
N1-M-N1'	94 57	90.79	146.81	96.76	102.37
N1-M-N2	115 89	123.16	96.90	101.19	114.68
N1-M-N3	121.02	116.35	95 93	133.75	102.37
N1'-M-N2	115.89	116.35	95.93	133.86	104.54
N1'-M-N3	121.02	123.16	96.90	100.88	128.86
N2-M-N3	90.49	90.26	133.94	96.91	104.54

Table 3.5: The $\angle$N-M-N bond angles in $K_2[Cd(NO_2)_4]$, $Mg[Cd(NO_2)_4]$, $Ca[Cd(NO_2)_4]$, $Cs_2[Zn(NO_2)_4]$ and $K_3[Hg(NO_2)_4](NO_3)$[6-8].

There has been considerable interest in the way in which a set of ligands arranges itself about a metal ion in forming a complex. A model developed by Kepert, described briefly below, considers the likely geometry of any complex if this is dominated by ligand-ligand repulsions[10].

It is possible to imagine the stereochemical arrangement of ligands (or atoms) around a central atom as a polyhedron, with atoms at each vertex to minimise repulsion. The octahedral arrangement in a six-coordinate complex and the tetrahedral arrangement of a four-coordinate complex are two such examples. Eight coordinate complexes may be treated in a similar manner, giving a number of theoretical polyhedral arrangements. When taking repulsion into account, the two most stable structures, are the dodecahedron and the square antiprism (Figure 3.9)[19].
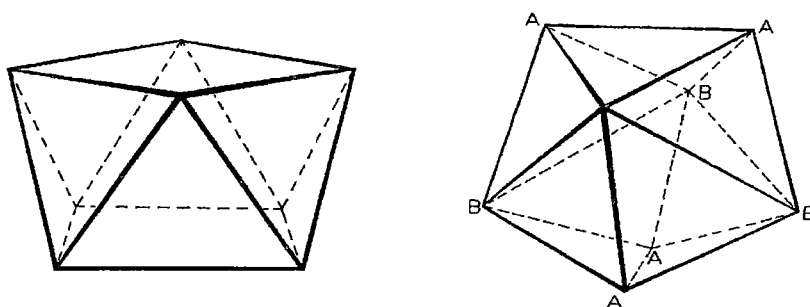

Figure 3.9: The square antiprism (D_4) and dodecahedron (D_{2d}).

For complexes with bidentate ligands, it has been suggested that the normalised bite angle, b, should provide a guide to the stereochemistry of the complex[10]. The

normalised bite angle can be calculated by determining the average bite angle for the complex and then using the average bite angle in the formula

$$b = 2\sin(\text{average bite angle}/2).$$

Complexes with normalised bite angles of less than ~1.1 are expected to have the D_{2d} dodecahedral stereochemistry. As b increases, the stereochemistry distorts and is progressively replaced by intermediate stereochemistries until the D_4 square antiprism is reached (b~1.28). The b values for the present complexes are listed in Table 3.6.

COMPLEX	b
$K_2[Cd(NO_2)_4]$	0.86
$Mg[Cd(NO_2)_4]$	0.88
$Ca[Cd(NO_2)_4]$	0.91
$Cs_2[Zn(NO_2)_4]$	0.89
$K_3[Hg(NO_2)_4]NO_3$	0.82

Table 3.6: Normalised bite angles for the tetranitrite complexes.

From this information, D_{2d} dodecahedral stereochemistries would be expected for the present complexes. This is clearly the case for the $[Cd(NO_2)_4]^{2-}$ ion when the counterion is Ca^{2+} (Figure 3.10).
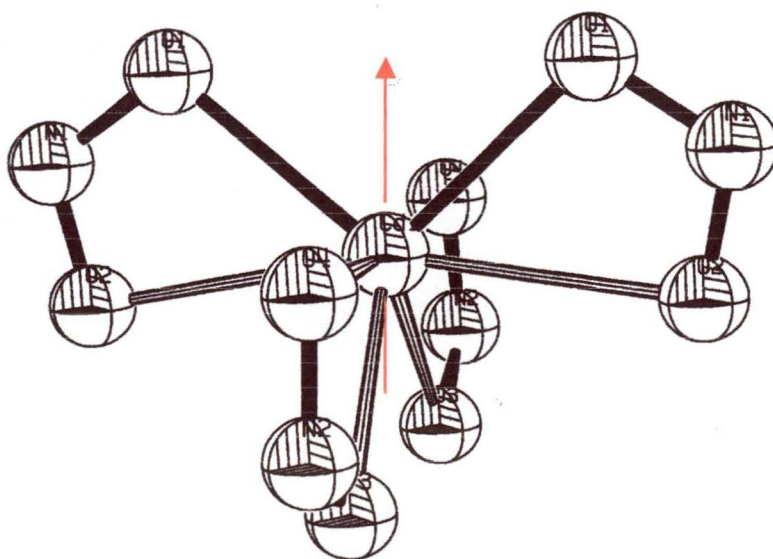

Figure 3.10: The stereochemistry of the $[Cd(NO_2)_4]^{2-}$ ion in $Ca[Cd(NO_2)_4]$.

One of the C_2 axes for this complex is marked in red in Figure 3.10. There are two C_2 axes perpendicular to this axis, and two σ_d mirror planes that bisect the angle between the two C_2 axes that are perpendicular to the marked C_2 axis. This arrangement is of D_{2d} symmetry, and can be represented by the polyhedron shown in Figure 3.11.
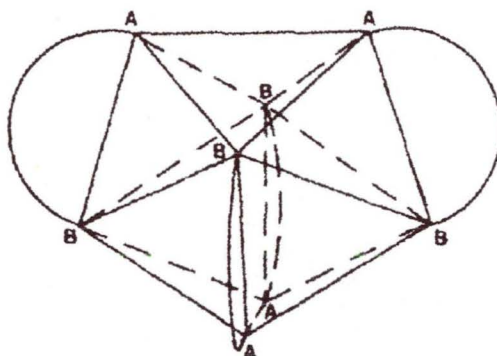

Figure 3.11: The D_{2d} dodecahedral arrangement of a [M(bidentate)$_4$] complex with two distinct types of vertices, labelled A and B.

However, when the bond lengths become inequivalent, a lower symmetry stereochemistry results. The asymmetry of the zinc-oxygen bonds of $[Zn(NO_2)_4]^{2-}$ means that the symmetry of this complex lowers from D_{2d} to D_2, as the mirror planes of the D_{2d} structure no longer exist (Figure 3.12). One $Zn(NO_2)$ plane is also tilted at an angle of 11° with respect to the other, which also lowers the symmetry of the complex. Also shown on this diagram are two C_2 axes, with the third directed into the page.
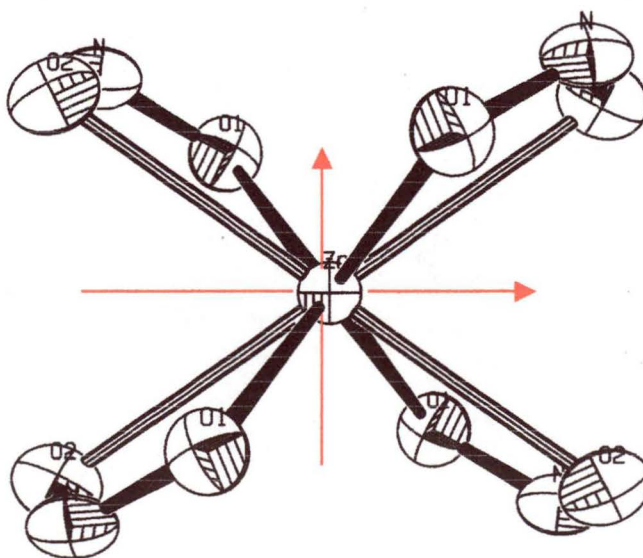

Figure 3.12: The stereochemistry of the $[Zn(NO_2)_4]^{2-}$ ion in $Cs_2[Zn(NO_2)_4]$.

The symmetry of the $[Cd(NO_2)_4]^{2-}$ ion in the compound $K_2[Cd(NO_2)_4]$ is also lower than that seen for the ion in $Ca[Cd(NO_2)_4]$, as two C_2 axes are no longer present. In this case the point group is C_{2v} as two mirror planes are present for this geometry (Figure 3.13). The C_2 axis is in one of the mirror planes, with the other perpendicular to this plane.
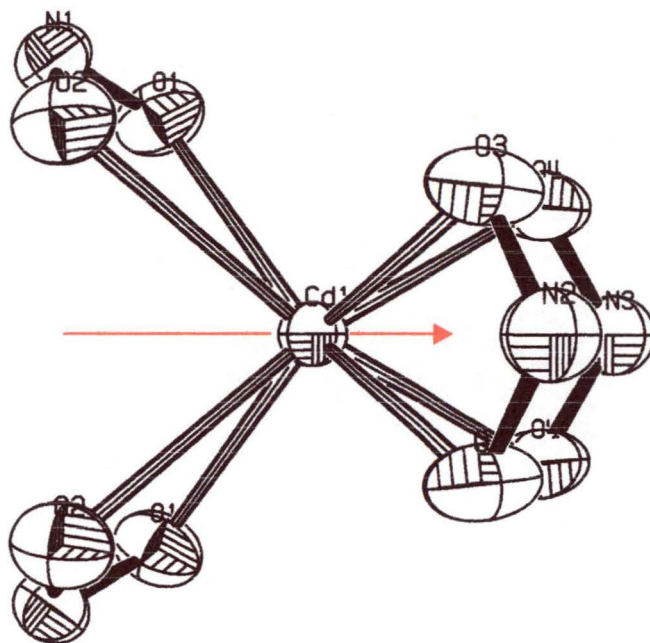
Figure 3.13: The stereochemistry of the $[Cd(NO_2)_4]^{2-}$ ion in $K_2[Cd(NO_2)_4]$.

This structure is a little unusual, as it is best modelled by a cube with bidentate groups (Figure 3.14). The only prior example of this is uranium tetrabipyridine, $[U(bipy)_4]$[10].
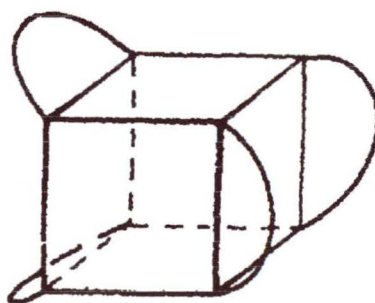
Figure 3.14: The cubic structure seen for $[U(bipy)_4]$ and $[Cd(NO_2)_4]^{2-}$ in the complex $K_2[Cd(NO_2)_4]$.

The disposition of the nitrite ligands about the Cd^{2+} ion and the inequivalence of bond lengths in the complex $Mg[Cd(NO_2)_4]$ result in a lowering of symmetry to C_2.

In this case, no mirror planes are seen, and there is only one C_2 axis, which is marked on Figure 3.15.
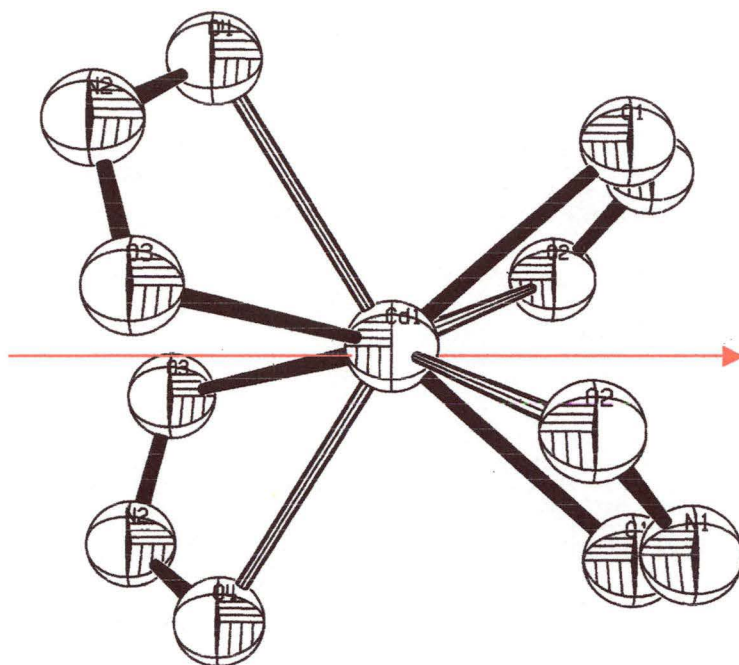
Figure 3.15: The geometry of the $[Cd(NO_2)_4]^{2-}$ ion in $Mg[Cd(NO_2)_4]$.

The geometry of the $[Hg(NO_2)_4]^{2-}$ ion in $K_3[Hg(NO_2)_4](NO_3)$ also deviates significantly from D_{2d} symmetry (Figure 3.16).
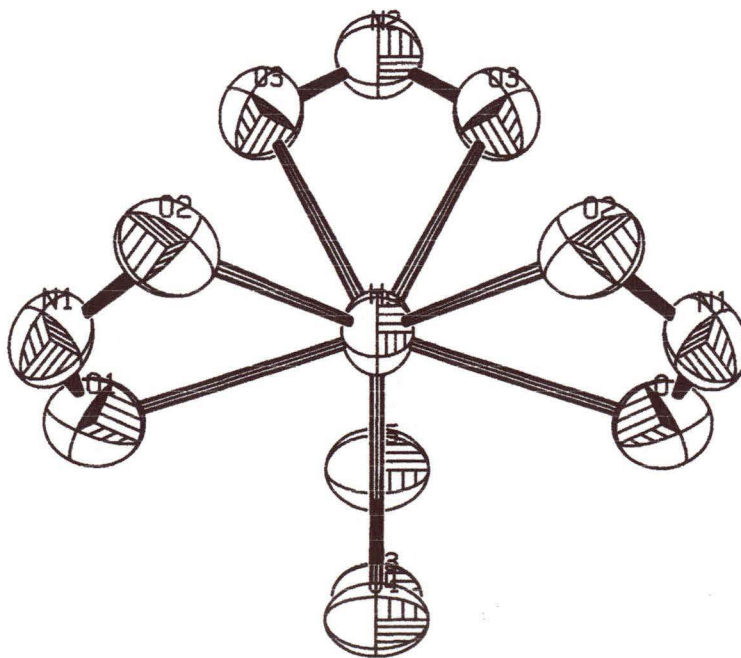
Figure 3.16: The geometry of the $[Hg(NO_2)_4]^{2-}$ ion in $K_3[Hg(NO_2)_4](NO_3)$.

Kepert has suggested that this last complex has a particularly unusual stereochemistry[10]. He describes it as a greatly distorted square antiprism, with one bidentate ligand lying on a mirror plane spanning a diagonal of the square face (Figure 3.17).
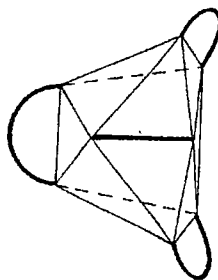

Figure 3.17: The unusual stereochemistry of $K_3[Hg(NO_2)_4](NO_3)$[10].

In summary, the $[Zn(NO_2)_4]^{2-}$ ion in $Cs_2[Zn(NO_2)_4]$ adopts the D_{2d} point group expected for four equivalent bidentate ligands bound to a metal, except that the marked difference in Zn-O bond lengths, accompanied by a slight tilting of the planes of the nitrite ligands, lowers the symmetry from D_{2d} to D_2. The $[Cd(NO_2)_4]^{2-}$ ion adopts the expected D_{2d} stereochemistry in the compounds $Ca[Cd(NO_2)_4]$ and $Sr[Cd(NO_2)_4]$, and different geometries in $K_2[Cd(NO_2)_4]$ and $Mg[Cd(NO_2)_4]$, while the $[Hg(NO_2)_4]^{2-}$ ion in $K_3[Hg(NO_2)_4](NO_3)$ adopts a highly asymmetric geometry. These different geometries are relevant to the results of the density functional theory calculations carried out for these complexes, described below.

3.4 Density Functional Theory (DFT) Calculations

DFT methods have become increasingly popular for calculations involving transition metal complexes[20]. These calculations have been used to give good descriptions of the ground electronic state and other properties such as molecular geometry and the reactivity of the complexes[20-23]. In the present work, these were carried out to investigate the relative stabilities of the complex ions. The geometries of the complex ions were first optimised using as starting points the geometry observed in the crystal structure, and then this was repeated with Zn(II) and Hg(II) replacing Cd(II) in each $[Cd(NO_2)_4]^{2-}$ structure, and Cd(II) replacing the Zn(II) and Hg(II) ions in these structures.

3.4.1 *Computational details*

The calculations were performed on Linux/Pentium II based computers using the density functional program ADF99[24-27]. The Local Density Approximation of Vosko, Wilk and Nusair[28] was used, as was the gradient correction of Becke[29] and the correlation term of Perdew[30]. For the main group atoms N and O, triple-ξ basis functions were employed, and the 1s cores on the N and O were frozen. For the Zn atom, triple-ξ functions were used with a 3p frozen core. For Cd and Hg, triple-ξ functions were used with a 3p frozen core, and relativistic effects were included using the ZORA approach[31]. Geometry optimisations were performed using the algorithm of Versluis and Ziegler[25].

3.4.2 *Geometry of the $[Zn(NO_2)_4]^{2-}$ ion*

The optimised structures of $[Zn(NO_2)_4]^{2-}$ based on the geometries of the complexes in $Cs_2[Zn(NO_2)_4]$, $Ca[Cd(NO_2)_4]$ as the most representative Cd(II) compound, and $K_3[Hg(NO_2)_4](NO_3)$ as a starting point are compared with the observed structure in Figure 3.18. Table 3.7 lists the calculated and measured bond lengths in these species, and Table 3.8 lists the calculated and measured bond angles.
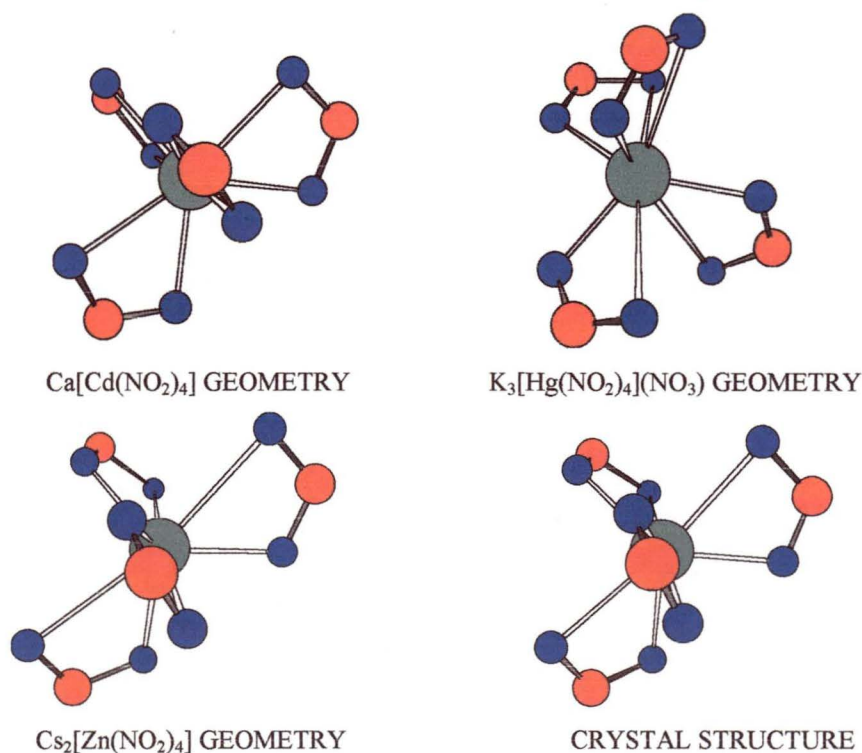

Ca[Cd(NO₂)₄] GEOMETRY   K₃[Hg(NO₂)₄](NO₃) GEOMETRY

Cs₂[Zn(NO₂)₄] GEOMETRY   CRYSTAL STRUCTURE

Figure 3.18: Calculated and observed geometries of $[Zn(NO_2)_4]^{2-}$ from different starting geometries.

BOND	$Cs_2Zn(NO_2)_4$	$CaCd(NO_2)_4$	$K_2Cd(NO_2)_4$	$[Hg(NO_2)_4]^{2-}$	EXPT
Zn-O11	2.130	2.238	2.397	2.106	2.080
-O12	2.766	2.509	2.408	2.621	2.516
-O21	2.125	2.238	2.352	2.111	2.080
-O22	2.773	2.510	2.353	2.970	2.516
-O31	2.125	2.303	2.274	2.762	2.080
-O32	2.782	2.401	2.517	2.147	2.516
-O41	2.127	2.302	2.274	2.970	2.080
-O42	2.781	2.402	2.517	2.145	2.516
O11-N1	1.301	1.284	1.276	1.298	1.211
O12-N1	1.254	1.267	1.275	1.255	1.250
O21-N2	1.301	1.284	1.275	1.308	1.211
O22-N2	1.254	1.267	1.275	1.247	1.250
O31-N3	1.301	1.277	1.285	1.256	1.211
O32-N3	1.254	1.272	1.265	1.308	1.250
O41-N4	1.301	1.277	1.285	1.254	1.211
O42-N4	1.254	1.272	1.265	1.303	1.250

Table 3.7: Comparison of calculated and experimental bond lengths (Å) for $[Zn(NO_2)_4]^{2-}$ from different starting geometries.

ANGLE	Cs₂Zn(NO₂)₄	CaCd(NO₂)₄	K₂Cd(NO₂)₄	[Hg(NO₂)₄]²⁻	EXPT
Zn-O11-N1	112.0	102.5	97.0	107.9	107.3
Zn-O12-N1	82.4	90.0	96.1	84.4	84.50
O11-N1-O12	115.3	114.3	95.9	114.9	115.0
O11-Zn-O12	50.3	53.3	52.9	52.8	52.8
Zn-O21-N2	112.3	102.4	114.3	119.1	-
Zn-O22-N2	82.1	89.8	95.9	78.1	-
O21-N2-O22	115.4	114.4	114.2	115.9	-
O21-Zn-O22	50.2	53.3	54.1	46.8	-
Zn-O31-N3	112.5	98.2	101.9	82.9	-
Zn-O32-N3	81.9	93.6	90.8	111.6	-
O31-N3-O32	115.5	114.1	114.4	115.2	-
O31-Zn-O32	50.1	54.0	52.9	50.2	-
Zn-O41-N4	112.5	98.2	101.9	79.0	-
Zn-O42-N4	82.0	93.7	90.8	117.9	-
O41-N4-O42	115.5	114.0	114.4	116.0	-
O41-Zn-O42	50.1	54.0	52.9	47.0	-

Table 3.8: Comparison of calculated and experimental bond angles (°) for
[Zn(NO₂)₄]²⁻ from different starting geometries.

Reasonable agreement was reached between the calculated and measured values when the starting point of the calculation was the geometry observed for the Zn(II) complex. Generally, the calculated bond lengths are longer than the measured values. This was seen for many calculations, and can be attributed to the introduction of the generalised gradient approximation in the calculations. In particular, the high asymmetry in the Zn-O distances for each nitrite ligand is maintained in the optimum calculated structure.

When the starting point of the calculation for the [Zn(NO₂)₄]²⁻ ion was the geometry observed for the [Cd(NO₂)₄]²⁻ and [Hg(NO₂)₄]²⁻ ions, the optimum geometry differed from that observed experimentally in Cs₂[Zn(NO₂)₄]. The symmetry of the Hg(II) and Cd(II) geometries was maintained, though some of the bonds have lengthened to produce an asymmetric chelation mode. The disposition of the nitrite ligands around

the zinc ion was maintained for the $[Cd(NO_2)_4]^{2-}$ molecular geometry, but this changed considerably for $[Zn(NO_2)_4]^{2-}$ placed in the $[Hg(NO_2)_4]^{2-}$ geometry (Figure 3.19).

$[Zn(NO_2)_4]^{2-}$ $Cs_2[Zn(NO_2)_4]$ CRYSTAL STRUCTURE

$[Zn(NO_2)_4]^{2-}$ $Ca[Cd(NO_2)_4]$ CRYSTAL STRUCTURE

$[Zn(NO_2)_4]^{2-}$ $K_3[Hg(NO_2)_4](NO_3)$ CRYSTAL STRUCTURE

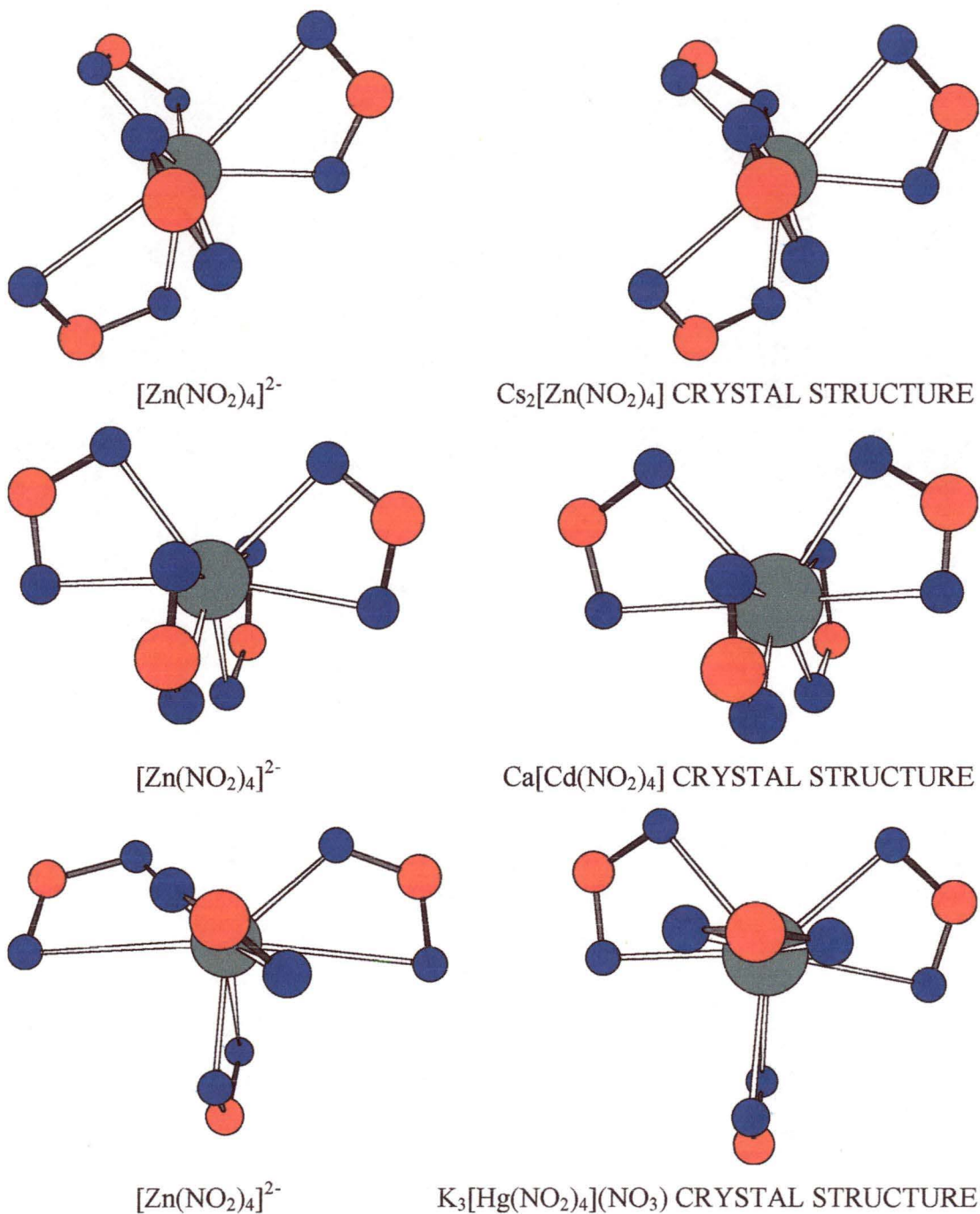**Figure 3.19**: A comparison of the calculated geometries of $[Zn(NO_2)_4]^{2-}$ from the starting geometries of $[Cd(NO_2)_4]^{2-}$ and $[Hg(NO_2)_4]^{2-}$ with the observed geometries of these complexes, and with that of $Cs_2[Zn(NO_2)_4]$.

The fact that the optimum geometry calculated for the $[Zn(NO_2)_4]^{2-}$ differs depending on the starting geometry suggests that these structures lie on a shallow potential energy curve. A comparison of the energies calculated for these complexes (Table 3.9) shows that the greatest energy difference between these structures was relatively small (0.286eV), and this is the reason that it was not possible to move from the local minima to the global minimum when allowing geometries to optimise. The values in this table indicate that, as expected, the lowest energy was associated with the experimentally observed geometry. Also included in Table 3.9 is the energy calculated when using the geometry of the $[Cd(NO_2)_4]^{2-}$ in the Mg^{2+} lattice; the results from these calculations are listed in full in Appendix B.

STARTING GEOMETRY	ENERGY (eV)
$Cs_2[Zn(NO_2)_4]$	-79.745
$Ca[Cd(NO_2)_4]$	-79.668
$Mg[Cd(NO_2)_4]$	-79.721
$K_2[Cd(NO_2)_4]$	-79.459
$K_3[Hg(NO_2)_4](NO_3)$	-79.683

Table 3.9: The energy of the optimum structures of $[Zn(NO_2)_4]^{2-}$ from the listed starting geometries.

3.4.3 Geometry of the $[Cd(NO_2)_4]^{2-}$ ion

The optimised structures of $[Cd(NO_2)_4]^{2-}$ based on the geometries of the complexes in $Ca[Cd(NO_2)_4]$, $Cs_2[Zn(NO_2)_4]$ and $K_3[Hg(NO_2)_4](NO_3)$ as a starting point are compared with the observed structure in Figure 3.20. Table 3.10 lists the calculated and measured bond lengths in these species, and Table 3.11 lists the calculated and measured bond angles.
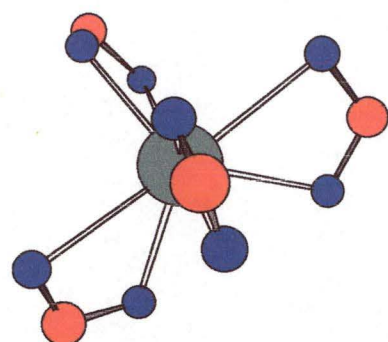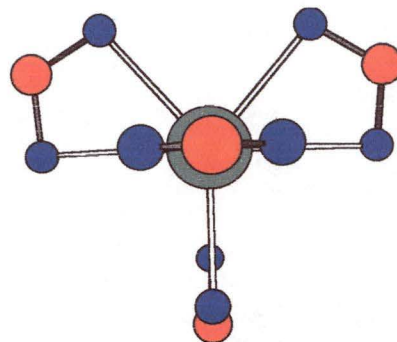
Cs₂[Zn(NO₂)₄] GEOMETRY   K₃[Hg(NO₂)₄](NO₃) GEOMETRY
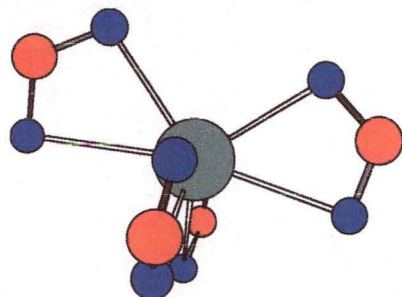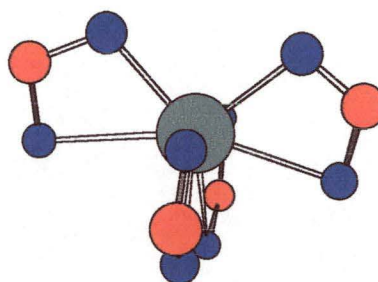
Ca[Cd(NO₂)₄] GEOMETRY   CRYSTAL STRUCTURE

Figure 3.20: Calculated and observed geometries of $[Cd(NO_2)_4]^{2-}$ from different starting geometries.

BOND	CaCd(NO₂)₄	Cs₂Zn(NO₂)₄	K₃[Hg(NO₂)₄](NO₃)	MEASURED (Å)
Cd-O11	2.462	2.413	2.469	2.313
-O12	2.667	2.785	2.658	2.532
-O21	2.462	2.413	2.512	2.313
-O22	2.667	2.785	2.647	2.532
-O31	2.519	2.413	2.516	2.381
-O32	2.590	2.785	2.638	2.439
-O41	2.525	2.413	2.574	2.381
-O42	2.583	2.785	2.576	2.439
O11-N1	1.283	1.287	1.282	1.279
O12-N1	1.266	1.264	1.266	1.248
O21-N2	1.283	-	1.281	1.281
O22-N2	1.266	-	1.266	1.252
O31-N3	1.274	-	1.280	-
O32-N3	1.274	-	1.266	-
O41-N4	1.274	-	1.274	-
O42-N4	1.275	-	1.266	-

Table 3.10: Comparison of calculated and experimental bond lengths for $[Cd(NO_2)_4]^{2-}$ from different starting geometries.

ANGLE	CaCd(NO₂)₄	Cs₂Zn(NO₂)₄	K₃[Hg(NO₂)₄](NO₃)	MEASURED (°)
Cd-O11-N1	102.3	106.6	101.7	102.6
Cd-O12-N1	92.8	89.2	93 1	92.8
O11-N1-O12	115.4	115.7	115.6	113 2
O11-Cd-O12	49.5	48.5	49 6	51.4
Cd-O21-N2	102.3	-	100.7	98.1
Cd-O22-N2	92.8	-	94.6	96.1
O21-N2-O22	115.4	-	115.3	113.6
O21-Cd-O22	49.5	-	49.2	52.1
Cd-O31-N3	99 1	-	100 4	102.6
Cd-O32-N3	95.7	-	94.9	92.8
O31-N3-O32	115.3	-	115.3	113.2
O31-Cd-O32	49.8	-	49.3	51.4
Cd-O41-N4	98.8	-	97.7	-
Cd-O42-N4	96.0	-	97.6	-
O41-N4-O42	115.3	-	115.3	-
O41-Cd-O42	49.8	-	49.4	-

Table 3.11: Comparison of calculated and experimental bond angles for
$[Cd(NO_2)_4]^{2-}$ from different starting geometries.

As for $[Zn(NO_2)_4]^{2-}$, the calculated geometry for $[Cd(NO_2)_4]^{2-}$ with $Ca[Cd(NO_2)_4]$ as
the starting point is in good agreement with the observed geometry in this lattice. In
the case of the $[Zn(NO_2)_4]^{2-}$ geometry as the starting point, the introduction of the
Cd^{2+} ion greatly reduced the difference between the longer and shorter bonds of the
nitrite ligands. This showed that the nitrite is moving back towards a symmetric
chelation mode. A difference between these calculated geometries and those for
$[Zn(NO_2)_4]^{2-}$ is that the disposition of the nitrites around the metal ions has not
altered greatly when using the $[Hg(NO_2)_4]^{2-}$ geometry as a starting point. This may
be because the $[Cd(NO_2)_4]^{2-}$ is closer in size to $[Hg(NO_2)_4]^{2-}$.

The optimised geometries of the $[Cd(NO_2)_4]^{2-}$ ion obtained from the different starting
geometries are not identical. This suggests that, as for the $[Zn(NO_2)_4]^{2-}$ ion, the
geometry may be changed relatively easily. A comparison of the energies calculated
for the optimised geometries confirms that these also lie on a shallow potential
energy curve (Table 3.12). In this case, the most stable geometry is that from the

complex $Ca[Cd(NO_2)_4]$, which is not unexpected as this is the shape that is most stable according to the theoretical model of Kepert[10].

STARTING GEOMETRY	ENERGY (eV)
$Ca[Cd(NO_2)_4]$	-79.033
$Mg[Cd(NO_2)_4]$	-78.955
$K_2[Cd(NO_2)_4]$	-78.916
$Cs_2[Zn(NO_2)_4]$	-78.966
$K_3[Hg(NO_2)_4](NO_3)$	-78.936

Table 3.12: The energy of the optimum structures of $[Cd(NO_2)_4]^{2-}$ from the listed starting geometries.

3.4.4 *Geometry of the $[Hg(NO_2)_4]^{2-}$ ion*

The geometry optimisation of the $[Hg(NO_2)_4]^{2-}$ ion starting from various points did not agree particularly well with experiment (Figure 3.21)[8]. Also shown are the geometries calculated from the starting geometries of $[Zn(NO_2)_4]^{2-}$ and $[Cd(NO_2)_4]^{2-}$ in the Ca^{2+} lattice. Tables 3.13 and 3.14 list the bond lengths and angles calculated for these complexes.

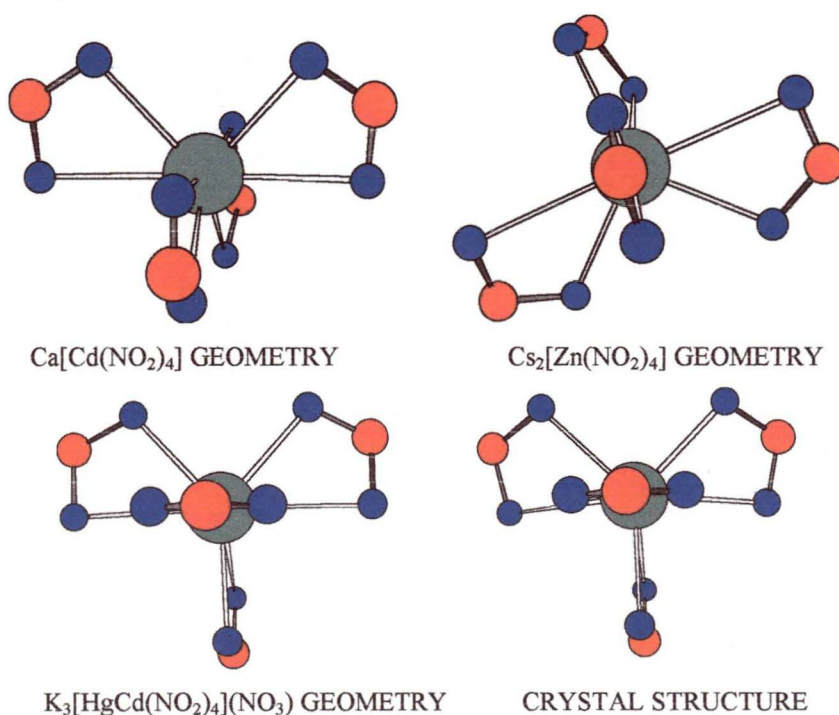$Ca[Cd(NO_2)_4]$ GEOMETRY $Cs_2[Zn(NO_2)_4]$ GEOMETRY

$K_3[HgCd(NO_2)_4](NO_3)$ GEOMETRY   CRYSTAL STRUCTURE

Figure 3.21: Calculated and observed geometries of $[Hg(NO_2)_4]^{2-}$ from different starting geometries.

BOND	K$^+$ lattice	Ca^{2+} lattice	Cs$^+$ lattice	MEASURED (Å)
Hg-O11	2.489	2 521	2 465	2.394
-O12	2.742	2.787	2.890	2 566
-O21	2.514	2.574	2.465	2.414
-O22	2.832	2.700	2.890	2.494
-O31	2.657	2.521	2.465	2.548
-O32	2.666	2.787	2.890	2.548
-O41	2.821	2 681	2.465	2.494
-O42	2.507	2.588	2.890	2.414
O11-N1	1.280	1.280	1.284	1.250
O12-N1	1.260	1.260	1.257	1.232
O21-N2	1.283	1.273	1.283	1.248
O22-N2	1.259	1.264	1.258	1.231
O31-N3	1.271	1.280	1.283	1.235
O32-N3	1.270	1.260	1.258	1.235
O41-N4	1.258	1.266	1.283	1.232
O42-N4	1.283	1.272	1.258	1.248

Table 3.13: Comparison of calculated and experimental bond lengths for $[Hg(NO_2)_4]^{2-}$ from different starting geometries.

ANGLE	K$^+$ lattice	Ca^{2+} lattice	Cs$^+$ lattice	MEASURED (°)
Hg-O11-N1	103.3	104.0	108 1	101.7
Hg-O12-N1	91.6	91.7	88.1	93.7
O11-N-O12	116.6	116.6	116.8	114.8
O11-Hg-O12	48.5	47.7	46 9	49.7
Hg-O21-N2	105 5	100.6	108.2	99.5
Hg-O22-N2	90.7	94.7	88.1	95.9
O21-N2-O22	116.6	116.5	116.8	114.3
O21-Hg-O22	47.2	48.2	46.8	50.2
Hg-O31-N3	98.1	104.0	108.2	98.5
Hg-O32-N3	97.7	91.7	88.2	98.5
O31-N3-O32	116.3	116.6	116.8	114 7
O31-Hg-O32	47.8	47.7	46.9	48.2
Hg-O41-N4	90.7	95.5	108.1	96.0
Hg-O42-N4	105.3	99.8	88 2	99.5
O41-N4-O42	116.6	116.5	116.8	114.3
O41-Hg-O42	47.4	48.3	46.9	50.4

Table 3.14: Comparison of calculated and experimental bond angles for $[Hg(NO_2)_4]^{2-}$ from different starting geometries.

The main discrepancy between the calculated and measured values can be seen for the bonds Hg-O21, Hg-O22, Hg-O41 and Hg-O42. The crystal structure has these bonds almost equal, with Hg-O21 and Hg-O42 of 2.494Å and Hg-O22 and Hg-O41 of 2.414Å. However, the optimised geometry has lengthened both of these bonds, and one more so than the other to give Hg-O21 of 2.515, Hg-O22 = 2.832 and Hg-O41 = 2.821 and Hg-O42 = 2.507Å.

The symmetry of the other geometries has been maintained. Although the metal-nitrite bond lengths obtained for the $[Hg(NO_2)_4]^{2-}$ ion when starting from the geometry of the $[Zn(NO_2)_4]^{2-}$ in $Cs_2[Zn(NO_2)_4]$ are not the same, as they would be for a symmetric chelation, it can be seen that the difference between the longer and shorter bond has reduced from that calculated for the $[Zn(NO_2)_4]^{2-}$ under the same conditions (Table 3.7). This indicates that the structure is moving back toward a symmetrically chelating structure, whilst maintaining the symmetry of the $[Zn(NO_2)_4]^{2-}$ ion. This can be seen even more clearly for the $[Cd(NO_2)_4]^{2-}$, where the difference between the longer and shorter bonds is even less than that seen for the $[Hg(NO_2)_4]^{2-}$ ion (Table 3.10).

The rather poor general agreement between the optimised geometries and that observed in $K_3[Hg(NO_2)_4](NO_3)$, even when the experimental geometry is used as the starting point, implies that the stereochemistry of the $[Hg(NO_2)_4]^{2-}$ ion is quite "flexible". This means that the geometry can be altered easily, even by subtle lattice forces. This may be related to the rather large ionic size of the Hg^{2+} compared with Cd^{2+} and, in particular, Zn^{2+}.

A comparison of the energies calculated for these structures supports this idea of flexible stereochemistry, as again there is very little difference in the energies of the most and least stable geometries (Table 3.15).

STARTING GEOMETRY	ENERGY (eV)
$K_3[Hg(NO_2)_4](NO_3)$	-77.300
$Ca[Cd(NO_2)_4]$	-77.395
$Mg[Cd(NO_2)_4]$	-77.308
$K_2[Cd(NO_2)_4]$	-77.285
$Cs_2[Zn(NO_2)_4]$	-77.373

Table 3.15: The energy of the optimum structures of $[Hg(NO_2)_4]^{2-}$ from the listed starting geometries.

Interestingly, in this case the geometry of greatest stability is not the experimentally observed geometry. The $Ca[Cd(NO_2)_4]$ starting geometry is of the highest symmetry, this being the shape predicted by Kepert's theory, and this is the most stable geometry calculated for the $[Hg(NO_2)_4]^{2-}$ ion.

3.5 Summary

The major aim of the present work was to investigate the difference between the nitrite coordination mode for the complex $Cs_2[Zn(NO_2)_4]$ and the quite symmetric bidentate nitrite coordination observed in $K_3[Hg(NO_2)_4](NO_3)$ and $[Cd(NO_2)_4]^{2-}$ with various counterions. To this end, the crystal structure of $Cs_2[Zn(NO_2)_4]$ was measured, and this showed the highly asymmetric chelation mode adopted by the nitrite ion. A comparison of this structure with those of the known transition metal tetranitrite complexes discussed in this chapter revealed that there were a number of structures that the $[M(NO_2)_4]^{2-}$ ion may adopt. This had significant bearing on the DFT calculations, which were carried out to determine the relative stabilities of the different geometries. These results generally agreed with experiment, but also indicated that tetranitrites can adopt a number of geometries, with similar energies, depending on the lattice forces which change with the counter-ion. This suggests that these stereochemistries lie on a shallow potential energy curve. The most stable geometry calculated for the $[Zn(NO_2)_4]^{2-}$ and $[Cd(NO_2)_4]^{2-}$ ions was that observed experimentally, but that calculated for $[Hg(NO_2)_4]^{2-}$ was not that found in $K_3[Hg(NO_2)_4](NO_3)$, but rather that with the highest symmetry, as predicted by simple theories based on ligand-ligand repulsions.

The use of infrared and Raman spectroscopy to give complementary information was also demonstrated. The use of both of these techniques was necessary for the unambiguous assignment of the symmetric and asymmetric stretching vibrations of the coordinated nitrite ions. Further examples of this will be discussed in the following chapters.

3.6 References

1. le Postollec M., Mathieu J.P. and Poulet H., *J. Chim. Phys.*, **60**, 1319-1333, (1963).

2. Mathieu J.P. and Cornevin S., *J. Chim. Phys.*, **36**, 271-291, (1939).

3. Lang J., *J. Prakt. Chem.*, **86**, 295-307, (1862).

4. Fock A., *Z. Krist.*, **17**, 188-202, (1889).

5. Goodgame D.M.L. and Hitchman M.A., *J. Chem. Soc. (A)*, 612-615, (1967).

6. Ohba S., Matsumoto F., Takazawa H. and Saito Y., *Acta Cryst.*, **C43**, 191-194, (1987).

7. Aoyama T., Ohba S. and Saito Y., *Acta Cryst.*, **C44**, 1703-1707, (1988).

8. Power L., King J. and Moore F., *J. Chem. Soc. Dalton Trans.*, 93-96, (1976).

9. Cotton F.A. and Dunne T.G., *J. Amer. Chem. Soc.*, **84**, 2013-2014, (1962).

10. Kepert D.L., *Inorganic Stereochemistry*, Springer-Verlag, Berlin, (1982).

11. Hall S.R., King G.S.D. and Steward J.M., *The Xtal User's Manual Version 3.0*, Universities of Western Australia and Maryland, (1990).

12. Goodgame D.M.L. and Hitchman M.A., *J. Chem. Soc. (A)*, 1933-1935, (1970).

13. Finney A.J., Hitchman M.A., Raston C.L., Rowbottom G.L. and White A.L., *Aust. J. Chem.*, **34**, 2061-2067, (1981).

14. Irish D.E. and Thorpe R.V., *Can. J. Chem.*, **53**, 1414-1423, (1975).

15. Cram A.G. and Davies M.B., *J. Inorg. Nucl. Chem.*, **37**, 1693-1696, (1975).

16. Farrugia L.J., *J. Appl. Cryst.*, **30**, 565, (1997).

17. Figgis B.N. and Hitchman M.A., *Ligand Field Theory and its Applications*, Wiley-VCH, New York, (2000).

18. Hitchman M.A. and Rowbottom G.L., *Coord. Chem. Rev.*, **42**, 55-132, (1982).

19. Muetterties E.L. and Wright C.M., *Quart. Revs. Chem. Soc.*, **21**, 109-194, (1967).

20. Deeth R.J., *J. Chem. Soc. Dalton Trans.*, 664-669, (2001).

21. Ziegler T., *Can. J. Chem.*, **73**, 743-761, (1995).

22. Nguyen K.A. and Pachter R., *J. Chem. Phys.*, **114(24)**, 10757-10767, (2001).

23. Ricciardi G., Rosa A. and Baerands E.J., *J. Phys. Chem. A*, **105(21)**, 5242-5254, (2001).

24. Baerends E.J., Ellis D.E. and Ros P., *Chem. Phys.*, **2**, 41-51, (1973).

25. Versluis L. and Ziegler T., *J. Chem. Phys.*, **88**, 322-328, (1988).

26. te Velde G. and Baerends E.J., *J. Comput. Phys.*, **99(1)**, 84-98, (1992).

27. Fonscca Guerra C., Snijders J.G., te Velde G. and Baerends E.J., *Theor. Chem. Acc.*, **99**, 391-403, (1998).

28. Vosko S.H., Wilk L. and Nusair M., *Can. J. Phys.*, **58**, 1200-1211, (1980).

29. Becke A.D., *Phys. Rev. A*, **38**, 3098-3100, (1988).

30. Perdew J.P., Chevary J.A., Vosko S.H., Jackson K.A., Pederson M.R., Singh D.J. and Fiolhais C., *Phys. Rev. B*, **46**, 6671-6687, (1992).

31. van Lenthe E., Baerends E.J. and Snijders J.G., *J. Chem. Phys.*, **99**, 4597-4610, (1993).

CHAPTER 4

Cobalt(III) and Chromium(III) Nitrite Complexes

Some of the earliest transition metal complexes synthesised were cobalt(III) complexes, with some preparation methods dating from the early nineteenth century[1,2]. The ambidentate nature of the nitrite ligand was first recognised later in the nineteenth century, with the preparation and isolation of the linkage isomers $[Co(NH_3)_5NO_2]^{2+}$ and $[Co(NH_3)_5ONO]^{2+}$ [3]. As well as being of interest in themselves, these isomers were also of importance in the controversy over the very nature of coordination compounds. As discussed in Chapter 1, it was Jørgensen[3] who realised that this was an example of linkage isomerism, but he was ultimately incorrect about the nature of coordination compounds, losing this argument to Werner[4].

From these early beginnings, these linkage isomers have been used in a range of studies. Kinetic studies have shown how the thermodynamically unstable nitrito complex forms, and have suggested ways in which this isomer rearranges to the more stable nitro complex[5-8]. Further studies have examined the photochemical rearrangement of the nitro isomer to the nitrito isomer[9-18].

Cobalt(III) nitrite complexes are still of interest today. The crystallisation behaviour of numerous cobalt amine complexes has been investigated as part of ongoing studies into the phenomenon of conglomerate crystallisation[19,20]. Attempts have been made to use similar complexes as precursors for semiconductors[21]. Studies of linkage isomerism have continued in recent years, with the measurement of crystal structures of $[Co(NH_3)_5NO_2]^{2+}$ and its nitrito isomer over a range of pressures and temperatures[22-26].

Some chromium(III) nitrite complexes have also been reported[27,28]. To date, the nitrite ligand has only been seen to adopt the monodentate nitrito coordination mode in these complexes. Of particular interest is the photochemical behaviour of these complexes. This differs from that of analogous cobalt(III) complexes in that linkage

isomerism has not been observed for chromium(III) complexes. The other photochemical processes undergone by cobalt(III) nitrite complexes upon irradiation, such as photoaquation, photoreduction and photodecomposition, are also seen for chromium(III)[14]. Photodecomposition results in the cleavage of the ONO nitrite ligand to give a nitric oxide (NO) molecule, leaving an oxygen atom coordinated to the Cr^{3+} ion. All of these reactions may occur to varying degrees for a particular complex, but it is photodecomposition that is of current interest as it may allow the delivery of the bioregulatory molecule NO to specific body tissues[28].

These few examples indicate that the chemistry of cobalt(III) and chromium(III) nitrite complexes is still of current interest. However, there have been very few attempts to explain why the O-bonded nitrito coordination mode is preferred in chromium(III) complexes, while the N-bonded nitro coordination mode occurs in cobalt(III) complexes. Therefore, a major aim of the present work is to investigate the bonding in $[Co(NH_3)_5NO_2]^{2+}$, its nitrito isomer and the chromium analogue, and to determine what may be influencing the way in which the nitrite coordinates. Single crystal polarised optical spectra were measured when possible to provide information for use in the Angular Overlap Model (AOM) parameterisation scheme, and these results were correlated with those obtained using Density Functional Theory (DFT) calculations. The Raman spectra for these complexes are also reported, and compared with the previously reported infrared spectra to confirm published nitrite vibrational energies.

4.1 Experimental

$[Co(NH_3)_5NO_2]Cl_2$ was prepared by the method of Pentland et al[29]. Recrystallising the yellow complex slowly at room temperature from an aqueous solution resulted in small orange crystals. Microanalysis: found, calculated: %N 32.14, 32.20%; %H 5.64, 5.79%. A comparison of the infrared spectrum measured for this complex with that measured by Johnson and Pashman[30] confirmed that this was the desired complex.

$[Co(NH_3)_5ONO]Cl_2$ was also prepared by the method of Pentland et al[29]. Recrystallising the red complex at room temperature from aqueous solution gave

very small red crystals. These converted to the orange nitro complex within a week. Leaving the aqueous solutions of the nitrito complex to recrystallise for a week also produced crystals of the nitro complex. The infrared spectra of the small red crystals and red precipitate, were used to confirm that the nitrito complex was the only isomer.

$[Co(NH_3)_5NO_2](CF_3SO_3)_2$ was prepared in the following manner. $[Co(NH_3)_5Cl]Cl_2$ (0.001mol), which was prepared via the method of Pentland et al.[29], was dissolved in the minimum amount of water. Solid silver triflate $(AgCF_3SO_3, 0.002mol)$ was added and the solution was shaken vigorously. The precipitate of silver chloride was removed via filtration, and solid sodium nitrite (0.001mol) was added. This solution was stirred and left overnight. It was difficult to remove all of the fine silver chloride that formed, so the yellow-brown precipitate had to be recrystallised slowly from aqueous solution at room temperature to give large plate-like yellow crystals suitable for the measurement of single crystal optical spectra. Microanalysis: found, calculated: %C 4.86, 4.92%; %N 16.75, 17.21%; %H 3.26, 3.10%; %S 13.24, 13.13%.

It was also possible to prepare crystals of $[Co(NH_3)_5NO_2](CF_3SO_3)_2$ by displacing the chloride ions of the complex $[Co(NH_3)_5NO_2]Cl_2$. This was done by dissolving the nitro complex in water and then adding solid silver triflate to this solution. Again, the silver chloride formed was quite difficult to remove, and slow recrystallisation of the crude brown-yellow precipitate was essential for the formation of large yellow crystals of the nitro complex. Infrared spectroscopy was used to compare the crystals formed in this manner with those of the first, and these measurements indicated that both methods allowed the preparation of the desired complex.

Attempts to prepare crystals of $[Co(NH_3)_5ONO](CF_3SO_3)_2$ suitable for single crystal polarised optical spectroscopy were unsuccessful. The complex could be formed in a similar manner to the second method described for the nitro complex using the appropriate nitrito starting complex, but only a finely divided powder was obtained. Leaving this to recrystallise for a few days resulted in the formation of the nitro complex, so this preparation was abandoned as a method for growing larger $[Co(NH_3)_5ONO]^{2+}$ crystals.

$[Cr(NH_3)_5ONO]X_2$, X = Cl, Br, were prepared following the method of Mori[31]. Although the alternative synthesis of Kyuno et al.[32] was less time consuming, it was found that Mori's method was more reliable. Microanalysis: found, calculated (X= Br): %N 24.64, 24.64%; %H 4.68, 4.43; (X= Cl): %N 33.23, 33.08%; %H 5.96, 5.95%. Recrystallising these two complexes to obtain crystals of good optical quality presented many problems. The complexes were insoluble in all common solvents apart from water, and changing the halide to perchlorate or triflate did not improve this. Leaving aqueous solutions of the complexes at room temperature promoted the formation of very finely divided purple complexes, which were found to be some form of chromium oxide. This contaminated the precipitates of the desired complexes, and also removed chromium from solution. The formation of these undesired complexes was slowed at lower temperature, and very small orange crystals of $[Cr(NH_3)_5ONO]Cl_2$ were grown at approximately 4°C after three days.

As discussed in Chapter 2, the O,O'-bridging nitrito coordination mode has not been seen experimentally. Since the only coordination mode seen for chromium(III) has been the monodentate nitrito mode, it was thought that it might be possible to prepare a chromium(III) complex in which two Cr^{3+} ions were bridged by a nitrite ion in the above manner. This was attempted in collaboration with Professor W.G. Jackson of the University of New South Wales. Initially, a procedure involving cobalt(III) was investigated, before using the analogous chromium(III) complexes. $[Co(NH_3)_5NO_2](CF_3SO_3)_2$ was prepared by first dissolving $[Co(NH_3)_5NO_2]Cl_2$ (0.002mol) in the minimum amount of water and adding solid silver acetate (0.004mol). After removing the silver chloride precipitate, triflic acid (0.004mol) was added with stirring. Yellow crystals of $[Co(NH_3)_5NO_2](CF_3SO_3)_2$ were filtered from solution and washed with isopropanol (0.0015mol, 75% yield). $[Co(NH_3)_5CF_3SO_3](CF_3SO_3)_2$ (0.002mol), which had been prepared by the method of Dixon et al.[33], was dissolved in acetone. This solution was added to an acetone solution of $[Co(NH_3)_5NO_2](CF_3SO_3)_2$ (0.0015mol) and was left to reflux at 60°C for one hour. The dark red solution was then pipetted into cold ether, with the immediate formation of a light pink precipitate. After separating the components of this precipitate on a Sephadex column, it was found that the only complexes present were the starting materials and an aquo complex, $[Co(NH_3)_5H_2O]^{3+}$. A similar

preparation in which tetramethylene sulfone was substituted for the acetone solvent was also unsuccessful.

Another method was tried to obtain the desired $[(NH_3)_5Co-NO_2-Co(NH_3)_5]^{5+}$ complex. $[Co(NH_3)_5NO_2](ClO_4)_2$ (0.001mol) and $[Co(NH_3)_5(DMSO)](ClO_4)_3$ (0.0015mol) were dissolved in ~5mL of dimethylsulfoxide (DMSO). This was refluxed at 100°C for one hour. This oily solution was poured into a large volume of a 1:1 ether and isopropanol solution (~25mL) to extract the excess DMSO. The precipitate was filtered from the solution and dissolved in water. This was separated on a Biorex column, and a dark orange precipitate was collected. The UV-VIS spectrum of this complex indicated that an N-bonded nitrite may be present, so this was recrystallised from water and a crystal structure was obtained. This indicated that this complex was in fact $[Co(NH_3)_6](ClO_4)_3$ [34].

Attempts to use the above methods for the preparation of the complex ion $[(NH_3)_5Cr-ONO-Cr(NH_3)_5]^{5+}$ were also unsuccessful. The starting complexes did not appear to have reacted to any great extent when using DMSO, or tetramethyl sulfone. Furthermore, the separation process was not particularly successful, as these had to be carried out quickly to prevent the formation of chromium hydroxides. Attempts to produce a mixed metal dimer were also unsuccessful.

Infrared and Raman spectroscopic measurements were carried out as described in Chapter 3, as were the microanalytical measurements.

Measurements of the optical spectra were carried out in three different ways. Single crystals of $[Co(NH_3)_5NO_2]Cl_2$ and $[Co(NH_3)_5NO_2](CF_3SO_3)_2$ were mounted over small holes cut into thin copper masks. The mounted crystals were held in place on a metal stage that was connected to a CTI Cryogenics cooling system and a diffusion pump that reduced the pressure within the sample holder to less than 10^{-4} atm. Another copper mask was placed in the reference beam of the Cary 5e spectrophotometer, along with other light absorbing material if necessary. Room and low temperature (15K) measurements were carried out for each crystal, and the extinction directions of the crystal were aligned with a polarising prism to give polarised spectra.

Crystals of good optical quality could not be obtained for $[Co(NH_3)_5ONO]Cl_2$, so room and low temperature optical spectra of KBr discs of this complex were measured in the above manner, with a blank KBr disc in the reference beam and without the use of a polariser.

Although the crystals of $[Cr(NH_3)_5ONO]Cl_2$ were of good optical quality, they were also very small and below the limit of detection for the Cary 5e spectrophotometer. Spectra were therefore measured at the Australian National University, under the supervision of Dr Elmars Krausz, using specialised equipment (see Chapter 2).

4.2 Vibrational Spectroscopy

The measurement of both infrared (IR) and Raman spectra provides complementary information about the nitrite vibrational energies. For this reason, both the IR and Raman spectra were measured for the $[Co(NH_3)_5NO_2]^{2+}$, $[Co(NH_3)_5ONO]^{2+}$ and $[Cr(NH_3)_5ONO]^{2+}$ complex ions with various counterions. Perhaps the first feature to be noted is that, unlike the spectra of nickel(II) nitrite complexes and the polynitrites discussed in Chapter 3, the peak intensities suggest that the asymmetric stretch is of higher energy than the symmetric stretch for Co(III) and Cr(III) complexes. This has been discussed in Chapter 2, and can be seen when comparing the Raman spectrum of $[Co(NH_3)_5NO_2](CF_3SO_3)_2$ (Figure 4.1) with the IR spectrum measured for this complex (Figure 4.2).

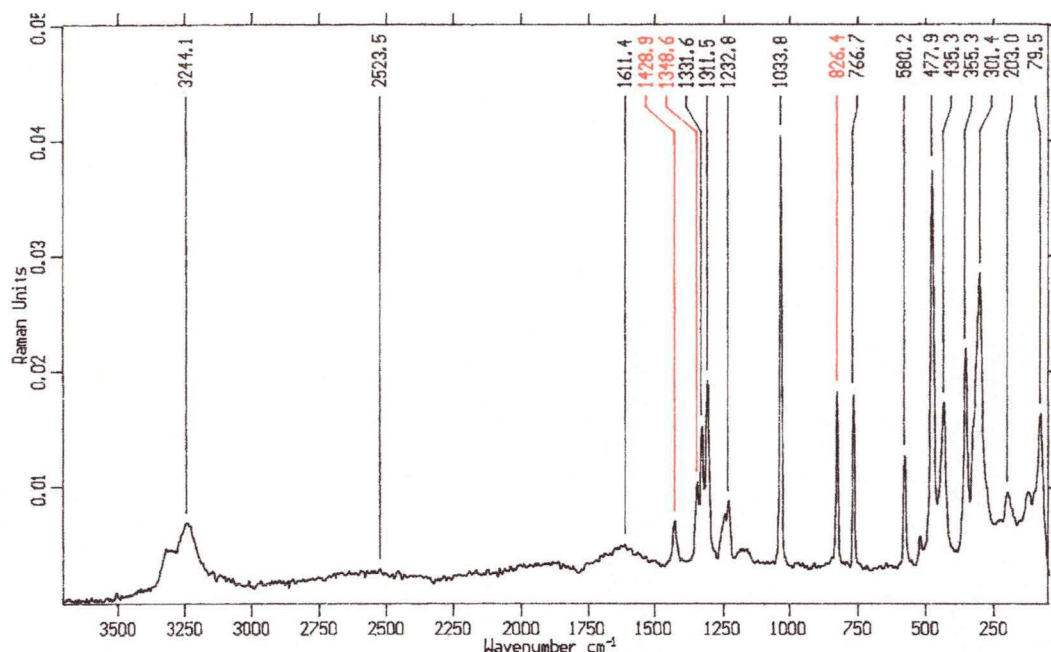**Figure 4.1**: The Raman spectrum of $[Co(NH_3)_5NO_2](CF_3SO_3)_2$.

The wagging mode is a sharp peak at $826cm^{-1}$. The ν_3 can be seen as a relatively weak peak at $1\,428cm^{-1}$, and a more intense ν_2 is at $1\,348cm^{-1}$.
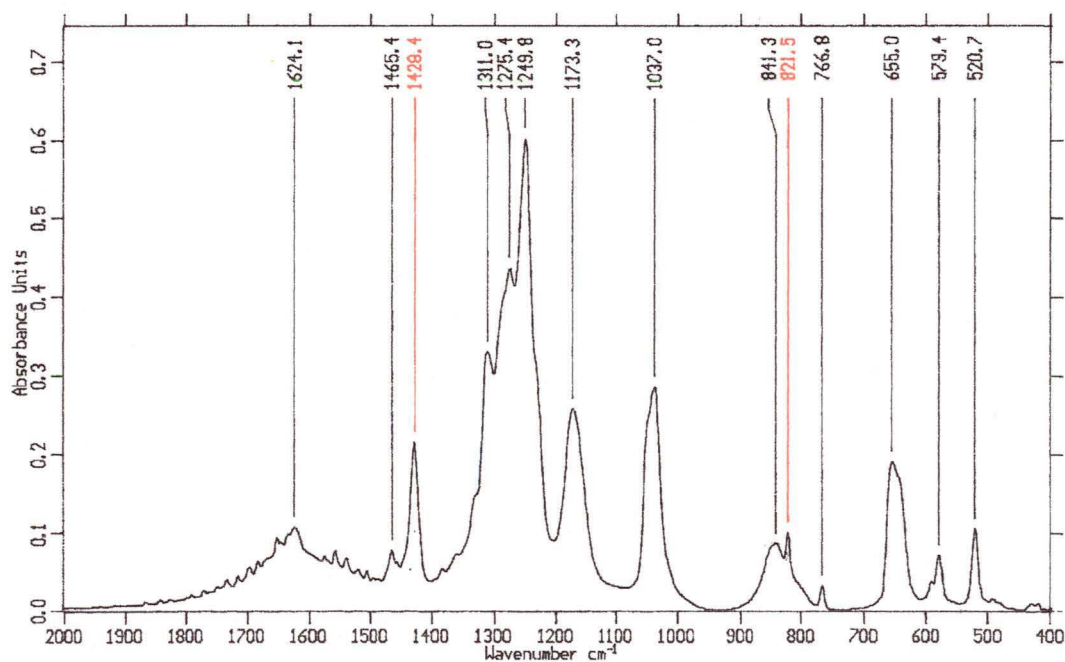

Figure 4.2: The IR spectrum of $[Co(NH_3)_5NO_2](CF_3SO_3)_2$.

The wagging mode is also visible in the infrared at $821cm^{-1}$, but in this case it is associated with a second, broader peak at $841cm^{-1}$. This broad peak may be assigned

as a rocking vibration of the ammine ligands, $\rho_r(NH_3)$. The ν_2 is obscured in this spectrum by triflate peaks, but one would expect this to be of relatively low intensity at about $1\,348cm^{-1}$. The ν_3 peak is clearly visible at $1\,428cm^{-1}$, and corresponds well with the Raman spectrum. Another peak that is seen only for nitro coordination is at $580cm^{-1}$. This is due to another nitrite wagging mode (ρ_w). These nitrite vibrational energies correspond well with those published for other $[Co(NH_3)_5NO_2]^{2+}$ salts[17,30,35], although Le Postollec does not report observing the higher energy vibration in his Raman spectrum[36]. He encountered some difficulties when measuring the Raman spectrum for this complex, so perhaps this vibration of relatively low intensity was not resolved in the spectrum that he obtained.

IR spectra of the $[Co(NH_3)_5ONO]^{2+}$ ion have also been reported[17,30,37]. Nakamoto et al.[37] list the nitrite vibrational energies as $\nu_1 = 825cm^{-1}$, $\nu_2 = 1\,065cm^{-1}$ and $\nu_3 = 1\,468cm^{-1}$. The Raman spectrum measured for the complex $[Co(NH_3)_5ONO]Cl_2$ is shown in Figure 4.3.

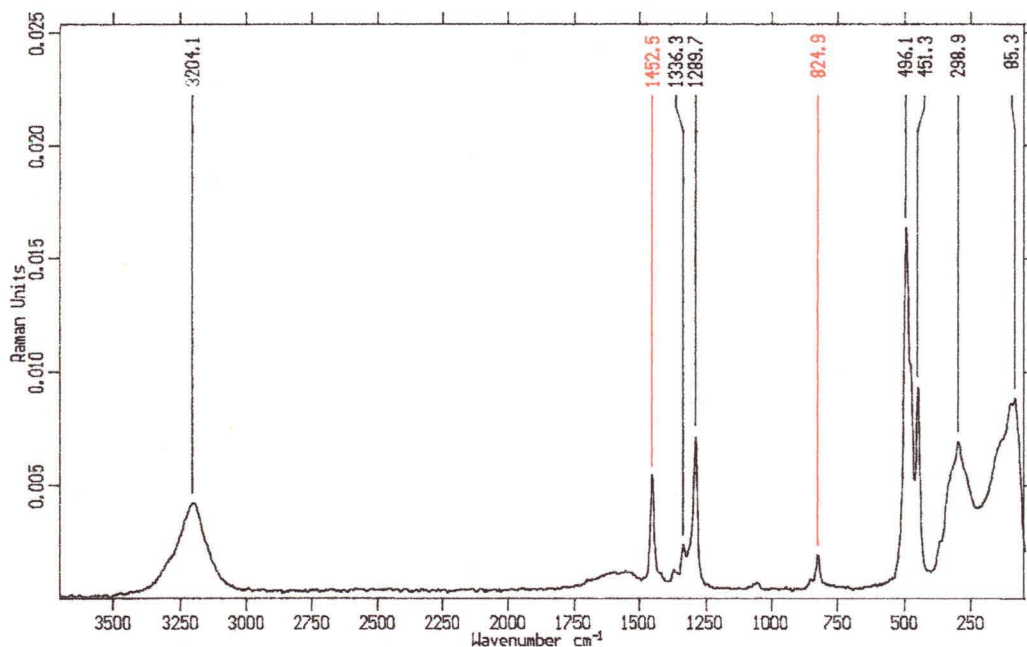**Figure 4.3**: The Raman spectrum of $[Co(NH_3)_5ONO]Cl_2$.

The energy of ν_1 is identical to that quoted for the IR spectrum ($825cm^{-1}$). The energy of ν_3 was found to be $1\,452cm^{-1}$, which is close to the IR value, and a ν_2 peak does not appear in the Raman spectrum.

A problem was encountered when measuring the Raman spectrum of $[Cr(NH_3)_5ONO]Cl_2$ (Figure 4.4). The sample fluoresced, which resulted in the unusually shaped baseline seen in Figure 4.4. However, the nitrite ligand vibrations were still visible in this spectrum, with $v_1 = 840cm^{-1}$, $v_3 = 1\ 462cm^{-1}$ and $v_2 = 1\ 043cm^{-1}$ as a peak of very low intensity.
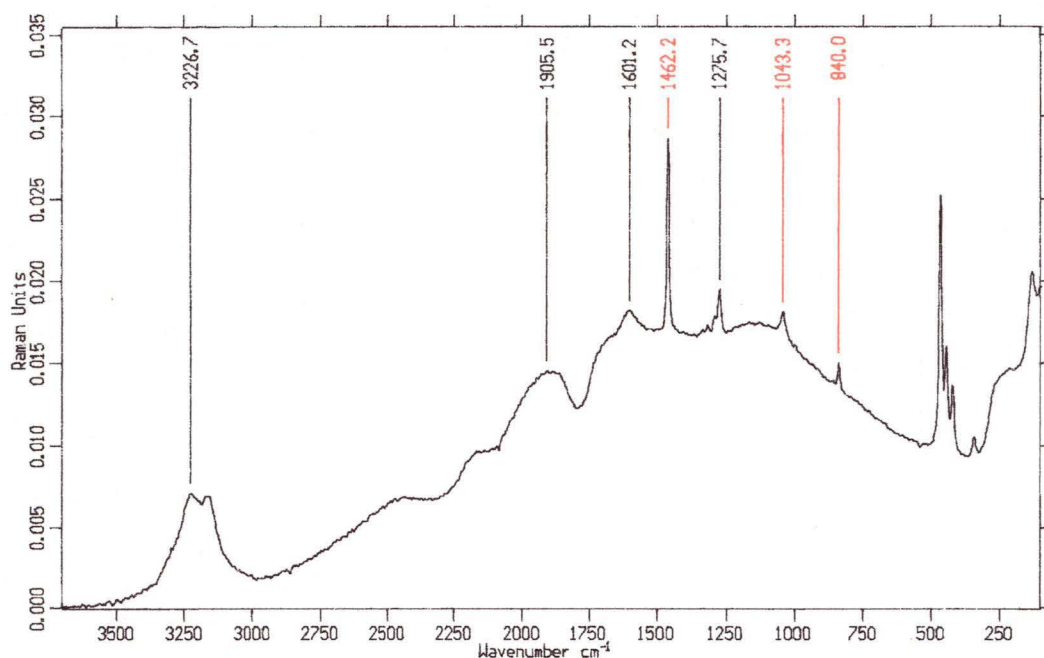
Figure 4.4: The Raman spectrum of $[Cr(NH_3)_5ONO]Cl_2$.

The infrared spectrum of $[Cr(NH_3)_5ONO]Cl_2$ (Figure 4.5) had peak energies which corresponded to those of the Raman, although in this case, the intensities of v_2 and v_3 have changed in relation to each other, with v_2 now being the more intense of the two. These values are in good agreement with Fee et al.[27], who found $v_1 = 838cm^{-1}$, $v_2 = 1\ 030cm^{-1}$ and $v_3 = 1\ 470cm^{-1}$.
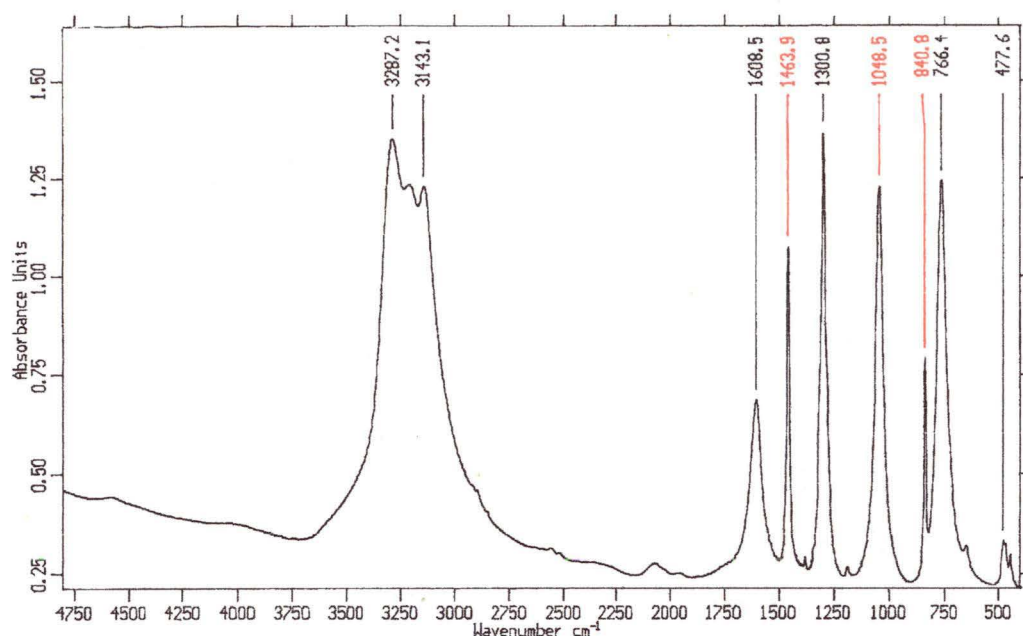
Figure 4.5: The infrared spectrum of $[Cr(NH_3)_5ONO]Cl_2$.

4.3 Optical Spectroscopy

Cobalt(III) and chromium(III) are quite kinetically inert, so a large range of complexes has been prepared and studied using optical spectroscopy[38]. This range included many cobalt and chromium amine complexes, and, in the case of cobalt, a number of cobalt amine nitrite complexes. However, there are very few studies of single crystals of these complexes. As part of the present work single crystal polarised optical spectra were attempted for the ions $[Co(NH_3)_5NO_2]^{2+}$, $[Co(NH_3)_5ONO]^{2+}$ and $[Cr(NH_3)_5ONO]^{2+}$, as these measurements can provide a great deal of information regarding the nature of bonding in these complexes.

Kiss and Czeglédy[39] measured the solution spectrum of $[Co(NH_3)_5NO_2]Cl_2$ in 1938. They assigned the two bands centred at 21 740 and 30 675cm^{-1} as the two d-d transitions, $^1T_1 \leftarrow {}^1A_{1g}$ and $^1T_2 \leftarrow {}^1A_{1g}$, respectively. Linhard et al.[40,41] agreed with the position and assignment of the first band, but questioned the interpretation of the second band. It had been established that $n \rightarrow \pi^*$ internal nitrite transitions occur in the range from 25 000 to 30 000cm^{-1}, and so it was possible that the higher energy band was due to this rather than a d-d transition[42].

The optical spectrum of a single crystal of $[Co(NH_3)_5NO_2]Cl_2$ was measured, and the position of the first band (21 865cm^{-1}) is in good agreement with the measurements by the above authors. The second, higher energy band is not clearly defined, as it coincided with an intense internal nitrite transfer band seen for all of the transition metal nitrite complexes in this work (Figures 4.6 and 4.7). Both the room temperature (Figure 4.6) and low temperature spectra (Figure 4.7) are shown below, and the additional information obtained when cooling a crystal can be seen when comparing the low temperature spectra with those measured at higher temperature. Spin forbidden peaks can be seen at low temperature, and poorly resolved vibrational fine structure can be seen on the band in one polarisation. As the spectra do not show strong polarisation, the molecular projections for the two extinction directions have not been determined for this crystal face. The labels I and II will be used throughout the present work whenever this is the case.
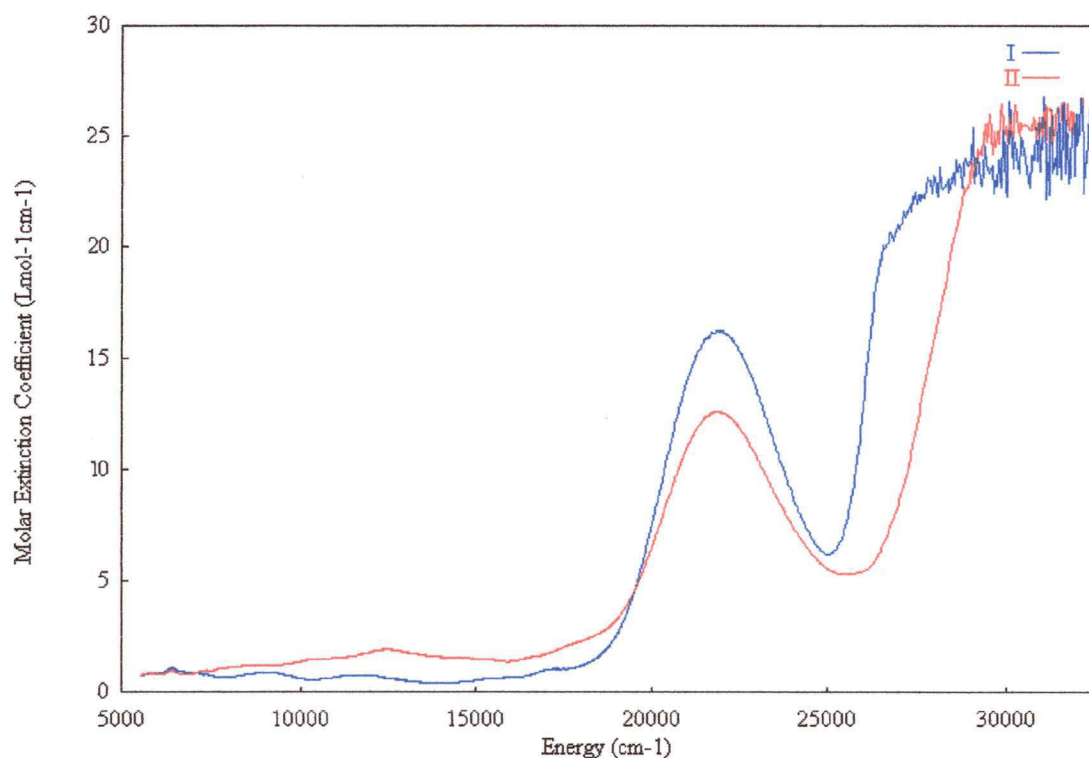

Figure 4.6: The single crystal optical spectrum of $[Co(NH_3)_5NO_2]Cl_2$ at room temperature, with the electric vector parallel to the extinction directions of an arbitrary crystal face.

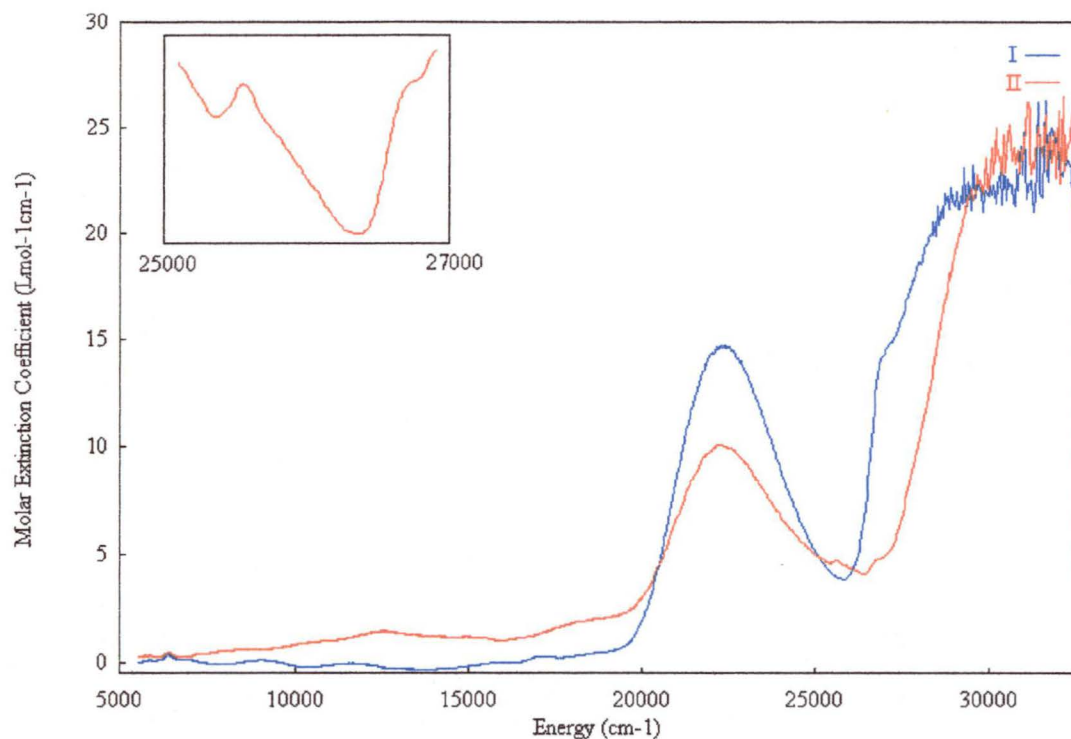**Figure 4.7**: The single crystal optical spectrum of $[Co(NH_3)_5NO_2]Cl_2$ at 15K with the electric vector parallel to the extinction directions of an arbitrary crystal face, with inset enlarging the 25 000 to 27 000cm^{-1} area.

The spin-forbidden peaks are positioned at 25 800cm^{-1} and 26 450cm^{-1}. Only the higher energy transition can be seen in the low temperature spectrum of $[Co(NH_3)_5NO_2](CF_3SO_3)_2$ (Figure 4.8).

The vibrational fine structure has a progression of ~380cm^{-1}. This can be attributed to a symmetric metal-nitrogen stretching vibration, which is also seen in the low temperature single crystal optical spectrum of $[Co(NH_3)_6]^{3+}$ [43]. This can also be seen in the spectra measured for $[Co(NH_3)_5NO_2](CF_3SO_3)_2$ (Figure 4.8), and is more clearly resolved for this crystal. The fine structure is also visible for both polarisations in this case. Note that the extinction coefficients for this crystal are only approximate, as the crystal structure of this complex has not been measured and so the density of the crystal is unknown.
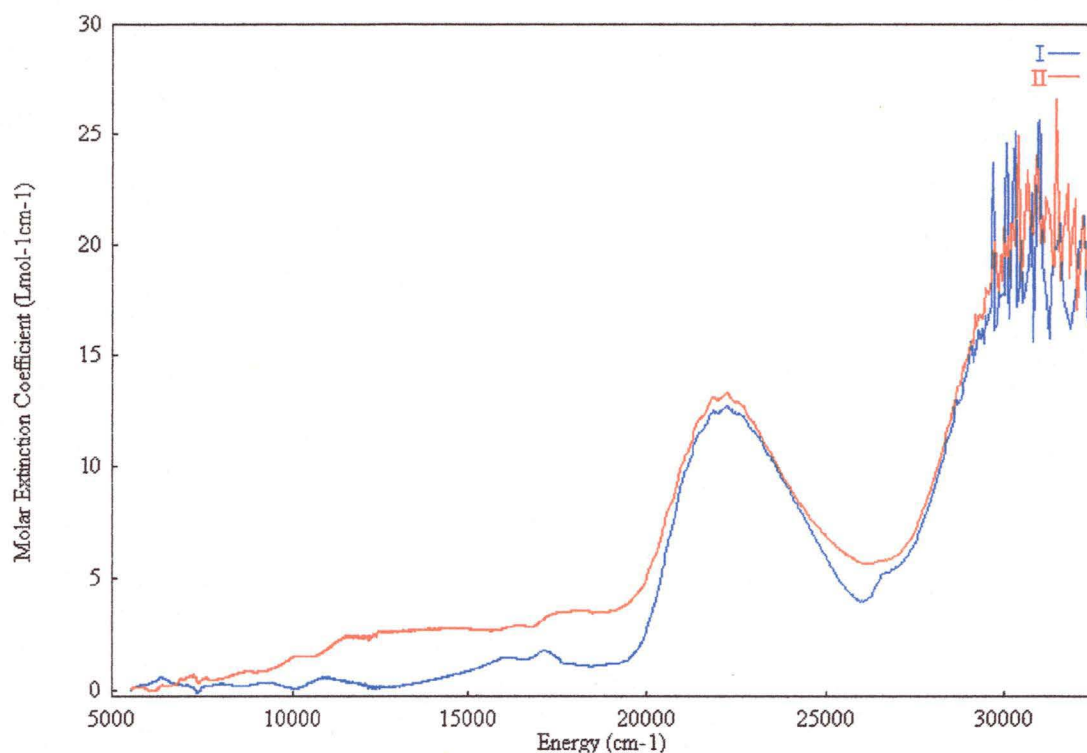
Figure 4.8: The single crystal optical spectrum of $[Co(NH_3)_5NO_2](CF_3SO_3)_2$ at 15K with the electric vector parallel to the extinction directions of an arbitrary crystal face.

As well as being ideal for the measurement of detailed optical spectra, the large plate-like crystals of $[Co(NH_3)_5NO_2](CF_3SO_3)_2$ were also used in the present study for another reason. It has been found that nitro complexes convert to nitrito complexes upon exposure to UV light. It has also been reported that the structure of the photochemically prepared nitrito isomer is different to that prepared by the method of Pentland et al[26]. To see if these differences could be observed in the optical spectrum, the mounted $[Co(NH_3)_5NO_2](CF_3SO_3)_2$ crystal that was used to measure the nitro complex optical spectrum was irradiated for a week with a 254nm source. After confirming that the crystal was still of good optical quality, and did not have the cracks reported by Boldyreva et al.[44] when they tried to irradiate crystals of the complex $[Co(NH_3)_5NO_2]X_2$, X = Cl, Br, I, NO_3, the optical spectrum was remeasured and compared with that of the nitro complex. No differences could be seen, suggesting that isomerization had not occurred to a significant extent. This may have been due to the use of an inadequate UV source, or it could be that the photoisomerism reaction only occurs at the surface of the sample. An examination

of previous literature indicated that this nitro → nitrito photoisomerism has only been measured when using powdered samples or solutions[12-17, 30]. As the latter method results in a much greater surface area compared with a crystal, the second reason may be why no noticeable change was detected for these crystals. Furthermore, Kubota and Ohba[10] cite the experiment carried out by Boldyreva et al.[45], in which they observed a crystal bending toward the irradiating light source, suggesting that this indicates a structural change induced by photoisomerisation at the surface only.

Attempts to prepare crystals of $[Co(NH_3)_5ONO]Cl_2$ were unsuccessful, so the optical spectrum was measured using KBr discs. The spectra measured at room and 15K are shown in Figure 4.9. The room temperature spectrum has been repositioned above the low temperature spectrum for clarity.
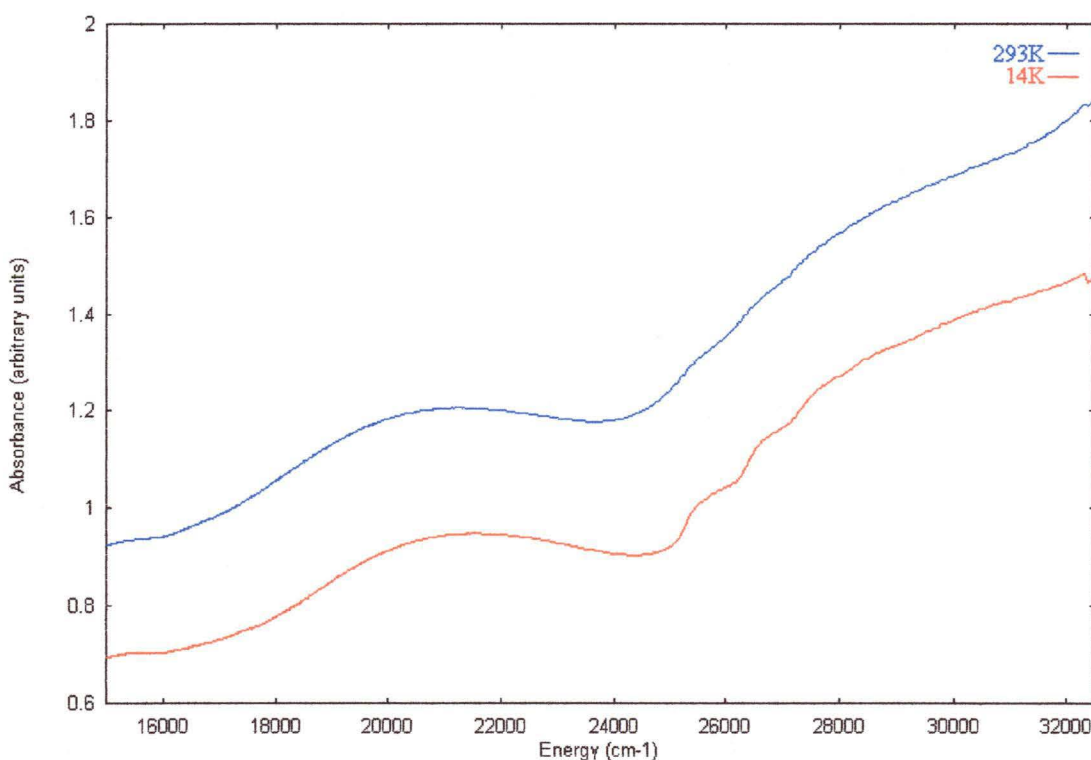

Figure 4.9: The optical spectrum of a KBr disc of $[Co(NH_3)_5ONO]Cl_2$ at room temperature and 14K.

The first broad band is centred at approximately 21 000cm^{-1}. This is higher than the energy of 20 350cm^{-1} measured for an aqueous solution of the complex by Linhard et al.[41] and Seel and Meyer[46], and also higher than the 20 580cm^{-1} quoted by Hitchman and Rowbottom[42]. However, this band is actually three unresolved transitions of

varying intensity, including one at approximately 22 000cm^{-1}, which corresponds to the $^1A_2$ component of the $^1T_1$ transition. This is also present in the $[Co(NH_3)_6]^{3+}$ and $[Co(NH_5NO_2]^{2+}$ spectra as it is unaffected by the axial ligands of the complex, and this may be responsible for the asymmetric shape and relatively high energy for this band.

Perhaps the most interesting feature of this spectrum is the vibrational structure visible on the shoulder of the high intensity charge transfer band above 25 000cm^{-1}. This has a progression of ~1 000cm^{-1}, which is greater than the ~600cm^{-1} progression seen in the same region for $[Cr(NH_3)_5ONO]^{2+}$ ions[27]. In this latter case, the band has been assigned as an n $\rightarrow$ π^* internal nitrite transition, with the 600cm^{-1} progression being in the δ_{NO2} nitrite wagging mode in an excited state, where an electron has been transferred to the nitrite π^* orbital[42]. The band seen in the present spectrum, with a 1 000cm^{-1} progression, may also be due to an internal nitrite n $\rightarrow$ π^* transition. The free nitrite ion has the asymmetric stretch at 1 260cm^{-1} [47], so the peak at ~1 000cm^{-1} may be due to this vibration in an excited state where an electron occupies the antibonding π^* orbital.

The room and low temperature (5K) spectra measured for a single crystal of $[Cr(NH_3)_5ONO]Cl_2$ are shown in Figures 4.10 and 4.11. The first band is centred at 21 550cm^{-1}, which is slightly higher in energy than that measured for this complex in aqueous solution. This was given as 20 750cm^{-1} by Fee et al.[27], and 20 730cm^{-1} by Linhard and Weigel[40]. Very sharp spin forbidden lines are also visible in the low temperature spectrum at 14 895, 14 923 and 15 042cm^{-1} (inset of Figure 4.11).
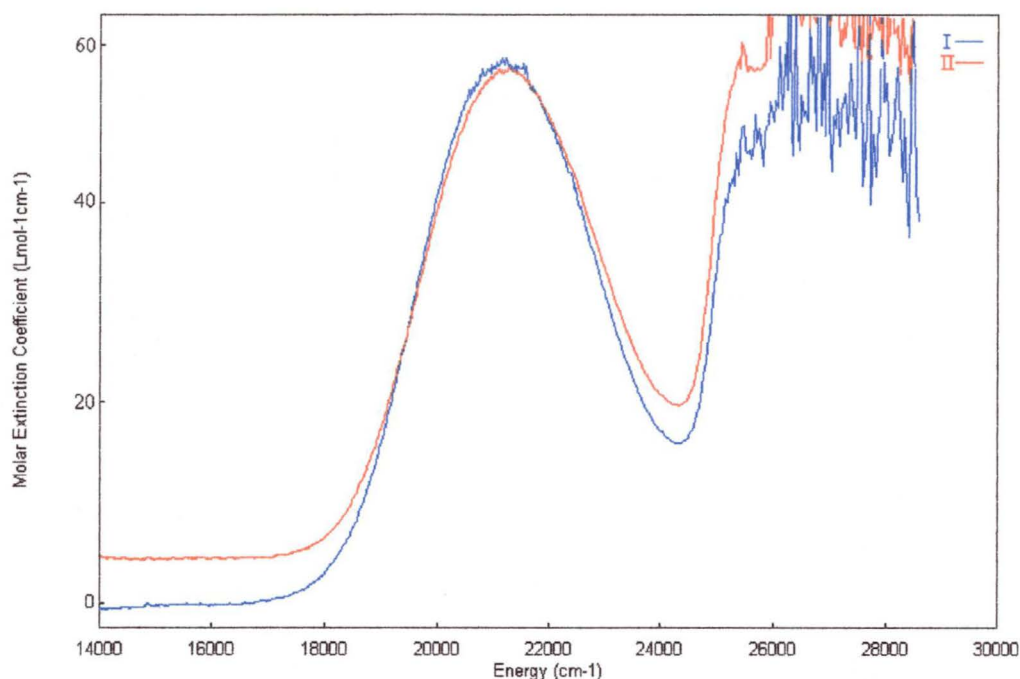
Figure 4.10: The single crystal optical spectrum of $[Cr(NH_3)_5ONO]Cl_2$ at room temperature with the electric vector parallel to the extinction directions of an arbitrary crystal face.

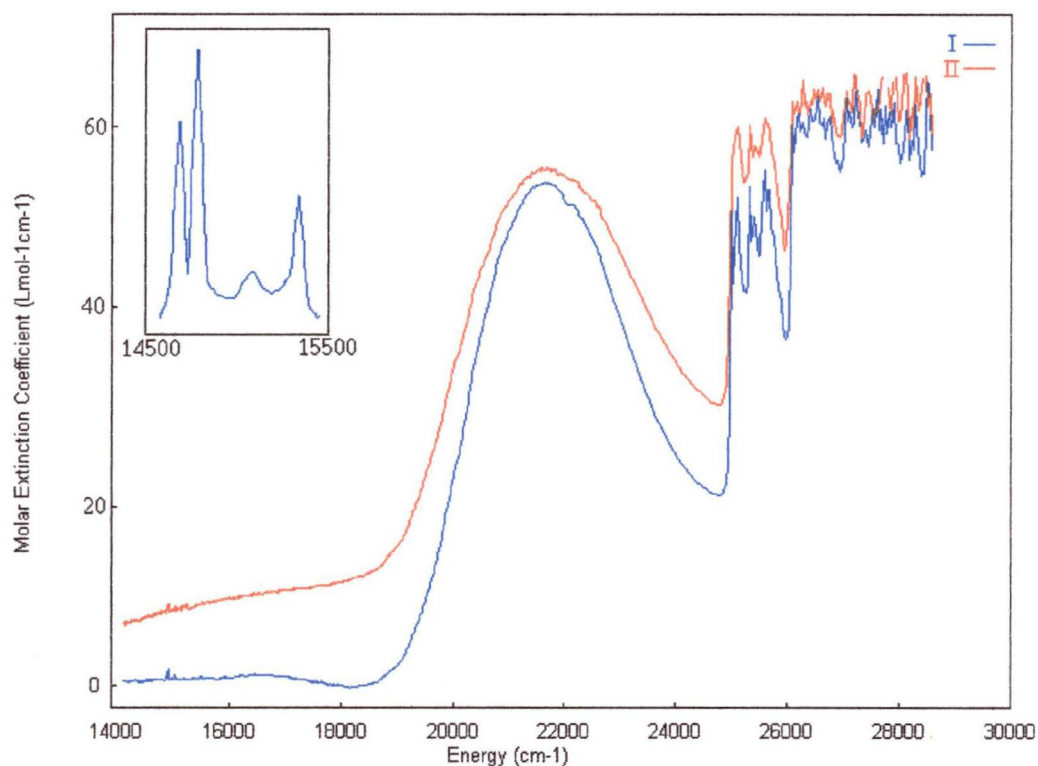**Figure 4.11**: The single crystal optical spectrum of $[Cr(NH_3)_5ONO]Cl_2$ at 5K with the electric vector parallel to the extinction directions of an arbitrary crystal face. The inset is an enlarged section from 14 500 to 15 500cm^{-1} showing the sharp spin-forbidden peaks.

The vibrational progression reported by Fee et al.[27] is not seen in the low temperature spectrum. It is difficult to say what causes the sudden dip at 26 000cm^{-1}, but it may be due to the spectrophotometer rather than any 'real' spectral feature of this complex.

4.4 Analysis of the Band Energies Using the Angular Overlap Model

4.4.1 Cobalt(III)

Unlike chromium(III) complexes, there have been few studies that have used the Angular Overlap Model (AOM) to obtain bonding parameters for ligands in cobalt(III) complexes[38]. A major problem in analysing Co(III) spectra is that few peaks are observed, so there is relatively little experimental data. However, as the cobalt(III) complexes of interest in this work only had two ligand types, it was possible to use the observed transition energies to estimate AOM parameters.

The single crystal optical spectrum of $[Co(NH_3)_6](ClO_4)_2Cl.KCl$ has been measured at low temperature by Wilson and Solomon[43]. It was possible to determine AOM parameters for the amine ligands by making a few assumptions. As is normally assumed for a saturated amine[48], π-bonding was taken to be negligible ($e_\pi = 0cm^{-1}$) and, to simplify matters, each metal-amine bond length was assumed to be equal. Using the Racah parameters of B = 615 and C = 2 640 quoted by Figgis and Hitchman[48] and the program CAMMAG[49], a value of 7 850cm^{-1} for e_σ (NH_3) gave calculated transitions close to those measured by Solomon and Wilson[43]. This is summarised in Table 4.1.

TRANSITION	CALCULATED	OBSERVED
$^1T_1 \leftarrow {}^1A_g$	21 831, 21 834, 21 868	21 900
$^1T_2 \leftarrow {}^1A_g$	30 123, 30 187, 30 267	30 300

Table 4.1: The observed and calculated energies for $[Co(NH_3)_6]^{3+}$ using the AOM model with B = 615, C = 2 640; $e_\sigma(NH_3)$ = 7 850cm^{-1}.

As the bond angles $\angle$N-Co-N do not equal 90°, three slightly different transition energies are calculated for each component of the bands. If an ideal complex of O_h symmetry is used in this calculation, rather than the actual crystal structure, only one value would be calculated for each band.

The $e_\sigma(NH_3)$ determined for $[Co(NH_3)_6]^{3+}$ allows the determination of the AOM parameters for the nitrite ligands in $[Co(NH_3)_5NO_2]^{2+}$ and $[Co(NH_3)_5ONO]^{2+}$. The ammine parameters were scaled in the manner described in Chapter 2 to take into account the different cobalt-ammine bond lengths in these complexes. As the crystal structure of $[Co(NH_3)_6](ClO_4)_2Cl.KCl$ was unavailable, an average bond length of 1.960Å was used in these scaling calculations, as it has been found that the counterion does not greatly affect the geometry of the $[Co(NH_3)_6]^{3+}$ cation in a number of complexes[50].

Using scaled parameters appropriate for the Co-NH$_3$ bonds in $[Co(NH_3)_5NO_2]^{2+}$, a reasonable fit of the spin allowed transition is obtained using just $e_\sigma(NO_2) =$ 8 150cm^{-1} (Table 4.2).

TRANSITION	CALCULATED	OBSERVED
$^1T_1 \leftarrow {}^1A_{1g}$	21 890, 21 932, 22 110	21 865

Table 4.2: The calculated and observed transition energies for $[Co(NH_3)_5NO_2]^{2+}$ with B = 615, C = 2 640; $e_\sigma(NO_2)$ = 8 150cm^{-1}.

However, including the additional data of the spin forbidden peaks allowed the parameter $e_{\pi y}(NO_2)$ to be determined also. The values C = 2 400cm^{-1}, $e_\sigma(NO_2)$ = 7 900cm^{-1} and $e_{\pi y}(NO_2)$ of $-$ 400cm^{-1} resulted in a reasonable fit to the experimental energies (Table 4.3).

TRANSITION	CALCULATED	OBSERVED
$^1T_1 \leftarrow {}^1A_{1g}$	21 844, 22 068, 22 149	21 865
$^3T_1 \leftarrow {}^1A_{1g}$	25 939	25 850
$^3T_2 \leftarrow {}^1A_{1g}$	26 338	26 480
$^1T_2 \leftarrow {}^1A_{1g}$	30 066, 30 566, 30 653	[30 675][a]

Table 4.3: The calculated and observed transition energies for $[Co(NH_3)_5NO_2]^{2+}$ with $B = 615$, $C = 2\,400$; $e_\sigma(NO_2) = 7\,900cm^{-1}$, $e_{\pi y}(NO_2) = -\,400cm^{-1}$ a: $30\,675cm^{-1}$ was the d-d transition assigned by Kiss and Czeglédy[39].

Note that the contentious higher energy band first assigned as a d-d transition by Kiss and Czeglédy[39] and later designated an internal nitrite transition by Linhard et al.[40,41] has also been included in Table 4.3. The calculated values indicate that it is not unreasonable for this peak to be identified as a d-d transition.

Some limitations were encountered when using the above process to determine the AOM parameters for the nitrito ligand in $[Co(NH_3)_5ONO]Cl_2$. Although it is possible to transfer the $e_\sigma(NH_3)$ parameters in a similar manner, the presence of only one band in this spectrum (Figure 4.9) prevented the calculation of both e_σ and $e_{\pi y}$ parameters for the nitrite ligand. Assuming $e_{\pi x} = 0cm^{-1}$, $e_{\pi y} \approx e_\sigma / 7$, as found for various nickel(II) complexes (see Chapter 5), retaining the Racah parameters of $B = 615$ and $C = 2\,640$, and scaling the ammine parameters to take into account differences in bond lengths, values of $e_\sigma(ONO) = 7\,050cm^{-1}$ and $e_{\pi y}(ONO) = 1\,005cm^{-1}$ provided an adequate fit to the experimental data (Table 4.4).

TRANSITION	CALCULATED	OBSERVED
$^1T_1 \leftarrow {}^1A_{1g}$	20 368, 21 008, 22 140	21 000

Table 4.4: The calculated and observed transition energies for $[Co(NH_3)_5ONO]^{2+}$ with $B = 615$, $C = 2\,640$; $e_\sigma(ONO) = 7\,050cm^{-1}$ and $e_{\pi y}(ONO) = 1\,005cm^{-1}$.

Ethylenediamine is a saturated amine, so it is possible to use a scaled value of $e_\sigma(NH_3)$ obtained from the spectrum reported[51] for $[Co(en)_3]^{3+}$, where en = ethylenediamine, to derive bonding parameters for the nitro groups from the spectrum reported for cis-$[Co(en)_2(NO_2)_2]^+$. The two spin allowed d-d transitions at 21 550 and 29 600cm^{-1} could be fitted using B = 615 and $e_\sigma(amine)$ = 7850cm^{-1} as for $[Co(NH_3)_6]^{3+}$ but scaled for bond distance (Table 4.5).

TRANSITION	CALCULATED	OBSERVED
$^1T_1 \leftarrow {}^1A_g$	21 576, 21 577, 21 592	21 550
$^1T_2 \leftarrow {}^1A_g$	29 787, 29 788, 30 254	29 600

Table 4.5: The calculated and observed transition energies for $[Co(en)_3]^{3+}$ with B = 615, C = 2 640; see text for $e_\sigma(amine)$ values.

However, Jørgensen[51] also reports a very broad (halfwidth = 1 700cm^{-1}) spin-forbidden peak centred at approximately 13 700cm^{-1}. Using the above parameters, the lowest energy spin-forbidden peak is at 16 294cm^{-1}. Generally, the parameter C may be altered to obtain a reasonable fit for the spin-forbidden peaks, but in this case this parameter would have to be lowered to an unreasonable value to achieve this. This very broad, low intensity band may be due to an impurity, possibly involving Co(II) as this has d-d transitions that are much lower in energy than Co(III).

It is a more straightforward task to calculate transition energies comparable to experiment for cis-$[Co(en)_2(NO_2)]^+$. Lever[38] quotes values of 22 885 and 31 055cm^{-1} for the two spin-allowed d-d transitions present in the spectrum of this complex. Scaling the AOM parameters previously obtained for the ammine and nitro ligands for the bond lengths in $[Co(NH_3)_5NO_2]^{2+}$, and using B = 615 and C = 2 400, yields transition energies agreeing well with experiment (Table 4.6).

TRANSITION	CALCULATED	OBSERVED
$^1T_1 \leftarrow {}^1A_g$	21 891, 22 776, 22 958	22 885
$^1T_2 \leftarrow {}^1A_g$	30 335, 31 067, 31 637	31 055

Table 4.6: The calculated and observed transition energies for cis-$[Co(en)_2(NO_2)_2]^+$ with B = 615, C = 2 400; see text for e_σ(amine), $e_\sigma(NO_2)$ and $e_{\pi y}(NO_2)$ values.

There has been some disagreement about the assignment of the optical spectrum of the cobalt(III) hexanitro complex, $[Co(NO_2)_6]^{3-}$. Early studies of aqueous solutions assigned a weak band at around 20 830cm^{-1} as the d-d transition, $^1T_{1g} \leftarrow {}^1A_{1g}$[52]. However, Caulton and Fenske[53] pointed out that this suggests a Δ value for the nitro group which is much lower than that suggested by the spectra of mixed ligand nitrite complexes such as $[Co(NH_3)_5NO_2]^{2+}$. They assigned it as a spin-forbidden ligand to metal charge transfer transition. It must also be noted that Buist et al.[52] have used ^{59}Co nmr spectra to suggest that this low energy was due to a pentanitro complex with an aquo or nitrito ligand.

The $e_\sigma(NO_2)$ and $e_{\pi y}(NO_2)$ parameters determined for the mixed ligand complex ion $[Co(NH_3)_5NO_2]^{2+}$ imply a Δ value of $\sim 24\ 500$cm^{-1}. This is close to the position of the first band measured as a potassium chloride disc by Caulton and Fenske[53] for $[Co(NO_2)_6]^{3-}$ with various counterions. However, the molar absorptivity of this peak in solution suggests that it is in fact a charge transfer transition, and not a d-d transition.

The bond length of the cobalt-nitrite bond is shorter in $[Co(NH_3)_5NO_2]Cl_2$ (1.919Å)[54] than in the hexanitro complex (1.952Å)[55]. When this difference is taken into account, the energy of the lowest energy d-d transition can be estimated as 20 600cm^{-1}, which is close to the weak peak originally assigned as a d-d transition. The second d-d transition is calculated at 28 891cm^{-1}, which would be hidden underneath the charge transfer transition at this energy.

The AOM results for cobalt(III) nitrite complexes thus show that the parameters from one calculation may be transferred to another, provided that the difference in bond lengths between the complexes is taken into account by using the r^{-6} relationship described in Chapter 2. The bonding parameters deduced for the nitro group, $e_\sigma \approx 7\ 900 cm^{-1}$ and $e_{\pi y} \approx -400 cm^{-1}$ suggest that this ligand has a similar σ-bonding strength to a saturated amine such as ammonia, and acts as a weak π-acceptor. Although it was not possible to calculate an $e_{\pi y}(ONO)$ parameter for the nitrito group, the spectral analysis shows that this is a much weaker ligand than the nitro group, and the spectra are consistent with it being a weaker σ-donor than NH_3 and a weak π-donor. Further evidence for this will be presented when comparing these parameters with those of nickel(II) nitrite linkage isomers in Chapter 5.

4.4.2 Chromium(III)

A large range of chromium(III) six-coordinate complexes have been studied by optical spectroscopy, as they are of interest photochemically. Sometimes, all three spin allowed transitions and some spin-forbidden peaks are visible in the spectrum[38]. Similarly, a number of workers have used the AOM to parameterise the bonding seen in these complexes[56-62]. One spectral feature of interest for many workers has been the 'ruby' lines, which are very narrow spin-forbidden peaks seen for most chromium(III) complexes. The use of ligand field theory to fit the large splitting of this lowest energy excited state has been the subject of many previous studies, with various interpretations being presented[56-62].

To determine AOM parameters for the nitrito ligand in the complex $[Cr(NH_3)_5ONO]Cl_2$, it was necessary to first determine the $e_\sigma(NH_3)$ parameter. This was calculated in a similar manner to the cobalt(III) complex, by first using the spectrum of $[Cr(NH_3)_6]^{3+}$ to obtain the AOM parameters for the chromium-ammine bonds[47]. Relatively good agreement was reached with the optical spectrum using the Racah parameters $B = 700$, $C = 3\ 100$ and $e_\sigma(NH_3) = 7\ 200 cm^{-1}$ (Table 4.7).

TRANSITION	CALCULATED	OBSERVED
$^2E \leftarrow {}^4A_2$	15 032	15 300
$^4T_2 \leftarrow {}^4A_2$	21 578, 21 587, 21 593	21 550
$^4T_1 \leftarrow {}^4A_2$	28 782, 28 843, 29 097	28 500

Table 4.7: The calculated and observed transition energies for $[Cr(NH_3)_6]^{2+}$ with $B = 700$, $C = 3\ 100$; $e_\sigma(NH_3) = 7\ 200cm^{-1}$.

These results are very similar to those of Vanquickenbourne et al.[63], who found $e_\sigma(NH_3) = 7\ 180cm^{-1}$ and Schönherr et al.[59] who quote a value of $7\ 200cm^{-1}$.

Again, this $e_\sigma(NH_3)$ parameter could be transferred to the $[Cr(NH_3)_5ONO]^{2+}$ ion with appropriate scaling. As described for the cobalt nitrito complex, the $e_{\pi y}(ONO)$ value was calculated by assuming that $e_{\pi y} = e_\sigma / 7$. A reasonable fit of the d-d transition was obtained using $B = 700$, $C = 3\ 150$ and $e_\sigma(ONO) = 6\ 055cm^{-1}$ and $e_{\pi y}(ONO) = 865cm^{-1}$ (Table 4.8).

TRANSITION	CALCULATED	OBSERVED
$^2E \leftarrow {}^4A_2$	14 714, 14 743	14 895, 14 923
$^2T \leftarrow {}^4A_2$	15 193	15 042
$^4T_2 \leftarrow {}^4A_2$	20 768, 21 547, 22 993	21 550

Table 4.8: The calculated and observed transition energies for $[Cr(NH_3)_5ONO]^{2+}$ with $B = 700$, $C = 3\ 150$; $e_\sigma(ONO) = 6\ 055cm^{-1}$, $e_{\pi y}(ONO) = 865cm^{-1}$.

In some cases, it is difficult to calculate a reasonable fit of the low energy spin-forbidden peaks using the AOM. This has been the subject of some discussion, with some authors including spin-orbit coupling to improve their calculations, and resorting to a number of approximations to obtain the Racah parameters[57-62]. Tree's corrections have also been included in these calculations, but from the experimental

data obtained for the complex $[Cr(NH_3)_5ONO]Cl_2$, it was not possible to include these without encountering the problem of overparameterisation.

As in the case for cobalt(III) nitrito complexes, the lack of spectroscopic and structural studies of chromium(III) nitrite complexes meant that there were no further examples to test the transferability of AOM parameters for this type of complex. However, the bonding parameters deduced for the nitrito group in $[Cr(NH_3)_5ONO]^{2+}$ suggest this to be a weaker σ-donor than ammonia, and a weak π-donor. The parameters are similar to those in the analogous Co(III) nitrito complex, though ~14% smaller. This follows the trend in the e_σ parameter which is ~10% smaller for the $[Cr(NH_3)_6]^{3+}$ ion compared with $[Co(NH_3)_6]^{3+}$.

4.5 Density Functional Theory Calculations

Although Density Functional Theory (DFT) has been successfully used to calculate properties of transition metal complexes, there are few studies involving nitrite complexes. Lelj and Adamo[64,65] have used the cobalt pentaammine nitro-nitrito linkage isomerism as an example of inorganic isomeric equilibrium when testing a solvent model that they included in an early version of the DFT program used in the present work. Although they managed to calculate a reasonable geometry for the $[Co(NH_3)_5NO_2]^{2+}$ and $[Co(NH_3)_5ONO]^{2+}$ ions, they were using a basis set which has since been superseded. Their studies were also limited to investigating the effect on the relative energies of the isomers with the inclusion of a self-consistent reaction field to model solvent effects.

A hybrid Hartree Fock- Density Functional Theory (HF-DFT) functional has been used by Ciofini and Adamo[66] to examine the linkage isomerism of $[Co(NH_3)_5ONO]^{2+}$. They have identified a transition state for the nitrito $\rightarrow$ nitro reaction. They also studied this reaction in solution through the use of a polarisable continuum model.

These previous studies have not examined the electronic differences between the cobalt(III) nitro and nitrito isomers, nor has DFT been used in studies of chromium(III) nitrite complexes. Furthermore, there are few studies in which the

results of a DFT or *ab initio* calculation have been compared with those of a ligand field theory model[63,67]. It was therefore decided to carry out DFT calculations as part of the present work.

4.5.1 *Geometry of the Cobalt(III) and Chromium(III) Complex Ions*

A number of calculations were carried out when optimising the geometry of the $[Co(NH_3)_5NO_2]^{2+}$, $[Co(NH_3)_5ONO]^{2+}$, $[Cr(NH_3)_5NO_2]^{2+}$ and $[Cr(NH_3)_5ONO]^{2+}$ complex ions. Chapter 3, Section 3.4.1 describes the general computational method used. In addition to this, four different methods were used: a double-ξ basis set with a polarisation function without (A) and with (B) a gradient correction, and a triple-ξ basis set with a polarisation function and without (C) or with (D) gradient corrections. The letters in brackets will be used throughout this text to denote the different calculations.

The important bond lengths and angles calculated by each method for $[Co(NH_3)_5NO_2]^{2+}$ are listed in Table 4.9. Included in this table are the bond lengths and angles measured experimentally for this complex. Figure 4.12 has also been included to show the numbering system used for this complex and the nitrito complexes.
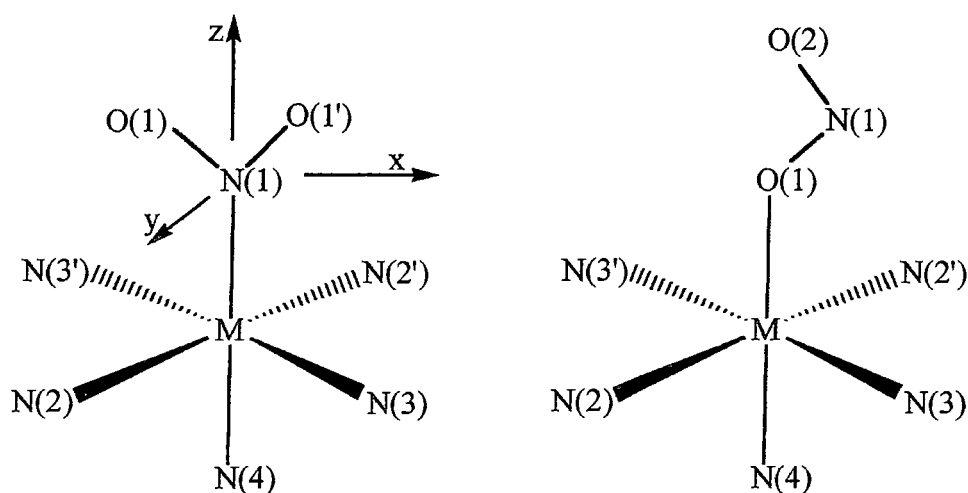

Figure 4.12: The numbering system used for $[Co(NH_3)_5NO_2]^{2+}$, $[Co(NH_3)_5ONO]^{2+}$ and $[Cr(NH_3)_5ONO]^{2+}$ and the axes defined for the complexes.

	A	**B**	**C**	**D**	**EXPT**[54]
Co-N(1)	1.877	1.944	1.885	1.954	1.930
N-O(1)	1.216	1.221	1.210	1.231	1.231
Co-N(2)	1.965	2.034	1.967	2.039	1.967
Co-N(3)	1.965	2.033	1.967	2.035	1.964
Co-N(4)	2.061	2.162	2.061	2.166	1.990
∠O-N-O	125.4	126.0	125.3	125.8	119.8
∠Co-N(1)-O(1)	117.0	117.6	117.4	117.3	120.4

Table 4.9: The calculated bond lengths (Å) and angles (°) of $[Co(NH_3)_5NO_2]^{2+}$ compared with the crystal structure values.

As shown in Table 4.9, and described by previous authors[65], the Local Density Approximation (LDA) is a relatively poor approximation in modelling the weak metal-ligand interactions, but the inclusion of gradient corrections produces calculated bond lengths of the nitro group which are reasonably close to those measured by Boldyreva et al[54]. However, introducing these corrections also lengthens the other bonds as well. Particularly noticeable is the anomalous length of the cobalt-ammine bond *trans* to the cobalt-nitrite bond compared with that observed in the crystal.

The calculated nitrite bond lengths are close to those measured experimentally. However, the bond angles differ somewhat, with the ∠ONO calculated to be up to 6° larger than the measured value. This may be due to hydrogen bonding, as the hydrogens of the equatorial amines are oriented in such a way as to allow an interaction with the oxygens of the nitro group.

The calculated geometries for the $[Co(NH_3)_5ONO]^{2+}$ ion do not compare so well with the experimentally obtained bond lengths and angles (Table 4.10). Note that two sets of experimental data have been included in this table. The first is that measured by Grenthe and Nordin[13] for $[Co(NH_3)_5ONO]Cl_2$ and the second is that measured by Masciocchi et al.[15] for $[Co(NH_3)_5ONO]Br_2$.

	A	B	C	D	EXPT[13]	EXPT[15]
Co-O(1)	1.854	1.880	1.854	1.893	1.927	2.240
O(1)-N(1)	1.379	1.459	1.418	1.477	1.244	
N(1)-O(2)	1.179	1.180	1.172	1.177	1.037	1.136
Co-N(2)	1.955	2.022	1.956	2.022	1.913	2.001
Co-N(3)	1.967	2.033	1.964	2.031	1.952	2.001
Co-N(4)	2.002	2.099	2.012	2.087	1.948	2.162
∠O-N-O	109.6	110.0	112.1	111.0	131.3	
∠Co-O(1)-N	121.3	117.3	114.7	117.1	125.3	180.0

Table 4.10: The calculated bond lengths and angles of $[Co(NH_3)_5ONO]^{2+}$ compared with the crystal structure values. Note that not all of the important bond lengths and angles are given by Masciocchi et al[15].

It is clear that there is considerable variation between the two experimentally obtained structures. The first, reported by Grenthe and Nordin[13], was determined for a single crystal of $[Co(NH_3)_5ONO]Cl_2$. This can be regarded as quite unreliable, especially for the nitrito group, as this was disordered. The second was measured by X-ray powder diffraction, and this was a photochemically prepared sample of the nitrito isomer from $[Co(NH_3)_5NO_2]Br_2$. The 180° angle, ∠Co-O(1)-N, is particularly unusual as in other cobalt nitrito complexes this angle is not linear. The calculations also show that the cobalt-ammine bond *trans* to the cobalt-nitrito bond is again slightly longer than the other bonds, but this is not as pronounced as it is in the nitro isomer.

Table 4.11 lists the important bond lengths and angles for the complex ion $[Cr(NH_3)_5ONO]^{2+}$.

	A	B	C	D	EXPT[68]
Cr-O(1)	1.861	1.849	1.863	1.859	1.970
O(1)-N	1.427	1.556	1.436	1.563	1.191
N-O(2)	1.166	1.160	1.165	1.160	1.190
Cr-N(2)	2.091	2.165	2.091	2.166	2.062
Cr-N(3)	2.104	2.176	2.107	2.178	2.062
Cr-N(4)	2.148	2.258	2.144	2.248	2.063
∠O-N-O	113.3	110.9	113.6	111.6	122.0
∠Cr-O(1)-N	118.0	121.9	118.5	122.5	125.9

Table 4.11: The calculated bond lengths and angles of $[Cr(NH_3)_5ONO]^{2+}$ compared with the crystal structure values.

Again, the nitrito group is not well modelled by the calculations. This nitrito group is unusual in that it has N-O bonds of equal length. As with the other complexes, the Cr-NH$_3$ bond *trans* to the Cr-ONO bond is calculated to be much longer than that seen experimentally.

4.5.2 Comparison of the Calculated Energies of the Co(III) and Cr(III) Isomers

Total energies were calculated for the cobalt(III) isomers and the analogous chromium(III) isomers (Table 4.12).

	A (eV)	B (eV)	C (eV)	D (eV)
$[Co(NH_3)_5NO_2]^{2+}$	-118.34	-108.47	-118.74	-109.00
$[Co(NH_3)_5ONO]^{2+}$	-117.49	-107.86	-117.98	-108.59
$[Cr(NH_3)_5NO_2]^{2+}$	-119.77	-110.74	-120.23	-111.32
$[Cr(NH_3)_5ONO]^{2+}$	-119.70	-110.79	-120.23	-111.52

Table 4.12: The calculated energies for the cobalt(III) and chromium(III) isomers.

There is a clear difference between the energies calculated when using gradient corrections and when not using these. For the cobalt(III) isomers, the energy of the nitrito isomer is always higher than the nitro isomer, which is in agreement with experiment. However, for chromium(III), this changes depending on which method

is used. Given that the only isomer seen experimentally is the nitrito complex, it may be assumed that the nitrito isomer is lower in energy than the nitro isomer. This is the case when incorporating gradient corrections into the calculation, but not when these are absent. The calculated energy difference between the nitro and nitrito isomers of $[Co(NH_3)_5NO_2]^{2+}$ was 0.41eV, which is of the same order of magnitude as the experimental value of 0.943eV [69].

The greater stability of the nitro isomer for Co(III) may be related to the filled t_{2g} d-shell which occurs for this metal ion. The empty π^* orbital can interact with the t_{2g} orbitals when the nitrite is N-bonded, and this has a stabilizing effect, as represented by the simple molecular orbital diagram shown in Figure 4.13.
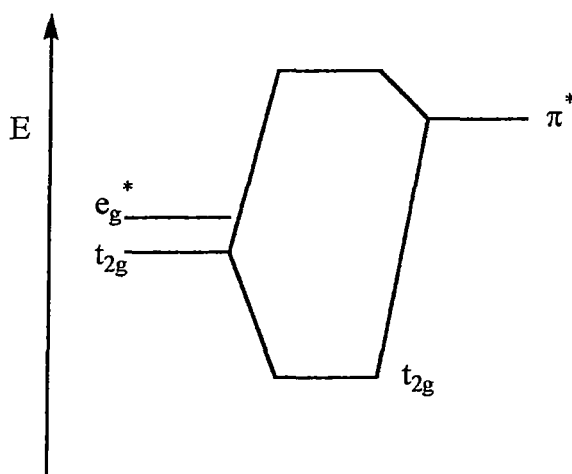

Figure 4.13: The effect of the interaction between the π^* orbital of NO_2^- and the t_{2g} orbitals of a metal ion.

As the chromium(III) ion has only half-filled t_{2g} orbitals, this stabilising effect would only be half as great as that for cobalt(III). However, the interaction of the filled π ligand orbitals of the nitrito group on the t_{2g} orbitals (Figure 4.14) is destabilizing when the t_{2g} orbitals are filled, and stabilizing when these are not filled. Therefore, it is possible that the effect of this stabilizing interaction for the Cr(III) is greater than the stabilizing effect of the nitro coordination π^* interaction discussed above, and this leads to a more stable nitrito isomer for chromium(III).
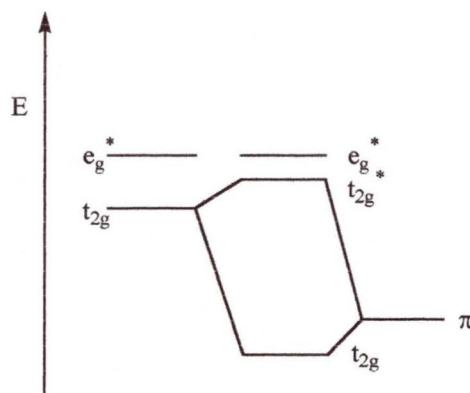
Figure 4.14: The effect of the interaction between the filled π orbital of the nitrito ligand and the t_{2g} orbitals.

4.5.3 Comparison of the DFT Calculations with the AOM Results

The important orbital energies calculated using DFT for the complex ions $[Co(NH_3)_5NO_2]^{2+}$ and $[Co(NH_3)_5ONO]^{2+}$ are shown in Figure 4.15.
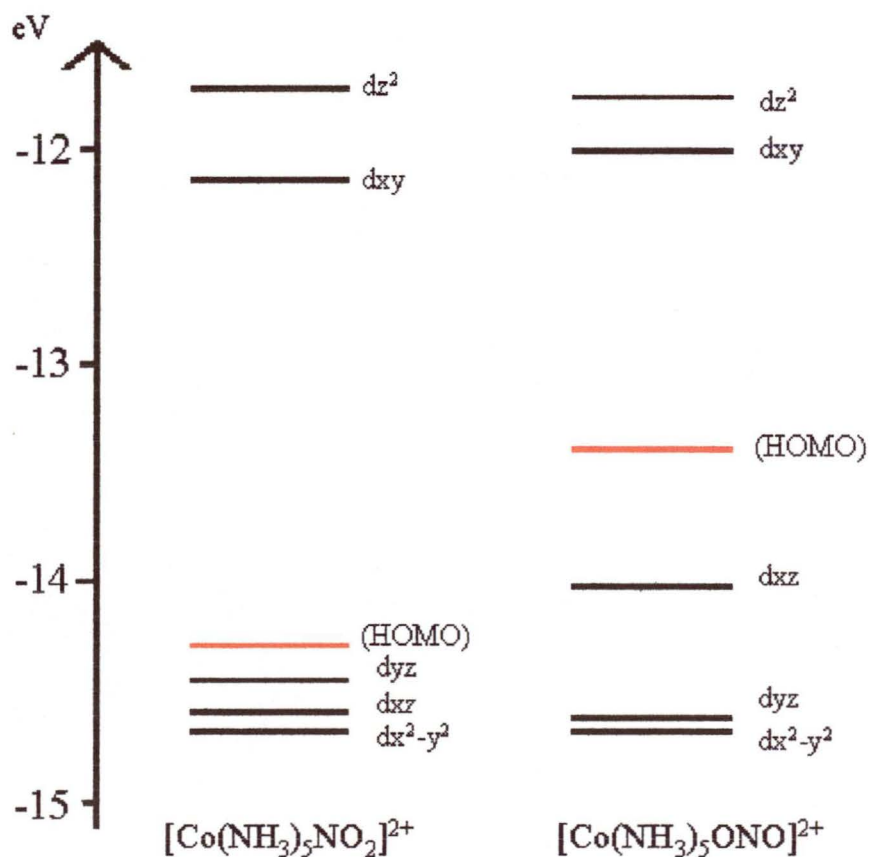
Figure 4.15: The calculated energies of the important orbitals of $[Co(NH_3)_5NO_2]^{2+}$ and $[Co(NH_3)_5ONO]^{2+}$. Ligand based orbitals are marked in red.

Marked upon this diagram is a ligand-based orbital which is calculated to lie between the t_{2g} and e_g d orbitals for both the nitro and nitrito complexes. For the nitro complex, the t_{2g} orbitals are quite similar in energy, with the difference between the dyz and dxy orbitals being 0.3eV, and the filled ligand based orbital is only 0.1eV higher in energy than the dyz orbital. As DFT tends to underestimate the energy of the metallic orbitals, it is possible that this ligand-based orbital should really be below these metal orbitals, thus conforming to the simple molecular orbital approach to bonding in transition metal complexes.

There is also quite a high degree of covalency in these higher energy d-orbitals. The dx^2-y^2 and dxz orbitals of the nitro isomer have greater than 88% d character, but this reduces to 62% for the empty dxy orbital, and only 50% for the empty dz^2 and filled dyz orbitals. Similar results are seen for the nitrito isomer, with the highest energy t_{2g} orbital, dxz, having only 46% d character.

It is possible to calculate a Δ value for the two isomers by subtracting the average energy of the t_{2g} orbitals from that of the e_g orbitals. This gave $\Delta = 21\ 525\text{cm}^{-1}$ for the nitro complex and $\Delta = 20\ 594\text{cm}^{-1}$ for the nitrito complex. These values are comparable to those obtained via the AOM, which are $23\ 280\text{cm}^{-1}$ and $21\ 506\text{cm}^{-1}$, respectively. The DFT calculations correctly reproduce the fact that nitrite is a "weaker" ligand when it bonds via oxygen compared with nitrogen. Figure 4.15 shows that the dz^2 orbital is considerably higher in energy than dxy for $[Co(NH_3)_5NO_2]^{2+}$, in agreement with the nitro group being a stronger σ-donor than NH_3. While this energy difference is much smaller for $[Co(NH_3)_5ONO]^{2+}$, dz^2 is still higher in energy than dxy, implying that the nitrito ligand is a stronger σ-donor than ammonia, which contradicts the AOM interpretation. The dyz orbital is very close in energy to dx^2-y^2 for both isomers, in agreement with the expectation that these two orbitals should be essentially non-bonding. For the nitro isomer, the dxz orbital is slightly lower in energy than dyz, while for the nitrito isomer dxz is somewhat higher than dyz. This is consistent with the AOM analysis which deduced that the nitro group is a weaker π-acceptor, while the nitrito group acts as a moderate π-donor.

The dxz orbitals of $[Co(NH_3)_5NO_2]^{2+}$ and $[Co(NH_3)_5ONO]^{2+}$ are illustrated in Figure 4.16. It can be seen for the nitro isomer that there appears to be little π-bonding, which is consistent with the small interaction suggested by the AOM. For the nitrito isomer, there is considerably more, again being consistent with the AOM results, which implied a significant π-donor interaction of the nitrite in this coordination mode.
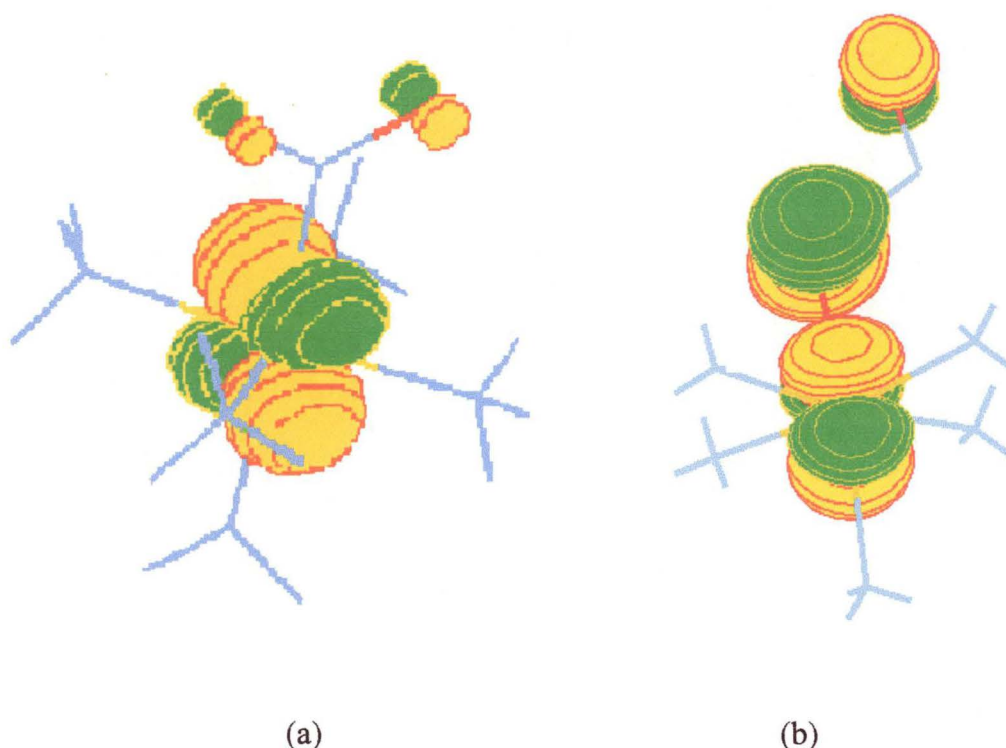

(a)   (b)

Figure 4.16: The dxz orbital of (a) $[Co(NH_3)_5NO_2]^{2+}$ and (b) $[Co(NH_3)_5ONO]^{2+}$.

Similar comparisons may be made for the chromium nitro and nitrito complexes. In this case, the energy diagram (Figure 4.17) is complicated by the presence of unpaired electrons, which results in the calculation of two sets of orbitals for the two possible electron spins.
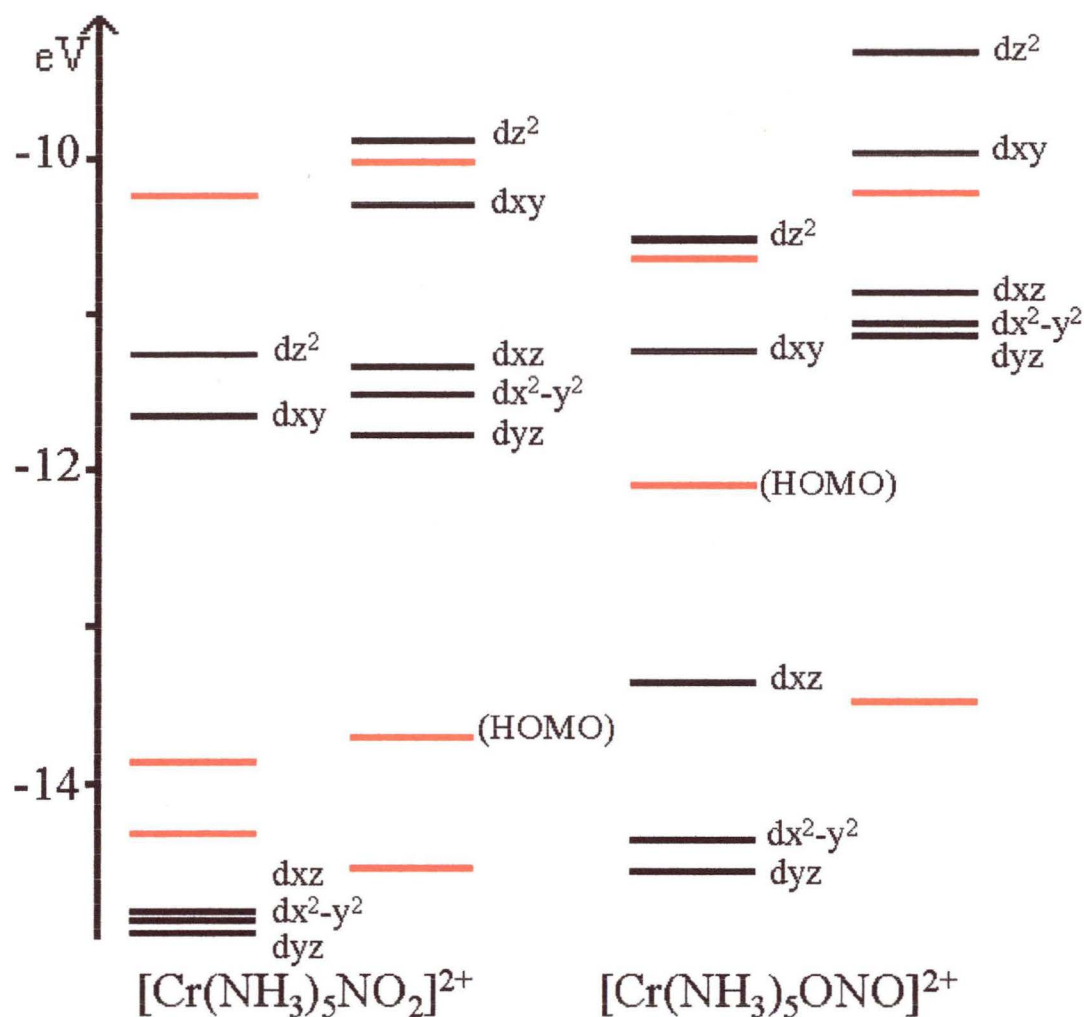
Figure 4.17: The calculated energies of the important orbitals of $[Cr(NH_3)_5NO_2]^{2+}$ and $[Cr(NH_3)_5ONO]^{2+}$. Note the two spins, α and β have been separated and that the orbitals marked in red are predominantly ligand based.

Again, predominantly ligand based orbitals lie between the metal orbitals and the orbitals are quite covalent, with the higher energy e_g orbitals of the nitro complex having 67% and 52% d character for the dxy and dz^2 orbitals, respectively. The nitrito complex has a lower degree of covalency, with both the dxy and dz^2 orbitals with over 70% d character.

The Δ values calculated for the nitro and nitrito isomers were 27 705cm^{-1} and 26 176cm^{-1} respectively. This follows the trend seen for the analogous cobalt(III) complexes. The relative energies of the d-orbitals are also similar to the Co(III) complexes.

4.6 Summary

The infrared and Raman spectra of $[Co(NH_3)_5NO_2]^{2+}$, $[Co(NH_3)_5ONO]^{2+}$ and $[Cr(NH_3)_5ONO]^{2+}$ have been used to confirm the assignments of the three nitrite vibrations. For these complexes, unlike the free nitrite ion, the asymmetric stretch is higher in energy than the symmetric stretch.

Single crystal optical spectra of $[Co(NH_3)_5NO_2]^{2+}$ and $[Cr(NH_3)_5ONO]^{2+}$ were used to obtain AOM bonding parameters for the nitrite ion in its two monodentate coordination modes. These showed that the nitro group is the stronger ligand, with a higher value of e_σ and a negative $e_{\pi y}$ parameter, indicating back-bonding. In contrast, the nitrito group is a weak σ-donor and a π-donor.

DFT calculations have been used to determine the ground state orbital energies and confirm that nitrito coordination is slightly less stable for the Co(III) ion. The Δ values from these calculations were similar to those obtained using the AOM and the orbital energies confirmed that, relatively speaking, the nitrite ion acts as a π-acceptor when it bonds via nitrogen compared with when it bonds via oxygen.

4.7 References

1. Tassaert, *Ann. Chem. Phys.*, **28**(1), 92, (1798).

2. Gibbs W. and Genth F.A., *American Journal of Science*, **24**, 86-107, (1857).

3. Jørgensen S.M., *Z. Anorg. Chem.*, **5**, 169, (1894).

4. Werner A., *Neuere Anschauungen*, Vieweg, Braunschwieg, (1920).

5. Basolo F., Pearson R., Henry P.M. and Bergmann J.G., *J. Amer. Chem. Soc.*, **76**, 5920-5923, (1954).

6. Murmann R.K. and Taube H., *J. Amer. Chem. Soc.*, **78**, 4886-4890, (1956).

7. Wendlandt W.W. and Woodlock J.H., *J. Inorg. Nucl. Chem.*, **27**, 259-260, (1965).

8. Jackson W.G., Lawrance G.A., Lay P.A. and Sargeson A.M., *Inorg. Chem.*, **19**, 904-910, (1980).

9. Balzani V., Moggi L., Scandola F. and Carassiti V., *Inorg. Chim. Acta Rev.*, 7-34, (1967).

10. Kubota M. and Ohba S., *Acta Cryst.*, **B48**, 627-632, (1992).

11. Sastri V.S., *Z. Phys. Chem.*, **84(1-4)**, 10-17, (1973).

12. Scandola M.A., Bartocci C., Scandola F. and Carassiti V., *Inorg. Chim. Acta*, **28**, 151-158, (1978).

13. Grenthe I. and Nordin E., *Inorg. Chem.*, **18(7)**, 1869-1875, (1979).

14. Valentine Jr. D., *Adv. Photochem.*, **6**, 123-192, (1968).

15. Masciocchi N., Kolyshev A., Dulepov V., Boldyreva E. and Sironi A., *Inorg. Chem.*, **33**, 2579-2585, (1994).

16. Scandola F., Bartocci C. and Scandola M.A., *J. Phys. Chem.*, **78(6)**, 572-575, (1974).

17. Heyns A.M. and Dc Waal D., *Spectrochim. Acta*, **45A(9)**, 905-909, (1989).

18. Balzani V., Ballardini R., Sabbatini N. and Moggi L., *Inorg. Chem.*, **7(7)**, 1398-1404, (1968).

19. Cai J., Myrczek J., Chun H. and Bernal I., *J. Chem. Soc. Dalton Trans.*, 4155-4160, (1998).

20. Bernal I. and Certrullo J., *Inorg. Chim. Acta*, **134**, 105-112, (1987).

21. Palmer B.J. and Hill R.H., *J. Photochem. Photobiol. A: Chem.*, **72**, 243-249, (1993).

22. Boldyreva E.V., Ahsbahs H., Naumov D.Y. and Kutoglu A., *Acta Cryst.*, **C54**, 1378-1383, (1998).

23. Boldyreva E.V., Naumov D.Y. and Ahsbahs H., *Acta Cryst.*, **B54**, 798-808, (1998).

24. Boldyreva E.V., Kuzmina S.L. and Ahsbahs H., *J. Struct. Chem.*, **39(3)**, 343-349, (1998).

25. Boldyreva E.V., Naumov D.Y. and Ahsbahs H., *J. Struct. Chem.*, **39(3)**, 350-361, (1998).

26. Boldyreva E.V., Kuzima S.L. and Ahsbahs H., *J. Struct. Chem.*, **39(5)**, 762-773, (1998).

27. Fee W.W., Garner C.S. and Harrowfield J.N.MacB., *Inorg. Chem.*, **6(1)**, 87-92, (1967).

28. De Leo M.A. and Ford P.C., *Coord. Chem. Rev.*, **208**, 47-59, (2000).

29. Pentland R.B., Lane J.J. and Quagliano J.V., *J. Amer. Chem. Soc.*, **78**, 887-889, (1956).

30. Johnson D.A. and Pashman K.A., *Inorg. Nucl. Letters*, **11**, 23-28, (1975).

31. Mori M., *Inorg. Synth.*, **5**, 133-135, (1957).

32. Kyuno E., Kamada M. and Tanaka N., *Bull. Chim. Soc. Jpn.*, **40**, 1848-1854, (1967).

33. Dixon N.E., Jackson W.G., Lawrance G.A. and Sargeson A.M., *Inorg. Synth.*, **22**, 103-107, (1983).

34. The structure of the chloride analogue, $[Co(NH_3)_6]Cl_3$, has been previously reported: Reynhardt E.C., *J. Solid State Chem.*, **43(3)**, 334-338, (1982).

35. Nakagawa I. and Shimanouchi T., *Spectrochim. Acta*, **23A**, 2099-2117, (1967).

36. Le Postollec M., *J. Chim. Phys. Phys-Chem. Biol.*, **72(5)**, 675-683, (1975).

37. Nakamoto K., Fujita J. and Murata H., *J. Amer. Chem. Soc.*, **80**, 4817-4823, (1958).

38. Lever A.B.P., *Inorganic Electronic Spectroscopy (2nd Edition)*, Elsevier Science Publishers, Amsterdam, (1984).

39. Kiss A. and Czeglédy D., *Z. anorg. allg. Chem.*, **235**, 407-426, (1938).

40. Linhard M. and Weigel M., *Z. anorg. Chem.*, **267**, 113-120, (1951).

41. Linhard M., Siebert H. and Weigel M., *Z. anorg. Chem.*, **278**, 287-298, (1955).

42. Hitchman M.A. and Rowbottom G.L., *Coord. Chem. Rev.*, **42**, 55-132, (1982).

43. Wilson R.B. and Solomon E.I., *J. Amer. Chem. Soc.*, **102(12)**, 4085-4095, (1980).

44. Boldyreva E.V., Virovets A.V., Burleva L.P., Dulepov V.E. and Podberezskaya N.V., *J. Struct. Chem.*, **34(4)**, 602-614, (1993).

45. Boldyreva E.V., Sidel'nikow A.A., Chupakhin A.P., Lyakhov N.Z. and Boldyrev V.V., *Dokl. Acad. Nauk. SSSR*, **277(4)**, 893-896, (1984).

46. Seel F. and Meyer D., *Z. anorg. allg. Chem.*, **408**, 275-282, (1974).

47. Chatt J., Duncanson L.A., Gatehouse B.M., Lewis J., Nyholm R.S., Tobe M.L., Todd P.F. and Venanzi L.M., *J. Chem. Soc.*, 4073-4080, (1959).

48. Figgis B.N. and Hitchman M.A., *Ligand Field Theory and its Applications*, Wiley-VCH, New York, (2000).

49. Cruse D.A., Davies J.E., Gerloch M., Harding J.H., Mackey D., McMeeking R.F., CAMMAG, a Fortran Package, University of Cambridge, (1979).

50. Bygott A.M.T. and Sargeson A.M., *Inorg. Chem.*, **37**, 4795-4806, (1998).

51. Jørgensen C.K., *Acta Chem. Scand.*, **8**, 1502-1512, (1954).

52. Buist R.I., Au-Yeng S.C.F. and Eaton D.R., *Can. J. Chem.*, **63**, 3558-33567, (1985).

53. Caulton K.G. and Fenske R.F., *Inorg. Chem.*, **6**, 562-568, (1967).

54. Boldyreva E.V., Kiviskoski J. and Howard J.A.K., *Acta Cryst.*, **C53**, 523-526, (1997).

55. Ohba S., Toriumi K., Sato S. and Saito Y., *Acta Cryst.*, **B34**, 3535-3542, (1978).

56. Lowry R.K. and Perumareddi J.R., *J. Phys. Chem.*, **74(6)**, 1371-1376, (1970).

57. Flint C.D. and Matthews A.P., *J. Chem. Soc. Faraday Trans. 2*, **69**, 419-425, (1973).

58. Decurtins S., Güdel H.U. and Neuenschwander K., *Inorg. Chem.*, **16(4)**, 796-799, (1977).

59. Schönherr T., Wiskemann R. and Mootz D., *Inorg. Chim. Acta*, **221**, 93-98, (1994).

60. Schönherr T., Itoh M. and Urushiyama A., *Bull. Chem. Soc. Jpn.*, **68**, 2271-2276, (1995).

61. Urushiyama A., Itoh M. and Schönherr T., *Bull. Chem. Soc. Jpn.*, **68**, 594-603, (1995).

62. Schönherr T., Atanasov M. and Hauser A., *Inorg. Chem.*, **35**, 2077-2084, (1996).

63. Vanquickenbourne L.G., Coussens B., Postelman D., Ceulemans A. and Pierloot K., *Inorg. Chem.*, **30**, 2978-2986, (1991).

64. Adamo C. and Lelj F., *Chem. Phys. Lett.*, **223**, 54-60, (1994).

65. Lelj F. and Adamo C., *Theor. Chim. Acta*, **91**, 199-214, (1995).

66. Ciofini I. and Adamo C., *J. Phys. Chem. A*, **105**, 1086-1092, (2001).

67. Deeth R.J., *J. Chem. Soc. Dalton Trans.*, 664-669, (2001).

68. Nordin E., *Acta Cryst.*, **B34**, 2285-2288, (1978).

69. Bozoglián F., González G., Martinez M., Queirolo M. and Sienra B., *Inorg. Chim. Acta*, **318**, 191-196, (2001).

CHAPTER 5

Nickel(II) Complexes with Monodentate Nitrite Ligands

The nitrite ion may adopt a number of different coordination modes in nickel(II) complexes. Most of the coordination modes illustrated in Chapter 1, Figure 1.3, have been seen experimentally for such complexes[1]. Some of these modes are monodentate and these will be discussed in this chapter. Complexes in which the nitrite ligand coordinates via chelating and bridging will be the subjects of Chapter 6.

Previous studies of nickel(II) nitrites with amine ligands of varying steric bulk have been carried out[2-4]. One of the aims of these studies was to investigate the idea that steric crowding may influence the manner of nitrite coordination. Although this is difficult to prove, it has been suggested that the nitrito coordination mode is favoured over the more usual nitro mode when the steric bulk of the amine ligands is increased[1]. The reason for this is illustrated in Figure 5.1.

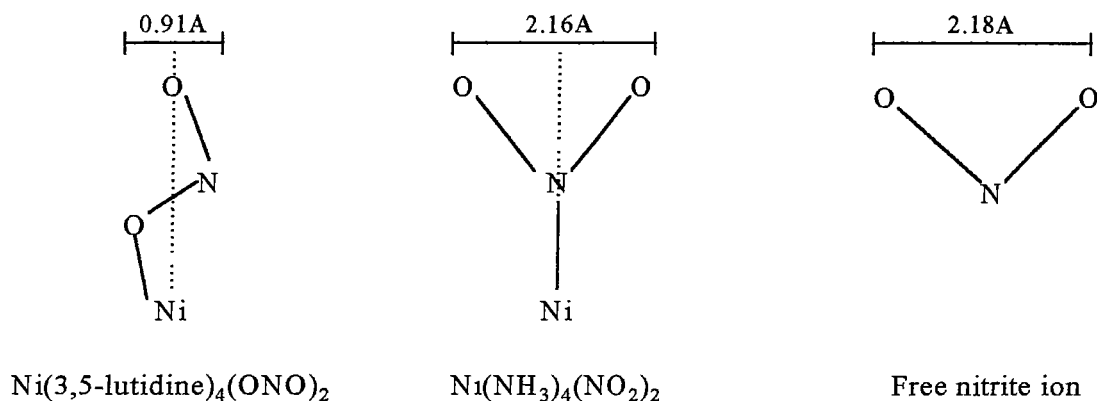Ni(3,5-lutidine)$_4$(ONO)$_2$ Ni(NH$_3$)$_4$(NO$_2$)$_2$ Free nitrite ion

Figure 5.1: A comparison of the geometry of the nitrite ligand in different coordination modes.

Figure 5.1 shows that the nitrito coordination mode takes up less space in the first coordination sphere, which may be advantageous when the nickel ion is surrounded by bulky ligand groups. It must be noted, however, that it is possible that a

combination of factors may cause this behaviour, and it was hoped that the present work would clarify this.

In general, nickel(II) complexes have been well studied by optical spectroscopy, partly due to the interest resulting from the fact that these can have coordination numbers ranging from two to seven[5]. Up to three bands occur for octahedral nickel(II) complexes and spin forbidden peaks may also be seen. Tetragonally distorted, high spin octahedral complexes with the general formula *trans*-NiL_4X_2 are of particular interest, as the bands may split into two or three components. The information obtained from spectra of this type of complex has contributed to the development of the theory of low symmetry complex spectra[5]. Nickel(II) nitrite complexes of the general formula $Ni(diamine)_2(NO_2)_2$ fall into this category, as the nitrite ligands generally adopt a *trans* configuration.

There have been few studies involving the derivation of nitrite AOM bonding parameters[6-11]. Nickel(II) nitrite complexes are ideal for this purpose, for not only can a comparison be made between the different coordination modes, but the spectra also tend to have many features, which helps reduce the number of assumptions made when using the AOM to fit the data. The recent preparation of nitro and nitrito isomers of the complex $[Ni(1-(2-aminoethyl)piperidine)_2(NO_2)_2]$[12] has provided a good example for a direct comparison of the AOM bonding parameters derived for monodentate nitro and nitrito coordination.

To compare the O-bonded and N-bonded coordination modes, single crystal optical spectra were measured, and AOM bonding parameters were determined for both modes. These results were correlated with those obtained by DFT calculations. DFT results were also used in an attempt to identify the nature of the transition seen in the spectrum of the nitro complexes at approximately $20\ 000cm^{-1}$. Again, both infrared and Raman spectra were recorded to determine the nitrite vibrational energies, to supplement previous measurements.

5.1 Experimental

The complex [Ni(3,5-lut)$_4$(ONO)$_2$], where 3,5-lut = 3,5-lutidine, was prepared by adding neat 3,5-lutidine (0.01mol) to a methanolic nickel nitrite solution (0.002mol in 10mL methanol). This methanolic solution had been prepared via the metathetic reaction of nickel nitrite and sodium nitrite in cold methanol. Recrystallisation from a 50:50 mixture by volume of acetonitrile and dichloromethane gave large, deep blue crystals. Microanalysis: found, calculated: %N 14.47, 14.51; %C 57.92, 58.02; %H 6.39, 6.26%. [Ni(3,5-lut)$_4$Br$_2$] was prepared by the addition of an ethanolic solution of 3,5-lutidine (0.01mol) to an ethanolic solution of nickel bromide (0.002mol). The light blue complex precipitated immediately from solution, and could be recrystallised from ethanol to give very small blue crystals. Microanalysis: found, calculated: %N 8.61, 8.66; %C 51.93, 51.97; %H 5.57, 5.61%.

K$_4$[Ni(NO$_2$)$_6$].H$_2$O (0.01mol) was prepared via the method of Goodgame and Hitchman[13]. This was ground to a fine powder and added to an excess of neat N,N-dimethylethylenediamine (0.05mol). The addition of chloroform (10mL) resulted in a pink solution, from which large blue crystals of [Ni(N,N-dimen)$_2$(ONO)$_2$] formed after a few days at room temperature. Microanalysis: found, calculated: %N 25.53, 25.70; %C 29.44, 29.38; %H 7.33, 7.39%.

Although the preparation of [Ni(isoquinoline)$_4$(ONO)$_2$] has been published[14], it was found that the following method provided small crystals of suitable quality for single crystal spectroscopic measurements. An excess of neat isoquinoline (0.05mol) was added to ground K$_4$[Ni(NO$_2$)$_6$].H$_2$O (0.01mol). This was stirred for approximately half an hour. The addition of chloroform (15mL) dissolved the desired complex, leaving the unreacted K$_4$[Ni(NO$_2$)$_6$].H$_2$O and sodium nitrite to be filtered from this dark green solution. This solution was left to slowly evaporate at room temperature, with small grey crystals forming after a few days. Microanalysis: found, calculated: %N 12.39, 12.60; %C 64.51, 64.79; %H 4.17, 4.23%.

[Ni(tn)$_2$(NO$_2$)$_2$], with tn = 1,3-diaminopropane, was prepared via the method of Green and Bell[15]. Recrystallisation from methanol gave very large pink crystals of

good optical quality. Microanalysis: found, calculated: %N 28.07, 28.12; %C 24.24, 24.10; %H 6.77, 6.74%.

[Ni(1,2-diamino-2-methylpropane)$_2$(NO$_2$)$_2$].0.5H$_2$O and the nitro and nitrito isomers of [Ni(1-(2-aminoethyl)piperidine)$_2$(NO$_2$)$_2$] were prepared as described by Laskar et al.[16] and Das et al[12]. Microanalysis: [Ni(1-(2-aminoethyl)piperidine)$_2$(NO$_2$)$_2$] found, calculated: %N 20.69, 20.65; %C 41.49, 41.30%; %H 8.05, 7.92; [Ni(1-(2-aminoethyl)piperidine)$_2$(ONO)$_2$] found, calculated: %N 20.79, 20.65; %C 41.29, 41.30; %H 8.11, 7.92%. [Ni(1,2-diamino-2-methylpropane)$_2$(NO$_2$)$_2$].0.5H$_2$O was characterised by its infrared spectrum. [Ni(1-(2-aminoethyl)piperidine)$_2$Br$_2$].H$_2$O was prepared by adding the ligand (0.002mol) to a methanolic suspension of nickel bromide (0.001mol). The green solution was stirred and decanted. After leaving it overnight, very small pale blue crystals of the desired product were collected. Microanalysis found, calculated: %N 10.64, 10.67; %C 32.03, 32.21; %H 6.36, 6.52%.

Infrared, Raman and optical spectroscopic measurements were carried out as described in Chapters 3 and 4, as were the microanalyses.

5.2 Vibrational Spectroscopy

The infrared spectra of many of these nickel(II) amine nitrite complexes have been measured previously, but few Raman spectra are available for such complexes. As numerous peaks due to the amine ligands can be seen in the IR spectrum, it was found that the measurement of both spectra was of great assistance when assigning the nitrite peaks. For some of the compounds with more complex spectra, a comparison of their infrared and Raman spectra with those measured for analogous nickel halide complexes also assisted in the peak assignment. Figures 5.2, 5.3 and 5.4 are included as examples of this, as these show the infrared and Raman spectra of the complex [Ni(1-(2-aminoethyl)piperidine)$_2$(ONO)$_2$] and the infrared spectrum of its corresponding halide.

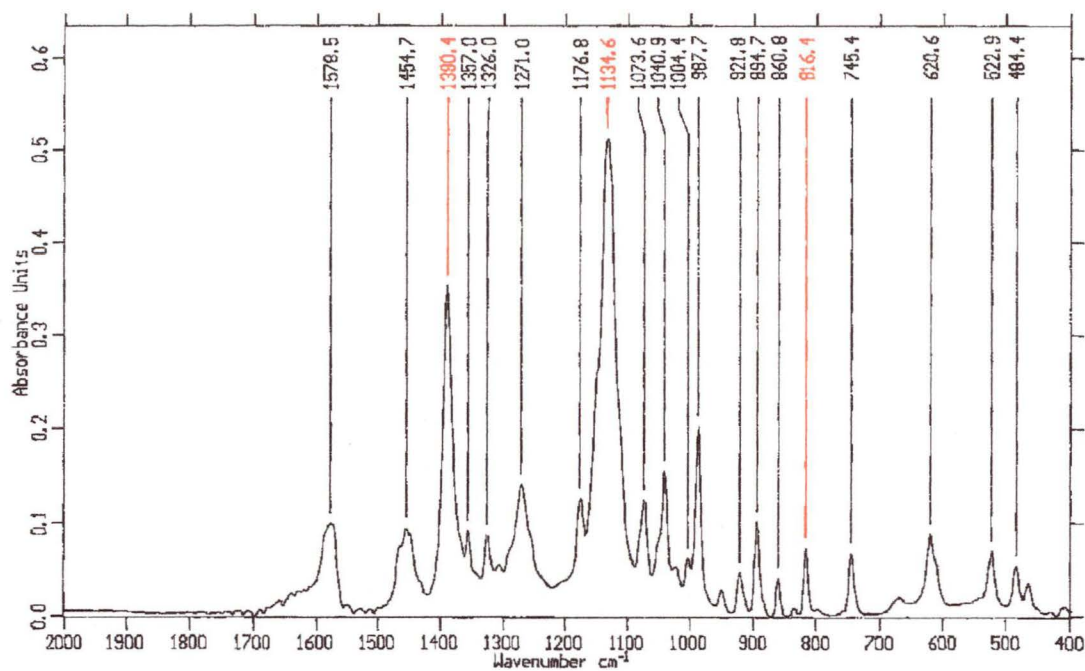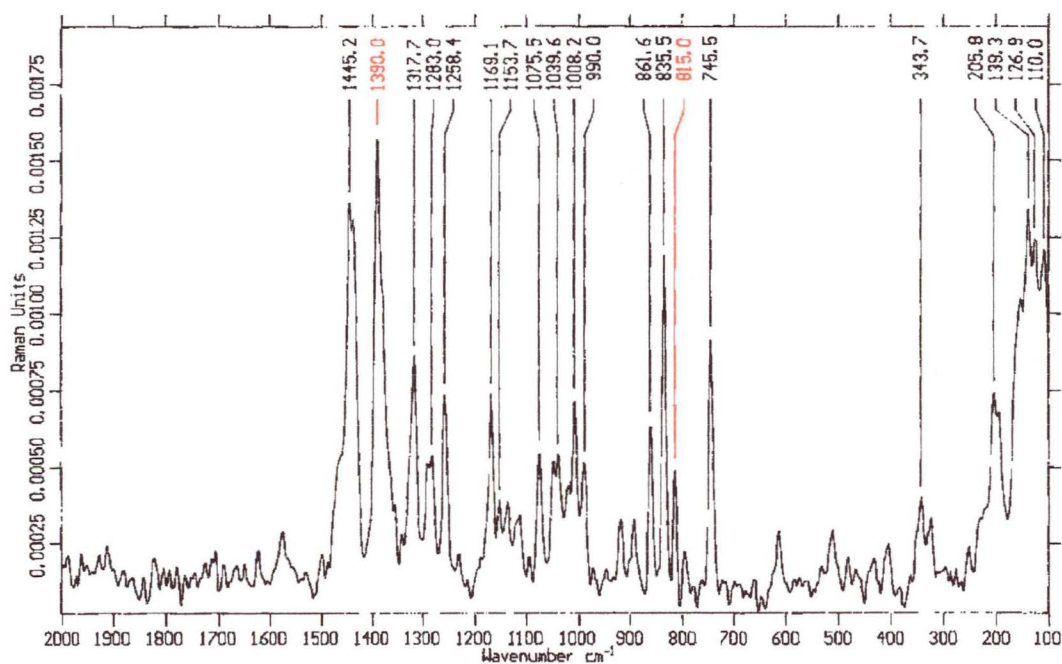**Figure 5.2**: The infrared spectrum of [Ni(1-(2-aminoethyl)piperidine)$_2$(ONO)$_2$].

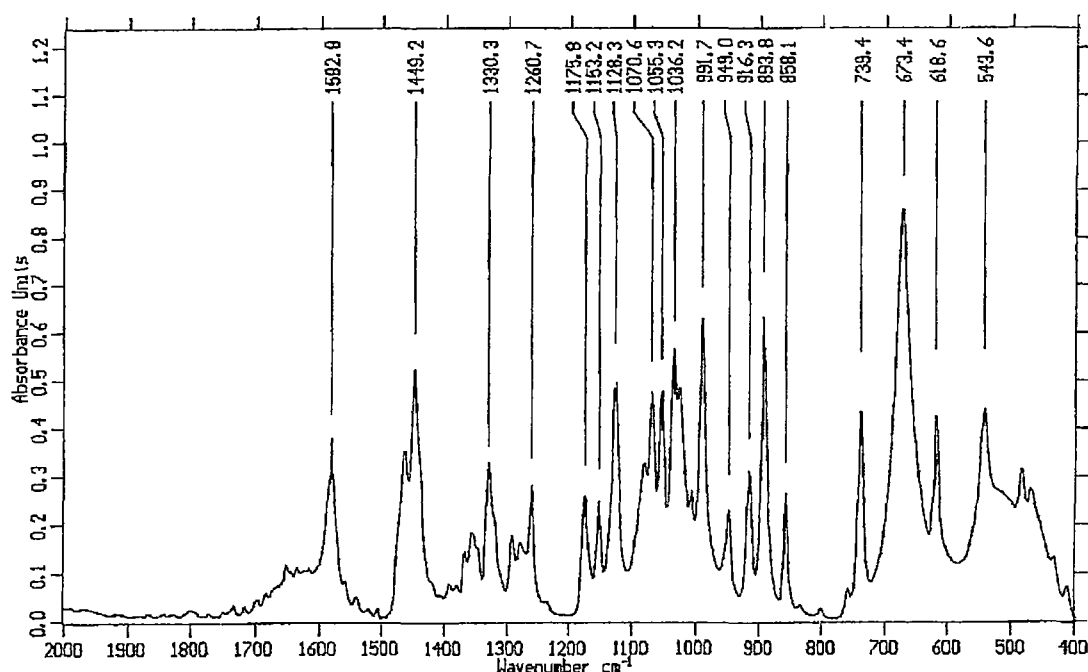**Figure 5.3**: The Raman spectrum of [Ni(1-(2-aminoethyl)piperidine)$_2$(ONO)$_2$].

Figure 5.4: The infrared spectrum of [Ni(1-(2-aminoethyl)piperidine)$_2$Br$_2$].

Table 5.1 summarises the infrared and Raman data obtained for these monodentate complexes. The previously reported IR spectra have also been included, when available, as the bracketed values.

	v_1 (cm^{-1})	v_2 (cm^{-1})	v_3 (cm^{-1})	Ref.
K$_4$[Ni(NO$_2$)$_6$].H$_2$O	810[a], 840[a] [810], [831]	1319[a] [1319]	1342[c] [1346]	8
[Ni(NH$_3$)$_4$(NO$_2$)$_2$]	812[c] [814]	1309[a] [1300]	1341[b] [1350]	6
[Ni(tn)$_2$(NO$_2$)$_2$]	819[c] [800]	1320[c] [1280]	1347[b] [1345]	17,18
[Ni(L1)$_2$(NO$_2$)$_2$]	810 [810]	1315 [1315]	1332 [1338]	16
[Ni(L2)$_2$(NO$_2$)$_2$]	809[c] [815]	obscured [1285]	1360[b] [1360]	12
[Ni(L2)$_2$(ONO)$_2$]	815[c] [820]	1135[a] [1138]	1390[c] [1385]	12
[Ni(3,5-lut)$_4$(ONO)$_2$]	825[c]	1137[a]	1393[c]	-
[Ni(N,N-dimen)$_2$(ONO$_2$)]	817[c] [820]	1138[c] [1130]	1390[b] [1387]	3
[Ni(isoquin)$_4$(ONO)$_2$]	820[b]	1125[a], 1315[a] [1125], [1315]	1390[b] [1400]	14

Table 5.1: The nitrite vibration energies for a number of nickel(II) nitrite complexes with monodentate nitrite ligands. L1 is 1,2-diamino-2-methylpropane and L2 is 1-(2-aminoethyl)piperidine. (a) seen in infrared only, (b) seen in Raman only, (c) seen in both spectra.

These values are in relatively good agreement with those reported by previous authors. For Ni^{2+} complexes, the asymmetric stretch is lower in energy that the symmetric stretch, and so some of these earlier reported spectra have the incorrect assignment of these two peaks[17]. The use of Raman spectroscopy was of great help in identifying v_3 for these complexes, as this was usually of very low intensity in the infrared spectrum. In some cases, v_2 and/or v_3 were obscured by the amine vibrations. The nitrite vibrations of $[Ni(1-(2-aminoethyl)piperidine)_2(NO_2)_2]$ in particular were very difficult to assign, even with access to the spectra of $[Ni(1-(2-aminoethlypiperidine)_2Br_2]$. For this reason, the energy of 1 285cm^{-1} given by Das et al.[12] for v_2 of this nitro complex is doubtful. The energy of 1 280cm^{-1} given by Ribas et al.[18] also appears to be a little low, and may be attributable to an amine vibration.

When the nitrite is N-bonded, the stretching vibrations v_2 and v_3 are quite similar in energy. Upon coordination via oxygen, v_2 decreases to ~1 135cm^{-1} and v_3 increases to ~1 390cm^{-1}. This marked decrease of v_2 was one of the ways that monodentate nitrito coordination was originally identified. However, a complication is that nitrito coordination may occur with the non-bonded oxygen either *trans* or, much less frequently, *cis* to the metal and these have similar vibrational energies, and some published examples exist in which these have been identified incorrectly[1].

The vibrational spectrum of $[Ni(isoquinoline)_4(ONO)_2]$ is particularly interesting. The peaks at 1 315 and 1 125cm^{-1} suggest that there may be both nitro and nitrito coordination in this complex. The peak at 1 390cm^{-1} would be due to the symmetric stretch of the nitrito group, but the corresponding vibration for the nitro group is obscured in both the infrared and Raman spectra by the isoquinoline vibrations. Hitchman and Ahsbahs[19] observed the changes in the infrared spectrum when it was measured at a range of pressures, and concluded that the complex has both nitro and nitrito coordination. Furthermore, their results seemed to indicate that rather than having a crystal structure with distinct nitro and nitrito isomers in the lattice, the molecules may have a statistically disordered distribution of nitro and nitrito groups.

A second example of this unusual type of nitrite complex has been reported. Cortes et al.[20] have determined the crystal structure of [Ni(terpy)(NO$_2$)(ONO)(H$_2$O)] where terpy = 2,2':6',2"-terpyridine. Each molecule has a monodentate nitro and nitrito coordinated nitrite ligand. They quote energies of 1 128 and 1 358cm^{-1} for v_2(ONO) and v_3(ONO), and 1 274 and 1 303cm^{-1} for the v_2 and v_3 of the nitro group. The latter values seem a little low and may be due to the terpy ligand rather than the N-coordinated nitrite ligands.

5.3 Optical Spectroscopy

5.3.1 *Nitro Complexes*

The electronic spectra of many nickel(II) nitro complexes have been reported[5]. These have bands at ~13 000 and ~20 000cm^{-1} and these were originally assigned as the first two spin-allowed transitions for octahedrally coordinated nickel. However, work by Reinen et al.[21] and Caulton and Fenske[22] cast doubt upon this assignment. From their spectroscopic measurements of nickel(II) hexanitro complexes, they concluded that the band at 20 000cm^{-1} is due to a charge transfer transition. Further spectroscopic studies of single crystals at low temperature have shown vibrational fine structure on the ~20 000cm^{-1} band with a progressional energy of ~600cm^{-1} [1]. This energy is too high to be due to a metal-ligand vibration, but is similar to the progression seen on the 28 000cm^{-1} band of NaNO$_2$ [23]. This has been assigned as due to an internal n $\rightarrow$ π^* transition[1]. This vibrational fine structure can be seen in the spectra of the nitro complexes studied in the present work.

To illustrate the benefit of measuring both room and low temperature spectra, both spectra measured for the complex [Ni(tn)$_2$(NO$_2$)$_2$] are shown (Figures 5.5 and 5.6).
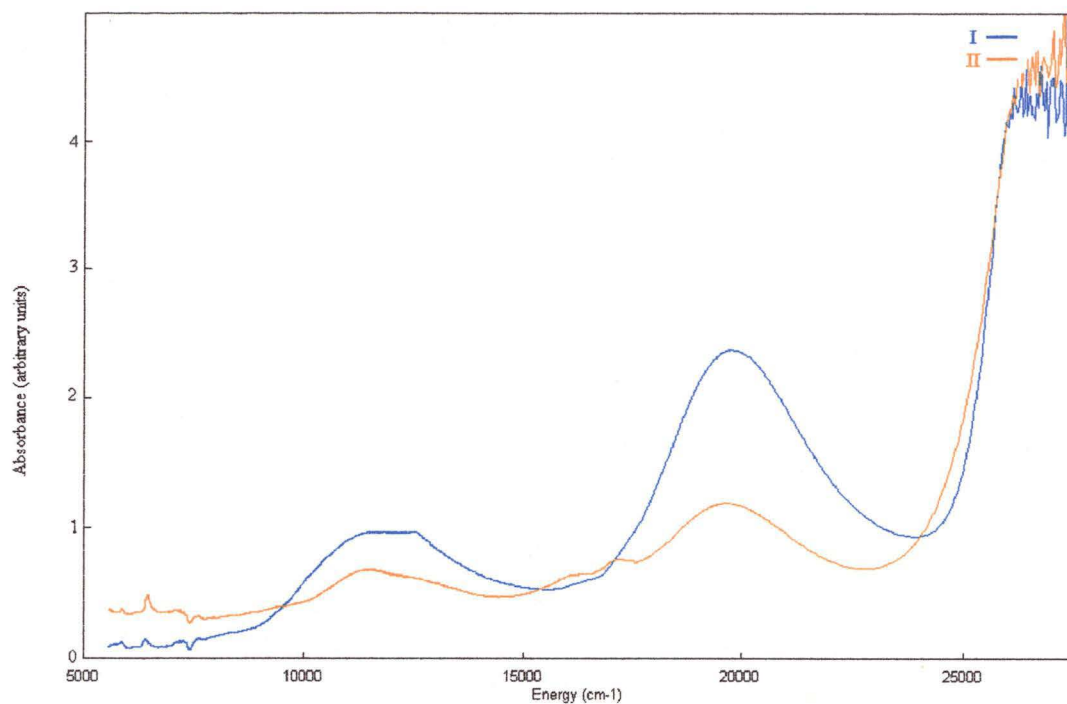
Figure 5.5: The single crystal optical spectrum of [Ni(tn)$_2$(NO$_2$)$_2$] at room temperature with the electric vector parallel to the extinction directions of an arbitrary crystal face.

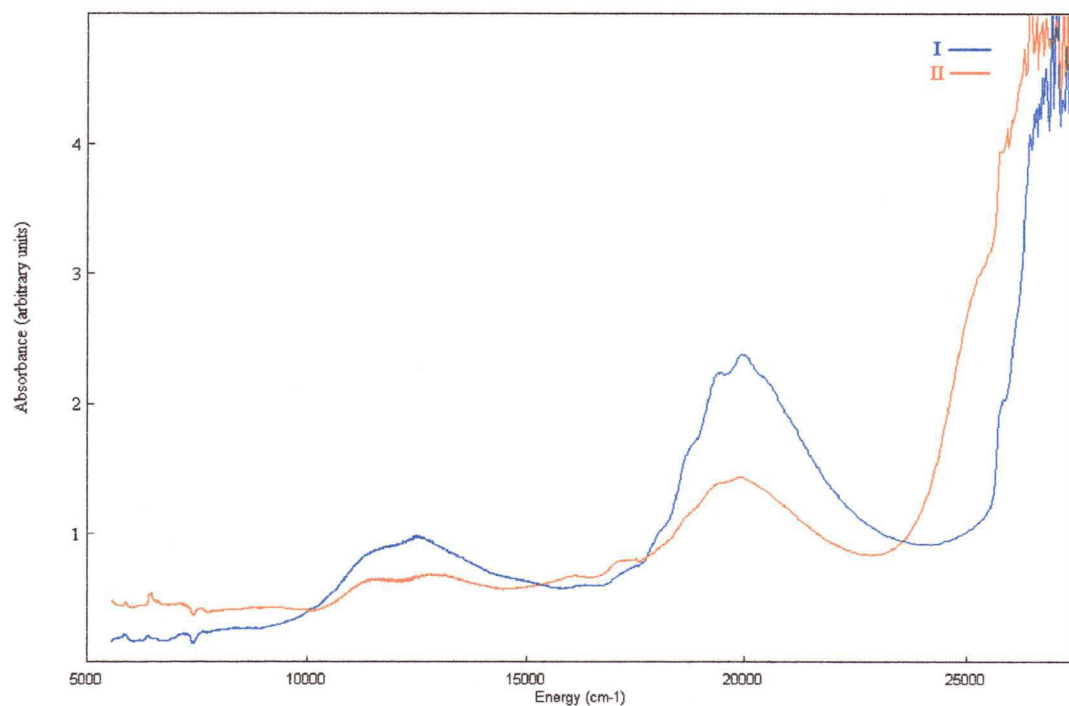**Figure 5.6**: The single crystal optical spectrum of [Ni(tn)$_2$(NO$_2$)$_2$] at 15K with the electric vector parallel to the extinction directions of an arbitrary crystal face.

Two bands are seen in these spectra. The first, at 11 600cm^{-1}, may be assigned to the transition $^3T_{2g} \leftarrow {}^3A_{2g}$. A distinct peak can be seen at 12 500cm^{-1}, and this is likely to be due to a spin-forbidden transition, $^1E_g \leftarrow {}^3A_{2g}$. The second band is centred at ~20 000cm^{-1} and a vibrational progression of ~670cm^{-1} is clearly visible on this band at low temperature. For reasons described earlier, this suggests that this band is not due to a d-d transition, but rather due to a transition in which an electron is promoted to the nitrite π^* orbital, possibly as a metal to ligand charge transfer transition. A peak of relatively low intensity is also visible at 17 400cm^{-1}. This may be due to the second d-d transition, the rest of which is obscured by the charge transfer transition. The peak at ~16 200cm^{-1} is too low in energy to be part of the second d-d transition for the complex, but may be the origin of the vibrational progression. The shoulders to the high energy charge transfer band are likely to be part of a vibrational progression on this charge transfer band.

Ribas et al.[18] and Takeuchi et al.[17] have reported the solution spectrum and reflectance spectrum, respectively. They report spectra that are similar to those at room temperature in the present work, though Takeuchi et al.[17] assume that the second band is a d-d transition, in keeping with the view at the time.

The complex [Ni(1,2-diamino-2-methylpropane)$_2$(NO$_2$)$_2$] is unusual because the two nitro groups are *cis* rather than *trans* to each other[16]. The low temperature spectra measured for this complex are shown in Figure 5.7. Note that the vibrational fine structure is present but is not as clear as in the other nickel(II) nitro spectra presented in this work.
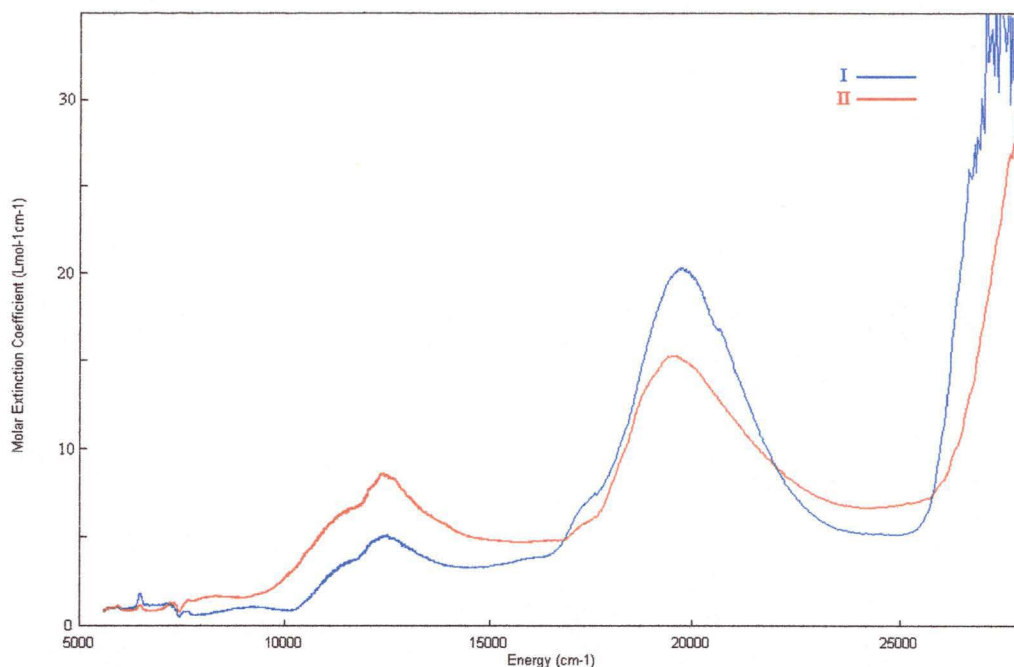
Figure 5.7: The single crystal optical spectrum of *cis*-[Ni(1,2-diamino-2 methylpropane)$_2$(NO$_2$)$_2$].0.5H$_2$O at 15K with the electric vector parallel to the extinction directions of an arbitrary crystal face.

These spectra are very similar to those measured for [Ni(tn)$_2$(NO$_2$)$_2$]. The first band has two distinct components at 11 380cm^{-1} and 12 415cm^{-1}, corresponding to split components of the $^3T_{2g}$ state. A shoulder to the second band is clearly visible at 17 325cm^{-1}, with the second band centred at ~19 740cm^{-1}. There are two indistinct shoulders to the intense charge transfer transition at 25 860cm^{-1} and 26 380cm^{-1}, which may be part of a vibrational progression.

Laskar et al.[16] also observed a change in the complex upon heating. They suggest that this complex changes from a *cis* form to a *trans* isomeric form, but there may be another explanation for this change. Their Nujol mull spectrum of the product of heating does not resemble that expected for a typical *trans* nitro complex. The first band, centred at ~8 000cm^{-1} seems to be too low in energy, and the presence of an intense band at 15 245cm^{-1} also seems unusual. However, this spectrum is not unlike those measured for [Ni(N,N'-diethylethylenediamine)$_2$(O$_2$N)](NO$_2$), [Ni(*meso*-1,2-diphenylethylenediamine)$_2$(O$_2$N)](NO$_2$) and [Ni(N,N'-dipropyl-1,2-ethylenediamine)$_2$(O$_2$N)](NO$_2$) which have a bidentate nitrito group and an ionic nitrite[10]. This is also consistent with the reported IR spectrum[16]. Moreover, the nitro

complex [Ni(en)$_2$(NO$_2$)$_2$] also undergoes a colour change on heating, and this has been shown to be due to the two nitro groups being replaced by a chelating and an ionic nitrite[24]. It thus seems likely that the same is true for cis-[Ni(1,2-diamino-2-methylpropane)$_2$(NO$_2$)$_2$], but as small crystals of this second complex could not be prepared, it was not possible to determine its crystal structure, or measure more detailed spectra.

5.3.2   Nitrito Complexes

Optical spectra of complexes of the type Ni(diamine)$_2$(ONO)$_2$ and Ni(L)$_4$(ONO)$_2$, where diamine is a substituted ethylenediamine and L is an aromatic amine, have been reported previously[1]. However, there are few studies of this type, as the monodentate O-bonded mode of coordination is less common than the N-bonded mode. Also, some of the complexes originally identified as having monodentate nitrito groups have since been determined to have an O,O'-chelating and ionic nitrite groups[10, 25, 26].

The crystal morphology of trans-[Ni(3,5-lutidine)$_4$(ONO)$_2$] determined by optical goniometry is shown in Figure 5.8. Figure 5.9 shows the spectra obtained when measuring parallel to the extinction directions of the (011) face.
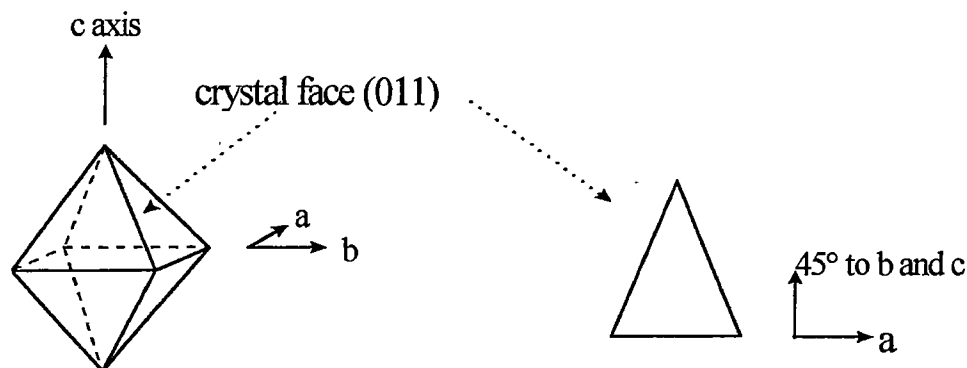

Figure 5.8: The crystal morphology of trans-[Ni(3,5-lutidine)$_4$(ONO)$_2$].
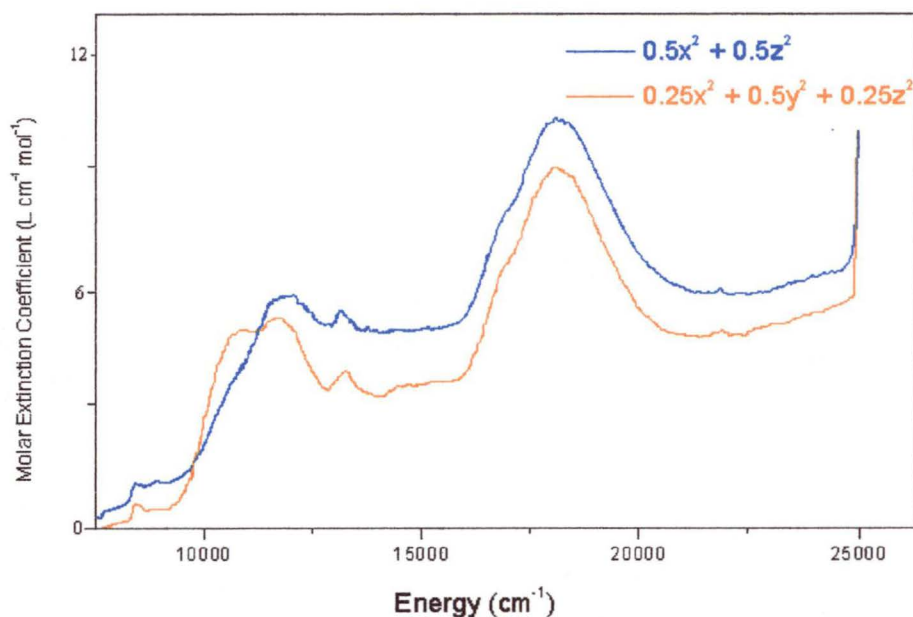
Figure 5.9: The single crystal optical spectrum of *trans*-[Ni(3,5-lutidine)$_4$(ONO)$_2$] at 15K with the electric vector parallel to the extinction directions of the (011) crystal face.

The molecular projections for the two spectra in Figure 5.9 are $0.5x^2 + 0.5z^2$, when the electric vector of the polarised light is parallel to the a axis, and $0.25x^2 + 0.5y^2 + 0.25z^2$. Here, z is parallel to the Ni-O bonds. The spectrum shows two broad bands. The first band contains peaks at 10 900 cm^{-1} and 11 800 cm^{-1}, which may be assigned to the transitions $^3E_g \leftarrow ^3B_{1g}$ and $^3B_{2g} \leftarrow ^3B_{1g}$. Assuming effective D$_{4h}$ symmetry, the noticeable change in intensity for the first transition is predicted by the selection rules, which indicate that the transition $^3B_{2g} \leftarrow ^3B_{1g}$ is forbidden in the z direction. Accordingly, this peak was expected to be much less intense in the //a direction, as it has twice the z-component. The second band consists of an intense peak at 17 970 cm^{-1} which is due to the $^3E_g \leftarrow ^3B_{1g}$ transition, with a shoulder at about 16 800 cm^{-1} corresponding to the $^3A_{2g} \leftarrow ^3B_{1g}$ transition. Spin-forbidden transitions that have 'borrowed' intensity due to their close proximity to the large spin-allowed peaks can be seen at 13 100 cm^{-1} and 21 700 cm^{-1}. The first of these can be seen quite clearly, and AOM calculations predict two spin-forbidden peaks close in energy to this observed peak assigned as the transitions $^1A_{1g} \leftarrow ^3B_{1g}$ and $^1B_{1g} \leftarrow ^3B_{1g}$.

No transitions of higher energy can be distinguished as an intense charge transfer peak obscures higher energy d-d transitions above 25 000 cm^{-1}.

The large blue crystals of *trans*-[Ni(N,N-dimethylethylenediamine)$_2$(ONO)$_2$] also had two well-developed faces. The crystal morphology was determined by measuring interfacial angles, and is shown in Figure 5.10, while the spectra obtained for the two faces are shown in Figures 5.11 and 5.12.
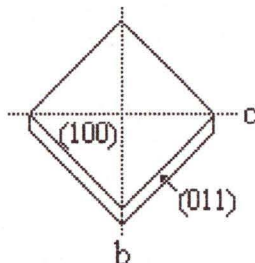

Figure 5.10: The crystal morphology of *trans*-[Ni(N,N-dimen)$_2$(ONO)$_2$].

When measuring the spectra of the (100) face, the extinction directions are parallel to the b and c axes. These correspond to the molecular projections $0.0919x^2 + 0.6623y^2 + 0.2458z^2$ and $0.2006x^2 + 0.1959y^2 + 0.6035z^2$, respectively, with z parallel to the Ni-O bond. As the spectrum measured for the (011) face does not show any polarisation, the molecular projections have not been determined for the extinction directions of this face.
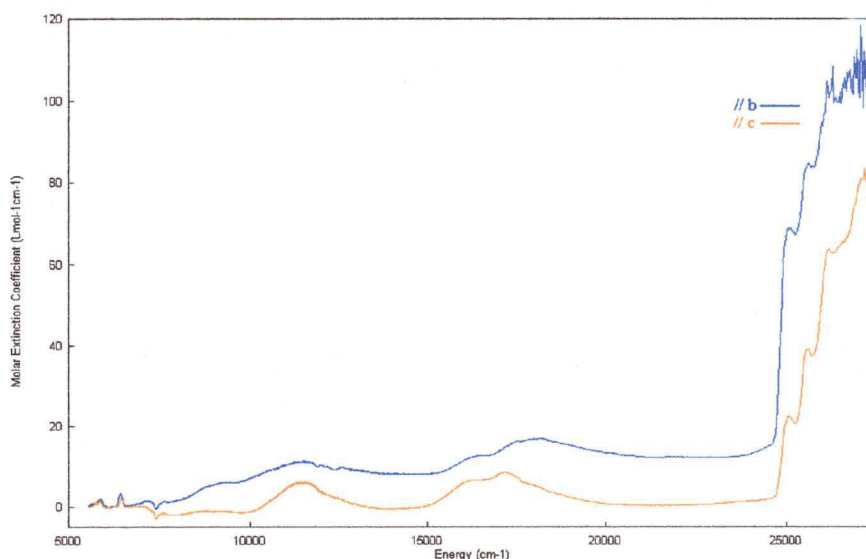

Figure 5.11: The single crystal optical spectrum of *trans*-[Ni(N,N-dimen)$_2$(ONO)$_2$] at 15K with the electric vector parallel to the extinction directions of the (100) face.
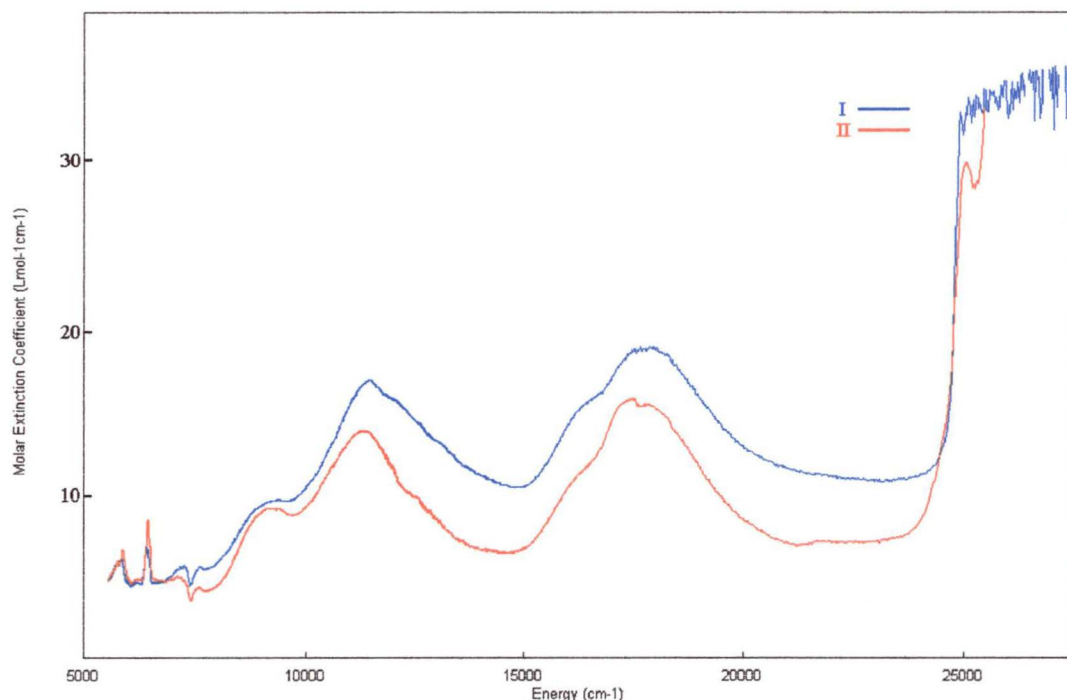
Figure 5.12: The single crystal optical spectrum of [Ni(N,N-dimen)$_2$(ONO)$_2$] at 15K
with the electric vector parallel to the extinction directions of the
(011) crystal face.

Two bands with distinct splitting patterns are seen in the spectra of this complex.
The first band consists of peaks at 9 500cm^{-1} and 11 600cm^{-1}. These correspond to
the transitions $^3B_{2g} \leftarrow {}^3B_{1g}$ and $^3E_g \leftarrow {}^3B_{1g}$, assuming approximate D$_{4h}$ symmetry.
The $^3B_{2g} \leftarrow {}^3B_{1g}$ transition is forbidden in the z-direction and as the z projection
varies for the two molecular projections, this transition would have less intensity in
the //c spectrum. The peak at 9 500cm^{-1} is weaker //c which therefore suggests its
assignment to the $^3B_{2g}$, with the 11 600cm^{-1} being to the ^3E_g level. The second band
has been split into peaks corresponding to the transitions $^3E_g \leftarrow {}^3B_{1g}$ and $^3A_{2g} \leftarrow$
$^3B_{1g}$, with energies of 16 125cm^{-1} and 18 050cm^{-1}. The transition $^3A_{2g} \leftarrow {}^3B_{1g}$ is also
forbidden in the z-direction, and this peak does not appear in the spectrum measured
//c, for the reasons described above. A spin forbidden peak is also present at
17 155cm^{-1}. A vibrational progression of ~600cm^{-1} commencing at ~25 000cm^{-1}
may be due to the n $\rightarrow \pi^*$ internal nitrite transition.

When this complex is dissolved in chloroform, the solution obtained is light pink in
colour. This has been interpreted as a nitrito $\rightarrow$ nitro isomerization, but another

possibility is a change from a dinitrito complex to a complex with a bidentate chelating O,O'-coordinated nitrite plus a nitrite counterion. As mentioned previously, such a change is known to occur in the solid state on heating [Ni(en)$_2$(NO$_2$)$_2$] to 110°C[24]. To determine which was the case, the conductivity of the [Ni(N,N-dimen)$_2$(ONO)$_2$] chloroform solution was measured. Using laboratory grade chloroform, the pink solution was high, suggesting that the reaction is indeed a nitrito → nitro isomerisation rather than a rearrangement to a chelating nitrite. Numerous attempts to repeat these measurements using freshly distilled chloroform failed as the complex always decomposed.

5.3.3 *Nitro and Nitrito Isomers and a Mixed Nitro-Nitrito Complex*

Complexes of this type are rare, with the nitro-nitrito isomers of [Ni(1-(2-aminoethyl)piperidine)$_2$(NO$_2$)$_2$] being the first example for which structural details are available for both isomers. The measurement of these spectra provides a direct comparison between a nitro and nitrito complex. The crystal morphologies of these two isomers determined by optical goniometry are shown in Figure 5.13. Marked upon the diagrams are the extinction directions for the two crystal faces measured.
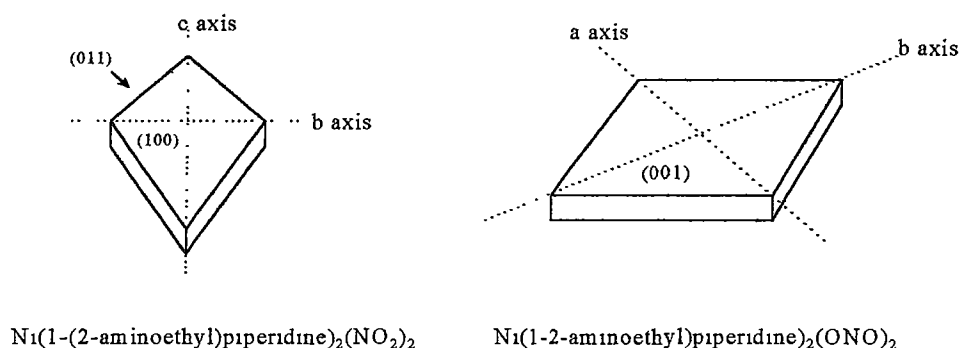

Ni(1-(2-aminoethyl)piperidine)$_2$(NO$_2$)$_2$ Ni(1-2-aminoethyl)piperidine)$_2$(ONO)$_2$

Figure 5.13: Crystal morphologies and extinction directions of the nitro and nitrito isomers of [Ni(1-(2-aminoethyl)piperidine)$_2$(NO$_2$)$_2$].

Although these complexes are formally of C$_i$ symmetry, the inner coordination sphere conforms to D$_{4h}$ symmetry if the amines are considered equivalent. The low temperature spectra (Figure 5.14) measured for the nitro isomer of

[Ni(1-(2-aminoethyl)piperidine)$_2$(NO$_2$)$_2$] show a pattern of polarisation that is consistent with D$_{4h}$ symmetry. The molecular projections for the extinction directions were $0.4162x^2 + 0.1410y^2 + 0.4428z^2$ when parallel to the b axis and $0.0001x^2 + 0.7659y^2 + 0.2340z^2$ when parallel to the c axis, and z is parallel to the Ni-nitrite bonds.
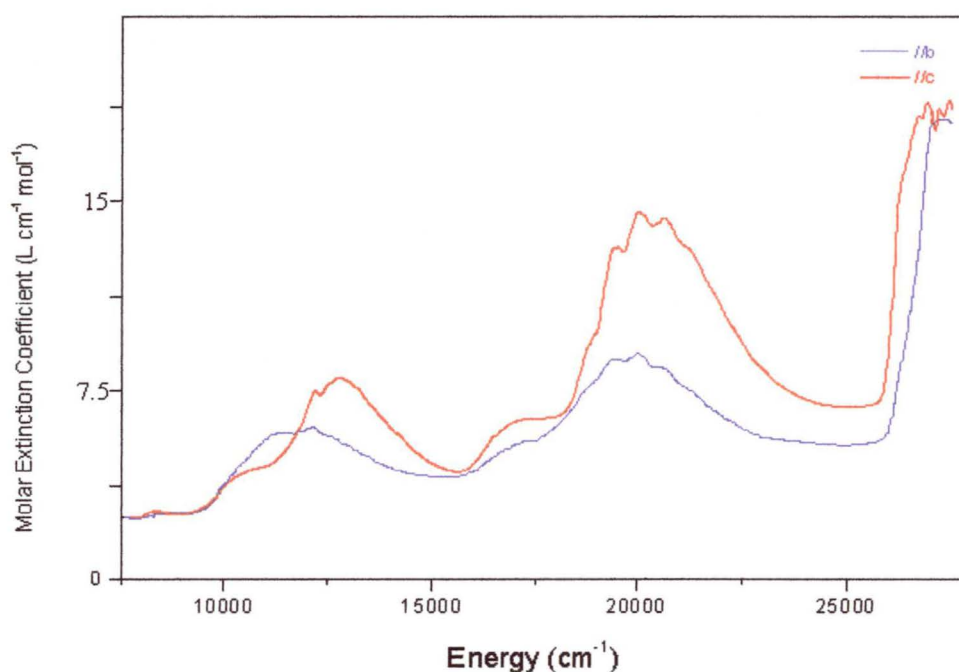

Figure 5.14: The single crystal optical spectrum of Ni(1-(2-aminoethyl)piperidine)$_2$(NO$_2$) at 15K with the electric vector parallel to the extinction directions of the (100) crystal face.

The first band was well resolved, with transitions at 10 540, 11 000 and 12 760cm^{-1}, respectively. Assuming an effective symmetry of D$_{4h}$, the transition $^3B_{2g} \leftarrow {}^3B_{1g}$ is forbidden in the z-direction. The peak at 12 760cm^{-1} is of lower intensity in the //b spectrum, which has a higher z-component in its molecular projection than that //c, and so this may be assigned as the transition $^3B_{2g} \leftarrow {}^3B_{1g}$. The first two peaks may be assigned as the transition $^3E_g \leftarrow {}^3B_{1g}$, where this level has been split by the relatively low symmetry of the complex overall. A sharp spin-forbidden transition, $^1A_{1g} \leftarrow {}^3B_{1g}$, can also be seen on this band at 12 200cm^{-1}. The mixed d-d and charge transfer transition band common to all nitro complexes is centred at approximately 20 000 cm^{-1}. Again, the vibrational structure has a progression of ~600 cm^{-1}. A

distinct shoulder is also seen for this peak at about 16 750 cm^{-1}, particularly for the polarisation parallel to the c axis, but the presence of the charge transfer band overlapping this d-d transition does not permit further assignment.

Figure 5.15 shows the optical spectra measured for the (001) face of a [Ni(1-(2-aminoethyl)piperidine)$_2$(ONO)$_2$] crystal. The extinction directions were parallel to the a axis and parallel to the b axis, with molecular projections of $0.1935x^2 + 0.7572y^2 + 0.0494z^2$ and $0.7892x^2 + 0.1484y^2 + 0.0624z^2$, respectively. Again, z is parallel with the nickel-nitrite bonds.
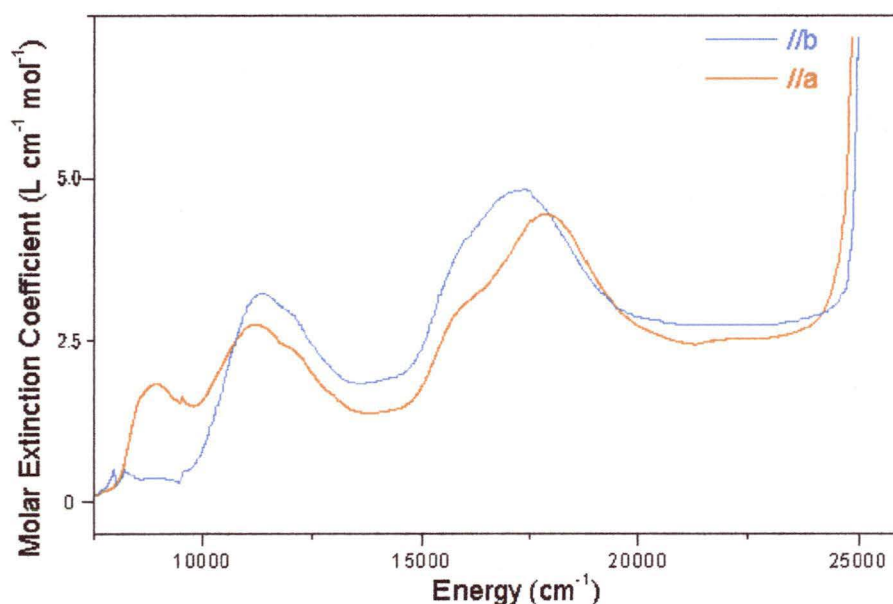

Figure 5.15: The single crystal optical spectrum of [Ni(1-(2-aminoethyl)piperidine)$_2$(ONO)$_2$] at 15K with the electric vector parallel to the extinction directions of the (001) crystal face.

Two bands are visible in the spectra, and the resolution obtained allowed the following detailed assignment. The first band is split into three components with the energies 8 900, 11 100 and 11 500cm^{-1}. These correspond to the transitions $^3B_{2g} \leftarrow$ $^3B_{1g}$ and the split components $^3E_g \leftarrow {}^3B_{1g}$, respectively. The first peak is highly polarised, as suggested by the D_{4h} vibronic selection rules. These predict that the $^3B_{2g} \leftarrow {}^3B_{1g}$ transition is forbidden in the z direction. It should have a lower intensity in the //b polarisation, as observed, since this has a slightly higher z component. The second band is also split into three with peaks at 15 900, 17 000 and 17 500cm^{-1}, which correspond to the $^3A_{2g} \leftarrow {}^3B_{1g}$, and the split components of $^3E_g \leftarrow {}^3B_{1g}$,

respectively. The selection rules predict that the $^3A_{2g} \leftarrow {}^3B_{1g}$ transition is forbidden in the z direction, and thus this peak should be less intense in the //b polarisation, as observed. A partly obscured transition could also be seen at 25 700 cm^{-1} (not shown in Figure 5.15), which corresponds to a spin-allowed transition of $^3A_{2g} \leftarrow {}^3B_{1g}$.

The single crystal spectra of [Ni(isoquin)$_4$(ONO)$_x$(NO$_2$)$_{2-x}$] at room and low temperature are shown in Figures 5.16 and 5.17.
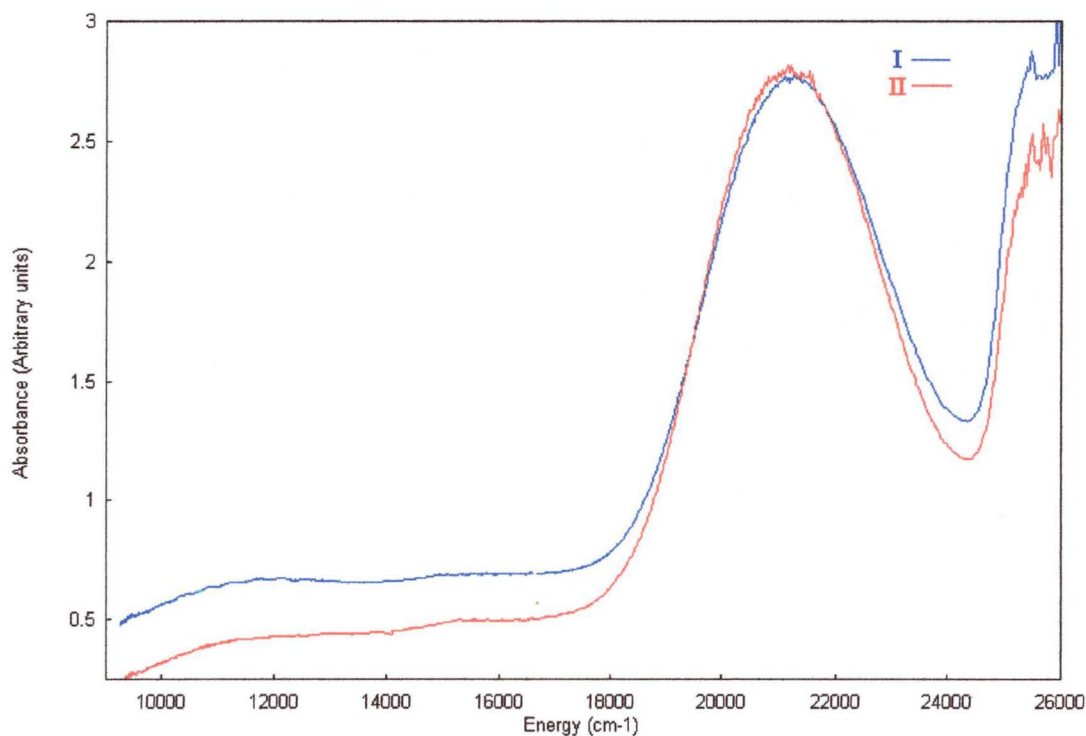

Figure 5.16: The single crystal optical spectrum of [Ni(isoquin)$_4$(ONO)$_x$(NO$_2$)$_{2-x}$] at room temperature, with the electric vector of the polarised light parallel to the extinction directions of an arbitrary crystal face.
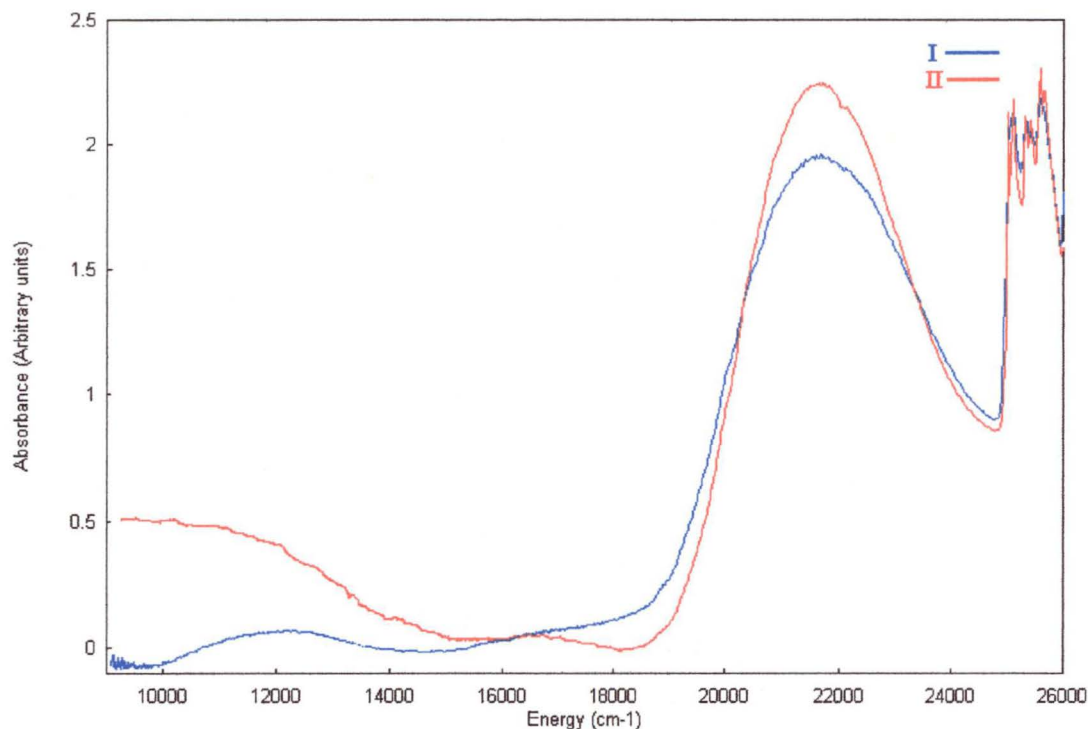
Figure 5.17: The single crystal optical spectrum of $[Ni(isoquin)_4(ONO)_x(NO_2)_{2-x}]$ at 15K, with the electric vector of the polarised light parallel to the extinction directions of an arbitrary crystal face.

The two bands centred at $12\,270cm^{-1}$ and $21\,600cm^{-1}$ are similar to those seen for the other nitro complexes discussed in this chapter. The lower energy band would correspond to the $^3T_{2g} \leftarrow {}^3A_{2g}$ transition, with the higher energy, more intense band likely due to a mixed d-d and charge transfer transition, although no vibrational structure could be resolved for this complex. A weak peak occurs at $16\,670cm^{-1}$ which may be due to a complex involving just monodentate nitrito coordinated ligands. If correct, this suggests that the compound is not a mixed nitro-nitrito complex of the fixed stoichiometry $[Ni(isoquin)_4(ONO)(NO_2)]$. It supports the conjecture that the nitro and nitrito groups are distributed randomly, that is, the formula is $[Ni(isoquin)_4(ONO)_x(NO_2)_{2-x}]$, where x is 0, 1 or 2 for any particular molecule[19]. The peak at $16\,670cm^{-1}$ arises from those molecules for which x = 2. It may be noted that, except for a sharpening of the peaks, and possibly an increase in intensity at ~$10\,000cm^{-1}$ for one polarisation, there is little change in the spectra on cooling. This suggests that the ratio of nitro to nitrito groups does not change drastically with temperature.

5.4 Analysis of the Band Energies Using the Angular Overlap Model

5.4.1 *Nitro Complexes*

Several workers have used the Angular Overlap Model (AOM) to determine bonding parameters in nickel(II) complexes[5]. A particular problem faced when attempting to derive nitrite bonding parameters for monodentate N-coordinated ligands in complexes of this type is that the relatively low energy charge transfer transition generally obscures the second d-d transition, thus limiting the number of peaks observed. However, as the complexes in the present work have only two ligand types, it was possible to use the observed transition energies to estimate AOM parameters.

It is possible to derive the e_σ parameter for the NH_3 ligand using the relationship

$$\Delta = 3e_\sigma - 4e_\pi.$$

Knowing that Δ for the complex $[Ni(NH_3)_6]^{2+}$ was 11 100cm^{-1} [27], and assuming that for an aliphatic amine $e_{\pi x} = e_{\pi y} = 0$cm^{-1}, an $e_\sigma(NH_3) = 3$ 700cm^{-1} was obtained. This parameter value has been used, with appropriate scaling for bond length where necessary, in the present work.

The transition energies calculated for the complex $[Ni(tn)_2(NO_2)_2]$ are shown in Table 5.2. These were calculated using amine parameters derived from $[Ni(NH_3)_6]^{2+}$ that had been scaled appropriately for bond length, $e_\sigma(NO_2) = 3$ 965cm^{-1} and $e_{\pi y}(NO_2) = -105$cm^{-1}. Here x is parallel to the plane of the nitrite and it is assumed that $e_{\pi x} = 0$cm^{-1} for the nitro group, that is, the π-bonding in the plane of the nitrite is negligible.

TRANSITION	CALCULATED (cm^{-1})	OBSERVED (cm^{-1})
$^3T_{2g} \leftarrow {}^3A_{2g}$	11 572	11 600
$^1E_g \leftarrow {}^3A_{2g}$	12 510	12 500
$^3T_{1g} \leftarrow {}^3A_{2g}$	17 550	17 400

Table 5.2: The calculated and observed transition energies for [Ni(tn)$_2$(NO$_2$)$_2$] when B = 750, C = 3 400, e$_\sigma$(amine) = 3 966 and 3 833cm^{-1}, e$_\sigma$(NO$_2$) = 3 965cm^{-1} and e$_{\pi y}$(NO$_2$) = -105cm^{-1}.

In a similar manner, the transition energies shown in Table 5.3 were calculated for the complex cis-[Ni(1,2-diamino-2-methylpropane)$_2$(NO$_2$)$_2$].0.5H$_2$O, using the nitro parameters e$_\sigma$(NO$_2$) = 3 966cm^{-1} and e$_{\pi y}$(NO$_2$) = -100cm^{-1}.

TRANSITION	CALCULATED (cm^{-1})	OBSERVED (cm^{-1})
$^3T_{2g} \leftarrow {}^3A_{2g}$	11 379	11 380
	12 419	12 415
$^3T_{1g} \leftarrow {}^3A_{2g}$	17 391	17 325

Table 5.3: The calculated and observed transition energies for the complex cis-[Ni(1,2-diamino-2-methylpropane)$_2$(NO$_2$)$_2$].0.5H$_2$O when B = 850, C = 3 500, e$_\sigma$(amine) = 3 551 and 4 344cm^{-1}, e$_\sigma$(NO$_2$) = 3 966cm^{-1} and e$_{\pi y}$(NO$_2$) = -100cm^{-1}.

The single crystal spectrum of [Ni(NH$_3$)$_4$(NO$_2$)$_2$] has been measured by Hitchman and Rowbottom[28]. Using their quoted transition energies for the components of the first d-d band and the e$_\sigma$(NH$_3$) value quoted above, the parameters e$_\sigma$(NO$_2$) = 3 850cm^{-1} and e$_{\pi y}$(NO$_2$) = -200cm^{-1} yield a reasonably good fit of the observed transitions (Table 5.4).

TRANSITION	CALCULATED (cm^{-1})	OBSERVED (cm^{-1})
$^3T_{2g} \leftarrow {}^3A_{2g}$	11 909	11 700
	12 123	12 350
$^1E_g \leftarrow {}^3A_{2g}$	13 142	13 105

Table 5.4: The calculated and observed transition energies for the $[Ni(NH_3)_4(NO_2)_2]$ when B = 850, C = 3 400, $e_\sigma(amine)$ = 4 035cm^{-1}, $e_\sigma(NO_2)$ = 3 850cm^{-1} and $e_{\pi y}(NO_2)$ = -200cm^{-1}.

Note that these values are considerably different from those quoted by Figgis et al.[6], which were $e_\sigma(NO_2)$ = 12 000 and $e_{\pi y}(NO_2)$ = 5 700cm^{-1}, but similar to the value of $e_\sigma(NO_2)$ = 4 400cm^{-1} deduced by Grey et al.[8] for the complex $K_4[Ni(NO_2)_6].H_2O$. The present parameters are also similar to those derived for the other nickel(II) nitro complexes in the current work.

The low temperature single crystal optical spectrum of the complex $[Ni(en)_2(NO_2)_2]$ where en = ethylenediamine has been reported by Bertini et al[7]. Using amine parameters scaled for bond length, the transition energies shown in Table 5.5 are obtained. This yields the values 3 800cm^{-1} and -100cm^{-1} for the $e_\sigma(NO_2)$ and $e_{\pi y}(NO_2)$ parameters, respectively.

TRANSITION	CALCULATED (cm^{-1})	OBSERVED (cm^{-1})
$^3E_g \leftarrow {}^3B_{1g}$	11 538	11 400
$^3B_{2g} \leftarrow {}^3B_{1g}$	12 176	12 200
$^1A_{1g} \leftarrow {}^3B_{1g}$	12 525	12 400

Table 5.5: The calculated and observed transition energies for $[Ni(en)_2(NO_2)_2]$ when B = 850, C = 3 500, $e_\sigma(amine)$ = 4 165 and 4 245cm^{-1}, $e_\sigma(NO_2)$ = 3 800cm^{-1} and $e_{\pi y}(NO_2)$ = -100cm^{-1}.

These nitro parameters are similar to those quoted by Bertini et al., $e_\sigma(NO_2) = 3\ 942$ and $e_{\pi y}(NO_2) = -191cm^{-1}$, though they derived their $e_\sigma(amine)$ parameters in a different way to the present work[7].

If it is assumed that the chelating 1-(2-aminoethyl)piperidine ligand can be treated as two independent amine groups, and that both the primary and ring nitrogens behave in a similar manner with respect to bonding parameters, then scaled amine parameters may be used to help derive the nitro parameters in this complex. The resulting parameters, $e_\sigma(NO_2) = 3\ 900cm^{-1}$ and $e_{\pi y}(NO_2) = -210cm^{-1}$, gave the transition energies shown in Table 5.6.

TRANSITION	CALCULATED (cm^{-1})	OBSERVED (cm^{-1})
$^3E_g \leftarrow {}^3B_{1g}$	10 515, 10 833	10 540, 11 000
$^1A_{1g} \leftarrow {}^3B_{1g}$	12 270	12 200
$^3B_{2g} \leftarrow {}^3B_{1g}$	12 780	12 760
$^3A_{2g} \leftarrow {}^3B_{1g}$	16 855	16 750

Table 5.6: The calculated and observed transition energies for [Ni(1-(2-aminoethyl)piperidine)$_2$(NO$_2$)$_2$] when B = 850, C = 3 100, $e_\sigma(amine)$ = 2 900 and 4 675cm^{-1}, $e_\sigma(NO_2)$ = 3 900cm^{-1} and $e_{\pi y}(NO_2)$ = -210cm^{-1}.

5.4.2 Nitrito Complexes

AOM parameters for the nitrito ligands in [Ni(1-(2-aminoethyl)piperidine)$_2$(ONO)$_2$] may be determined in a manner similar to that described for the nitro isomer. The calculated energies shown in Table 5.7 are similar in energy to the observed transition energies. The nitrito parameters are $e_\sigma(ONO) = 3\ 510cm^{-1}$ and $e_{\pi y}(ONO) = 525$.

TRANSITION	CALCULATED (cm^{-1})	OBSERVED (cm^{-1})
$^3B_{2g} \leftarrow ^3B_{1g}$	8 900	8 900
$^3E_g \leftarrow ^3B_{1g}$	11 025, 11 675	11 100, 11 500
$^3A_{2g} \leftarrow ^3B_{1g}$	15 850	15 900
$^3E_g \leftarrow ^3B_{1g}$	16 850, 17 500	17 000, 17 500
$^3A_{2g} \leftarrow ^3B_{1g}$	25 850	25 700

Table 5.7: The calculated and observed transition energies for [Ni(1-(2-aminoethyl)piperidine)$_2$(ONO)$_2$] when B = 750, C = 3 850, e$_\sigma$(amine) = 3 200 and 4 450cm^{-1}, e$_\sigma$(ONO) = 3 510cm^{-1} and e$_{\pi y}$(ONO) = 525cm^{-1}.

A comparison of the observed transition energies for [Ni(N,N-dimen)$_2$(ONO)$_2$] with those calculated using CAMMAG in the above way is shown in Table 5.8. The calculation yields the nitrito parameters e$_\sigma$(ONO) = 3 700cm^{-1} and e$_{\pi y}$(ONO) = 375cm^{-1}.

TRANSITION	CALCULATED (cm^{-1})	OBSERVED (cm^{-1})
$^3B_{2g} \leftarrow ^3B_{1g}$	9 501	9 500
$^3E_g \leftarrow ^3B_{1g}$	10 874, 11 830	11 600
$^3A_{2g} \leftarrow ^3B_{1g}$	16 122	16 125
$^1B_{1g} \leftarrow ^3B_{1g}$	17 141	17 155
$^3E_{2g} \leftarrow ^3B_{1g}$	17 800	18 050

Table 5.8: The calculated and observed transition energies for [Ni(N,N-dimen)$_2$(ONO)$_2$] when B = 770, C = 3 080, e$_\sigma$(amine) = 3 200 and 4 310cm^{-1}, e$_\sigma$(ONO) = 3 700cm^{-1} and e$_{\pi y}$(ONO) = 375cm^{-1}.

To determine the AOM parameters of the nitrito groups in the complex

[Ni(3,5-lutidine)$_4$(ONO)$_2$], parameters for the 3,5-lutidine ligand had to be derived from the pyridine parameters quoted by Astley et al[28]. The calculated energies shown in Table 5.9 could then be determined using e_σ(ONO) = 4 020cm^{-1} and $e_{\pi y}$(ONO) = 610cm^{-1} for the nitrito ligand.

TRANSITION	CALCULATED (cm^{-1})	OBSERVED (cm^{-1})
$^3B_{2g} \leftarrow {}^3B_{1g}$	10 930	10 900
$^3E_g \leftarrow {}^3B_{1g}$	12 014	11 800
$^1A_{1g}, \leftarrow {}^3B_{1g}$	12 968	13 100
$^3A_{2g} \leftarrow {}^3B_{1g}$	16 881	16 800
$^3E_g \leftarrow {}^3B_{1g}$	17 901	17 970
$^1A_{1g} \leftarrow {}^3B_{1g}$	21 578	21 700

Table 5.9: The calculated and observed transition energies for [Ni(3,5-lut)$_4$(ONO)$_2$] when B = 750, C = 3 600, e_σ(3,5-lut) = 4 530cm^{-1}, $e_{\pi y}$(3,5-lut) = 890cm^{-1} e_σ(ONO) = 4 020cm^{-1} and $e_{\pi y}$(ONO) = 610cm^{-1}.

5.4.3 A Comparison of the AOM Parameters for Monodentate Nitro and Nitrito Coordination Modes

If a bond length of 2.14Å is assumed for the nickel-nitrite bonds in each complex, it is possible to compare the AOM parameters obtained for the two coordination modes (Table 5.10). The bonding parameters are pleasingly self-consistent, particularly considering the marked differences between the other ligands in the set of complexes. This implies that AOM bonding parameters for a ligand may indeed be reliably transferred from one complex to another, provided that differences in bond length are properly accounted for.

	e_σ(nitrite)	$e_{\pi y}$(nitrite)
[Ni(NH$_3$)$_4$(NO$_2$)$_2$]	3 850	-200
[Ni(en)$_2$(NO$_2$)$_2$]	3 695	-100
[Ni(tn)$_2$(NO$_2$)$_2$]	3 700	-100
cis-[Ni(L1)$_2$(NO$_2$)$_2$]	3 900	-100
[Ni(L2)$_2$(NO$_2$)$_2$]	4 000	-205
[Ni(L2)$_2$(ONO)$_2$]	3 370	505
[Ni(3,5-lutidine)$_4$(ONO)$_2$]	3 400	515
[Ni(N,N-dimen)$_2$(ONO)$_2$]	3 430	350

Table 5.10: A summary of the e_σ(nitrite) and $e_{\pi y}$(nitrite) AOM parameters derived for the nickel(II) nitrite complexes with monodentate nitrite coordination. All have been scaled for a bond length of 2.14Å. L1 = 1,2-diamino-2-methylpropane and L2 = 1-(2-aminoethyl)piperidine.

The e_σ parameter for the N-bonded nitrite, $3\ 830 \pm 170\ \text{cm}^{-1}$, is slightly higher in energy than that for the nitrito ligand, $3\ 400 \pm 30\text{cm}^{-1}$. This implies that the nitro ligand is a marginally stronger σ-donor than the nitrito ligand. A much greater difference is noticed when comparing the $e_{\pi y}$ parameters for the two coordination modes. In this case, the nitrito has a significant value, $450 \pm 100\text{cm}^{-1}$, while the nitro parameter is negative and small, $-140 \pm 65\text{cm}^{-1}$. This suggests that the O-bonded nitrite is a moderate π-donor, whereas for the nitro coordination mode the ligand acts as a weak π-acceptor. The large difference in the overall ligand field strength, and very different position in the spectrochemical series, is thus due mainly to the difference in the π-bonding of the two coordination modes.

5.5 Density Functional Theory Calculations

Nickel(II) complexes have been the subject of relatively few DFT calculations. As calculations of this type provided a considerable amount of information about the cobalt(III) and chromium(III) nitrite complexes discussed in the previous chapter, similar calculations were undertaken for the complexes $[Ni(NH_3)_4(NO_2)_2]$, $[Ni(en)_2(NO_2)_2]$ and $[Ni(N,N-dimen)_2(ONO)_2]$. Molecular geometries were calculated for each complex and compared with those obtained experimentally. This was also carried out for possible nitro and nitrito isomers of each of these complexes, and the total energies calculated were compared. The results were also compared with those of the AOM model. The nature of the transition at ~20 000cm^{-1} in the optical spectrum of nickel(II) nitro complexes was also investigated.

5.5.1 *The Geometry of the Nickel(II) Nitrite Complexes*

The geometry optimisations for the nickel(II) complexes were done in the same manner as described in Chapter 3, Section 3.4.1. Successful optimisations were carried out for $[Ni(NH_3)_4(NO_2)_2]$, $[Ni(en)_2(NO_2)_2]$ and $[Ni(N,N-dimen)_2(ONO)_2]$. Attempts to calculate similar properties for the nitro and nitrito isomers of $[Ni(1-(2-aminoethyl)piperidine)_2(NO_2)_2]$ were unsuccessful, as the conformation of the amine ligands could not be resolved.

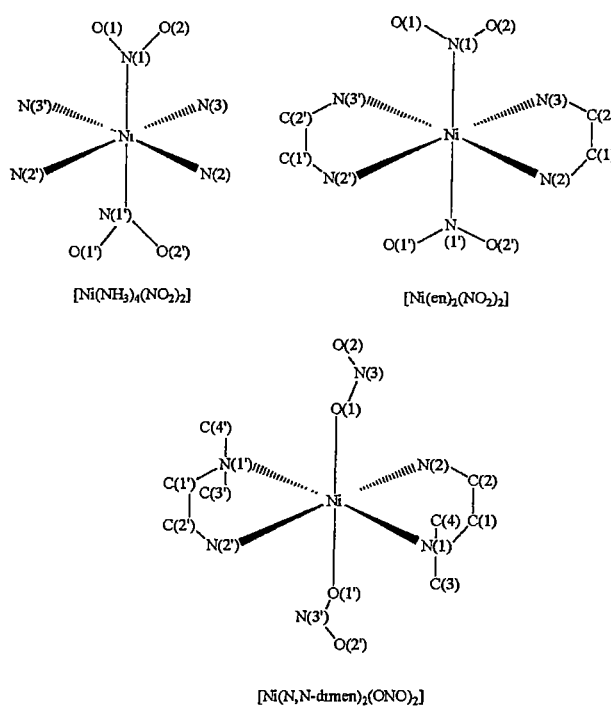The numbering systems for each complex are shown in Figure 5.18.

Figure 5.18: The numbering system used for the three complexes [Ni(NH₃)₄(NO₂)₂],
[Ni(en)₂(NO₂)₂] and [Ni(N,N-dimen)₂(ONO)₂] for the DFT
calculations.

The important bond lengths and angles calculated for [Ni(NH₃)₄(NO₂)₂] are listed in
Table 5.11.

	CALCULATED	CRYSTAL STRUCTURE[6]
Ni-N(1)	2.092	2.142
Ni-N(2)	2.176	2.109
Ni-N(3)	2.175	2.109
N1-O(1)	1.255	1.158
N1-O(2)	1.270	1.270
∠Ni-N(1)-O(1)	122.5	121.0
∠Ni-N(1)-O(3)	117.6	121.5
∠O(2)-N-O(3)	119.8	117.5
∠N(2)-Ni-N(3)	92.2	90.1

Table 5.11: The calculated bond lengths (Å) and angles (°) of [Ni(NH₃)₄(NO₂)₂]
compared with the crystal structure values[6].

Agreement between the calculated and observed bond lengths and angles is
moderate. The nickel-ammine lengths are calculated to be longer than the crystal

structure values, but this may be due to the use of gradient corrections, which tend to lengthen bonds.

Reasonable agreement between the calculated bond lengths and angles and structurally determined values was reached for the complex [Ni(en)$_2$(NO$_2$)$_2$] (Table 5.12).

	CALCULATED	CRYSTAL STRUCTURE[3]
Ni-N(1)	2.096	2.130
N(1)-O(1)	1.264	1.243
N(1)-O(2)	1.263	1.234
Ni-N(2)	2.138	2 089
Ni-N(3)	2.164	2.096
N(2)-C(1)	1.478	1.471
N(3)-C(2)	1.482	1 474
C(1)-C(2)	1.527	1.505
∠Ni-N(1)-O(1)	119.9	118.6
∠Ni-N(1)-O(2)	120.4	124.4
∠O(1)-N(1)-O(2)	119.7	117.0
∠N(2)-Ni-N(3)	82 1	82.1
∠Ni-N(2)-C(1)	108.4	108.0
∠Ni-N(3)-C(2)	107.2	109.5
∠N(2)-C(1)-C(2)	109.6	108.2
∠N(3)-C(2)-C(1)	109.4	109 2
∠N(1)-Ni-N(2)	89.7	89.5
∠N(1)-Ni-N(3)	91.5	92.8

Table 5.12: The calculated bond lengths (Å) and angles (°) of [Ni(en)$_2$(NO$_2$)$_2$] compared with the crystal structure values[3].

Again, the calculated geometry of [Ni(N,N-dimen)$_2$(ONO)$_2$] is similar to that measured experimentally. The significant lengthening of the Ni-N bonds to the tertiary amine group is reproduced successfully. Figure 5.19 also shows that the positions of the nitrito ligands in the crystal structure are the same as those calculated by DFT. Table 5.13 lists the important bond lengths and angles for this complex.
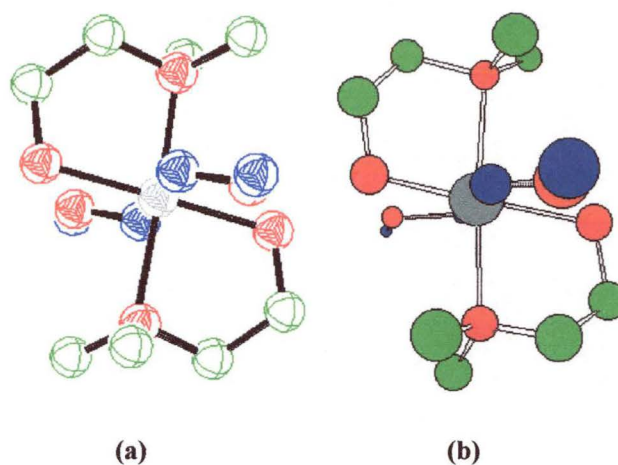
(a)   **(b)**

Figure 5.19: The observed (a) and calculated (b) molecular geometry for [Ni(N,N-dimen)$_2$(ONO)$_2$].

	CALCULATED	CRYSTAL STRUCTURE[3]
Ni-O(1)	2.101	2.113
O(1)-N(3)	1.328	1.288
O(2)-N(3)	1.233	1.215
Ni-N(1)	2.294	2.216
Ni-N(2)	2.123	2.077
N(1)-C(1)	1.486	1.481
C(1)-C(2)	1.524	1.511
N(1)-C(3)	1.478	1.472
N(1)-C(4)	1.480	1.478
∠Ni-O(1)-N(3)	115.8	119.3
∠O(1)-N(3)-O(2)	114.9	115.1
∠N(1)-Ni-N(2)	81.9	83.3
∠Ni-N(1)-C(1)	102.2	103.3
∠Ni-N(2)-C(2)	109.3	108.8
∠ C(3)-N(1)-C(4)	109.4	106.9
∠N(1)-Ni-O(1)	88.6	87.0
∠N(2)-Ni-O(1)	90.9	85.6
∠Ni-N(1)-C(3)	111.8	112.9
∠Ni-N(1)-C(4)	113.2	114.9
∠C(4)-N(1)-C(1)	109.5	108.4
∠C(3)-N(1)-C(1)	110.5	110.4

Table 5.13 : The calculated bond lengths (Å) and angles (°) of [Ni(N,N-dimen)$_2$(ONO)$_2$] compared with the crystal structure values[3].

5.5.2 *Comparison of the Calculated Energies of the Ni(II) Nitro and Nitrito Isomers*

The total energies for the possible nitrite isomers of the nickel(II) complexes are compared in Table 5.14.

	[Ni(NH₃)₄(NO₂)₂]	[Ni(en)₂(NO₂)₂]	[Ni(N,N-dimen)₂(ONO)₂]
Nitro	-121.28	-170.55	-234.45
Nitrito	-120.68	-170.08	-234.08

Table 5.14: A comparison of the energies (eV) calculated for nitro and nitrito isomers for the complexes [Ni(NH₃)₄(NO₂)₂], [Ni(en)₂(NO₂)₂] and [Ni(N,N-dimen)₂(ONO)₂].

These results suggest that for these three complexes, the nitro isomer is inherently slightly more stable than the nitrito isomer in every case. Although this is in agreement with observation in the solid state for the complexes [Ni(NH₃)₄(NO₂)₂] and [Ni(en)₂(NO₂)₂], this is not the case for [Ni(N,N-dimen)₂(ONO)₂]. However, the difference in energy is smallest for this complex. Furthermore, it must be remembered that these calculations are carried out for the gas phase. A nitro-nitrito equilibrium occurs for [Ni(N,N-dimen)₂(ONO)₂] in chloroform solution and here the nitro isomer is slightly more stable, though only by $2.8 \pm 1.2 \text{kJmol}^{-1}$ (~0.04eV). It is also possible that lattice forces in the crystal structure stabilise the nitrito isomer, but it is not possible to include these in the present calculations.

5.5.3 *Comparison of the DFT Calculations with the AOM Results*

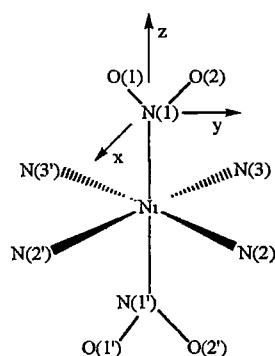The coordinate system used in the DFT calculation is shown overleaf (Figure 5.20).

Figure 5.20: The coordinate system for [Ni(NH$_3$)$_4$(NO$_2$)$_2$].

The important orbital energies calculated using DFT for the isomers of [Ni(NH$_3$)$_4$(NO$_2$)$_2$] are shown in Figure 5.21. This energy diagram is complicated by the presence of unpaired electrons, which results in the calculation of two sets of orbitals for the two possible electron spin states.
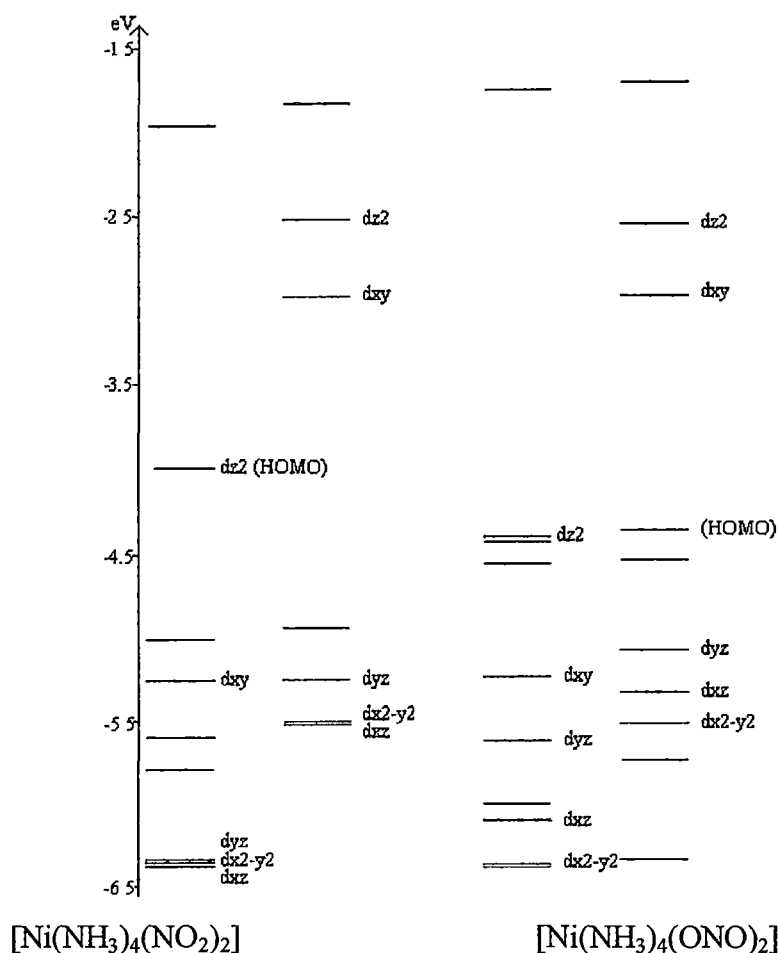

Figure 5.21: The calculated energies of the important orbitals of [Ni(NH$_3$)$_4$(NO$_2$)$_2$] and [Ni(NH$_3$)$_4$(ONO)$_2$]. Note that the two spins, α and β, have been separated and that the red orbitals are predominantly ligand-based.

The filled t_{2g} orbitals of both the nitro and nitrito complex are all of high d character (> 80%), but the α-spin dz^2 orbitals of both isomers are very covalent, with only ~30% d character. The other filled e_g orbital is less covalent, with ~50% d character. Several ligand based orbitals lie between the metal orbitals. This also occurred for the cobalt and chromium complexes (Chapter 4, Section 4.5).

The Δ values implied by the DFT results for the nitro and nitrito isomers of $[Ni(NH_3)_4(NO_2)_2]$ were 13 968cm^{-1} and 9 737cm^{-1}, respectively. As was the case for the cobalt and chromium complexes, these calculations have correctly reproduced the fact that the ligand is "weaker" when coordinating via oxygen, compared with N-coordination. This nitro value is comparable to that obtained from the AOM, 11 727cm^{-1}. Similar results were obtained for $[Ni(en)_2(NO_2)_2]$ and $[Ni(N,N\text{-dimen})_2(ONO)_2]$. The Δ values calculated for the nitro and nitrito isomers of $[Ni(en)_2(NO_2)_2]$ are 15 180cm^{-1} and 11 693cm^{-1}, and the AOM gave Δ = 12 133cm^{-1} for the nitro complex. The DFT-derived values of the nitro and nitrito isomers of $[Ni(N,N\text{-dimen})_2(ONO)_2]$ are 13 812cm^{-1} and 10 511cm^{-1}, respectively. The latter value is in excellent agreement with that obtained using the AOM, which is 10 404cm^{-1}.

Figure 5.21 shows that the dz^2 orbital is considerably higher in energy than the dxy orbital for the nitro isomer. This was also observed for the cobalt and chromium complexes, and implies that the nitro group is a stronger σ-donor than ammonia, as with the AOM interpretation. However, although the energy difference is smaller for the nitrito isomer, the dz^2 orbital is still higher in energy than the dxy orbital, which suggests that the nitrito ligand is a stronger σ-donor than ammonia, which contradicts the AOM interpretation. Similar results were obtained for the cobalt and chromium nitrito complexes.

The $dx^2\text{-}y^2$, dxz and dyz orbitals are of similar energy for the nitro isomer, while the dyz orbital is considerably higher in energy than the $dx^2\text{-}y^2$ and dxz orbitals for the nitrito isomer. This is consistent with the AOM results, which indicate that the nitro group is a weak π-acceptor, while the nitrito group acts as a moderate π-donor.

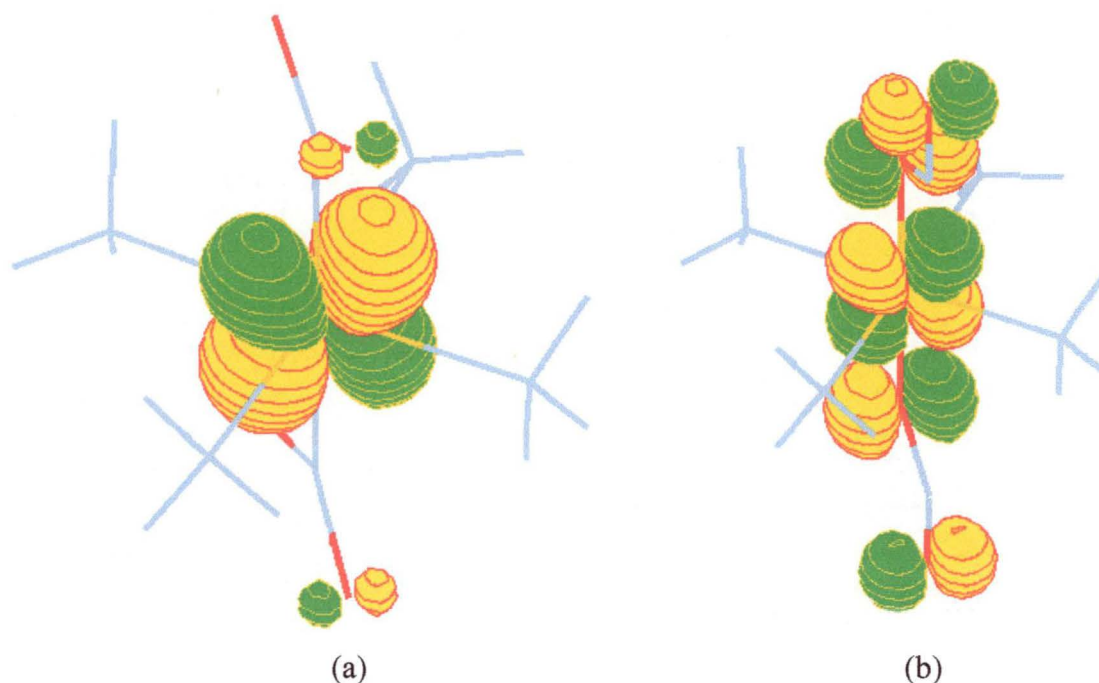Figure 5.22 illustrates the orbitals of predominantly dyz character for the nitro and nitrito isomers.

(a)   (b)

Figure 5.22: The α-spin dyz orbitals of the nitro (a) and nitrito (b) isomers of $[Ni(NH_3)_4(NO_2)_2]$.

The nitro isomer has little π-delocalisation, while the nitrito isomer shows a much greater π-interaction, which agrees with the AOM results.

The optical spectra of nickel(II) nitro complexes have an interesting feature at ~20 000cm^{-1}. Although this band was originally assigned as the second d-d transition expected for such complexes, more detailed spectroscopic studies carried out by Reinen et al.[21] and Caulton and Fenske[22] cast doubt upon this assignment. These authors concluded that it was most likely due to a charge transfer transition, though there was also evidence to suggest that it could be due to an internal nitrite n $\rightarrow \pi^*$ transition. During the present DFT studies, the energy difference between the highest filled e_g orbital and the lowest unoccupied orbital, the ligand-based π^* orbital (Figure 5.23), was calculated to be 16 110cm^{-1}.
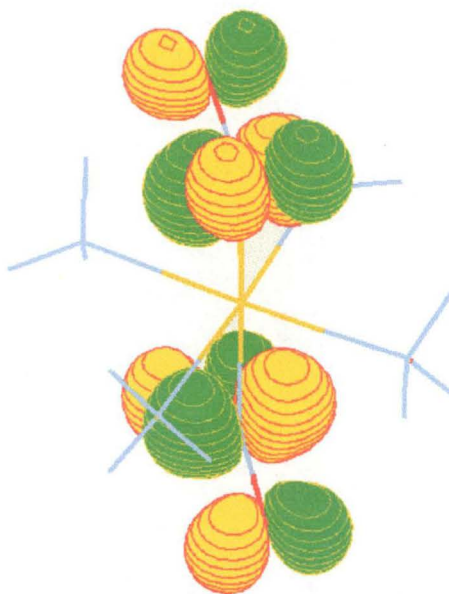
Figure 5.23: The empty π^* orbital of the complex $[Ni(NH_3)_4(NO_2)_2]$.

This is comparable to the energy of the "anomalous" band, so it is quite likely to be due to a metal $\rightarrow$ ligand π^* charge transfer transition. The reason why the peak has such a low intensity is not clear.

5.6 Summary

A number of nickel(II) nitrite complexes with monodentate nitro and nitrito ligands have been prepared. The infrared and Raman spectra measured for these complexes were used to assign the vibrational modes of the nitrite ligands. These showed that, upon nitrito coordination, ν_2 shifts significantly to lower energy compared with the ionic nitrite stretch. For nitro coordination, this stretching vibration shifts to higher energy, decreasing the energy difference between ν_2 and ν_3. The infrared and Raman spectra of the complex $[Ni(isoquinoline)_4(ONO)_x(NO_2)_{1-x}]$ suggested that both coordination modes are present in this sample.

Single crystal optical spectra were measured for a wide range of complexes. AOM parameters have been derived for the nitro and nitrito coordination modes, and these were found to be self-consistent, being $e_\sigma(NO_2) = 3\,830 \pm 170 cm^{-1}$ and $e_{\pi y}(NO_2) = -140 \pm 65 cm^{-1}$ for nitro coordination, and $e_\sigma(ONO) = 3\,400 \pm 30 cm^{-1}$ and $e_{\pi y}(ONO) = 450 \pm 100 cm^{-1}$ for nitrito coordination, normalised to a metal-ligand bond length of

2.14Å. This implies that a nitro group is a slightly stronger σ-donor than a nitrito ligand, and that the nitro group is a weak π-acceptor. The nitrito group is a moderate π-donor, and so the difference in the overall ligand field strength of these two coordination modes is mainly due to the difference in π-bonding.

The nitro and nitrito isomers of [Ni(NH$_3$)$_4$(NO$_2$)$_2$], [Ni(en)$_2$(NO$_2$)$_2$] and [Ni(N,N-dimen)$_2$(ONO)$_2$] were successfully modelled using DFT calculations. The calculated energies suggest that the nitro isomer is inherently slightly more stable than the nitrito isomer. This agrees with observation in the solid state for [Ni(NH$_3$)$_4$(NO$_2$)$_2$] and [Ni(en)$_2$(NO$_2$)$_2$], but not for [Ni(N,N-dimen)$_2$(ONO)$_2$]. However, the difference in the energies calculated for both isomers was the smallest for the complex with the substituted amines, and the nitro form is indeed the most stable isomer for this complex in chloroform solution.

DFT calculations were also used to derive Δ values, and these are similar to those obtained using the AOM. The results confirm that nitrite ions act as a π-donor when it is O-bonded, compared with that of the N-bonded ligand. The peak at ~20 000cm^{-1} observed in the electronic spectra of nickel(II) nitro complexes was deduced to be a metal to ligand charge transfer transition, from the highest occupied molecular orbital (predominantly the Ni^{2+} dz^2 orbital) to the lowest unoccupied molecular orbital, which was the π* orbital of the nitrite ligand.

5.7 References

1. Hitchman M.A. and Rowbottom G.L., *Coord. Chem. Rev.*, **42**, 55-132, (1982).

2. Porai-koshits M.A. and Minacheva L.Kh., *J. Struct. Chem.*, **5**, 595-597, (1964).

3. Finney A.J., Hitchman M.A., Raston C.L., Rowbottom G.L. and White A.H., *Aust. J. Chem.*, **34**, 2047-2060, (1981).

4. Finney A.J., Hitchman M.A., Raston C.L., Rowbottom G.L. and White A.H., *Aust. J. Chem.*, **34**, 2069-2084, (1981).

5. Lever A.B.P., *Inorganic Electronic Spectroscopy (2nd Edition)*, Elsevier Science Publishers, Amsterdam, (1984).

6. Figgis B.N., Reynolds P.A., White A.H., Williams G.A. and Wright S., *J. Chem. Soc. Dalton Trans.*, 997-1003, (1981).

7. Bertini I., Gatteschi D. and Scozzafava A., *Inorg. Chem.*, **15(1)**, 203-207, (1976).

8. Grey I.E., Hitchman M.A., Rowbottom G.L., Scarlett N.V.Y. and Wilson J., *J. Chem. Soc. Dalton Trans.*, 595-601, (1994).

9. Kennedy B.J., Murray K.S., Hitchman M.A. and Rowbottom G.L., *J. Chem. Soc. Dalton Trans.*, 825-830, (1987).

10. Walker I.M., Lever A.B.P. and McCarthy P.J., *Can. J. Chem.*, **58**, 823-832, (1980).

11. Lever A.B.P, Walker I.M. and McCarthy P.J., *Can. J. Chem.*, **69**, 495-500, (1982).

12. Das D., Laskar I.R., Ghosh A., Mondal A., Okomoto K. and Chaudhuri N.R., *J. Chem. Soc. Dalton Trans.*, 3987-3990, (1998).

13. Goodgame D.M.L. and Hitchman M.A., *Inorg. Chem.*, **6**, 813-816, (1967).

14. Goodgame D.M.L. and Hitchman M.A., *Inorg. Chim. Acta*, **3(2)**, 319-322, (1969).

15. Green R.W. and Bell B., *Aust. J. Chem.*, **26**, 1663-1668, (1973).

16. Laskar I.R., Ghosh A., Mostafa G., Das D., Mondal A. and Chaudhuri N.R., *Polyhedron*, **19**, 1015-1020, (2000).

17. Takeuchi A., Sato K., Sone K., Yamada S. and Yamasaki K., *Inorg. Chim. Acta*, **1(3)**, 399-402, (1967).

18. Ribas J., Diaz L., Monfort M., Vilana J., Solans X. and Font-Altaba M., *Trans. Met. Chem.*, **10**, 340-344, (1985).

19. Hitchman M.A. and Ahsbahs H., *Inorg. Chim. Acta*, **53**, L97-L98, (1981).

20. Cortes R., Arriortua M.I., Rojo T., Solans X. and Beltran D., *Polyhedron*, **5(12)**, 1987-1990, (1986).

21. Reinen D., Friebel C. and Reetz K.P., *J. Solid State Chem.*, **4**, 103-114, (1972).

22. Caulton K.G. and Fenske R.F., *Inorg. Chem.*, **6**, 562-568, (1967).

23. Sidman J.W., *J. Amer. Chem. Soc.*, **79**, 2675-2678, (1957).

24. Hitchman M.A. and James G., *Inorg. Chim. Acta*, **88**, L19-21, (1984).

25. El-Sayed L. and Ragsdale R.O., *Inorg. Chem.*, **6**, 1640-1643, (1967).

26. Goldberg M.J. and Marsh R.E., *Acta Cryst.*, **B35**, 960-962, (1979).

27. Jorgensen C.K., *Acta Chem. Scand.*, **9**, 1362-1377, (1955).

28. Hitchman M.A. and Rowbottom G.L., *Inorg. Chem.*, **21**, 823-825, (1982).

29. Astley T., Canty A.J., Hitchman M.A., Rowbottom G.L., Skelton B.W. and White A.H., *J. Chem. Soc. Dalton Trans.*, 1981-1984, (1991).

CHAPTER 6

Bridging and Chelating Nitrites

The ability of the nitrite ion to act as a bridging ligand between metal centres has been exploited in recent times. As well as being of interest to bioinorganic chemists studying polynuclear reaction sites common in biological processes, complexes of this type have been synthesised so as to produce materials with novel magnetic properties. The bridging nitrite coordination modes that have been seen experimentally are shown in Figure 6.1.
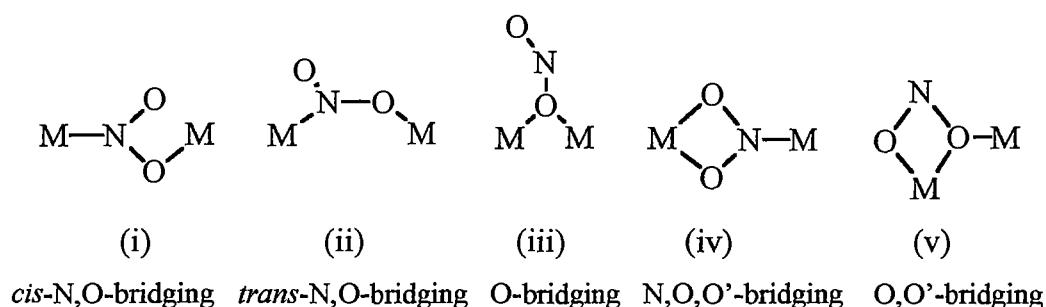

(i)	(ii)	(iii)	(iv)	(v)
cis-N,O-bridging	*trans*-N,O-bridging	O-bridging	N,O,O'-bridging	O,O'-bridging

Figure 6.1: The bridging coordination modes of the nitrite ion.

In this chapter, nickel(II) nitrite complexes with the coordination modes (i), (ii) and (iv) (Figure 6.1) will be discussed. Coordination mode (iii) has been seen in some nickel(II) nitrite complexes such as [Ni$_5$(N,N-dimen)$_4$(NO$_2$)$_8$(OH)$_2$].CH$_3$CN, where N,N-dimen = N,N-dimethylethylenediamine, which has two such groups per formula unit, as well as six nitrites with type (ii) coordination[1]. The only example of a complex with type (v) coordination is a mixed metal complex, [Cu(oxpn)Ni(trimen)NO$_2$]ClO$_4$, with trimen = N,N,N'-trimethylethylenediamine and oxpn = N,N-bis(3-aminopropyl)oxamide[2].

As well as bidentate coordination by bridging, the nitrite ion may also coordinate via an O,O'-chelating mode. Complexes of this type have been investigated in the present work as they are expected to exhibit "bent bonding". The bite angle ($\angle$ O-M-O') in these complexes is approximately 60°, which is much less than the "ideal" octahedral angle of 90° (Figure 6.2).
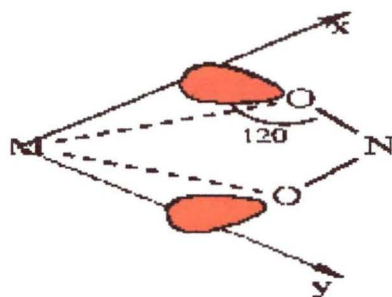
Figure 6.2: Oxygen orbital positions for a chelating nitrite.

In this situation, the ligand lone pair orbitals bend significantly away from the metal-oxygen bond vectors and the σ-orbital overlap is reduced. This lowers the σ bonding and introduces an interaction with the d orbitals of π symmetry. An important aspect of the present work is to test the extension of the AOM to include bent bonding. As the bite angles of chelating O,O'-nitrito ligands are so much less than 90°, it is possible that the effect of bent bonding is quite large for these complexes, making them ideal candidates to study this extension of the AOM.

Few optical spectroscopic studies involving nickel(II) complexes with chelating and bridging nitrite ligands have been carried out[1]. For this reason, a number of these complexes have been prepared and their low temperature, single crystal optical spectra were measured. Information obtained from these measurements was then used to derive AOM parameters for the nitrite ligands. Infrared and Raman spectra were also measured for these complexes.

6.1 Experimental

The complexes [Ni(2,3-lutidine)$_2$(O$_2$N)$_2$] and [Ni(2,5-lutidine)$_2$(O$_2$N)$_2$] were prepared in the following manner. Methanolic solutions of 2,3-lutidine (0.01mol) and 2,5-lutidine (0.01mol) were added to methanolic solutions of nickel(II) nitrite (0.02mol in 10mL methanol). These nickel(II) nitrite solutions had been prepared metathetically from the reaction of nickel(II) nitrate with sodium nitrite. After leaving these solutions for a few days at room temperature, the green precipitates were collected and recrystallised from methanol. Microanalytical results for [Ni(2,3-lutidine)$_2$(O$_2$N)$_2$]: found, calculated: %N 15.41, 15.35; %C 46.19, 46.06; %H 4.97,

4.97%. The complex [Ni(2,5-lutidine)$_2$(O$_2$N)$_2$] has been shown by X-ray diffraction to invariably have approximately one nitrate molecule present for every four molecules in the crystal structure[3], and the sample prepared in the current work appears to have a similar nitrate to nitrite ratio. Attempts to prepare this complex from the starting material K$_4$[Ni(NO$_2$)$_6$].H$_2$O to avoid possible nitrate contamination from the metathetically prepared nickel(II) nitrite solutions were unsuccessful. Microanalysis, assuming that one nitrite in four is replaced by nitrate: found, calculated: %N 14.60, 14.71; %C 43.70, 44.13; %H 4.87, 4.76%.

[Ni(quinoline)$_2$(O$_2$N)$_2$] was prepared via the method of Goodgame and Hitchman[4]. Small green crystals were obtained after recrystallisation from methanol. Microanalysis: found, calculated: %N 13.90, 13.70; %C 52.93, 52.85; %H 3.50, 3.43%.

[(CH$_3$)$_4$N]Ni(NO$_2$)$_3$ was prepared by the method described by Goodgame and Hitchman[5]. Small crystals of better optical quality were also obtained in a manner similar to Chou et al[6]. An aqueous solution of nickel(II) bromide and tetramethylammonium bromide was layered on top of an aqueous solution of sodium nitrite, and these solutions were allowed to mix slowly. Very small light brown crystals formed at the interface of the two solutions, and these could be collected. As this complex is insoluble in all common solvents, larger crystals could not be obtained via recrystallisation. This complex was characterised by its infrared spectrum[5].

[Ni(en)$_2$NO$_2$]ClO$_4$, with en = ethylenediamine, was prepared by the method described by Hathaway and Slade[7]. Ethylenediamine (0.015mol) and sodium nitrite (0.05mol) were added to an aqueous solution of nickel perchlorate (0.05mol). After leaving the blue solution at room temperature for a few days, red crystals of the desired product could be isolated. Microanalysis: found, calculated: %N 21.48, 21.50; %C 14.87, 14.81; %H 5.11, 4.97%.

[Ni(tn)$_2$(NO$_2$)$_2$], with tn = 1,3-diaminopropane, was prepared via the method of Green and Bell[8]. This was then used in the synthesis of [Ni(tn)$_2$NO$_2$]ClO$_4$ as described by Ribas et al[9]. Microanalysis: found calculated: %N 19.74, 19.88; %C 20.40, 20.45; %H 5.94, 5.72%.

The series of complexes [Ni$_2$(dpt)$_2$(NCS)$_3$NO$_2$], [Ni$_2$(medpt)$_2$(NCS)$_3$NO$_2$].H$_2$O and [Ni(medpt)(NCS)NO$_2$], with dpt = bis(3-aminopropyl)amine and medpt = bis(3-aminopropyl)methylamine, were prepared by the method described by Escuer et al[10]. [Ni(medpt)(NO$_2$)$_2$] was prepared via the method of Wen et al[11]. Microanalysis for [Ni$_2$(dpt)$_2$(NCS)$_3$NO$_2$]: found, calculated: %N 23.35, 23.35; %C 30.06, 30.02; %S 15.87, 16.03; %H 5.73, 5.71%. [Ni$_2$(medpt)$_2$(NCS)$_3$NO$_2$].H$_2$O: found, calculated: %N 21.76, 21.76; %C 31.79, 31.70; %H 6.01, 5.95%. [Ni(medpt)(NCS)NO$_2$]: found, calculated: %N 22.54, 22.74, %C 30.99, 31.19; %H 6.15, 6.22. [Ni(medpt)(NO$_2$)$_2$]: found, calculated: %N 23.48, 23.67; %C 28.61, 28.41; %H 6.45, 6.47%.

Attempts to prepare analogous halide complexes for IR and Raman comparisons were unsuccessful. The Raman measurements for the complex [(CH$_3$)$_4$N]Ni(NO$_2$)$_3$ were also problematic, as this complex absorbed strongly at the wavelength of the laser used. The only solution was to measure at a different wavelength, and these measurements were carried out by Associate Professor Bill van Bronswijk at the School of Applied Science, Curtin University of Technology, Western Australia. All other IR and Raman measurements were carried out as described previously, as were the microanalyses.

Optical spectroscopic measurements were carried out as described previously. As the crystals of [(CH$_3$)$_4$N]Ni(NO$_2$)$_3$ were too small to be measured on the Cary 5e spectrophotometer, the room and low temperature spectra of these were measured using the specialised equipment at the Research School of Chemistry, ANU.

The crystal structure of [Ni(tn)$_2$(NO$_2$)]ClO$_4$ was measured by Professor Charles Simmons at the University of Hawaii at Hilo. This was done using an Enraf-Nonius CAD4 MACH diffractometer with graphite monochromatic Mo Kα radiation (λ = 0.71073Å). The unit cell constants and their standard deviations were determined by a least-squares treatment (CELDIM) of the angular coordinates of 25 high-angle 2θ reflections. The θ-2θ scan mode was used with a variable scan rate. The intensities of three check reflections showed no discernable decrease. All diffraction intensities were corrected for Lorentz and polarisation effects and for absorption using seven ψ scans. The structures were refined using full-matrix least squares methods with

anisotropic displacement factors for the non-H atoms and fixed isotropic B values for the H's. Refinements were based on F, and computations were performed on a Dec-alpha computer using the teXsan software package. The crystal structure of [Ni(quinoline)$_2$(O$_2$N)$_2$] was measured by Professor Allan White and Dr B.W. Skelton at the University of Western Australia (see Chapter 3 for general details).

6.2 Vibrational Spectroscopy

The problems faced when assigning the infrared and Raman spectra of nickel(II) complexes with monodentate nitrite ligands also had to be dealt with when assigning the spectra of the present nickel(II) complexes containing bridging and chelating ligands. An added complication in these assignments was that analogous halide complexes could not be prepared. However, using both the Raman and infrared spectra, it was possible to determine the energies of ν_1, ν_2 and ν_3 for most of the complexes, and these are listed in Table 6.1. Also included in this table are references to other infrared spectral data, where available, and the vibrational energies of ionic nitrite for comparative purposes.

	MODE	ν_1	ν_2	ν_3
Ni(2,3-lutidine)$_2$(O$_2$N)$_2$	O,O'-chelating	865[c]	1 200[a]	1 300[b]
Ni(quinoline)$_2$(O$_2$N)	O,O'-chelating	865[c]	1 200[a]	1 300[c]
Ni(2,5-lutidine)$_2$(O$_2$N)$_2$	O,O'-chelating	860[c]	1 210[a]	1 300[b]
[Ni(medpt)(NCS)NO$_2$]	O,O'-chelating	Obscured	1 209[c]	1 283[c]
[Ni(medpt)(NO$_2$)$_2$]	nitro and O,O'-chelating	815[c]	1 201[a], 1 271[a]	1 306[b]
[Ni(en)$_2$NO$_2$]ClO$_4$	cis-N,O-bridging	854[c] [860][7]	1 252[c] [1256][7]	1 380[b]
[Ni(tn)$_2$NO$_2$]ClO$_4$	cis-N,O-bridging	851[c] [815][9]	1 265[c] [1260][9]	1 365[c] [1365][9]
[(CH$_3$)$_4$N]Ni(NO$_2$)$_3$	trans-N,O-bridging	860[c] [852][5]	1 200[a] [1202][5]	1 431[b] [1435][5]
[Ni$_2$(NCS)$_3$(medpt)$_2$NO$_2$]	N,O,O'-bridging	Obscured	1 204[a]	1 298[b]
[Ni$_2$(NCS)$_3$(dpt)$_2$NO$_2$]	N,O,O'-bridging	Obscured	1200[a]	1 281[b]
Ionic nitrite (NaNO$_2$)		810	1 240	1 330

Table 6.1: The nitrite vibration energies for a number of nickel(II) nitrite complexes with bridging and/or chelating ligands. Also included are the reported vibrational energies for some of the complexes (bracketed values) and ionic nitrite. (a): infrared only, (b): Raman only, (c) seen in both spectra.

The energies of the nitrite stretching vibrations, v_2 and v_3, are shifted to slightly lower energy than those of the free ion upon bidentate O,O'-chelating coordination. The bridging mode present in the complexes [Ni(en)$_2$NO$_2$]ClO$_4$ and [Ni(tn)$_2$NO$_2$]ClO$_4$ does not have a great effect on the vibrational energies of the nitrite, and this may be due to the relatively long Ni-N and Ni-O bonds present in these complexes[13]. In addition, this manner of N,O-bridging leaves the non-coordinated oxygen in quite close proximity to the Ni^{2+} ion, so that the difference between the nitrite oxygen atoms is less pronounced than for the *trans* N,O-bridging mode (Figure 6.3). The energy difference between v_2 and v_3 may be correlated with the significant difference in the N-O bond lengths of the bridging nitrites.
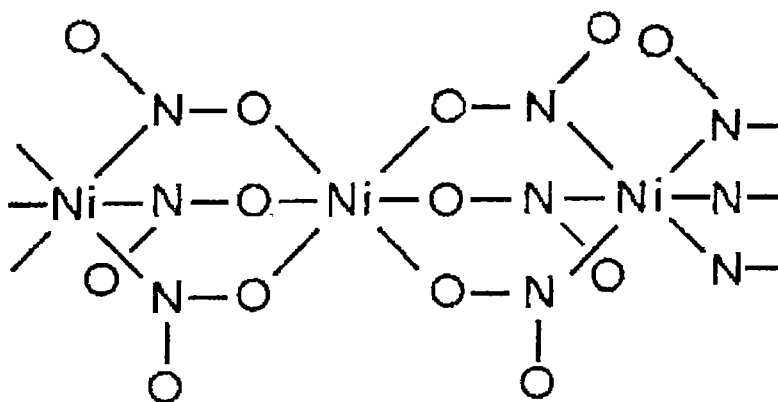

Figure 6.3: A simplified structure of [(CH$_3$)$_4$N]Ni(NO$_2$)$_3$ showing the two nickel(II) environments.

The N,O,O'-bridging mode seen in [Ni$_2$(NCS)$_3$(medpt)$_2$NO$_2$] and [Ni$_2$(NCS)$_3$(dpt)$_2$NO$_2$] results in similar energies to those seen for O,O'-chelation.

The complex [Ni(medpt)(NO$_2$)$_2$] has both a nitro-coordinated and an O,O'-chelating nitrite. The two energies quoted for v_2 in Table 6.1 can be assigned to these different nitrite groups.

6.3 The Crystal Structure of [Ni(tn)₂NO₂]ClO₄ and [Ni(quinoline)₂(O₂N)₂]

Although [Ni(tn)₂NO₂]ClO₄ has been prepared by Ribas et al.[9] they did not report its crystal structure. These authors assumed that it was structurally similar to [Ni(en)₂NO₂]ClO₄ by comparing the infrared and reflectance spectra obtained for the two complexes. To confirm this, the crystal structure was measured in the present study.

An ORTEP[14] diagram of [Ni(tn)₂NO₂]ClO₄ is shown in Figure 6.4. Hydrogen atoms have been omitted for clarity, as have the perchlorate counterions.

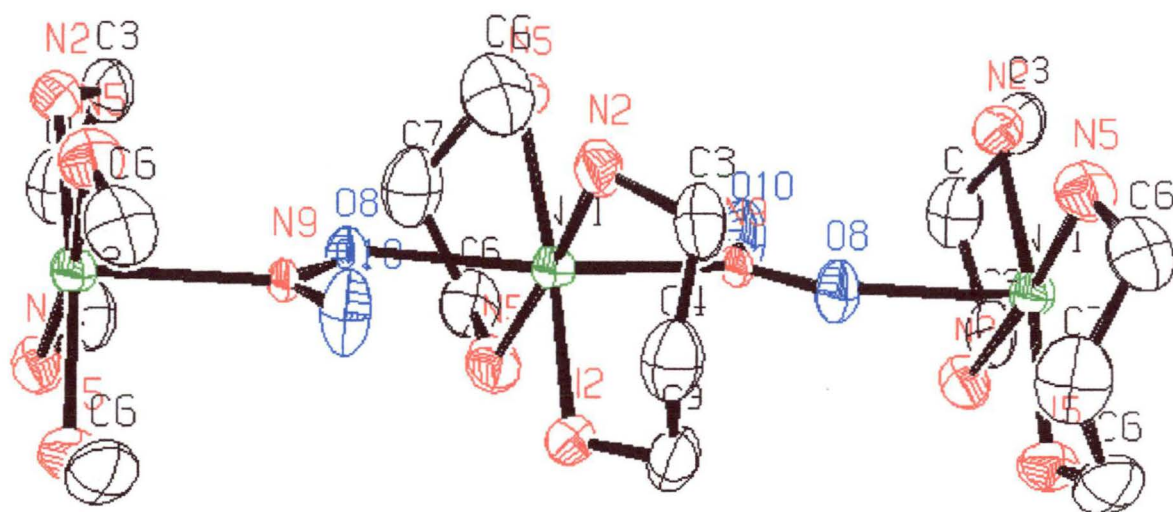**Figure 6.4**: The structure of [Ni(tn)₂NO₂]ClO₄.

Figure 6.4 shows three nickel ions and the nitrite bridges between these metal ions. Each nickel ion is bonded to the nitrogen atom of one nitrite ligand, and an oxygen atom from another, forming a polymeric complex. This is similar to the structure of [Ni(en)₂NO₂]ClO₄, though, unlike the ethylenediamine complex[13], there is no disorder in the present complex.

The important crystallographic details are listed in Table 6.2, and the important bond lengths and angles are listed in Tables 6.3 and 6.4. Further details are listed in Appendix C.

Molecular formula	$NiClO_6N_5C_6H_{20}$
Molecular weight	352.41
Crystal system	Orthorhombic
Space group	Pnma
A	10.5988(2) Å
B	8.5029(2) Å
C	15.4045(4) Å
V	1388.26(5)Å^3
Z	4
D	1.686g/cm^3
F(000)	736.00
T	296
R	0.059

Table 6.2: Summary of crystallographic data for $[Ni(tn)_2NO_2]ClO_4$.

	BONDLENGTH (Å)		**BONDLENGTH (Å)**
Ni-N(9)	2.163	Ni-N(5)	2.117
Ni-O(8)	2.290	N(2)-C(3)	1.468
O(8)-N(9)	1.250	C(3)-C(4)	1.528
O(10)-N(9)	1.235	N(5)-C(6)	1.491
Ni-N(2)	2.102	C(6)-C(7)	1.489

Table 6.3: Important bond lengths for the complex $[Ni(tn)_2NO_2]ClO_4$.

	ANGLE (°)		**ANGLE (°)**
Ni-O(8)-N(9)	130.7	O(8)-Ni-N(5)	83.7
O(8)-N(9)-O(10)	116.7	O(8)-Ni-N(2)	90.6
Ni-N(9)-O(8)	127.5	N(9)-Ni-N(5)	90.3
Ni-N(9)-O(10)	115.8	N(9)-Ni-N(2)	95.6
Ni-N(5)-C(6)	127.3	O(8)-Ni-N(9)	171.2
N(5)-C(6)-C(7)	118.7	N(2)-C(3)-C(4)	113.0
C(6)-C(7)-C(6')	115.8	Ni-N(2)-C(3)	119.7

Table 6.4: Important bond angles for the complex $[Ni(tn)_2NO_2]ClO_4$.

Apart from ∠O(8)-Ni-N(5), the coordination geometry around the nickel ions is very close to octahedral. This is not the case for [Ni(en)₂NO₂]ClO₄, where these angles differ from the ideal octahedral angles of 90° by up to 10° [13].

A comparison of the Ni-N(9) and Ni-O(8) bond lengths with corresponding bond lengths in complexes with monodentate nitro and nitrito ligands reveals that these bonds are longer in the complex [Ni(tn)₂NO₂]ClO₄. The Ni-N bond lengths in [Ni(NH₃)₄(NO₂)₂], [Ni(en)₂(NO₂)₂] and [Ni(1-(2-aminoethyl)piperidine)₂(NO₂)₂] are 2.14Å [15], 2.130Å [16] and 2.148Å, respectively, so that these are all shorter than the 2.163Å bond determined for [Ni(tn)₂NO₂]ClO₄. This Ni-N(9) length is the same as that measured for the complex [Ni(en)₂NO₂]ClO₄. Likewise, the Ni-O(8) length in [Ni(tn)₂NO₂]ClO₄ (2.290Å) is considerably longer than the analogous bond in [Ni(3.5-lutidine)₄(ONO)₂], [Ni(N,N-dimen)₂(ONO)₂] and [Ni(1-(2-aminoethyl)piperidine)₂(ONO)₂], which were 2.08Å, 2.169Å [16] and 2.113Å [17], respectively. It is also longer than that seen in the analogous complex [Ni(en)₂NO₂]ClO₄, where this bond length is 2.183Å. The complex Cs₂[Zn(ONO)₄] has asymmetrically chelating nitrites, with each nitrite having Zn-O bond lengths of 2.516Å and 2.081Å. The difference between these is much less than for the analogous Ni-O bond lengths of this complex, where Ni-O(8) is 2.290Å and Ni-O(10) is 3.336Å. This latter distance is much too large for this nitrite to be regarded as an asymmetrically chelating ligand, unlike the zinc complex in which the interaction between the zinc ion and oxygen atom of the longer bond was still regarded as significant.

It has been shown that the complexes [Ni(en)₂NO₂]X, X = ClO₄⁻, BF₄⁻ and PF₆⁻, are isomorphous [13]. The complexes [Ni(en)₂NO₂]X, X = Cl⁻,Br⁻, I⁻ and NO₃⁻, are also isomorphous, but with different structures from the former complexes [18]. The crystal structure determined for the chloride complex by Wen et al. [18] shows that the nickel ion has an O,O'-chelating nitrite bonded to it, and no bridging nitrite groups. The reason why the counterion affects the coordination mode of the nitrite ion in these complexes is not clear.

During the present study, the morphology of a crystal of [Ni(quinoline)₂(O₂N)₂] was determined, and it was found that the crystal structure of this sample (structure B)

was different to that previously published (structure A)[19]. Figure 6.5 is a diagram of the published molecular geometry. This is clearly different to that determined in the present work (Figure 6.6).

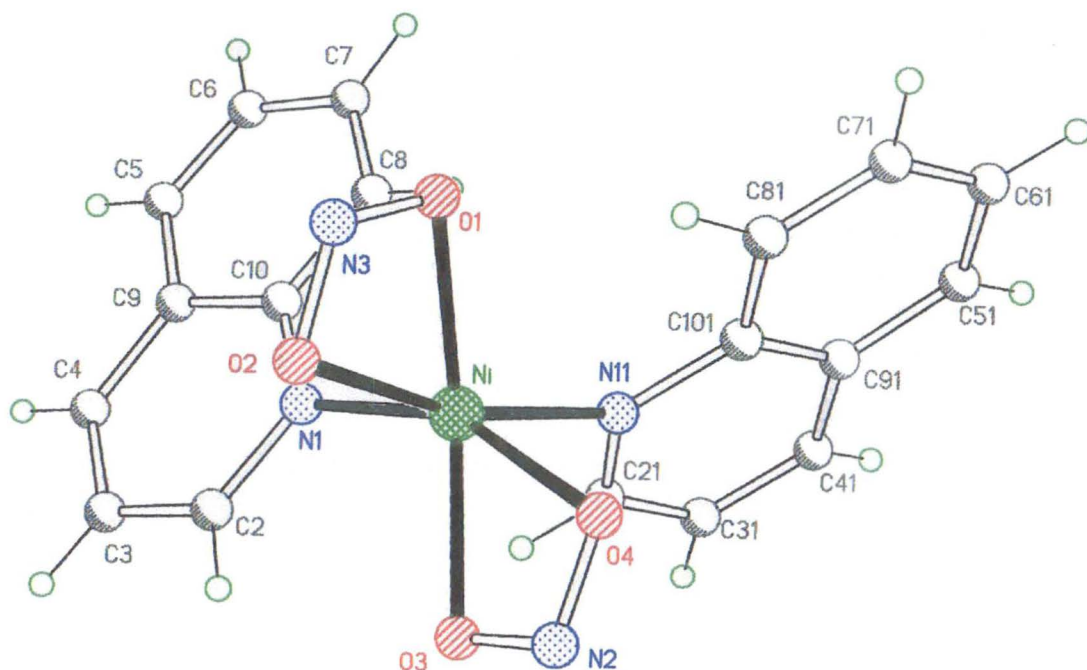**Figure 6.5**: The previously reported molecular geometry of [Ni(quinoline)$_2$(O$_2$N)$_2$] (Structure A) (from Hitchman et al.[19]).

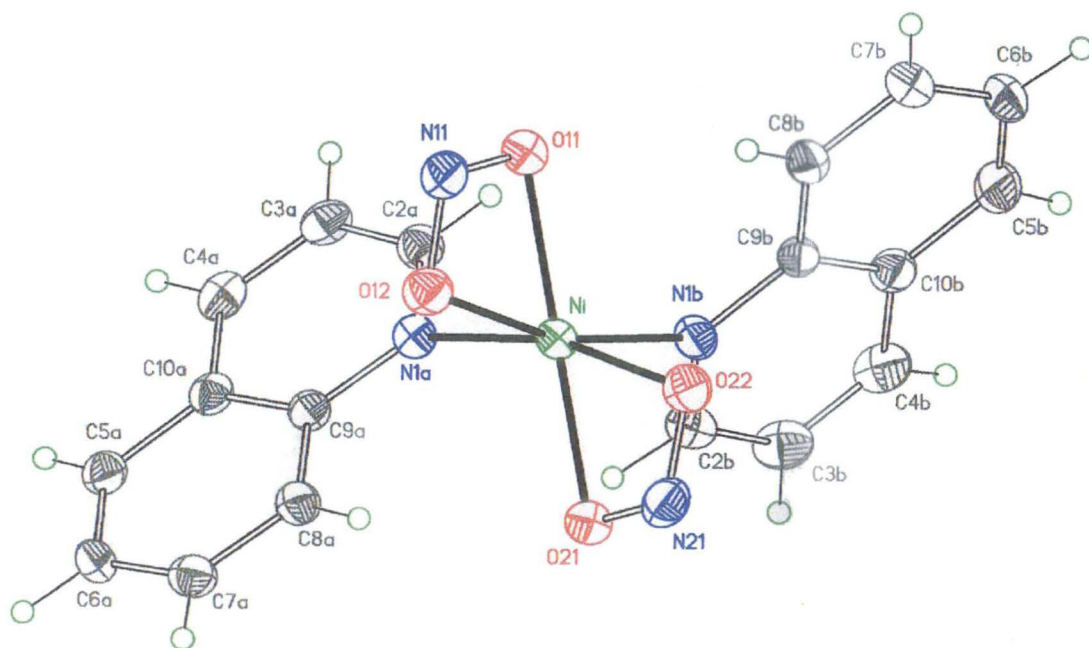**Figure 6.6**: The molecular geometry of [Ni(quinoline)$_2$(O$_2$N)$_2$] determined in the present work (Structure B).

The important crystallographic details for [Ni(quinoline)$_2$(O$_2$N)$_2$] obtained from these measurements are listed in Table 6.5, and the important bond lengths and angles are listed in Tables 6.6 and 6.7. Further details are listed in Appendix D.

Molecular formula	NiO$_4$N$_4$C$_{18}$H$_{14}$
Molecular weight	409.04
Crystal system	Monoclinic
Space group	P21/c
A	7.4040(15) Å
B	7.6200(15) Å
C	30.785(6) Å
V	1736.2(6) Å^3
α	90.0°
β	91.51°
γ	90.0°
Z	4
D	1.565g/cm^3
F(000)	840
T	150K
R	0.061

Table 6.5: Summary of crystallographic data for [Ni(quinoline)$_2$(O$_2$N)$_2$].

	BONDLENGTH (Å)			BONDLENGTH (Å)	
Ni-N(1a)	2.069	(2.065)	Ni-O(12)	2.117	(2.117)
Ni-N(1b)	2.063	(2.071)	O(11)-N(11)	1.275	(1.275)
Ni-O(21)	2.0715	(2.101)	O(12)-N(11)	1.264	(1.246)
Ni-O(22)	2.123	(2.138)	O(21)-N(21)	1.259	(1.251)
Ni-O(11)	2.0791	(2.068)	O(22)-N(21)	1.265	(1.249)

Table 6.6: Important bond lengths for the complex [Ni(quinoline)$_2$(O$_2$N)$_2$]. Bond lengths in brackets are the corresponding lengths for Structure A of the [Ni(quinoline)$_2$(O$_2$N)$_2$] complex (from Hitchman et al.[19]).

	ANGLE (°)			ANGLE (°)	
N(1b)-Ni-N(1a)	93.85	(97.1)	N(1a)-Ni-O(22)	165.40	(156.9)
N(1b)-Ni-O(21)	92.50	(89.3)	O(21)-Ni-O(22)	59.66	(59.8)
N(1a)-Ni-O(21)	106.37	(97.5)	O(11)-Ni-O(22)	101.12	(101.4)
N(1b)-Ni-O(11)	105.36	(107.3)	O(12)-Ni-O(22)	89.23	(88.5)
N(1a)-Ni-O(11)	90.77	(90.5)	O(12)-N(11)-O(11)	111.3	(113.2)
O(21)-Ni-O(11)	154.45	(151.9)	N(11)-O(11)-Ni	95.10	(94.8)
N(1b)-Ni-O(12)	165.01	(165.3)	N(11)-O(12)-Ni	93.66	(93.4)
N(1a)-Ni-O(12)	89.46	(90.5)	O(21)-N(21)-O(22)	111.5	(118.8)
O(21)-Ni-O(12)	100.60	(97.5)	N(21)-O(21)-Ni	95.72	(94.9)
O(11)-Ni-O(12)	59.93	(59.0)	N(21)-O(22)-Ni	93.09	(93.4)
N(1b)-Ni-O(22)	91.15	(89.3)			

Table 6.7: Important bond angles for the complex [Ni(quinoline)$_2$(O$_2$N)$_2$]. Bond angles in brackets are the corresponding angles for Structure A of the [Ni(quinoline)$_2$(O$_2$N)$_2$] complex (from Hitchman et al.[19]).

Perhaps the most obvious difference between structures A and B is the disposition of the aromatic rings around the metal ion. The second ring is *cis* in structure A, but *trans* in structure B. However, the bond lengths and angles are similar for both structures and the chelating nitrite groups are *cis* to each other in the two structures. This means that the optical spectra measured for crystals of the two structures are unlikely to differ to any great degree.

6.4 Optical Spectroscopy

6.4.1 *O,O'-Chelating Nitrite Ligands*

The complexes [Ni(2,3-lutidine)$_2$(O$_2$N)$_2$] and [Ni(quinoline)$_2$(O$_2$N)$_2$] have O,O'-chelating nitrite groups that are *cis* to each other (Figure 6.7)[20].

[Ni(2,3-lutidine)₂(O₂N)₂]   [Ni(quinoline)₂(O₂N)₂]
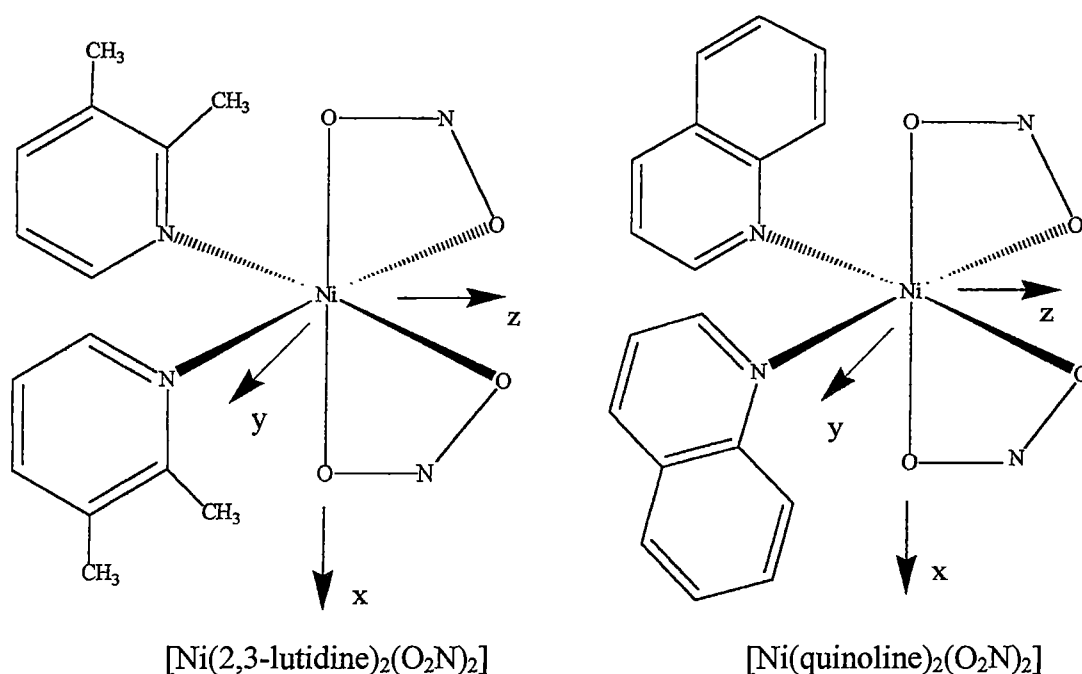
Figure 6.7: The geometry of Ni(2,3-lutidine)$_2$(O$_2$N)$_2$ and Ni(quinoline)$_2$(O$_2$N)$_2$, with molecular axes defined.

Figure 6.8 illustrates the crystal morphology determined by optical goniometry for the complexes [Ni(2,3-lutidine)$_2$(O$_2$N)$_2$] and [Ni(quinoline)$_2$(O$_2$N)$_2$]. The faces and extinction directions used for the low temperature spectral measurements are also marked on this diagram.
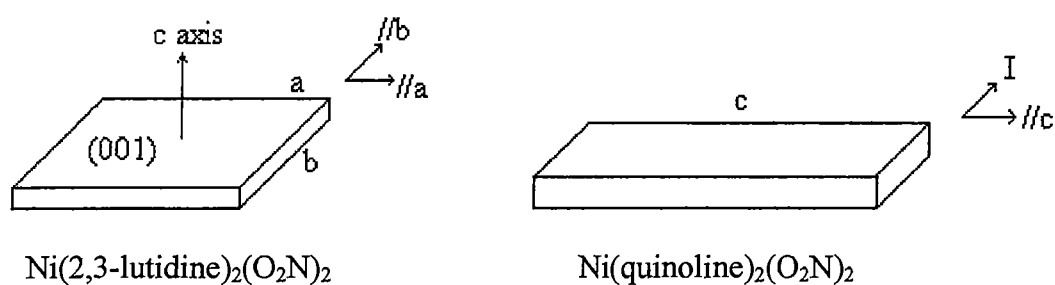

Ni(2,3-lutidine)$_2$(O$_2$N)$_2$ Ni(quinoline)$_2$(O$_2$N)$_2$

Figure 6.8: Crystal morphology and extinction directions of Ni(2,3-lutidine)$_2$(O$_2$N)$_2$ and Ni(quinoline)$_2$(O$_2$N)$_2$.

The spectra measured for Ni(2,3-lutidine)$_2$(O$_2$N)$_2$ are shown in Figure 6.9. The electric vector of light was positioned parallel to the a axis in one polarisation, which corresponded to a molecular projection of $0.0285x^2 + 0.5455y^2 + 0.4260z^2$. The second polarisation, parallel to the b axis, corresponded to a molecular projection of $0.3924x^2 + 0.3500y^2 + 0.2576z^2$. The molecular axes are shown in Figure 6.7.
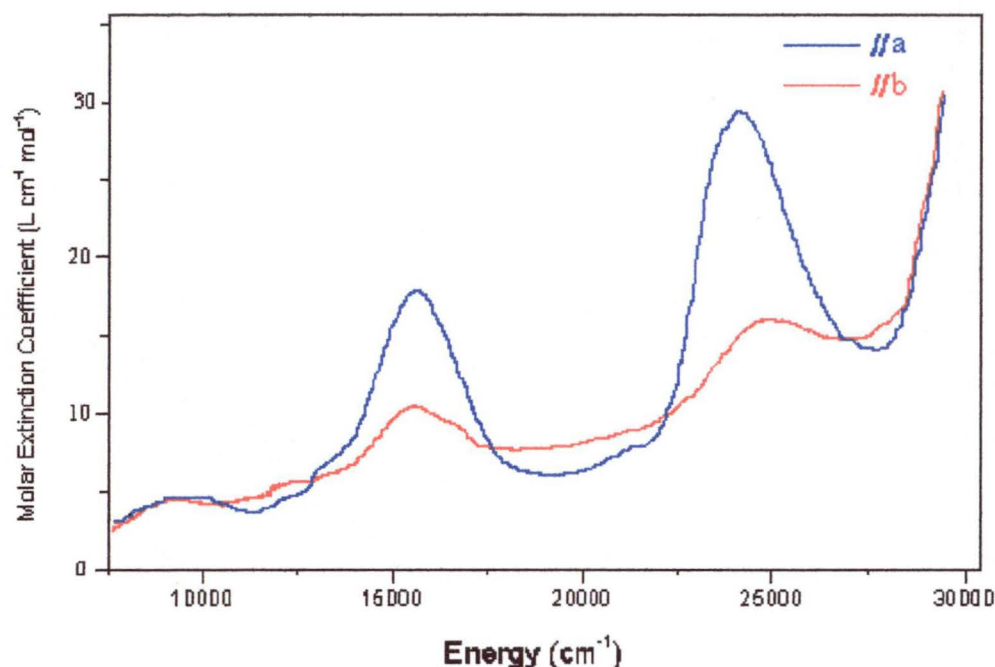
Figure 6.9: The single crystal optical spectrum of [Ni(2,3-lutidine)$_2$(O$_2$N)$_2$] at 16K with the electric vector parallel to the extinction directions of the (001) crystal face.

As may be seen in Figure 6.9, there is no complete polarisation, but rather a difference in peak intensities due to the differing molecular projections for each measurement. Both [Ni(2,3-lutidine)$_2$(O$_2$N)$_2$] and [Ni(quinoline)$_2$(O$_2$N)$_2$] have C$_{2v}$ symmetry and the selection rules show that the only allowed transitions are ^{3}A$_1 \leftarrow$ ^{3}B$_1$ in the x direction, ^{3}A$_2 \leftarrow$ ^{3}B$_1$ in the y direction and ^{3}B$_2 \leftarrow$ ^{3}B$_1$ in the z direction. The first band is centred at 9 600cm^{-1} and would be due to transitions to the ^{3}T$_{2g}$ state. The second band shows the ^{3}B$_1 \leftarrow$ ^{3}B$_1$, and ^{3}A$_2 \leftarrow$ ^{3}B$_1$ transitions at 15 800cm^{-1} and 16 350cm^{-1}. The intensity of both of these peaks would be expected to be greater in the //a polarisation, as the molecular projection for this extinction direction has higher y and z components than that for the //b polarisation. The third band has a peak and shoulder at 24 200 cm^{-1} and 25 000 cm^{-1}, which would correspond to the transitions ^{3}A$_2 \leftarrow$ ^{3}B$_1$ and ^{3}B$_1 \leftarrow$ ^{3}B$_1$. Again, these would be expected to be of higher intensity in the //a polarisation, for the same reason given above. Spin-forbidden peaks of low intensity were also visible at 13 250cm^{-1} (^{1}A$_1 \leftarrow$ ^{3}B$_1$) and 21 400cm^{-1} (^{1}B$_1 \leftarrow$ ^{3}B$_1$).

Figure 6.10 shows the low temperature spectra measured for an arbitrary face of a single crystal of Ni(quinoline)$_2$(O$_2$N)$_2$ with the electric vector of light parallel to the extinction direction. The flattened peak in the spectra measured for polarisation I indicated that the limit of the detector's sensitivity was reached, which is a common problem when measuring the spectra of small crystals.
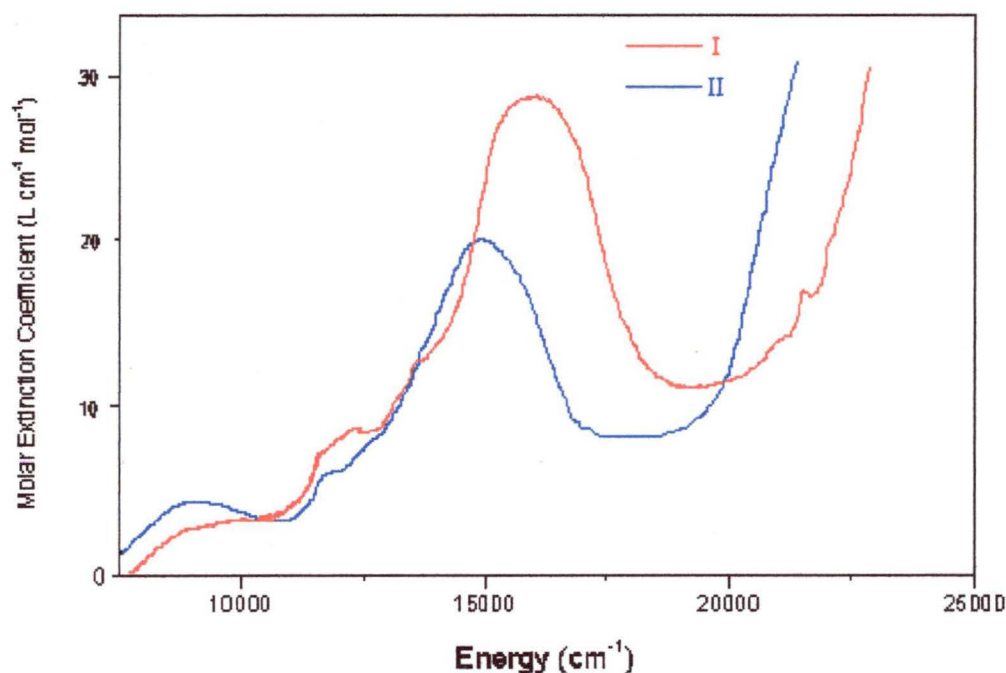

Figure 6.10: The single crystal optical spectrum of [Ni(quinoline)$_2$(O$_2$N)$_2$] at 16K with the electric vector parallel to the extinction directions of an arbitrary crystal face.

The splitting pattern expected for complexes with C$_{2v}$ symmetry is not as well resolved for this complex as it was for [Ni(2,3-lutidine)$_2$(O$_2$N)$_2$]. The first band is centred at 9 600cm^{-1} and this would be due to transitions to the ^{3}T$_{2g}$ state. The second band is split into two components at 15 000cm^{-1} and 17 000cm^{-1}. These correspond to the ^{3}A$_2 \leftarrow ^3$B$_1$ and ^{3}B$_1 \leftarrow ^3$B$_1$ transitions, where the assignment is that suggested by the AOM calculations. Spin forbidden peaks are also visible at 12 500cm^{-1} and 21 485cm^{-1}.

The complex [Ni(2,5-lutidine)$_2$(O$_2$N)$_2$] has nitrite groups that are *trans* to each other (Figure 6.11)[3].
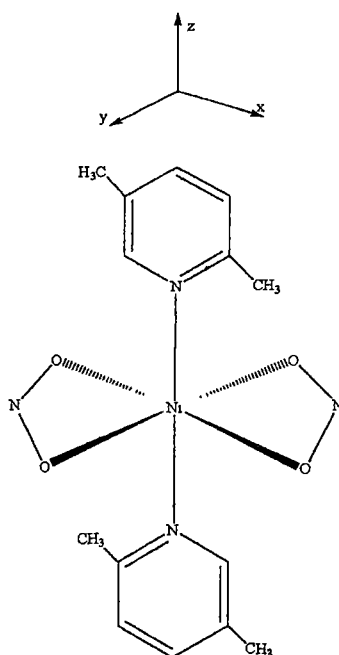
Figure 6.11: The geometry of [Ni(2,5-lutidine)₂(O₂N)₂]. The molecular axes defined for this complex are also shown on this diagram.

The morphology and extinction directions of the [Ni(2,5-lutidine)₂(O₂N)₂] crystal are shown in Figure 6.12.
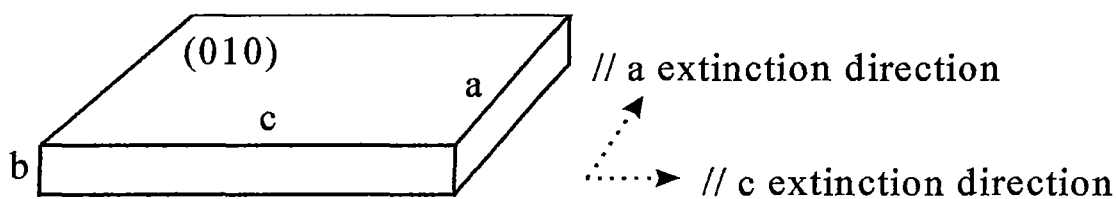
Figure 6.12: Crystal morphology of [Ni(2,5-lutidine)₂(O₂N)₂].

The spectra measured at 15K for the (010) face of the complex are shown in Figure 6.13. In D_{2h} symmetry there are no transitions forbidden by the vibronic selection rules, so the spectra are not strongly polarised.

Figure 6.13: The single crystal optical spectrum of [Ni(2,5-lutidine)$_2$(O$_2$N)$_2$] at 16K with the electric vector parallel to the extinction directions of the (010) crystal face.

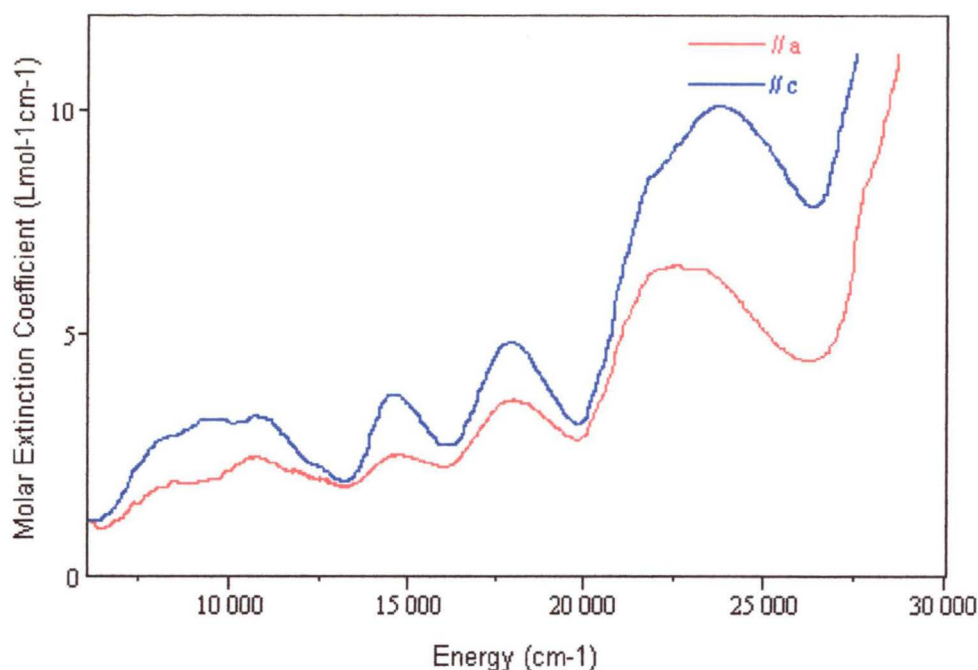The peak intensities are much lower than those for the C$_{2v}$ complexes, as expected for a centrosymmetric complex (see Chapter 2). The first broad band of low intensity consists of three clearly defined peaks at 8 650cm^{-1}, 9 450cm^{-1} and 10 650cm^{-1}. These corresponded to the $^3B_{1g} \leftarrow {}^3B_{1g}$, $^3B_{2g} \leftarrow {}^3B_{1g}$ and $^3B_{3g} \leftarrow {}^3B_{1g}$ transitions, assuming an effective symmetry of D$_{2h}$ and with the assignments being those suggested by the AOM calculations. The second band is resolved into two well-defined peaks at 14 900cm^{-1} and 17 700cm^{-1}, indicating a large splitting of the $^3T_{2g}$ state. The third band is less clearly resolved, and consists of an intense peak at approximately 24 600 cm^{-1}, and another at approximately 27 000 cm^{-1}. Two shoulders are also visible on this third band. These are at 21 000cm^{-1} and 23 000cm^{-1}, and would correspond to the $^1A_g \leftarrow {}^3B_{1g}$ and $^1B_{1g} \leftarrow {}^3B_{1g}$ spin-forbidden transitions.

The single crystal spectrum of [Ni(medpt)(NCS)NO$_2$] was measured at room temperature and 13K (Figure 6.15). This complex has a single O,O'-chelating nitrite ligand, a tridentate amine group and an N-bonded thiocyanate ion[10]. This complex is formally of very low symmetry, when each orbital triplet will be split into three

components. However, the observed splitting pattern may also suggest a higher effective symmetry. This may be explained by considering only the atoms bonded to the nickel ion. If it is assumed that the metal-thiocyanate and metal-amine bonds are similar, this complex may then be described as having four similar metal-nitrogen bonds and two metal-oxygen bonds from the bidentate nitrite. This geometry would have an effective symmetry of C_{2v} (Figure 6.14).
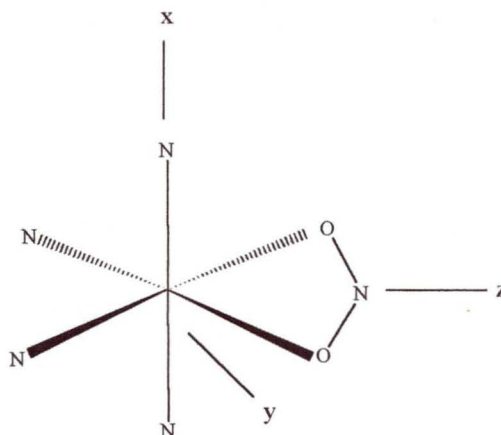

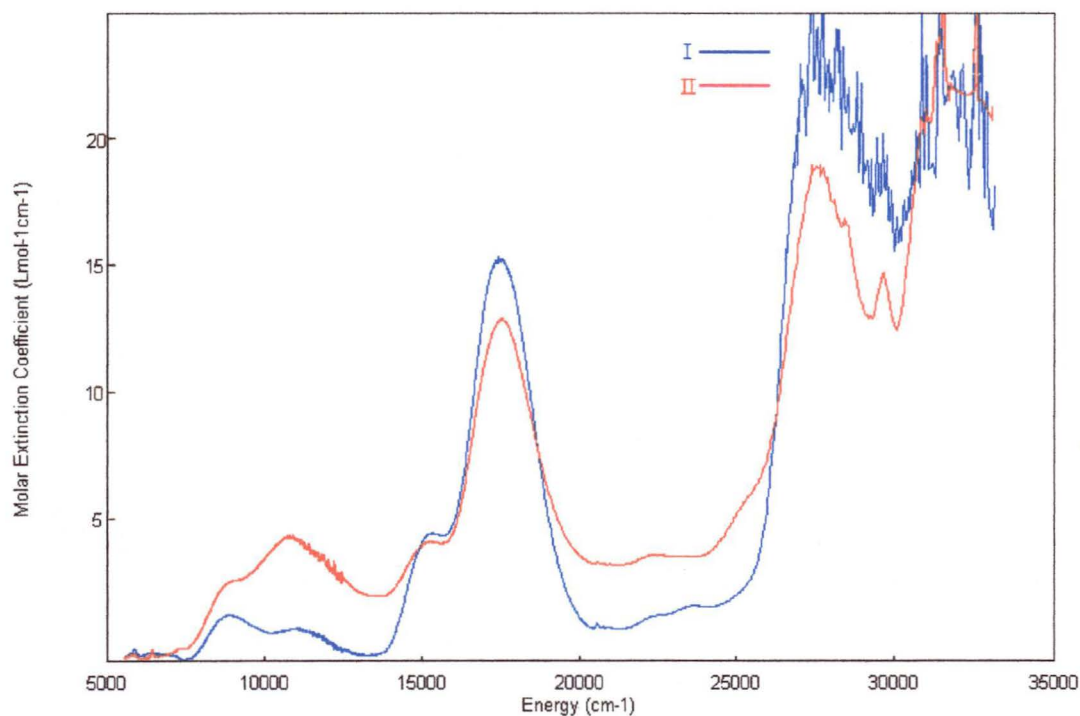**Figure 6.14**: The molecular geometry of $[Ni(medpt)(NCS)(NO_2)]$. Also shown on the diagram are the symmetry axes for the space group C_{2v}.

Figure 6.15: The single crystal spectrum of $[Ni(medpt)(NCS)NO_2]$ at 13K with the electric vector parallel to the extinction directions of an arbitrary crystal face.

The first band is split into two peaks, at 9 300cm^{-1} and 10 950cm^{-1}. Assuming C_{2v} symmetry, these transitions may be assigned as the $^3B_1 \leftarrow {}^3B_1$ and $^3A_1 \leftarrow {}^3B_1$ transitions from the AOM calculation. The second band consists of two peaks, one at 15 600cm^{-1} and the second at 17 300cm^{-1}. By comparison to the other C_{2v} nickel(II) nitrite complexes in the present work, it is likely that these would be due to the $^3B_1 \leftarrow {}^3B_1$ and the $^3A_1 \leftarrow {}^3B_1$ transitions. Peaks of low intensity are located at 22 300cm^{-1} and 23 100cm^{-1}. This spectrum is very similar to those seen for [Ni(2,3-lutidine)$_2$(O$_2$N)$_2$] and [Ni(quinoline)$_2$(O$_2$N)$_2$] which have two O,O'-chelating nitrites *cis* to each other, and to that seen for the complexes [Ni(*s*-Et$_2$en)$_2$(O$_2$N)]NO$_2$, *s*-Et$_2$en = *sym*-N,N'-diethylethylenediamine, and [Ni(*m*-stien)$_2$(O$_2$N)]NO$_2$, *m*-stien = *meso*-stilbenediamine, which have a single O,O'-chelating nitrite ligand[21,22].

The complex [Ni(medpt)(NO$_2$)$_2$] has both a N-bonded monodentate nitro ligand, and an O,O'-chelating nitrito ligand[11]. This complex would be of very low symmetry, for in this case the N-bonded nitro group cannot be thought of as being similar to amine groups. However, it can be seen in Figure 6.16 that the spectra measured for this complex are broadly similar to those of the previous complex, except for an additional peak at 20 750cm^{-1}.
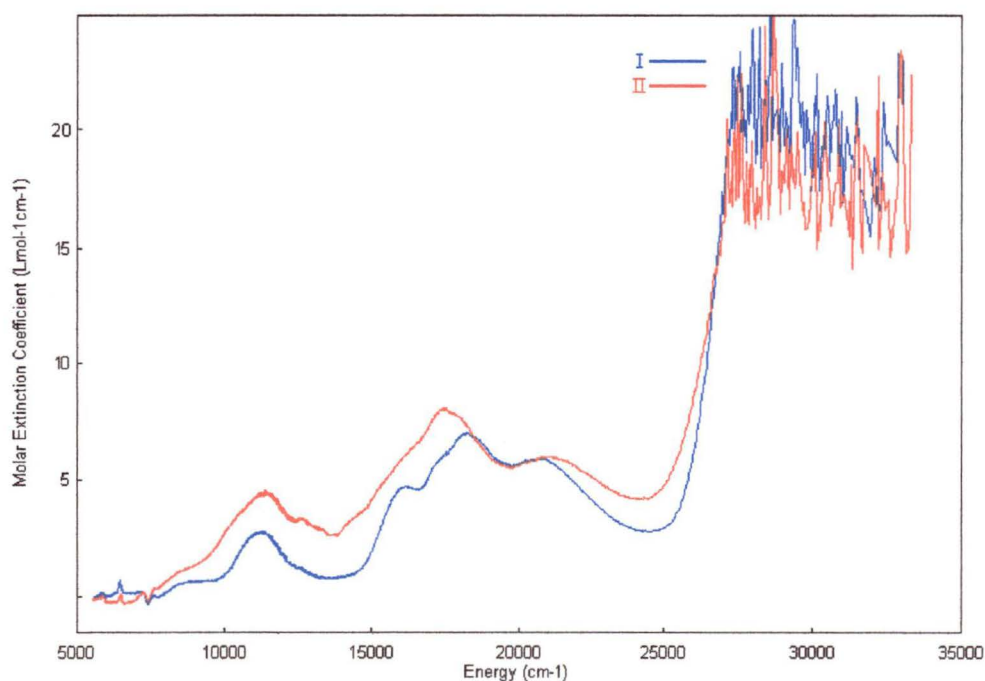
Figure 6.16: The single crystal spectrum of [Ni(medpt)(NO$_2$)$_2$] at 13K with the electric vector parallel to the extinction directions of an arbitrary crystal face.

The first band has been split into three components. These are located at 8 850cm^{-1}, 10 570cm^{-1} and 11 500cm^{-1}. Peaks of lesser intensity can be seen on the higher energy side of this band, at 12 530cm^{-1} and 13 420cm^{-1}. The three components of the second band are at 16 000cm^{-1}, 17 400cm^{-1} and 18 180cm^{-1}. These peaks are generally slightly higher in energy than those seen for [Ni(medpt)(NCS)NO$_2$], [Ni(2,3-lutidine)$_2$(O$_2$N)$_2$] and [Ni(quinoline)$_2$(O$_2$N)$_2$].

The broad peak centred at approximately 20 750cm^{-1} does not appear in the spectra of the other complexes with O,O'-chelating nitrites described in the present work. This peak is presumably due to the low energy metal $\rightarrow \pi^*$ charge transfer transition previously described for other nickel(II) nitrite complexes with monodentate nitro groups.

6.4.2 Bridging Complexes

As described in Section 6.3, the complexes [Ni(en)$_2$NO$_2$]ClO$_4$ and [Ni(tn)$_2$NO$_2$]ClO$_4$ have nitrite ligands that adopt an N,O-bridging mode. Each Ni^{2+} ion is coordinated to the nitrogen atom of one nitrite group and one oxygen atom of another nitrite (Figure 6.17).
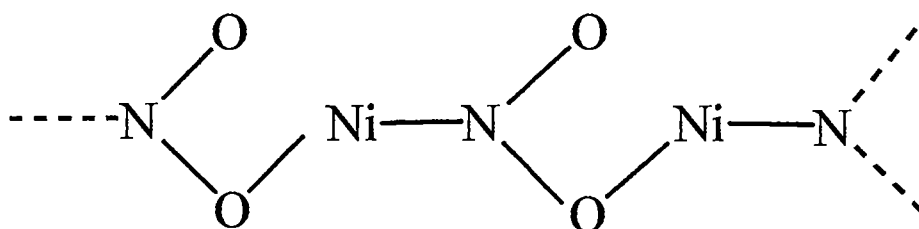
Figure 6.17: The N,O-bridging mode adopted by the nitrite ligands in [Ni(en)$_2$NO$_2$]ClO$_4$ and [Ni(tn)$_2$NO$_2$]ClO$_4$.

The single crystal spectrum of [Ni(en)$_2$NO$_2$]ClO$_4$ at 16K is shown in Figure 6.18.

Figure 6.18: The single crystal optical spectrum of $[Ni(en)_2(NO_2)]ClO_4$ at 16K with the electric vector parallel to the extinction directions of an arbitrary crystal face.

A number of peaks may be seen in this spectrum. Two relatively broad peaks can be seen in polarisation I at 9 800cm^{-1} and 12 000cm^{-1}, and these may be assigned to transitions to the split components of the $^3T_{2g}$ state of the parent octahedral complex. The second peak also has a relatively sharp peak on the side of it at 12 820cm^{-1}, which must be due to the spin-forbidden transition to a component of the ^1E_g state. At higher energy, two peaks may be seen at 16 000cm^{-1} and 16 900cm^{-1} for this polarisation, presumably due to transitions to components of the $^3T_{1g}$ state. A peak centred at approximately 20 600cm^{-1} which appears to have a vibrational progression of ~600cm^{-1} may be assigned to the charge transfer transition associated with the presence of an N-bonded nitrite (see Chapter 5). Polarisation II has peaks at 10 575cm^{-1} and 13 500cm^{-1} due to transitions to components of the $^3T_{1g}$ and/or ^1E_g levels, and a broad band centred at 20 100cm^{-1} due to the metal $\rightarrow$ ligand charge transfer transition. These results are consistent with those reported previously[23].

A particularly interesting and previously unreported feature of polarisation I can be seen when comparing the spectrum measured at room temperature with the low temperature spectrum (Figure 6.19).
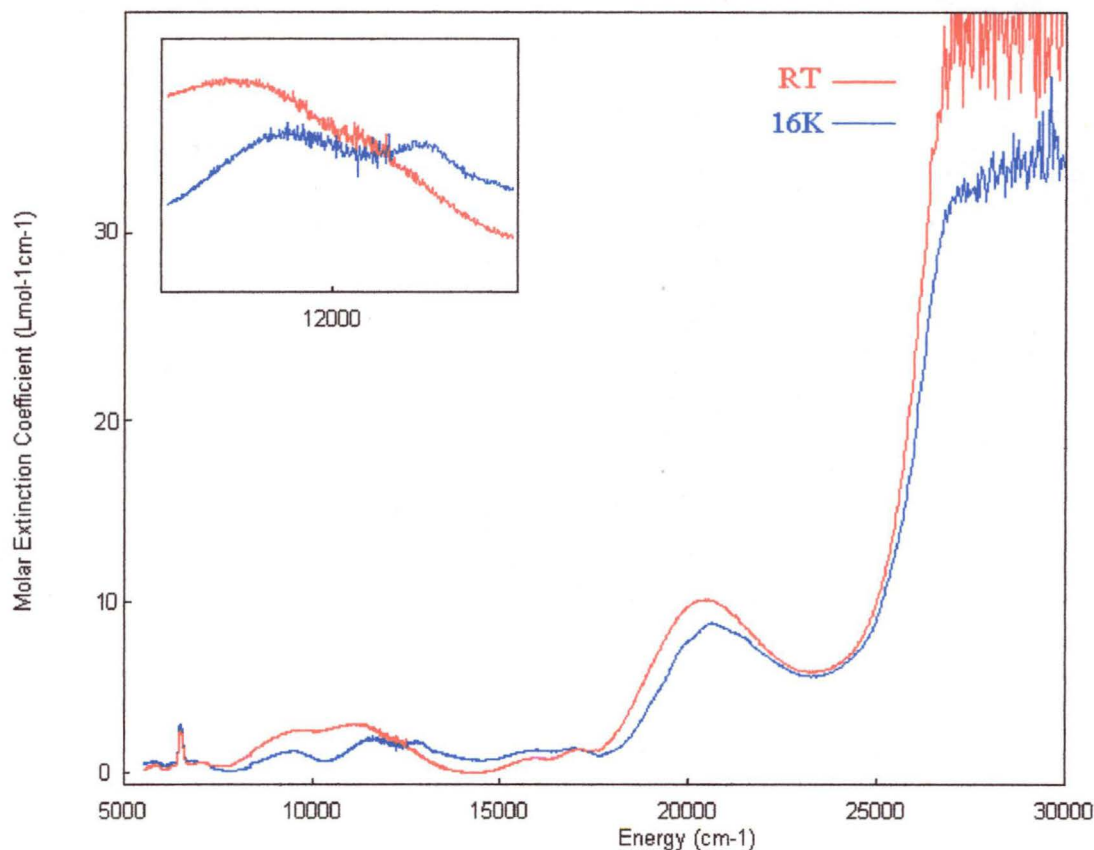
Figure 6.19: The room and low temperature spectra of polarisation I for an arbitrary crystal face of $[Ni(en)_2NO_2]ClO_4$. The inset shows an enlarged area of the spectra from $11\ 000cm^{-1}$ to $13\ 000cm^{-1}$.

The low temperature spectrum has a relatively sharp peak at $12\ 820cm^{-1}$ which does not appear in the room temperature spectrum. This is quite unusual, as peaks at low temperature usually have an intensity that is *less* than that seen at room temperature. This is because a variation of intensity is normally associated with a vibronic coupling mechanism, and vibrational amplitudes decrease on cooling. The peak at $12\ 820cm^{-1}$ is probably due to a spin-forbidden transition, and its intensification on cooling may possibly be due to the strong magnetic ordering which occurs in this complex. It is known that magnetic coupling sometimes influences the intensities of spin-forbidden transitions[24].

As described in Section 6.3, the structures of [Ni(tn)$_2$NO$_2$]ClO$_4$ and [Ni(en)$_2$NO$_2$]ClO$_4$ are very similar. Therefore, it was expected that the single crystal optical spectra of these complexes would also be similar. This was found to be the case, as the spectra measured for [Ni(tn)$_2$NO$_2$]ClO$_4$ show (Figure 6.20).
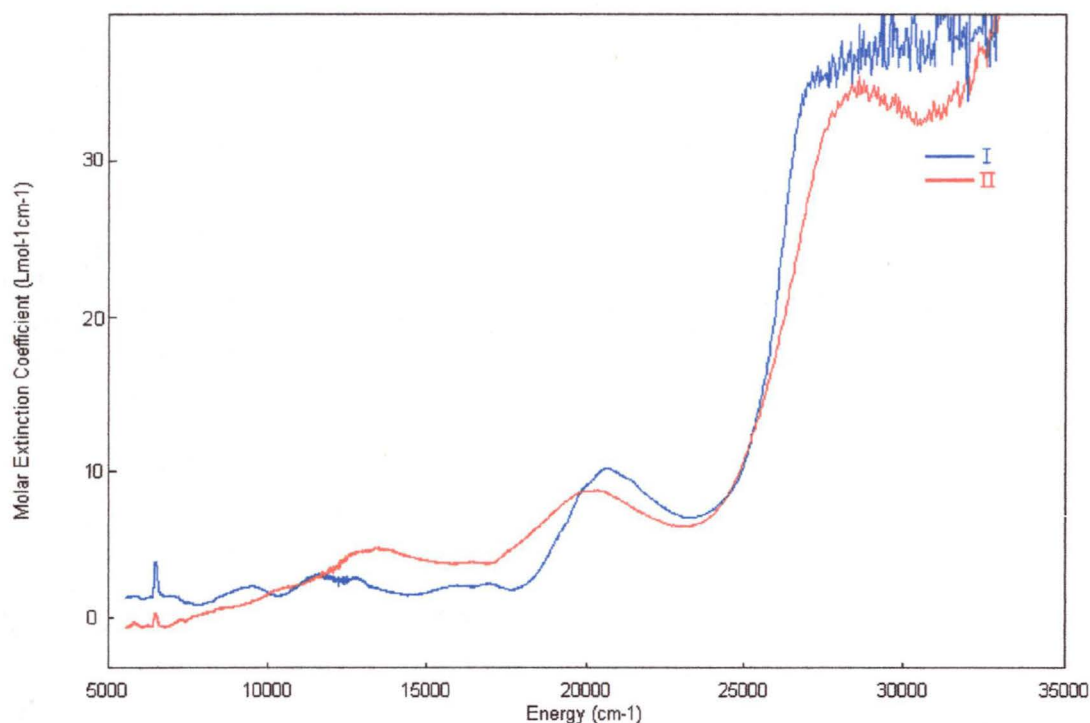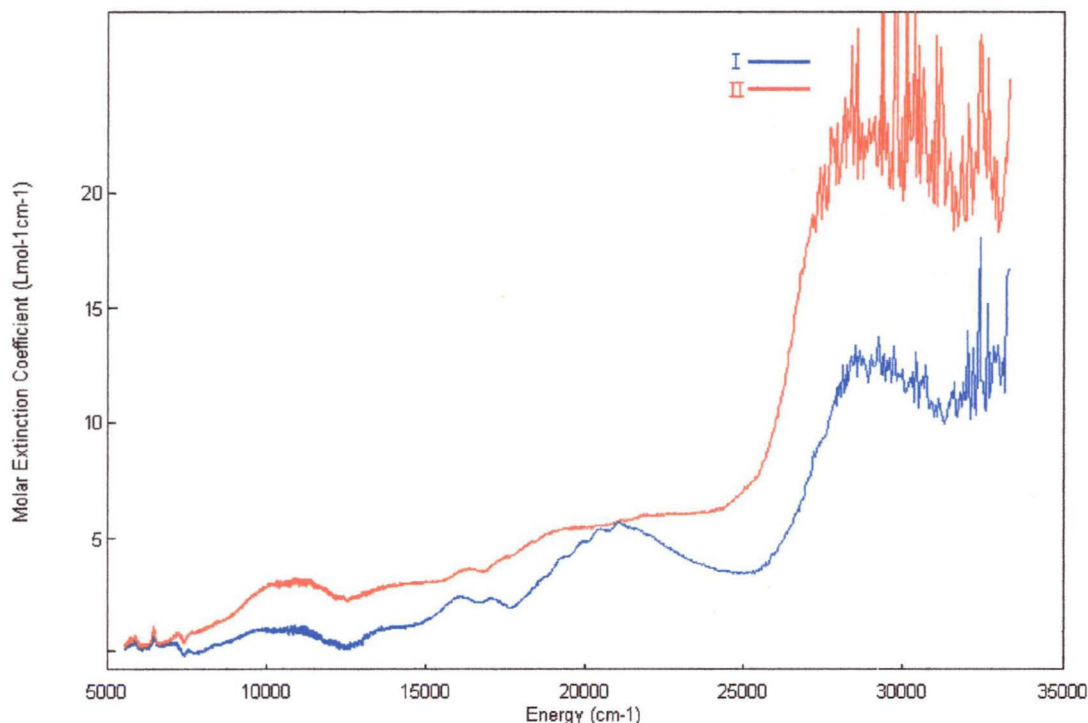

Figure 6.20: The single crystal optical spectrum of [Ni(tn)$_2$(NO$_2$)]ClO$_4$ at 16K with the electric vector parallel to the extinction directions of an arbitrary crystal face.

Both polarisations have peaks due to transitions to the components of the ^{3}T$_{2g}$ level at 9 760cm^{-1} and 10 400cm^{-1} and 11 900cm^{-1}. Further weak peaks are visible at 13 570cm^{-1}, 15 950cm^{-1} and 17 080cm^{-1}. Polarisation II has two wide peaks centred at 19 200cm^{-1} and 21 670cm^{-1}, while polarisation I has a peak centred at 21 100cm^{-1} which shows a progression of ~600cm^{-1}.

The structure of [(CH$_3$)$_4$N]Ni(NO$_2$)$_3$ is shown in Figure 6.3, and reproduced overleaf (Figure 6.21). As described in Section 6.2, two types of Ni^{2+} ions are present, octahedrally coordinated either to N atoms or to O atoms[7].
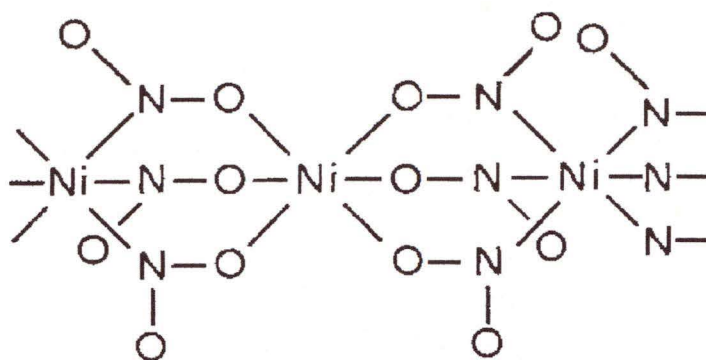
Figure 6.21: The chain structure of $[(CH_3)_4N]Ni(NO_2)_3$. The tetramethylammonium groups have been omitted in this diagram for clarity.

Due to the small crystal size, the spectra could only be measured over the limited range of 13 000 to 30 000cm^{-1}. The spectra for two extinction directions of an arbitrary face of the complex $[(CH_3)_4N]Ni(NO_2)_3$ are shown in Figure 6.22.
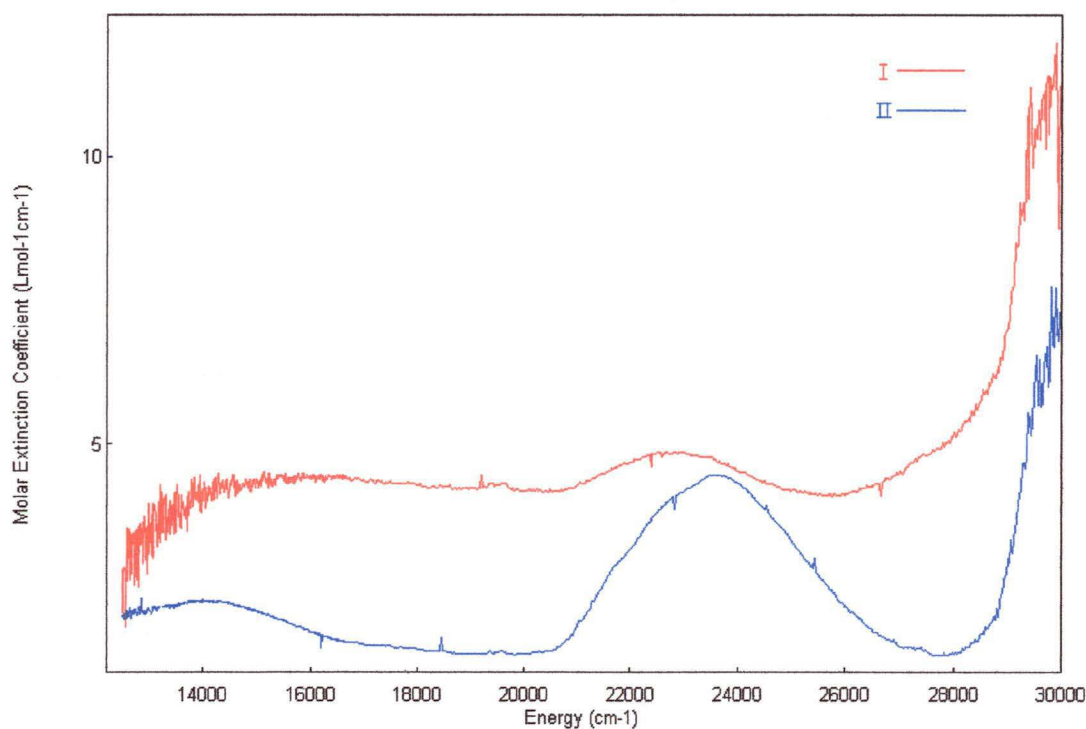
Figure 6.22: The single crystal optical spectrum of $[(CH_3)_4N]Ni(NO_2)_3$ at 4K with the electric vector parallel to the extinction directions of an arbitrary crystal face.

Two bands can be seen in the spectrum. The first broad band is centred at

14 300cm^{-1}. The second band appears to be made up of three peaks at 21 720cm^{-1}, 22 600cm^{-1} and 23 500cm^{-1}. Two sharp, low intensity peaks are also visible at 19 360cm^{-1} and 19 570cm^{-1}. The other sharp peaks visible in this spectrum are probably due to the detector.

Unlike the spectra of [Ni(en)$_2$NO$_2$]ClO$_4$ and [Ni(tn)$_2$NO$_2$]ClO$_4$ which have peaks at 16 000cm^{-1} and 17 000cm^{-1} that may be attributable to the second 'd-d' transition, the spectrum of [(CH$_3$)$_4$N]Ni(NO$_2$)$_3$ appears to be more like those measured for Ni(II) complexes with monodentate nitro groups. Given that the structure consists of Ni^{2+} ions that are separately octahedrally O-bonded and N-bonded, it is unclear as to why the octahedrally N-bonded nickel appears to dominate in the measured spectrum. Further optical spectroscopic measurements are necessary to determine this, and these will only be possible when a method to grow larger crystals of this complex has been developed.

The complexes [Ni$_2$(medpt)$_2$(NCS)$_3$NO$_2$].H$_2$O and [Ni$_2$(dpt)$_2$(NCS)$_3$NO$_2$] have a nitrite ligand coordinated via an N,O,O'-bridging mode (Figure 6.23)[10].
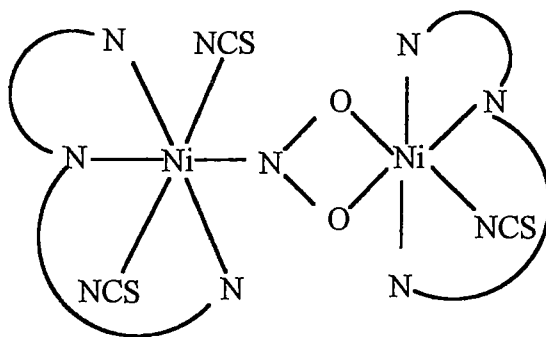
Figure 6.23: The N,O,O'-bridging mode adopted by the nitrite ligand in both the [Ni$_2$(medpt)$_2$(NCS)$_3$NO$_2$].H$_2$O and [Ni$_2$(dpt)$_2$(NCS)$_3$NO$_2$] complexes.

The low temperature single crystal optical spectra measured for these complexes are shown in Figures 6.24 and 6.25, respectively.
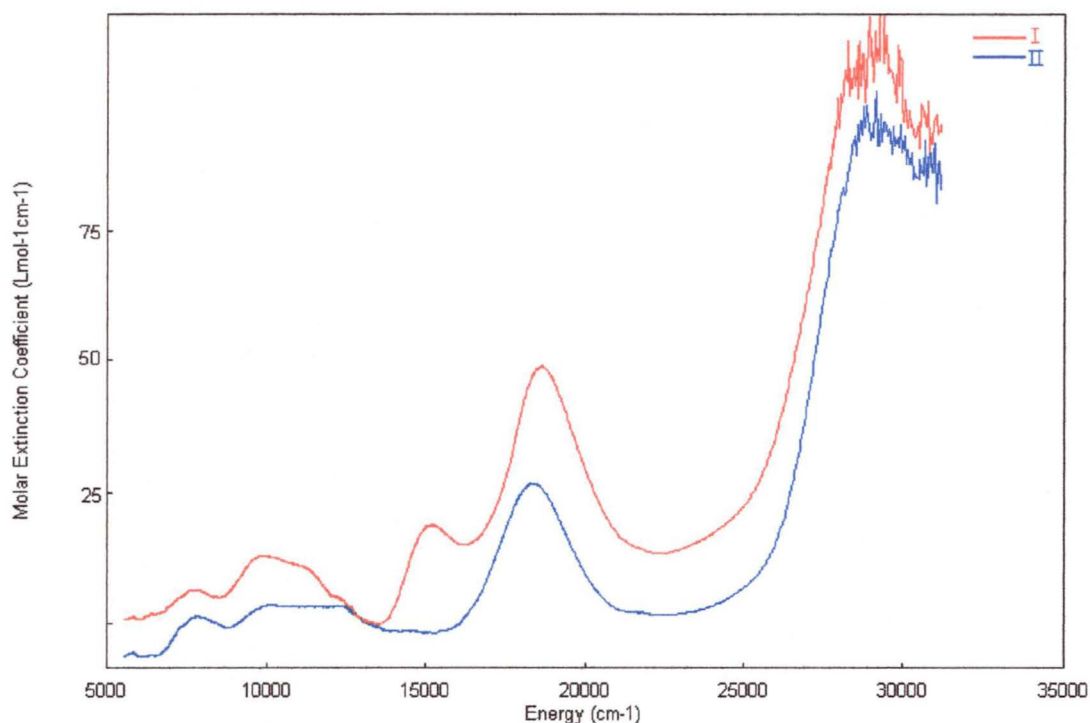
Figure 6.24: The single crystal optical spectrum of $[Ni_2(medpt)_2(NCS)_3NO_2].H_2O$ at 16K with the electric vector parallel to the extinction directions of an arbitrary crystal face.

The spectra of $[Ni_2(medpt)_2(NCS)_3NO_2].H_2O$ have peaks at 8 200cm^{-1}, 10 000cm^{-1} and 11 200cm^{-1} which must be due to transitions to the components of the $^3T_{2g}$ state, and 15 250cm^{-1} due to the components of the $^3T_{1g}$ state. The band centred at ~18 500cm^{-1} is likely to be due to the metal to ligand charge transfer transition characteristic of N-bonded nitrites. Two peaks probably due to the spin-forbidden transitions to components of the ^1E_g level are located at 12 430cm^{-1} and 12 700cm^{-1}. It should be noted that this spectrum is similar to the spectrum measured for the complex $[Ni(medpt)(NCS)NO_2]$ (Figure 6.15), although in the present case the first band is at lower energy and the second band is shifted to slightly higher energy than those of the complex with the O,O'-chelating nitrite. Also, the peak at 15 250cm^{-1} in the spectrum of $[Ni_2(medpt)_2(NCS)_3NO_2].H_2O$ is strongly polarised.
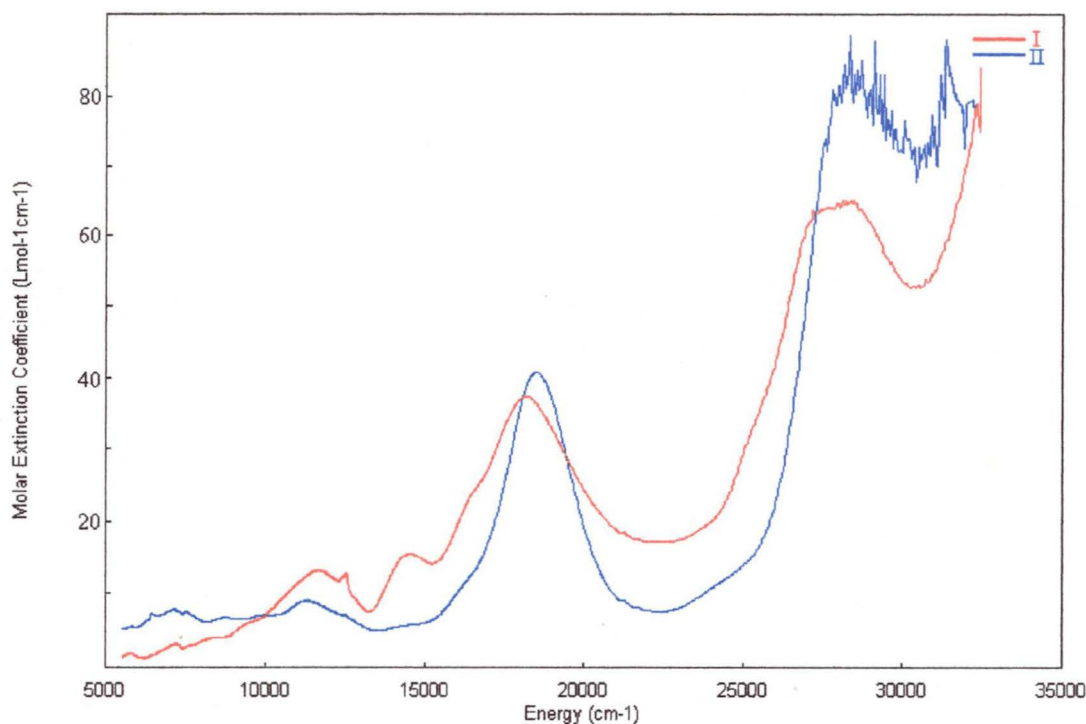
Figure 6.25: The single crystal optical spectrum of [Ni$_2$(dpt)$_2$(NCS)$_3$(NO$_2$)] at 16K with the electric vector parallel to the extinction directions of an arbitrary crystal face.

For [Ni$_2$(dpt)$_2$(NCS)$_3$(NO$_2$)], peaks are visible at 8 000cm^{-1}, 9 400cm^{-1} and 11 900cm^{-1} in both polarisations due to the components of the ^{3}T$_{2g}$ state. Peaks can also be seen at 14 450cm^{-1}, 16 430cm^{-1} and 18 100cm^{-1} in polarisation I, and at 18 690cm^{-1} in polarisation II due to components of the ^{3}T$_{1g}$ level and the charge transfer transition. A very sharp peak at 12 620cm^{-1} due to ^{1}E$_{1g}$ level is also observed both at 16K and room temperature. Vibrational fine structure on the peak at ~18 000cm^{-1} is absent in both this spectrum and that measured for [Ni$_2$(medpt)$_2$(NCS)$_3$(NO$_2$)].H$_2$O. The fact that both oxygen atoms are involved in the bridging mode adopted by the nitrite ligand in these complexes may influence the wagging vibrational mode of the nitrite, thus possibly preventing this from being observed as a progression on the charge transfer band.

6.5 Analysis of the Band Energies Using the Angular Overlap Model

6.5.1 *Complexes with O,O'-chelating nitrite ligands*

One of the basic assumptions of the AOM is that the energy change of a d-orbital when interacting with a ligand orbital depends on the square of the overlap integral. As well as its dependence on the bond length, this overlap integral also changes when misdirected valence, or "bent bonding" is present. A simplified diagram illustrating this is shown in Figure 6.26.

(i)   (ii)
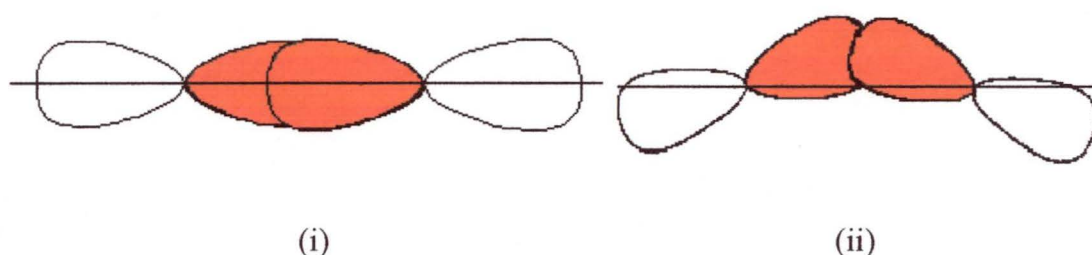
Figure 6.26: A simplified diagram of (i) a σ-bond without bent bonding and (ii) a bent bond.

The complexes most likely to exhibit bent bonding in the present study were those with O,O'-chelating nitrite ligands, such as [Ni(2,3-lutidine)$_2$(O$_2$N)$_2$], [Ni(quinoline)$_2$(O$_2$N)$_2$] and [Ni(2,5-lutidine)$_2$(O$_2$N)$_2$]. The bite angles, ∠O-Ni-O', for these complexes were 60.15°, 59.0° and 60.20°, respectively, which are much lower than the ideal 90° angle. This would lead to the situation shown in Figure 6.2, as illustrated below (Figure 6.27).
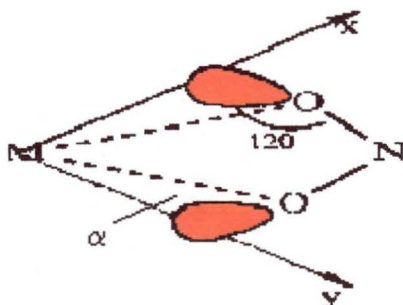
Figure 6.27: Oxygen orbital positions for a chelating nitrite.

In Figure 6.27, the oxygen orbitals are not directed along the metal-oxygen bond, but at some angle (α) to it. The 120° angle marked on this diagram assumes that the

oxygen orbitals of interest are sp^2 hybridised. For the present complexes, the angle α would be ~25°. This is estimated by subtracting the value of the $\angle$M-O-N from 120°. In this situation, the σ interaction would decrease, and an interaction with the d-orbitals of π symmetry would be introduced. A version of CAMMAG[25] has been developed recently to treat this situation by Dr Mark Riley of the University of Queensland. This includes a parameter, $e_{\sigma\pi}$, to describe this interaction.

To test this new version of CAMMAG, a relatively simple complex with bent bonding was modelled. The complex [Ni(cyanurate)$_2$(NH$_3$)$_4$] has the structure shown in Figure 6.28 at room temperature[26].
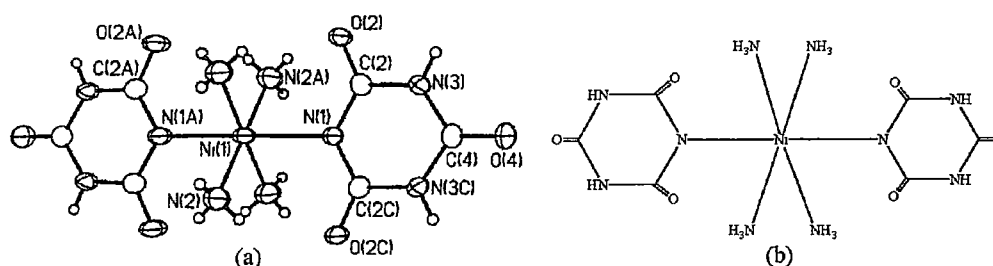
Figure 6.28: The structure of [Ni(cyanurate)$_2$(NH$_3$)$_4$] at room temperature (a) and a simple diagram (b) of the complex (from Falvello et al.[26]).

As the temperature decreases, the planar cyanurate rings bend in the manner shown in Figure 6.29.
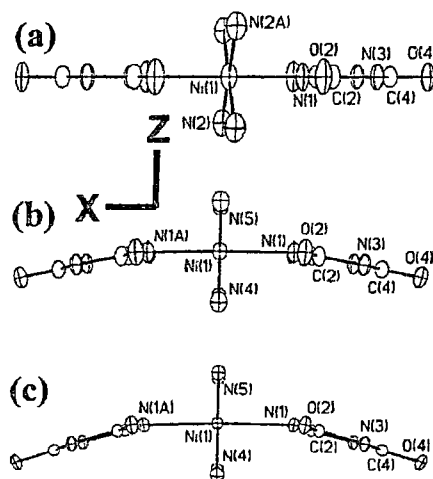
Figure 6.29: Lateral view of a molecule of [Ni(cyanurate)$_2$(NH$_3$)$_4$] showing the change in the dihedral angle between the cyanurate rings at (a) 298K, dihedral angle = 0°, (b) 223K, dihedral angle = 21.64° and (c) 139K, dihedral angle = 32.14° (from Falvello et al.[26]).

The first calculation confirmed that the energy levels calculated using the new CAMMAG program were the same as those calculated previously, neglecting bent bonding[26]. The parameters that gave a reasonable fit to the experimentally obtained band energies were e_σ(amine) = 4 395cm^{-1}, e_σ(cyanurate) = 1 815cm^{-1}, e_π(cyanurate) = 0cm^{-1} and B = 962. Assuming that the π-interaction resulting from the rotation of the σ-orbital is given by $E_{\pi x} = \frac{1}{4} E_\sigma$, as suggested by the overlap integral, and using the equations

$$e_{\pi x} = E_{\pi x}(\sin \alpha)^2$$

$$e_\sigma = E_\sigma(\cos \alpha)^2$$

and $\qquad e_{\sigma \pi} = [\sqrt{(e_\sigma)(e_{\pi x})}](\sin \alpha)(\cos \alpha),$

the following energy levels were obtained as α was changed from 0° to 50° (Figure 6.30).
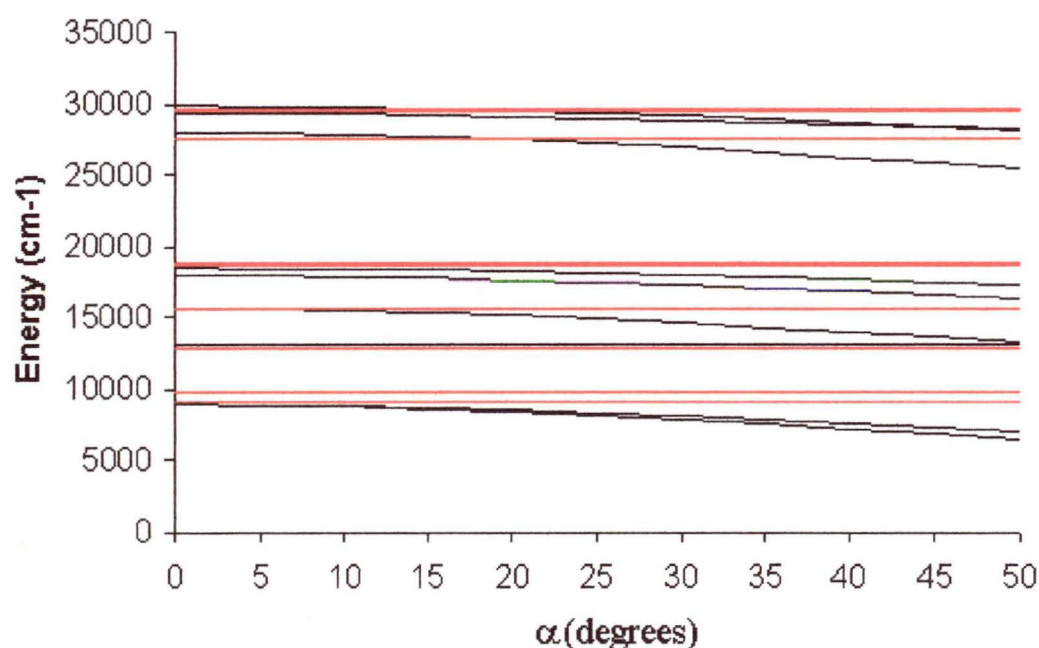
Figure 6.30: The energy levels calculated for the complex [Ni(cyanurate)$_2$(NH$_3$)$_4$] when α is varied from 0° to 50°. Observed energy levels are in red.

Perhaps the most obvious result from this calculation is that the inclusion of the parameter $e_{\sigma\pi}$ does not greatly affect the energy levels calculated for this complex until higher values of α are reached. As the angle reached is 16° at low temperature, this suggests that the effect of bent bonding is relatively minor for this complex. Decreasing the e_σ parameter for the cyanurate ligand to 1 750cm^{-1} and including bent

bonding fits the calculated energies to those determined experimentally, but the fit is not significantly better than that ignoring bent bonding.

A particular problem faced when including $e_{\sigma\pi}$ in AOM calculations is determining whether this is positive or negative. It is clear that the influence of bent bonding will be very different when the lone pair orbitals tilt towards one another, rather than away from one another. The former decreases the interaction along the octahedral cartesian axes, and will therefore have a much larger effect on the d-orbital energies than the latter. In the computer program, the sign of the rotation is related to the way in which the ligand axes are defined, and a detailed explanation for this is given in Appendix E. Figure 6.31 indicates the way in which the axes were defined for the nitrite ligands of the present complexes.
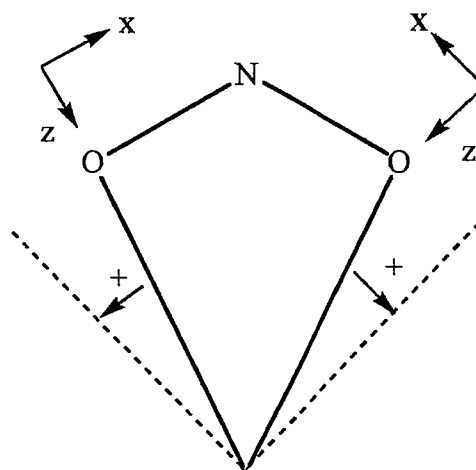
Figure 6.31: The way in which the axes were defined for the O,O'-nitrito ligand and the sign of rotation.

Neglecting the possible effects of bent bonding, and assuming bonding parameters similar to those observed for the complex [Ni(N,N-dimen)$_2$(ONO)$_2$], which contains monodentate nitrito groups, produces calculated transition energies in only moderate agreement with experiment. For [Ni(2,5-lutidine)$_2$(O$_2$N)$_2$], the 2,5-lutidine parameters were obtained in a similar way to those obtained for 3,5-lutidine (Chapter 5, Section 5.5). There are two values for the nitrite parameters as the Ni-O bond lengths are not equal. These parameters were derived from the monodentate nitrito parameters calculated in the present work, which had been scaled appropriately.

TRANSITION	CALCULATED (cm^{-1})	OBSERVED (cm^{-1})
$^3B_{1g} \leftarrow {}^3A_g$	6 532	8 650
$^3B_{3g} \leftarrow {}^3A_g$	8 463	9 450
$^3B_{2g} \leftarrow {}^3A_g$	11 048	10 650
$^3B_{2g} \leftarrow {}^3A_g$	14 879	14 900
$^3B_{1g}, {}^3B_{2g} \leftarrow {}^3A_g$	17 386, 18 110	17 700
$^3B_{2g} \leftarrow {}^3A_g$	23 045	24 600
$^3B_{1g} \leftarrow {}^3A_g$	27 189	27 000

Table 6.8: The calculated and observed transition energies for $[Ni(2,5\text{-lut})_2(O_2N)_2]$ when B = 800, C = 3 300, e_σ(2,5-lut) = 5 350cm^{-1}, $e_{\pi y}$(2,5-lut) = 1 050cm^{-1}, $e_\sigma(O_2N)$ = 4 610cm^{-1} and 4 015cm^{-1}, $e_{\pi y}(O_2N)$ = 635cm^{-1} and 555cm^{-1}, with $\alpha = 0°$.

The addition of the $e_{\sigma\pi}$ parameter enabled the calculation of energy levels while changing the angle, α, from 0° to 90° and these are compared with experiment in Figure 6.32.
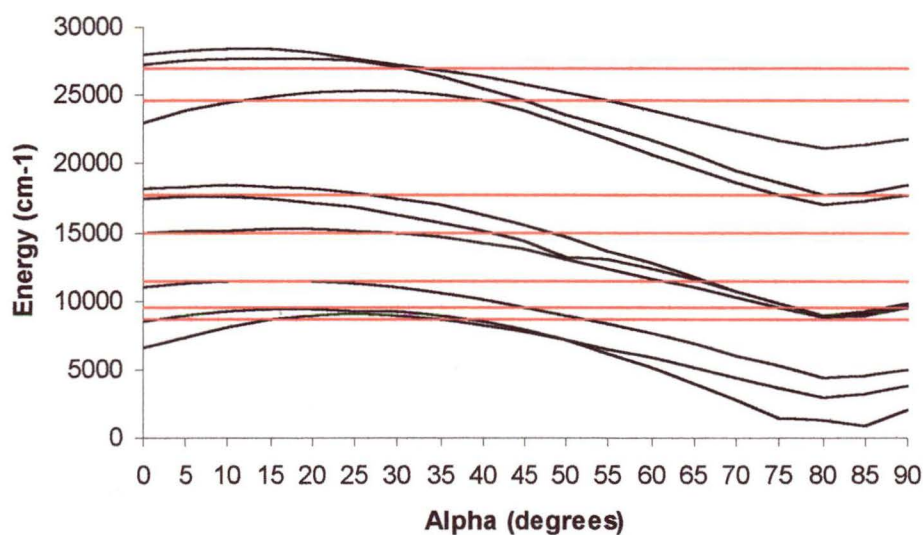
Figure 6.32: The calculated (black) and observed (red) transition energies for $[Ni(2,5\text{-lut})_2(O_2N)_2]$ when changing α from 0° to 90° ($e_{\sigma\pi}$ negative).

As mentioned previously, determining whether the $e_{\sigma\pi}$ parameter is a positive or negative value is very important. When the sign of $e_{\sigma\pi}$ is changed for this calculation, the energy levels shown in Figure 6.33 are obtained.
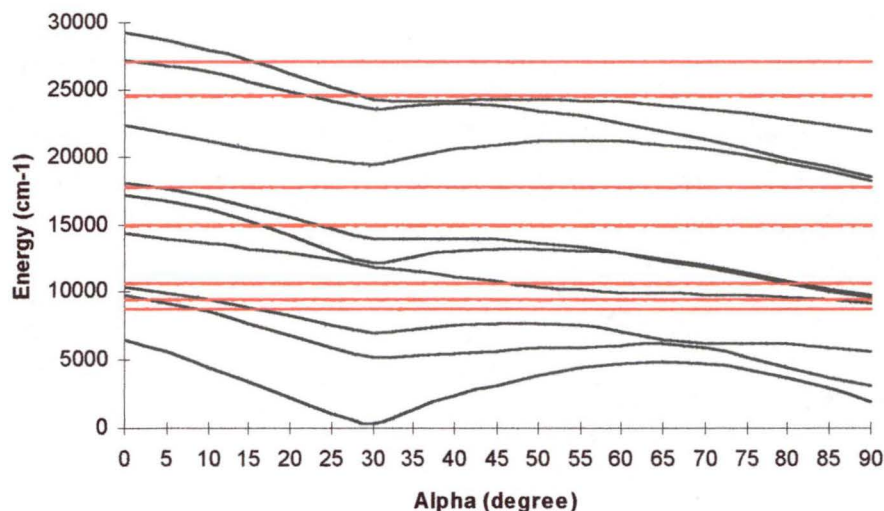
Figure 6.33: The calculated (black) and observed (red) transition energies for [Ni(2,5-lut)$_2$(O$_2$N)$_2$] when changing α from 0° to 90° ($e_{\sigma\pi}$ positive).

When $\alpha = 25°$, the value corresponding to the bite angle ~60° observed experimentally, a reasonable fit of the experimental data is obtained (Table 6.9).

TRANSITION	CALCULATED (cm^{-1})	OBSERVED (cm^{-1})
$^3B_{1g} \leftarrow {}^3A_g$	9 146	8 650
$^3B_{3g} \leftarrow {}^3A_g$	9 283	9 450
$^3B_{2g} \leftarrow {}^3A_g$	11 229	10 650
$^3B_{2g} \leftarrow {}^3A_g$	15 100	14 900
$^3B_{1g}, {}^3B_{2g} \leftarrow {}^3A_g$	16 780, 17 878	17 700
$^1B_{2g} \leftarrow {}^3A_g$	21 114	21 000
$^1B_{3g} \leftarrow {}^3A_g$	22 729	23 000
$^3B_{2g} \leftarrow {}^3A_g$	25 060	24 600
$^3B_{1g} \leftarrow {}^3A_g$	27 449	27 000

Table 6.9: The calculated and observed transition energies for [Ni(2,5-lut)$_2$(O$_2$N)$_2$]; $B = 800$, e_σ(2,5-lut) $= 5440$cm^{-1}, $e_{\pi y}$(2,5-lut) $= 1065$cm^{-1}, e_σ(O$_2$N) $= 3890$cm^{-1} and 4015cm^{-1}, $e_{\pi y}$(O$_2$N) $= 555$cm^{-1} and 575cm^{-1}; $\alpha = 25°$.

A similar situation occurs for the complexes with *cis* O,O'-chelating nitrites, [Ni(2,3-lutidine)$_2$(O$_2$N)$_2$] and [Ni(quinoline)$_2$(O$_2$N)$_2$].

A complication that is faced for the complex [Ni(2,3-lutidine)$_2$(O$_2$N)$_2$] is that this has two types of molecules in its unit cell[20]. However, when including the $e_{\sigma\pi}$ parameter, it can be seen that the fit between calculated and observed energies can be improved.
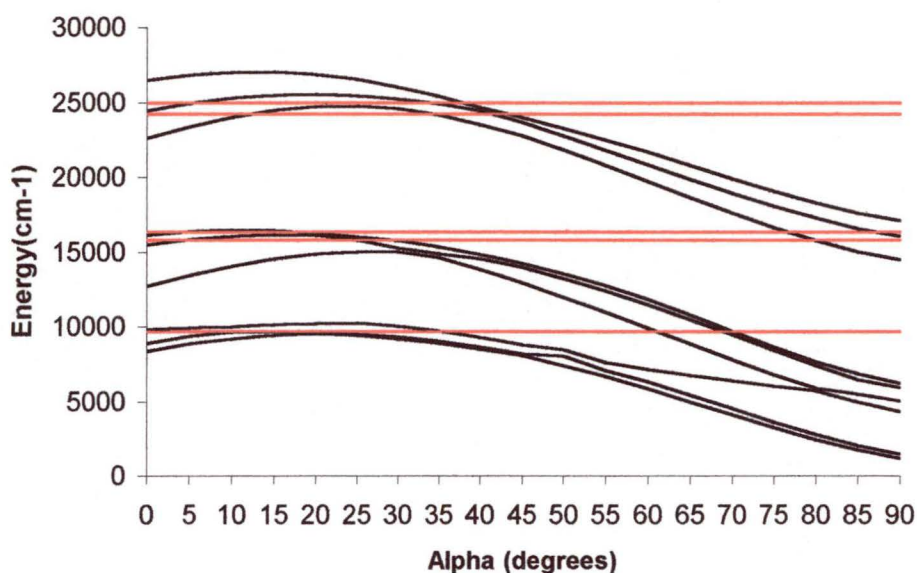
Figure 6.34: The energy levels calculated for molecule type I of [Ni(2,3-lutidine)$_2$(O$_2$N)$_2$] when changing α from 0° to 90°.
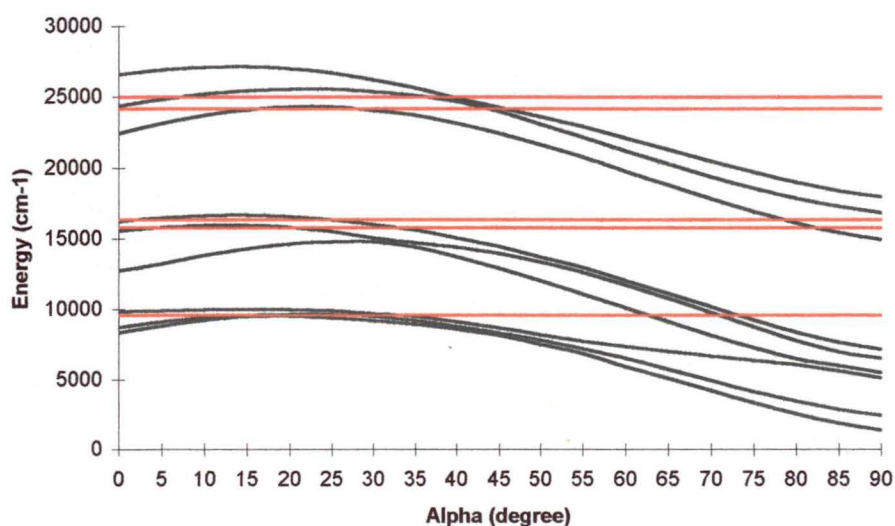
Figure 6.35: The energy levels calculated for molecule type II of [Ni(2,3-lutidine)$_2$(O$_2$N)$_2$] when changing α from 0° to 90°.

Using appropriately scaled e_σ and $e_{\pi y}$ parameters for the 2,3-lutidine and nitrite ligands derived from the 2,5-lutidine ligands and monodentate nitrito ligands, respectively, and including the $e_{\sigma\pi}$ parameter for an α value of 25°, the energy values shown in Table 6.10 were obtained for the complex [Ni(2,3-lutidine)$_2$(O$_2$N)$_2$]. The Racah parameters used for this calculation were B = 800cm^{-1} and C = 3 500cm^{-1}.

TRANSITION	CALCULATED (A)	CALCULATED (B)	OBSERVED
$^3B_1, {}^3B_2, {}^3A_2 \leftarrow {}^3B_1$	9 437, 9 513, 10 204	9 424, 9 676, 9 932	9 600
$^1B_1 \leftarrow {}^3B_1$	13 019	12 998	13 250
$^3B_1 \leftarrow {}^3B_1$	15 796	15 542	15 800
$^3A_1 \leftarrow {}^3B_1$	16 025	16 378	16 350
$^1B_1 \leftarrow {}^3B_1$	21 415	21 267	21 400
$^3B_1 \leftarrow {}^3B_1$	24 771	24 322	24 200
$^3A_2 \leftarrow {}^3A_1$	25 423	25 565	25 200

Table 6.10: The calculated and observed transition energies for [Ni(2,3-lut)$_2$(O$_2$N)$_2$]. (A) and (B) denote the two molecule types in the unit cell.

Similar calculations undertaken for the [Ni(quinoline)$_2$(O$_2$N)$_2$] provided the calculated energies shown in Table 6.11. Also included in this table are the results obtained when $\alpha = 0°$ as a comparison to those calculated using $\alpha = 25°$.

TRANSITION	CALCULATED ($\alpha = 0°$)	CALCULATED ($\alpha = 25°$)	OBSERVED
$^3B_1, {}^3B_2, {}^3A_2 \leftarrow {}^3B_1$	9 194, 9 428, 10 169	9 640, 10 641, 10 834	9 600
$^1B_1 \leftarrow {}^3B_1$	12 095	12 623	12 500
$^3B_1 \leftarrow {}^3B_1$	13 292	15 135	15 000
$^3A_2 \leftarrow {}^3B_1$	16572, 17256	17 051, 17 158	17 000
$^1B_1 \leftarrow {}^3B_1$	20 519	21 465	21 490

Table 6.11: A comparison of the observed transition energies for [Ni(quin)$_2$(O$_2$N)$_2$] with those calculated when $\alpha = 0°$ and $\alpha = 25°$.

The complex [Ni(medpt)(NO$_2$)$_2$] has a tridentate amine, a monodentate nitro and a bidentate O,O'-chelating nitrito ligand coordinated to the Ni^{2+} ion. It also has two

different molecule types in its unit cell[11]. When using appropriately scaled amine, nitro and nitrito AOM parameters, and accounting for bent bonding by the use of the parameter $e_{\sigma\pi}$ and $\alpha = 25°$, the transition energies listed in Table 6.12 may be calculated. The bite angle of this complex is $58°$ [11], which is comparable to those of the other complexes discussed in this section, so a similar α value was assumed.

TRANSITION	CALCULATED (A)	CALCULATED (B)	OBSERVED
	9 169	8 598	8 850
$^3T_{2g} \leftarrow {}^3A_{2g}$	10 939	10 683	10 570
	11 509	10 762	11 500
$^1E_g \leftarrow {}^3A_{2g}$	12 773, 13 459	12 673, 13 444	12 530, 13 420
	16 591	15 902	16 000
$^3T_{1g} \leftarrow {}^3A_{2g}$	16 699	16 077	17 380
	17 840	17 013	18 180

Table 6.12: The calculated and observed transition energies for $[Ni(medpt)(NO_2)_2]$. (A) and (B) denote the two molecule types in the unit cell.

As shown in Table 6.12, it can be seen that a relatively good agreement between observed and calculated transition energies was reached. However, it was necessary to calculate energies for both molecule types, and it appears that the observed spectrum has peaks attributable to the two different molecules.

In summary, for each of the complexes, agreement with the observed transition energies is significantly improved by including "bent bonding" in the AOM calculations.

6.5.2 Complexes with Bridging Nitrite Ligands

When calculating AOM parameters for the polymeric Ni^{2+} complexes $[Ni(en)_2NO_2]ClO_4$ and $[Ni(tn)_2NO_2]ClO_4$, each metal centre was considered to be independent, i.e. as a first approximation, the effect of neighbouring metal ions on the nitrite bonding parameters was ignored. This means that each nickel ion in these

complexes was considered to be coordinated to two bidentate amines, a monodentate nitro and a monodentate nitrito ligand (Figure 6.36).
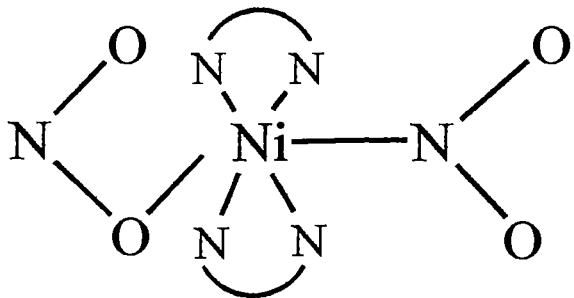
Figure 6.36: The inner coordination sphere for $[Ni(en)_2NO_2]ClO_4$ and $[Ni(tn)_2NO_2]ClO_4$.

Using amine and monodentate nitro and nitrito parameters appropriately scaled for bond length, the energies listed in Table 6.13 were calculated.

TRANSITION	CALCULATED (cm^{-1})	OBSERVED (cm^{-1})
	9 545	9 800
$^3T_{2g} \leftarrow {}^3A_{2g}$	10 137	10 575
	12 357	12 000
$^1E_g \leftarrow {}^3A_{2g}$	12 745	12 820
	13 386	13 500
	16 324	16 000
$^3T_{1g} \leftarrow {}^3A_{2g}$	16 463	16 900

Table 6.13: A comparison of the transition energies calculated for the complex $[Ni(en)_2NO_2]ClO_4$ using appropriately scaled AOM parameters with those obtained experimentally.

Initially, an attempt was made to assign the peak at ~13 500cm^{-1} to a spin-allowed transition, but this required unreasonable bonding parameters. However, the calculations suggested that this peak could be due to a spin-forbidden transition. This is a little surprising, as spin-forbidden peaks are usually very sharp in

appearance, whereas the 13 500cm^{-1} peak for [Ni(en)$_2$NO$_2$]ClO$_4$ is quite broad. This may be related to the unusual magnetic coupling present in this complex.

When calculating energies for the complex [Ni(tn)$_2$NO$_2$]ClO$_4$, a reasonable fit is obtained in a similar manner to that described for [Ni(en)$_2$NO$_2$]ClO$_4$. The results obtained using appropriately scaled amine, nitro and nitrito parameters, and B = 800, are shown in Table 6.14.

TRANSITION	CALCULATED (cm^{-1})	OBSERVED (cm^{-1})
	9 914	9 760
$^3T_{2g} \leftarrow {}^3A_{2g}$	10 161	10 400
	12 151	11 900
$^1E_g \leftarrow {}^3A_{2g}$	13 559	13 570
	16 330	15 950
$^3T_{1g} \leftarrow {}^3A_{2g}$	17 302	17 080

Table 6.14: A comparison of the transition energies calculated for [Ni(tn)$_2$NO$_2$]ClO$_4$ using appropriately scaled AOM parameters with those obtained experimentally.

Although the band observed at 13 570cm^{-1} appears to be quite broad in this spectrum as well (Figure 6.20), these calculations have again shown that it is likely to be a spin-forbidden transition rather than a spin-allowed transition. It is possible that a similar magnetic interaction to that described for the analogous complex [Ni(en)$_2$NO$_2$]ClO$_4$ is also occurring in this complex, thus broadening this peak.

The structure of the polymeric complex [(CH$_3$)$_4$N]Ni(NO$_2$)$_3$ is different to the N,O-bridged complexes discussed above. In this case, the nickel ions are in two different environments, either surrounded by N-bonded or O-bonded nitrite ligands. Table 6.15 shows the energies calculated for octahedrally coordinated nickel nitro and nitrito complexes where the AOM parameters used have been scaled for bond length. Also included in this table are the experimentally obtained values.

TRANSITION	CALCULATED (cm^{-1})	OBSERVED (cm^{-1})
	[12 270]	
	[13 179]	
$^3T_{2g} \leftarrow {}^3A_{2g}$	[14 092]	14 300
	14 369	
	14 568	
	14763	
$^3T_{2g} \leftarrow {}^3A_{2g}$	[19 297]	19 360
	[19 775]	19 570
.	[21 231]	
	21 839	21 720
$^3T_{1g} \leftarrow {}^3A_{2g}$	21 962	22 600
	22 394	23 500

Table 6.15: A comparison of the transition energies calculated for the complex [(CH$_3$)$_4$N]Ni(NO$_2$)$_3$ using appropriately scaled AOM parameters with those obtained experimentally. Bracketed values are those calculated for a monodentate nitrito complex.

These calculated values confirm that, as suggested in Section 6.4, the bands observed for this complex are due to the octahedrally N-coordinated nickel ions. It is possible that the peaks of very low intensity at 19 360cm^{-1} and 19 570cm^{-1} are due to the octahedrally O-coordinated nickel centres, but it is not clear as to why these would be of such low intensity in comparison to the other bands.

To a good approximation, the bonding parameters of N,O-bridged nitrites are similar to those of monodentate nitro and nitrito groups. That is, the bonding by one atom does not greatly influence the bonding power of the second atom involved in the bridging.

6.5.3 Complexes with Thiocyanate and Nitrite Ligands

The three nickel(II) nitrite complexes with thiocyanate ligands discussed in the present chapter are [Ni(medpt)(NCS)NO$_2$], [Ni$_2$(medpt)$_2$(NCS)$_3$NO$_2$].H$_2$O and [Ni$_2$(dpt)$_2$(NCS)$_3$NO$_2$]. The first of these complexes has one O,O'-nitrito ligand, while the latter two have an N,O,O'-bridging nitrito ligand (see Figure 6.23). The thiocyanate ligand can have different resonance structures. When changing from sp to sp^2 hybridisation on the nitrogen atom, the angle $\angle$MNC changes (Figure 6.37).
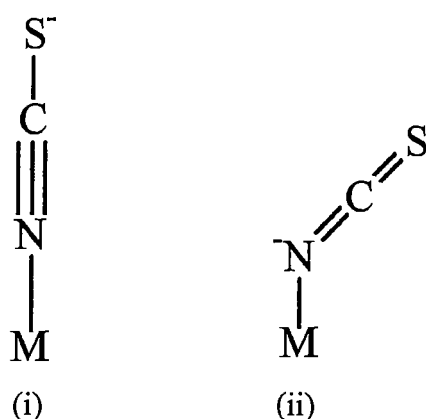
Figure 6.37: Linearly (i) and non-linearly (ii) coordinated thiocyanate ligands.

In the linear case (i), this ligand may have a negative value for the AOM parameter e_π, corresponding to π-acceptance, whereas in the non-linear case (ii), there is also the possibility that the π-interaction is anisotropic, leading to a difference between the in-plane e_π and out-of-plane e_π. The complexes discussed in the present section have this non-linear coordination, and so this has been considered in these calculations.

With the introduction of another ligand type, the problem of over-parameterisation becomes more pronounced. For this reason, a number of assumptions were made when using the AOM to calculate band energies for these complexes. Parameters for the amine ligands were estimated by scaling previously obtained amine parameters for bond length. The nitrite parameters used in these calculations were scaled from appropriate monodentate parameters (Section 5.4). For example, the complexes [Ni$_2$(medpt)$_2$(NCS)$_3$NO$_2$].H$_2$O and [Ni$_2$(dpt)$_2$(NCS)$_3$NO$_2$] have μ-N,O,O'-nitrito bridging nitrite ligands. The two nickel centres were considered to be independent

molecules, one of which had an O,O'-chelating nitrito group (centre I), and the other with a monodentate nitro ligand (centre II). Therefore, the first group had parameters derived from monodentate nitrito parameters, which has been shown in the present chapter to give reasonable energy values, and the latter parameters were derived from nitro parameters listed in Chapter 5. Bent bonding has also been taken into account, with an $\alpha = 25°$ used to determine $e_{\sigma\pi}$ where appropriate. This 25° value was chosen as the geometry of the nitrite ligand in these complexes was similar to that of the complexes with O,O'-chelating nitrites. For each complex, the value of e_σ and $e_{\pi x}$ and $e_{\pi y}$ for the thiocyanate ligand giving optimum agreement with the observed transition energies was then estimated. Here, x lies in the plane defined by the Ni^{2+} and thiocyanate. During this work, it was found that optimum agreement was obtained if $e_{\pi x}$ is negligible.

The complex [Ni(medpt)(NCS)NO$_2$] has one chelating O,O'-nitrito ligand. Assuming an $\alpha = 25°$, and using amine and nitrito parameters that had been scaled to take into account the different bond lengths, the transition energies listed in Table 6.16 were calculated. The values $e_\sigma(NCS) = 3\,400cm^{-1}$ and $e_{\pi y}(NCS) = 100cm^{-1}$ were used in this calculation, and B = 850.

TRANSITION	CALCULATED (cm^{-1})	OBSERVED (cm^{-1})
$^3B_1 \leftarrow {}^3B_1$	9 659	9 300
$^3A_1 \leftarrow {}^3B_1$	11 077	10 950
$^3B_1 \leftarrow {}^3B_1$	15 877	15 600
$^3A_1 \leftarrow {}^3B_1$	16 980	17 300
$^1A_1 \leftarrow {}^3B_1$	22 476	22 300
$^1B_1 \leftarrow {}^3B_1$	22 806	23 100

Table 6.16: The calculated and observed energies for [Ni(medpt)(NCS)NO$_2$].

As described above, the complexes [Ni$_2$(medpt)$_2$(NCS)$_3$NO$_2$].H$_2$O and [Ni$_2$(dpt)$_2$(NCS)$_3$NO$_2$] have bridging N,O,O'-nitrito ligands. When using the method discussed above, the transition energies listed in Table 6.17 were calculated. The $e_\sigma(NCS)$ and $e_{\pi y}(NCS)$ parameters used in these calculations were 3 000cm^{-1} and 125cm^{-1} for the nickel centre with the O,O'-nitrito ligand (centre I). The $e_\sigma(NCS)$

used for the other nickel centre (centre II) were 2 990cm^{-1} and 2 880cm^{-1} with $e_{\pi y}$(NCS) = 0cm^{-1} for both thiocyanate ligands.

TRANSITION	CALCULATED (cm^{-1})	OBSERVED (cm^{-1})
$^3T_{2g} \leftarrow {}^3A_{2g}$	[8 573]	
	9 565	8 200
	[10 087]	10 000
	[10 708]	11 200
	11 088	
	12 263	
$^1E_g \leftarrow {}^3A_{2g}$	[12 320], 12 745	12 430, 12 700
$^3T_{1g} \leftarrow {}^3A_{2g}$	[15 054]	
	[15 994]	
	[16 665]	15 250
	16 806	
	17 667	
	18 515	

Table 6.17: The calculated and observed energies for the complex [Ni$_2$(medpt)$_2$(NCS)$_3$NO$_2$].H$_2$O. The bracketed values are those calculated for the nickel centre surrounded by three amine ligands, a thiocyanate and an O,O'-nitrito ligand. The other values are those calculated for the nickel ion surrounded by three amine and two thiocyanate ligands, and a nitro ligand.

Using the above assumptions, the energies shown in Table 6.18 could be calculated for the complex [Ni$_2$(dpt)$_2$(NCS)$_3$NO$_2$]. The e_σ(NCS) values used were 3 395cm^{-1} for centre I and 3 070cm^{-1} and 2 850cm^{-1} for centre II, and $e_{\pi y}$(NCS) for centre I was 150cm^{-1}, and 0cm^{-1} for both thiocyanate ligands of centre II.

TRANSITION	CALCULATED (cm^{-1})	OBSERVED (cm^{-1})
	[8371]	
	[9130]	8 000
$^3T_{2g} \leftarrow {}^3A_{2g}$	9 952	9 400
	10 906	11 900
	[11 006]	
	12 186	
$^1E_g \leftarrow {}^3A_{2g}$	12 489	12 620
	[14 759]	
	[15 744]	14 450
$^3T_{1g} \leftarrow {}^3A_{2g}$	[16 451]	16 430
	16 715	18 100
	17 692	
	18 349	

Table 6.18: The calculated and observed energies for [Ni$_2$(dpt)$_2$(NCS)$_3$NO$_2$]. The bracketed values are those calculated for the nickel centre surrounded by three amine ligands, a thiocyanate and an O,O'-nitrito ligand. The other values are those calculated for the nickel ion surrounded by three amine and two thiocyanate ligands, and a nitro ligand.

To see whether the parameters obtained for the thiocyanate ligands were self-consistent, further calculations were carried out to determine the value of these parameters for the relatively simple complexes [Ni(en)$_2$(NCS)$_2$] and [Ni(NH$_3$)$_4$(NCS)$_2$]. Using appropriately scaled parameters for the ethylenediamine ligands of [Ni(en)$_2$(NCS)$_2$], a relatively good fit of the experimentally observed transition energies[27] was obtained when e_σ(NCS) = 2 350cm^{-1} and $e_{\pi y}$(NCS) = 100cm^{-1}. The parameter $e_{\pi x}$(NCS) had little effect on this calculation, and so was assumed to be negligible. A comparison of the calculated energies with those observed is shown in Table 6.19.

TRANSITION	CALCULATED (cm^{-1})	OBSERVED (cm^{-1})[27]
$^3E_g \leftarrow {}^3B_{1g}$	9 574	9 600
$^3B_{2g} \leftarrow {}^3B_{1g}$	11 808	12 000
$^3A_{2g} \leftarrow {}^3B_{1g}$	16 161	16 000
$^3E_g \leftarrow {}^3B_{1g}$	17 949	17 900
$^3E_g \leftarrow {}^3B_{1g}$	27 629	27 700

Table 6.19: The calculated and observed energies for [Ni(en)$_2$(NCS)$_2$]. Observed energies are those quoted by Lever[27].

In a similar manner, the transition energies shown in Table 6.20 were calculated for the complex [Ni(NH$_3$)$_4$(NCS)$_2$]. The parameter values e_σ(NCS) = 3 380cm^{-1} and $e_{\pi y}$(NCS) = -100cm^{-1} were used in this calculation. For simplicity, O$_h$ symmetry labels have been used to denote these transitions.

TRANSITION	CALCULATED (cm^{-1})	OBSERVED (cm^{-1})[28]
$^3T_{2g} \leftarrow {}^3A_{2g}$	10 879	10 750
	11 079	
$^3T_{1g} \leftarrow {}^3A_{2g}$	17 243	17 350
	17 798	17 500
$^3T_{1g} \leftarrow {}^3A_{2g}$	27 916	27 900

Table 6.20: The calculated and observed energies for [Ni(NH$_3$)$_4$(NCS)$_2$]. Observed energies are from Hare and Ballhausen[28].

The transition energies shown in Table 6.21 were calculated for the complex ion [Ni(NCS)$_6$]$^{4-}$. As the bond lengths of the thiocyanate groups in this complex are not equal, parameter values close to those of [Ni(NH$_3$)$_4$(NCS)$_2$] were used, with appropriate scaling for bond length.

TRANSITION	CALCULATED (cm^{-1})	OBSERVED (cm^{-1})[29]
	9 324	
$^3T_{2g} \leftarrow {}^3A_{2g}$	9 616	9 600
	9 946	
$^1E_g \leftarrow {}^3A_{2g}$	13 377	13 700
	15 492	
$^3T_{1g} \leftarrow {}^3A_{2g}$	15 590	15 950
	15 820	
$^1A_{1g} \leftarrow {}^3A_{2g}$	22 202	22 200
	25 911	
$^3T_{1g} \leftarrow {}^3A_{2g}$	25 999	25 800
	26 169	

Table 6.21: The calculated and observed energies for $[Ni(NCS)_6]^{4-}$. Observed energies are from Forster and Goodgame[29].

Table 6.22 summarises the AOM parameters determined for the thiocyanate ligands in these nickel(II) complexes. All of the values listed in this table have been scaled for a bond length of 2.1Å so that these can be compared easily.

COMPLEX	$e_\sigma(NCS)$	$e_{\pi y}(NCS)$
$[Ni(medpt)(NCS)NO_2]$	2 875	85
$[Ni_2(medpt)_2(NCS)_3NO_2].H_2O$	2 720; 2 725; 2 400	0; 0; 100
$[Ni_2(dpt)_2(NCS)_3NO_2]$	2 730; 2 730; 2 590	0; 0; 115
$[Ni(en)_2(NCS)_2]$	2 710	115
$[Ni(NH_3)_4(NCS)_2]$	2 900	-75
$[Ni(NCS)_6]^{4-}$	3 190; 3 130; 3 160	-75; -75; -75

Table 6.22: A comparison of the $e_\sigma(NCS)$ and $e_{\pi y}(NCS)$ AOM parameters derived for the nickel(II) complexes discussed in Section 6.5.3. All have been scaled for a bond length of 2.1Å.

It can be seen that, in general, these parameters transfer well from one complex to another. They suggest that N-bonded thiocyanate is a relatively weak ligand with a Δ value for an octahedral complex of $\sim 9000cm^{-1}$. The value observed for the $[Ni(NCS)_6]^{4-}$ ion is a little higher than this ($\Delta = 9\,600cm^{-1}$)[29]. The relatively low value obtained for one of the $e_\sigma(NCS)$ parameters for $[Ni_2(medpt)_2(NCS)_3NO_2].H_2O$ is still within experimental error. The negative values of $e_{\pi y}(NCS)$ for $[Ni(NH_3)_4(NCS)_2]$ and $[Ni(NCS)_6]^{4-}$ are possible as these complexes have linearly coordinated thiocyanate ligands. The higher values of $e_\sigma(NCS)$ determined for these two complexes may also be due to this, as the slight bent bonding that results from the non-linearly coordinating NCS ligands may result in a slightly less effective overlap, and thus a lower e_σ value in comparison to the linearly coordinated NCS groups.

6.6 Summary

A number of nickel(II) complexes with bridging and bidentate nitrite ligands have been synthesised. The crystal structure determination for $[Ni(tn)_2NO_2]ClO_4$ confirmed that this complex was similar to $[Ni(en)_2NO_2]ClO_4$ and had N,O-bridging nitrito ligands. A redetermination of the crystal structure of $[Ni(quinoline)_2(O_2N)_2]$ revealed a different crystal structure to that reported previously.

The infrared and Raman spectra measured for the complexes were used to assign the vibrational modes of the nitrite ligands. This showed that the energies of the nitrite stretching vibrations shifted to lower energy upon bidentate O,O'-chelation and N,O,O'-bridging in comparison to the free nitrite energies, whereas the *cis* N,O-bridging does not have a great effect on the nitrite vibrational modes. The *trans* N,O-bridging coordination mode has a considerable effect on these stretching modes, with ν_2 shifting to lower energy and ν_3 shifting to a higher energy, in relation to the free nitrite stretching energies.

Single crystal optical spectra were measured for all of the complexes discussed in the present chapter. AOM parameters for the nitrite ligands could be derived from monodentate nitro or nitrito values with appropriate scaling for bond length differences. An extension of the AOM has been used to include the effects of bent

bonding, which in the case of the present complexes is considerable. It was found that this extension to the AOM in its simple form significantly improved agreement with experiment. The polymeric complexes with bridging ligands were successfully modelled by considering each nickel ion coordination sphere in isolation, regarding the nitrites as having bonding parameters similar to monodentate nitro and nitrito ligands. The dimers [Ni$_2$(medpt)$_2$(NCS)$_3$NO$_2$].H$_2$O and [Ni$_2$(dpt)$_2$(NCS)$_3$NO$_2$] were also successfully modelled in this manner.

6.7 References

1. Hitchman M.A. and Rowbottom G.L., *Coord. Chem. Rev.*, **42(1)**, 55-132, (1982).

2. Diaz C., Ribas J., Costa, R., Tercero J., El Fallah M.S., Solans X. and Font-Bardía, M., *Eur. J. Inorg. Chem.*, 675-681, (2000).

3. Rowbottom, G.L., Ph.D. Thesis, University of Tasmania, (1980).

4. Goodgame D.M.L. and Hitchman M.A., *Inorg. Chem.*, **4**, 721-725, (1965).

5. Goodgame D.M.L. and Hitchman M.A., *Inorg. Chem.*, **6**, 813-816, (1967).

6. Chou L.K., Abboud K.A., Talham D.R., Kim W.W. and Meisel M.W., *Chem. Mater.*, **6**, 2051-2055, (1994).

7. Hathaway B.J. and Slade R.C., *J. Chem. Soc. (A)*, 952-955, (1967).

8. Green R.W. and Bell B., *Aust. J. Chem.*, **26**, 1663-1668, (1973).

9. Ribas J., Díaz C., Monfort M., Vilana J., Solans X. and Font-Altaba R., *Trans. Met. Chem.*, **10**, 340-344, (1985).

10. Escuer A., Font-Bardía M., Peñalba E., Sanz N., Solans X. and Vicente R., *J. Chem. Soc. Dalton Trans.*, 3115-3119, (1999).

11. Wen R., Bernal I., Somoza F., Li W. and Fronczek F.R., *Inorg. Chim. Acta*, **282**, 96-109, (1998).

12. Sidman J.W., *J. Amer. Chem. Soc.*, **79**, 2675-2678, (1957).

13. Meyer A., Gleizes A., Girerd J., Verdaguer M. and Kahn O., *Inorg. Chem.*, **21**, 1729-1739, (1982).

14. Farrugia L.J., *J. Appl. Cryst.*, **30**, 565, (1997).

15. Figgis B.N., Reynolds P.A., White A.H., Williams C.A. and Wright S., *J. Chem. Soc. Dalton Trans.*, 997-1003, (1981).

16. Finney A.J., Hitchman M.A., Raston C.L., Rowbottom G.L. and White A.H., *Aust. J. Chem.*, **34**, 2047-2060, (1981).

17. Das D., Laskar I.R., Ghosh A., Mondal A., Okamoto K. and Chaudhuri N.R., *J. Chem. Soc. Dalton Trans.*, 3987-3990, (1998).

18. Wen R., Bernal I. and Fronczek F.R., *J. Coord. Chem.*, **49**, 33-43, (1999).

19. Hitchman M.A., Thomas R., Skelton B.W. and White A.H., *J. Chem. Soc. Dalton Trans.*, 2273-2279, (1998).

20. Hitchman M.A., Oats S.G., Riley M. and Rowbottom. G.L., *J. Chem. Soc. Dalton Trans.*, submitted for publication.

21. Lever A.B.P., Walker I.M. and McCarthy P.J., *Can. J. Chem.*, **60**, 495-500, (1982).

22. Finney A.J., Hitchman M.A., Raston C.L., Rowbottom G.L. and White A.H., *Aust. J. Chem.*, **34**, 2069-2084, (1981).

23. Drew M.G.B., Goodgame D.M.L., Hitchman M.A. and Rogers D., *Chem. Comm.*, 477, (1965).

24. Yamamoto Y., Suzuki T. and Kaizaki S., *J. Chem. Soc. Dalton Trans.*, 1566-1572, (2001).

25. Cruse D.A., Davies J.E., Gerloch M., Harding J.H., Mackey D. and McMeeking R.F., CAMMAG, a FORTRAN Package, University of Cambridge, (1979).

26. Falvello L.R., Hitchman M.A., Palacio F., Pascual I., Schultz A.J., Stratemeier H., Tomás M, Urriolabeitia E.P. and Young D.M., *J. Amer. Chem. Soc.*, **121(12)**, 2808-2819, (1999).

27. Lever A.B.P., *Inorganic Electronic Spectroscopy (2nd Edition)*, Elsevier Science Publishers, Amsterdam, (1984).

28. Hare C.R. and Ballhausen C.J., *J. Chem. Phys.*, **40(3)**, 792-795, (1964).

29. Forster D. and Goodgame D.M.L., *Inorg. Chem.*, **4(6)**, 823-829, (1965).

CHAPTER 7

General Conclusions

The transition metal complexes prepared for the current work illustrate the versatility of the nitrite ion when coordinating to a metal ion. They have provided a series of complexes from which conclusions may be drawn about the possible factors influencing the nitrite coordination mode in a given complex, and the changes in the nature of the bonding between different metal ions and nitrite coordination modes. These are summarised in this chapter.

7.1 Factors Thought to Influence the Nitrite Coordination Mode

Kinetic, steric and electronic factors are the three main factors thought to influence the coordination mode of the nitrite ligands in a given complex. This work concentrates on steric and electronic factors. The complexes prepared for the present studies included tetranitrite complex ions of the formula $[M(NO_2)_4]^{2-}$, M = Zn(II), Cd(II) and Hg(II), a series of nickel(II) nitrite complexes with amines of varying degrees of substitution and the pentaammine nitrite complexes $[Co(NH_3)_5NO_2]^{2+}$, $[Co(NH_3)_5ONO]^{2+}$ and $[Cr(NH_3)_5ONO]^{2+}$. The Co(III) and Cr(III) complexes were selected as it was thought that the main influence on the nitrite coordination mode is electronic, whereas the other complexes are thought to have steric factors as the primary influence.

7.1.1 *Electronic Factors*

In general, N-bonded nitro coordination is the preferred coordination mode in cobalt(III) complexes, but O-bonded nitrito coordination is preferred in chromium(III) complexes. DFT calculations were used to determine the differences between the total energies calculated for the nitro and nitrito isomers of the Cr(III) and Co(III) pentammine nitrite complexes. As the only isomer seen experimentally for Cr^{3+} is the nitrito complex, it was expected that the nitrito isomer is lower in energy than the nitro isomer. This was found to be the case, with the nitrito isomer

being 0.2eV lower in energy than the nitro isomer. This was the reverse for the cobalt(III) isomers, with a calculated energy difference between the nitro and nitrito isomers of $[Co(NH_3)_5NO_2]^{2+}$ of 0.41eV, which is of the same order of magnitude as the experimental value of 0.943eV.

The greater stability of nitro coordination may possibly be related to the filled t_{2g} d-shell, which occurs for the cobalt(III) ion. This is stabilized by the interaction with the empty π^* orbital of the nitrite ion for nitro coordination, but not when the nitrite bonds via oxygen. This stabilization is only half as great for Cr^{3+}, as here the t_{2g} orbitals are only half filled.

7.1.2 Steric Factors

The nitrite groups in the complex ion $[M(NO_2)_4]^{2-}$, M = Zn(II), Cd(II) and Hg(II), adopt an O,O'-nitrito coordination mode. This bidentate coordination is relatively symmetric for the cadmium and mercury complexes, with the M-O and M-O' bonds being similar in length. The crystal structure measured for the zinc complex ion in the present work shows that these bonds differ considerably in length for this complex, resulting in very asymmetric chelation. Given that Zn(II), Cd(II) and Hg(II) are all d^{10} transition metal ions, so no effects due to a partly filled d-shell are present, it is thought that the size of the metal ion is influencing the nitrite coordination mode. Zinc(II) is much smaller that cadmium(II) and mercury(II), and it is possible that there is simply not enough space for the nitrite groups to chelate symmetrically.

Density functional theory calculations were carried out for the complexes $[M(NO_2)_4]^{2-}$, M = Zn(II), Cd(II) and Hg(II). It was hoped that these would indicate the relative stabilities of the different coordination geometries for the complexes. However, it was found that the stereochemistry of these complexes is very flexible, with a number of geometries being very similar in energy. The most stable geometry calculated for $[Zn(NO_2)_4]^{2-}$ is that observed experimentally, while for $[Cd(NO_2)_4]^{2-}$ it is the geometry of highest symmetry observed experimentally; this latter complex has a number of different geometries in different crystal structures. For

$[Hg(NO_2)_4]^{2-}$, the most stable calculated geometry is not that observed in the solid state for the complex $K_3[Hg(NO_2)_4](NO_3)$, but rather that of the highest symmetry, as predicted by simple theories based on ligand-ligand repulsions. It is likely that the large size of the Hg^{2+} ion means that the disposition of the nitrite ions may easily be influenced by crystal lattice forces.

A number of nickel(II) nitrite complexes with amine and pyridine ligands of varying degrees of substitution were prepared. The complexes $[Ni(NH_3)_4(NO_2)_2]$, $[Ni(en)_2(NO_2)_2]$ and $[Ni(N,N-dimen)_2(ONO)_2]$ were successfully modelled using DFT calculations. The calculated energies for the nitro and nitrito isomers of the above complexes suggest that the nitro isomer is inherently slightly more stable than the nitrito isomer. This agreed with observation in the solid state for $[Ni(NH_3)_4(NO_2)_2]$ and $[Ni(en)_2(NO_2)_2]$, but not for $[Ni(N,N-dimen)_2(ONO)_2]$. However, the difference in the energies calculated for both isomers was the smallest for the complex with the substituted amines, and the nitro form of this complex is indeed the most stable isomer for this complex in chloroform solution.

7.2 The Nature of the Metal-Nitrite Bond

Single crystal optical spectra were measured for the Co(III), Cr(III) and Ni(II) complexes in the present study. The observed transition energies for these complexes are compared with those calculated using the Angular Overlap Model (AOM). These calculations have been used to derive e_σ and e_π parameters for the nitrite ligands, and the parameters are shown to be transferable not only to other complexes with the same transition metal ion and nitro or nitrito coordination mode, but also to complexes with bridging and chelating nitrites.

The bonding parameters deduced for the nitro group when coordinated to cobalt(III) are $e_\sigma \approx 7\,900cm^{-1}$ and $e_{\pi y} \approx -400cm^{-1}$. This suggests that the ligand has a similar σ-bonding strength to a saturated amine such as ammonia, and acts as a weak π-acceptor. Spectral analysis for the cobalt(III) nitrito isomer showed that the nitrito ion is a much weaker ligand than the nitro group, being a weaker σ-donor than NH_3 and a weak π-donor. The parameters are similar to those determined for the nitrito ligand in $[Cr(NH_3)_5ONO]^{2+}$, which are $e_\sigma = 6\,055cm^{-1}$ and $e_{\pi y} = 865cm^{-1}$.

Similar results were obtained for the nickel(II) nitrite complexes. The e_σ parameter for the N-bonded nitrite, $3\,830 \pm 170\text{cm}^{-1}$ is slightly higher in energy than that for the nitrito ligand, $3\,400 \pm 30\text{cm}^{-1}$, which implies that the nitro ligand is a marginally stronger

σ-donor than the nitrito ligand. The difference between the $e_{\pi y}$ parameters derived for the nitrito and nitro coordination modes is much greater. The nitrito ligand has a significant positive value, $450 \pm 100\text{cm}^{-1}$, while the nitro parameter is small and negative, $-140 \pm 65\text{cm}^{-1}$. This suggests that the O-bonded nitrite is a moderate π-donor, whereas the N-bonded nitrite is a weak π-acceptor. The difference in π-bonding is consistent with the way in which the orientation of the non-bonding and antibonding nitrite π-orbitals changes as the ligand alters its manner of coordination. The large difference in the overall field strength, and very different position in the spectrochemical series, is thus due mainly to the difference in the π-bonding of the two coordination modes.

The nitro and nitrito AOM parameters determined for the nickel(II) complexes with monodentate nitrite ligands were found to be transferable to complexes with bridging and chelating nitrite groups, with appropriate scaling for the difference in bond lengths. However, an added complication for the complexes with O,O'-chelating and N,O,O'-bridging nitrites is the presence of "bent bonding". To account for the change in orbital overlap in this situation, another parameter, $e_{\sigma\pi}$, was introduced into the calculations. The calculated transition energies are then in good agreement with the observed energies when the angle between the position of the oxygen orbital and the M-O bond, α, is 25°. This is in agreement with the α value estimated from the crystal structural data of these complexes.

DFT calculations also provided an insight into the nature of the bonding when the nitrite is N-bonded or O-bonded. These confirm that nitrite acts as π-donor when these are O-bonded, compared with that of the N-bonded ligands. Δ values comparable to those derived via the AOM, and estimated from the optical spectra, were also derived from these DFT calculations. The Δ values of the nitro complexes are greater than those of the analogous nitrito isomer, and this correlated well with the respective positions of the nitro and nitrito group in the spectrochemical series.

The nickel(II) nitro complexes studied in the current work have an unusual peak in their optical spectra at $\sim$ 20 000cm^{-1}. Originally assigned as a d-d transition, and then as a n $\rightarrow \pi^*$ transition, evidence provided by the optical spectra, AOM and DFT calculations in the present work suggests that it is in fact a relatively low energy metal to ligand charge transfer transition, from the highest occupied molecular orbital (predominantly the Ni^{2+} dz^2 orbital) to the lowest unoccupied molecular orbital, the π^* orbital of the nitrite.

Infrared and Raman spectra were measured for each complex prepared in the present work. As well as allowing the unambiguous assignment of the fundamental nitrite vibrations, these have shown that, upon nitrito coordination, v_2 shifts significantly to lower energy compared with the free ion. For nitro coordination, this vibration shifts to higher energy, decreasing the energy difference between v_2 and v_3. The energies of these nitrite stretching vibrations, v_2 and v_3, are shifted to slightly lower energy than those of the free ion upon bidentate O,O'-chelating coordination. The *cis*-N,O-bridging mode does not have a great effect on the vibrational energies of the nitrite, and this may be due to the relatively long Ni-N and Ni-O bonds present in complexes with this coordination mode. In addition, this manner of N,O-bridging leaves the non-coordinated oxygen in quite close proximity to the Ni^{2+} ion, so that the difference between the nitrite oxygen atoms is less pronounced than for the *trans* N,O-bridging mode. This latter mode causes v_2 to shift to lower energy and v_3 to shift to much higher energy than observed for free nitrite. The energy difference between v_2 and v_3 may be correlated with the significant difference in the N-O bond lengths of the bridging nitrites.

7.3 Future Work

Attempts were made in the present work to prepare the first complex with a nitrite ion adopting the O,O'-bridging coordination mode. Although these attempts were unsuccessful, it would be interesting to compare the bonding parameters and spectral data obtained for such a complex with those listed in this thesis. As chromium(III) is oxophilic, it may well be possible to prepare a Cr(III) complex with this desired coordination mode, if the right experimental procedure is discovered.

The DFT calculations involving nitro and nitrito isomers of nickel(II) complexes may be expanded as more powerful computers and programs become available. Possible future work may include modelling the isomers of [Ni(N,N-dimen)$_2$(ONO)$_2$] in solution, and calculating total energies for [Ni(1-(2-aminoethyl)piperidine)$_2$(NO$_2$)$_2$] and its nitrito isomer. This latter work may be achieved by using a combination of DFT and molecular modelling methods, to explore the steric interactions in the two crystal modifications of this complex.

The spectroscopic and computational studies discussed in this thesis have provided much information about the nature of the metal-nitrite bond in a number of transition metal complexes, and allowed a comparison of this bonding when the nitrite ion adopts many different coordination modes. The factors likely to exert an influence on the coordination mode adopted by the nitrite ion in a given complex have also been discussed, providing greater insight into the coordination chemistry of this versatile ligand. It is hoped that in future this may help in the many applied areas of biochemistry and solid state chemistry, in which the nitrite ion plays an important role.

APPENDIX A

The Crystal Structure of $Cs_2[Zn(NO_2)_4]$

Atom	x/a	y/b	z/c	U(eq) A**2
Cs	3/8	-1/8	0.05658(1)	* 0.0232(2)
Zn	1/8	1/8	1/8	* 0.0201(4)
N	-0.1520(4)	0.0441(3)	0.0566(1)	* 0.029(2)
O(1)	-0.0585(4)	0.0084(2)	0.0930(1)	* 0.034(1)
O(2)	-0.1148(4)	0.1364(3)	0.0478(1)	* 0.035(1)

Table A1: The atomic positional and isotropic displacement parameters.

Atom	U11	U22	U33	U12	U13	U23
Cs	0.0337(2)	0.0167(2)	0.0192(2)	0.00608(8)	0	0
Zn	0.0236(4)	0.0135(4)	0.0232(4)	0	0	0
N	0.024(1)	0.018(2)	0.044(2)	-0.002(1)	0.001(1)	-0.009(1)
O(1)	0.040(1)	0.027(1)	0.035(1)	-0.005(1)	-0.001(1)	0.004(1)
O(2)	0.037(2)	0.022(2)	0.047(1)	0.0015(8)	-0.006(1)	0.006(1)

Table A2: Atomic displacement parameters.

BOND	LENGTH (Å)	BOND	LENGTH (Å)
Cs-O(1)	3.346(3)	Zn-O(1)	2.080(3)
Cs-O(2[1])	3.132(3)	Zn-O(2)	2.516(3)
Cs-O(1[2])	3.185(3)	N-O(1)	1.211(4)
Cs-N[3]	3.441(3)	N-O(2)	1.251(5)
Cs-O(2[3])	3.181(3)		

Symmetry operations: [1] ¼ - x, ¼ -y, z; [2] ¼-x, y, ¼-z; [3] -x,-y, -z

Table A3: Bond lengths for $Cs_2[Zn(NO_2)_4]$.

ANGLE	°	ANGLE	°	ANGLE	°
O(1)-Zn-O(2)	52.8(1)	O(1[1])-Zn-O(1[8])	85.6(1)	O(1)-N-O(2)	115.4(3)
O(1)-Zn-O(1[1])	132.5(1)	O(1[1])-Zn-O(2[8])	133.7(1)	O(1)-N-Cs[3]	172.4(2)
O(1)-Zn-O(2[1])	87.5(1)	O(1[1])-Zn-O(1[2])	113.6(1)	O(2)-N-Cs[3]	67.6(2)
O(1)-Zn-O(1[8])	113.6(1)	O(1[1])-Zn-O(2[2])	87.5(1)	Cs-O(1)-Zn	93.32(9)
O(1)-Zn-O(2[8])	87.5(1)	O(2[1])-Zn-O(1[8])	133.7(1)	Cs-O(1)-N	111.2(2)
O(1)-Zn-O(1[2])	85.6(1)	O(2[1])-Zn-O(2[8])	173 2(1)	Cs-O(1)-Cs[2]	93 09(7)
O(1)-Zn-O(2[2])	133.7(1)	O(2[1])-Zn-O(1[2])	87.5(1)	Zn-O(1)-N	107.3(2)
O(2)-Zn-O(1[1])	87.5(1)	O(2[1])-Zn-O(2[2])	107.49(9)	Zn-O(1)-Cs[2]	98.06(9)
O(2)-Zn-O(2[1])	72.93(9)	O(1[8])-Zn-O(2[8])	52.8(1)	N-O(1)-Cs[2]	143 2(2)
O(2)-Zn-O(1[8])	87.5(1)	O(1[8])-Zn-O(1[2])	132.5(1)	Zn-O(2)-N	84.5(2)
O(2)-Zn-O(2[8])	107.49(9)	O(1[8])-Zn-O(2[2])	87.5(1)	Zn-O(2)-Cs[1]	90.7(1)
O(2)-Zn-O(1[2])	133.7(1)	O(2[8])-Zn-O(1[2])	87.5(1)	Zn-O(2)-Cs[3]	171 6(1)
O(2)-Zn-O(2[2])	173.2(1)	O(2[8])-Zn-O(2[2])	72.93(9)	N-O(2)-Cs[1]	161.0(2)
O(1[1])-Zn-O(2[1])	52.8(1)	O(1[2])-Zn-O(2[2])	52.8(1)	Cs[1]-O(2)-Cs[3]	95.71(9)

Symmetry Operations: [1] ¼-x, ¼-y, z; [2] ¼-x, y, ¼-z; [3] -x, -y, -z; [4] ¾+x, y–¼, -z; [5] ½+x, y–½, z; [6] ¾-x, -y-¼, z; [7] ½+x, -y-¼, ½-z; [8] x, ¼-y, ½-z.

Table A4: Bond angles for $Cs_2[Zn(NO_2)_4]$.

APPENDIX B

DFT Calculations for Mg[Cd(NO$_2$)$_4$], K$_2$[Cd(NO$_2$)$_4$] and "Mg[Zn(NO$_2$)$_4$]"

(a)   (b)
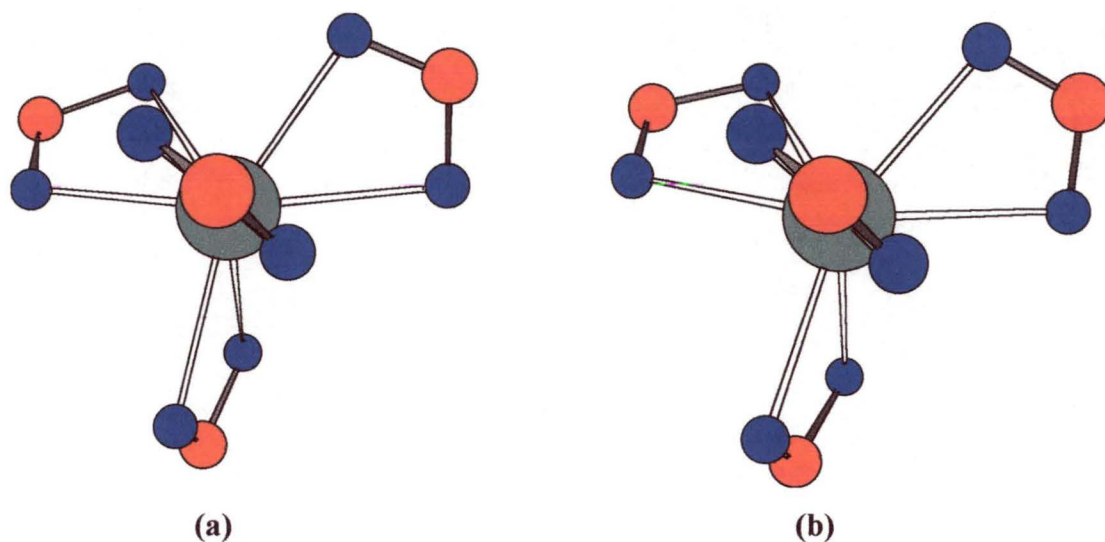
Figure B1: The observed (a) and calculated (b) geometry of the [Cd(NO$_2$)$_4$]$^{2-}$ in the complex Mg[Cd(NO$_2$)$_4$]$^{2-}$.

	CALCULATED	OBSERVED [1]
Cd-O(11)	2.530Å	2.366Å
Cd-O(12)	2.587Å	2.428Å
Cd-O(21)	2.504Å	2.362Å
Cd-O(22)	2.636Å	2.636Å
∠N(1)-Cd-N(2)	92.71°	90.79°
∠N(1)-Cd-N(3)	121.32°	123.16°
∠N(1)-Cd-N(4)	115.62°	116.35°
∠N(2)-Cd-N(3)	115.72°	116.35°
∠N(2)-Cd-N(4)	121.34°	123.16°
∠N(3)-Cd-N(4)	92.66°	90.79°

Table B1: A comparison of the calculated bond lengths and angles for [Cd(NO$_2$)$_4$]$^{2-}$ in Mg[Cd(NO$_2$)$_4$] with the experimental values[1].

(a)   (b)
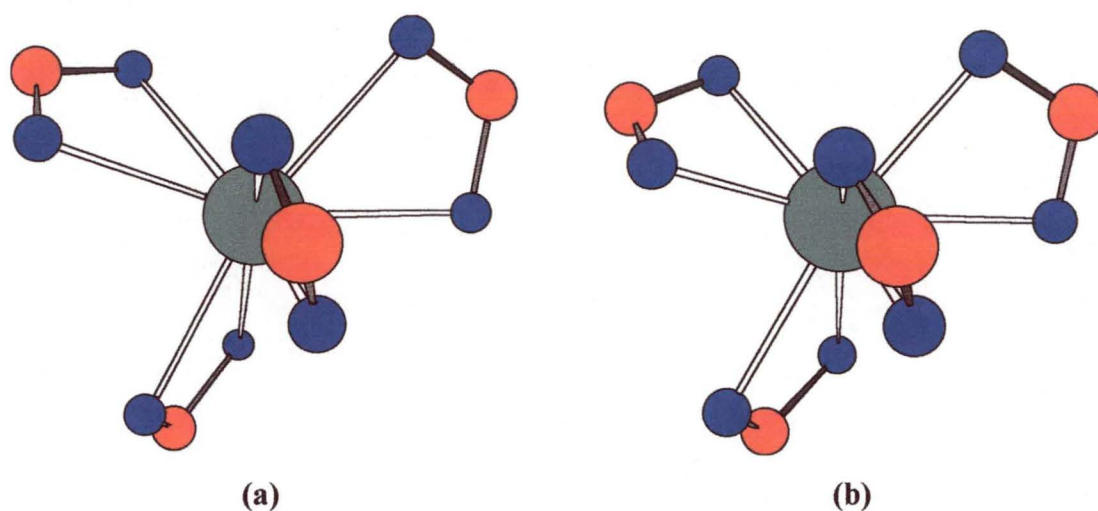
Figure B2: The observed (a) and calculated (b) geometry of the $[Cd(NO_2)_4]^{2-}$ in the complex $K_2[Cd(NO_2)_4]^{2-}$.

	CALCULATED	OBSERVED [1]
Cd-O(1)	2.497Å	2.377Å
Cd-O(1')	2.644Å	2.377Å
Cd-O(2)	2.647Å	2.414Å
Cd-O(2')	2.500Å	2.414Å
Cd-O(3)	2.577Å	2.435Å
Cd-O(3')	2.550Å	2.435Å
Cd-O(4)	2.563Å	2.525Å
Cd-O(4')	2.579Å	2.525Å
∠N(1)-Cd-N(1')	94.1°	94.6°
∠N(1)-Cd-N(2)	116.0°	115.9°
∠N(1)-Cd-N(3)	119.4°	121.0°
∠N(2)-Cd-N(3)	93.0°	90.5°

Table B2: A comparison of the calculated bond lengths and angles for $[Cd(NO_2)_4]^{2-}$ in $K_2[Cd(NO_2)_4]$ with the experimental values[1].

BOND	Mg[Zn(NO₂)₄]	EXPT
Zn-O11	2.138	2.080
-O12	2.877	2.516
-O21	2.276	2.080
-O22	2.384	2.516
-O31	2.126	2.080
-O32	2.949	2.516
-O41	2.223	2.080
-O42	2.467	2.516
O11-N1	1.299	1.211
O12-N1	1.254	1.250
O21-N2	1.273	1.211
O22-N2	1.281	1.250
O31-N3	1.302	1.211
O32-N3	1.254	1.250
O41-N4	1.285	1.211
O42-N4	1.266	1.250
Zn-O11-N1	101.31	107.3
Zn-O12-N1	90.29	84.50
O11-N1-O12	114.36	115.0
O11-Zn-O12	54.09	52.8

Table B3: Bond lengths (Å) and angles (°) for $[Zn(NO_2)_4]^{2-}$ calculated from the starting geometry $Mg[Cd(NO_2)_4]$ compared with the observed values in $Cs_2[Zn(NO_2)_4]$.

References:

1. Ohba S., Matsumoto F., Takazawa H. and Saito Y., *Acta Cryst.*, **C43**, 191-194, (1987).

Appendix C

Crystal Structure of [Ni(tn)₂NO₂]ClO₄

Crystal Structure of [Ni(tn)$_2$NO$_2$]ClO$_4$
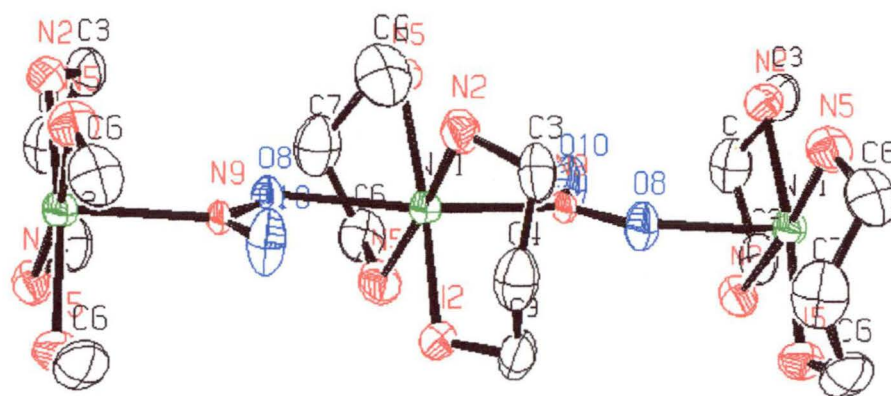
Figure C1: The structure of [Ni(tn)$_2$NO$_2$]ClO$_4$.

	Distance (Å)		Distance (Å)
Ni(1)-O(2)	2.290(6)	Ni(1)-N(2)	2.163(8)
Ni(1)-N(4)	2.102(6)	Ni(1)-N(4)	2.102(6)
Ni(1)-N(5)	2.117(6)	N(4)-H(5)	0.96
Cl(1)-O(1)	1.372(8)	N(4)-H(6)	0.89
Cl(1)-O(3)	1.41(1)	C(1)-H(8)	0.88
Cl(1)-O(4)	1.37(2)	C(1)-H(9)	0.87
N(4)-C(3)	1.468(9)	C(2)-H(1)	0.99
N(5)-C(1)	1.491(11)	C(2)-H(2)	0.86
C(1)-C(4)	1.489(12)	C(3)-H(3)	0.91
C(2)-C(3)	1.528(10)	C(3)-H(4)	0.87
O(2)-N(2)	1.250(10)	C(4)-H(7)	1.07
O(5)-N(2)	1.235(11)	C(4)-H(10)	1.08

Table C1: Bond lengths for [Ni(tn)$_2$NO$_2$]ClO$_4$.

	ANGLE (°)		ANGLE (°)
O(2)-Ni(1)-N(2)	171.2(3)	H(5)-N(4)-H(6)	100
O(2)-Ni(1)-N(4)	90.6(2)	Ni(1)-N(5)-C(1)	121.3(5)
O(2)-Ni(1)-N(5)	83.7(2)	N(5)-C(1)-C(4)	115.7(8)
N(2)-Ni(1)-N(4)	95.6(2)	N(5)-C(1)-H(8)	100
N(2)-Ni(1)-N(5)	90.3(2)	N(5)-C(1)-H(9)	106
N(4)-Ni(1)-N(4)	89.9(3)	N(4)-C(1)-H(8)	106
N(4)-Ni(1)-N(5)	87.7(2)	C(4)-C(1)-H(9)	116
N(5)-Ni(1)-N(5)	94.1(4)	H(8)-C(1)-H(9)	109
O(1)-Cl(1)-O(1)	111.4(10)	C(3)-C(2)-C(3)	115.5(9)
O(1)-Cl(1)-O(3)	108.9(6)	C(3)-C(2)-H(1)	107
O(1)-Cl(1)-O(4)	105.7(8)	C(3)-C(2)-H(2)	106
O(3)-Cl(1)-O(4)	116.2(14)	H(1)-C(2)-H(2)	112
Ni(1)-O(2)-N(2)	130.7(6)	N(4)-C(3)-C(2)	113.0(7)
Ni(1)-N(2)-O(2)	127.5(6)	N(4)-C(3)-H(3)	106
Ni(1)-N(2)-O(5)	115.8(6)	N(4)-C(3)-H(4)	108
O(2)-N(2)-O(5)	116.7(7)	C(2)-C(3)-H(3)	110
Ni(1)-N(4)-C(3)	119.7(5)	C(2)-C(3)-H(4)	110
Ni(1)-N(4)-H(5)	112	H(3)-C(3)-H(4)	107
Ni(1)-N(4)-H(6)	105	C(1)-C(4)-C(1)	115.8(11)
C(3)-N(4)-H(5)	105	C(1)-C(4)-H(7)	107
C(3)-N(4)-H(6)	110	C(1)-C(4)-H(10)	107

Table C2: Important bond angles for [Ni(tn)$_2$NO$_2$]ClO$_4$.

|	ANGLE (°)		ANGLE (°)
Ni(1)-O(2)-N(2)-O(5)	0.0000	N(2)-O(2)-Ni(1)-N(5)	-132.6(2)
Ni(1)-N(4)-C(3)-C(2)	-55.9(8)	N(4)-Ni(1)-N(4)-C(3)	-38.6(6)
Ni(1)-N(5)-C(1)-C(4)	37.1(10)	N(4)-Ni(1)-N(5)-C(1)	116.7(22)
O(2)-Ni(1)-N(4)-C(3)	129.2(5)	N(4)-C(3)-C(2)-C(3)	66.1(11)
O(2)-Ni(1)-N(5)-C(1)	-93.1(6)	N(5)-Ni(1)-N(4)-C(3)	-147.1(5)
N(2)-O(2)-Ni(1)-N(4)	-44.9(2)	N(5)-C(1)-C(4)-C(1)	-68.7(14)

Table C3: Torsion angles for [Ni(tn)$_2$NO$_2$]ClO$_4$.

	x	y	z	B_{eq}
Ni(1)	0.85505(2)	0.2500	0.23158(2)	1.808(6)
Cl(11)	0.59373(7)	0.7500	0 25145(5)	3 64(2)
O(8)	0.63913(13)	0.2500	0.22397(10)	2.71(4)
O(10)	0.5969(1)	0.2500	0.35856(11)	3.75(4)
O(12)	0.6017(6)	0.5944(9)	0.2662(5)	5.5(2)
O(13)	0.6971(7)	0.7500	0.1977(5)	10.6(2)
O(14)	0.7312(8)	0.7500	0.2478(6)	4.6(3)
O(15)	0.5808(3)	0.8828(3)	0.3106(2)	6.41(6)
O(16)	0.4574(8)	0.7500	0.2154(5)	4.8(2)
O(17)	0.5085(5)	0.7500	0 1794(3)	8.0(2)
N(2)	0.85016(13)	0.4246(2)	0.32757(10)	2.50(3)
N(5)	0.8395(2)	0.4302(2)	0 13809(11)	2.99(3)
N(9)	0.5568(2)	0.2500	0.28318(12)	1.27(4)
C(3)	0.9220(2)	0.3997(2)	0.40921(11)	3.18(4)
C(4)	0.8877(3)	0.2500	0.4541(2)	3.63(7)
C(6)	0.8449(2)	0.3971(3)	0.0440(1)	3.42(5)
C(7)	0.7821(3)	0.2500	0.0178(2)	4.86(8)
H(2A)	0.869(2)	0.513(3)	0.292(2)	4.9(5)
H(2B)	0.773(2)	0.437(2)	0.3335(11)	3.5(4)
H(3A)	1.004(2)	0.379(2)	0.3943(11)	3.8(4)
H(3B)	0.9080(13)	0.499(2)	0.4484(10)	2.2(3)
H(4A)	0.917(3)	0.2500	0.513(2)	6.0(8)
H(4B)	0.801(3)	0.2500	0.468(2)	4.4(6)
H(5A)	0.889(2)	0.509(2)	0.1536(12)	3.8(5)
H(5B)	0.782(2)	0.487(3)	0.142(2)	6.8(7)
H(6A)	0.821(2)	0.472(2)	0.0269(12)	3.0(5)
H(6B)	0.923(2)	0.389(3)	0.030(2)	7.6(7)
H(7A)	0.772(3)	0.2500	-0.036(2)	5.3(8)
H(7B)	0.681(3)	0.2500	0.040(2)	6.4(8)

$$B_{eq} = 8/3\ \pi^2(U_{11}(aa^*)^2 + U_{22}(bb^*)^2 + U_{33}(cc^*)^2 + 2U_{12}(aa^*bb^*)\cos \gamma + 2U_{13}(aa^*cc^*)\cos \beta + 2U_{23}(bb^*cc^*)\cos \alpha)$$

Table C4: Atomic coordinates of $[Ni(tn)_2NO_2]ClO_4$

APPENDIX D

The Crystal Structure of [Ni(quinoline)$_2$(O$_2$N)$_2$]
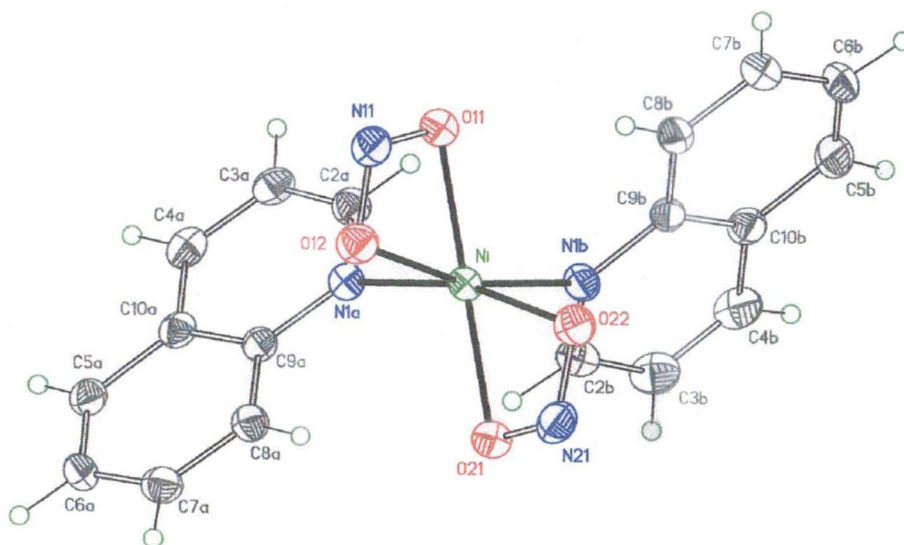
Figure D1: The structure of [Ni(quinoline)$_2$(O$_2$N)$_2$].

BOND	LENGTH (Å)	BOND	LENGTH (Å)	BOND	LENGTH (Å)
Ni-N(1B)	2.063(2)	C(5A)-C(10A)	1.422(4)	C(4B)-H(4B)	0.94(3)
Ni-N(1A)	2.069(2)	C(5A)-H(5A)	0.91(3)	C(5B)-C(6B)	1.345(5)
Ni-O(21)	2.0715(19)	C(6A)-C(7A)	1.409(4)	C(5B)-C(10B)	1.428(4)
Ni-O(11)	2.0791(19)	C(6A)-H(6A)	0.96(3)	C(5B)-H(5B)	0.93(3)
Ni-O(12)	2.117(2)	C(7A)-C(8A)	1.374(4)	C(6B)-C(7B)	1.411(4)
Ni-O(22)	2.123(2)	C(7A)-H(7A)	0.96(3)	C(6B)-H(6B)	0.97(3)
N(1A)-C(2A)	1.321(4)	C(8A)-C(9A)	1.414(4)	C(7B)-C(8B)	1.374(4)
N(1A)-C(9A)	1.381(3)	C(8A)-H(8A)	0.93(3)	C(7B)-H(7B)	0.95(3)
C(2A)-C(3A)	1.405(4)	C(9A)-C(10A)	1.417(4)	C(8B)-C(9B)	1.407(4)
C(2A)-H(2A)	0.93(3)	N(1B)-C(2B)	1.326(3)	C(8B)-H(8B)	0.93(3)
C(3A)-C(4A)	1.359(4)	N(1B)-C(9B)	1.389(3)	C(9B)-C(10B)	1.411(4)
C(3A)-H(3A)	0.94(3)	C(2B)-C(3B)	1.394(4)	N(11)-O(12)	1.264(3)
C(4A)-C(10A)	1.414(4)	C(2B)-H(2B)	0.99(3)	N(11)-O(11)	1.275(3)
C(4A)-H(4A)	0.94(3)	C(3B)-C(4B)	1.353(4)	N(21)-O(21)	1.259(3)
C(5A)-C(6A)	1.353(4)	C(4B)-C(10B)	1.419(4)	N(21)-O(22)	1.265(3)

Table D1: Bond lengths for the complex [Ni(quinoline)$_2$(O$_2$N)$_2$].

ANGLE	(°)	ANGLE	(°)	ANGLE	(°)
N1B-Ni-N1A	93.85(9)	C9A-N1A-Ni	125.62(18)	N1B-C2B-C3B	123.9(3)
N1B-Ni-O21	92.50(8)	N1A-C2A-C3A	124.2(3)	C4B-C3B-C2B	119.2(3)
N1A-Ni-O21	106.37(8)	C4A-C3A-C2A	118.7(3)	C3B-C4B-C10B	119.5(3)
N1B-Ni-O11	105.36(8)	C3A-C4A-C10A	119.6(3)	C6B-C5B-C10B	120.7(3)
N1A-Ni-O11	90.77(8)	C6A-C5A-C10A	120.7(3)	C5B-C6B-C7B	120.6(3)
O21-Ni-O11	154.45(8)	C5A-C6A-C7A	120.3(3)	C8B-C7B-C6B	120.6(3)
N1B-Ni-O12	165.01(8)	C8A-C7A-C6A	121.0(3)	C7B-C8B-C9B	119 8(3)
N1A-Ni-O12	89.46(8)	C7A-C8A-C9A	119.6(3)	N1B-C9B-C8B	119.8(2)
O21-Ni-O12	100.60(8)	N1A-C9A-C8A	119.7(2)	N1B-C9B-C10B	120.4(2)
O11-Ni-O12	59.93(7)	N1A-C9A-C10A	120.9(2)	C8B-C9B-C10B	119.8(4)
N1B-Ni-O22	91.15(8)	C8A-C9A-C10A	119.4(2)	C9B-C10B-C5B	118.6(3)
N1A-Ni-O22	165.40(8)	C4A-C10A-C9A	118.5(2)	O12-N11-O11	111.3(2)
O21-Ni-O22	59.66(8)	C4A-C10A-C5A	122.5(3)	N11-O11-Ni	95.10(15)
O11-Ni-O22	101.12(8)	C9A-C10A-C5A	119 0(3)	N11-O12-Ni	93.66(15)
O12-Ni-O22	89.23(8)	C2B-N1B-C9B	118.3(2)	O21-N21-O22	111.5(2)
C2-N1A-C9A	118.1(2)	C2B-N1B-Ni	116.19(18)	N21-O21-Ni	95.72(15)
C2A-N1A-Ni	115.93(18)	C9B-NiB-Ni	125.31(17)	N21-O22-Ni	93.09(15)

Table D2: Bond angles for the complex [Ni(quinoline)$_2$(O$_2$N)$_2$].

ATOM	x	y	z	U(eq)
H(2A)	0.374(4)	0.561(4)	0.389(1)	0.042(9)
H(3A)	0.394(4)	0.801(4)	0.437(1)	0.034(8)
H(4A)	0 310(4)	0.760(4)	0.5077(9)	0 024(7)
H(5A)	0.202(4)	0.556(4)	0.564(1)	0.032(8)
H(6A)	0 124(4)	0.276(4)	0.587(1)	0.036(9)
H(7A)	0.121(4)	0.046(4)	0.5378(8)	0.020(7)
H(8A)	0.193(3)	0.092(4)	0.4665(8)	0.012(6)
H(2B)	-0.022(3)	0.364(4)	0.3769(9)	0.020(7)
H(3B)	-0.234(4)	0.500(4)	0.326(1)	0.035(9)
H(4B)	-0.142(4)	0.562(4)	0.256(1)	0.042(9)
H(5B)	0.082(4)	0.530(4)	0.201(1)	0.040(9)
H(6B)	0.367(4)	0.430(4)	0.178(1)	0.037(8)
H(7B)	0.563(4)	0.296(4)	0.2316(9)	0.027(8)
H(8B)	0.476(4)	0.254(4)	0.299(1)	0.030(8)

Table D3: Hydrogen coordinates and isotropic displacement parameters for

[Ni(quinoline)$_2$(O$_2$N)$_2$].

	x	y	z	U(eq)
Ni	0.31355(4)	0.19572(4)	0.38162(1)	0.0207(1)
N(1A)	0.2895(3)	0.3876(3)	0.42867(7)	0.0223(5)
C(2A)	0 3395(4)	0.5474(4)	0.41739(9)	0.0260(6)
C(3A)	0.3500(4)	0.6907(4)	0 44606(9)	0.0257(6)
C(4A)	0 3037(4)	0.6662(4)	0.48806(9)	0.0265(6)
C(5A)	0.1986(4)	0.4633(4)	0.54540(9)	0.0274(6)
C(6A)	0.1525(4)	0.2992(4)	0.55774(9)	0.0289(6)
C(7A)	0.1523(4)	0.1604(4)	0.52749(9)	0.0267(6)
C(8A)	0.1969(4)	0.1885(4)	0.48502(8)	0.0239(5)
C(9A)	0.2449(3)	0.3592(3)	0.47137(8)	0.0208(5)
C(10A)	0.2479(3)	0 4983(4)	0.50191(9)	0.0230(6)
N(1B)	0.1685(3)	0.3356(3)	0.33517(7)	0.0230(5)
C(2B)	0.0043(4)	0.3864(4)	0.34595(9)	0.0282(6)
C(3B)	-0.1169(4)	0.4713(4)	0.3176(1)	0.0328(7)
C(4B)	-0.0671(4)	0.5055(4)	0.2765(1)	0.0327(7)
C(5B)	0.1665(4)	0.4795(4)	0.21969(9)	0.0328(7)
C(6B)	0.3302(4)	0.4231(4)	0.20793(9)	0.0345(7)
C(7B)	0.4468(4)	0.3382(4)	0.23824(9)	0.0310(7)
C(8B)	0.3951(4)	0.3120(4)	0.28028(8)	0.0246(6)
C(9B)	0.2233(3)	0.3679(3)	0.29311(8)	0.0210(5)
C(10B)	0.1065(4)	0.4531(4)	0.26292(9)	0.0263(6)
N(11)	0.6451(3)	0.1607(3)	0.40231(7)	0.0288(5)
O(11)	0.5822(3)	0.2638(3)	0.37299(6)	0.0276(4)
O(12)	0.5204(3)	0.0754(3)	0.41993(6)	0.0289(4)
N(21)	0.1525(3)	-0.0877(3)	0.36250(8)	0.0305(5)
O(21)	0.1031(2)	0.0213(3)	0.39052(6)	0 0277(4)
O(22)	0.2928(3)	-0.0363(3)	0.34366(6)	0.0296(4)

Table D4: Atomic coordinates and equivalent isotropic displacement parameters for [Ni(quinoline)$_2$(O$_2$N)$_2$].

APPENDIX E

Bent Bonding

Single Ligand[1]

A ligand has an orbital along the z axis (Figure E1), and the bond is rotated by $\alpha = 20°$ about the y_L axis.
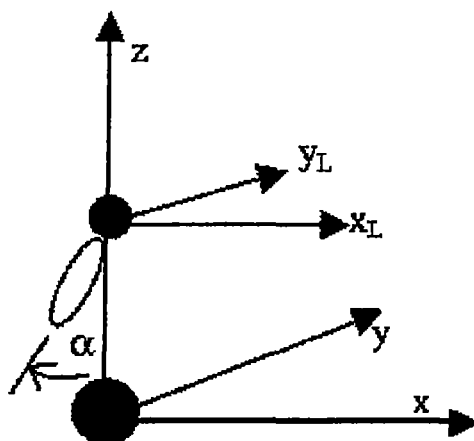

Figure E1: Ligand and global axes for a single ligand.

If the bonding orbital is thought of as acting as a p_z orbital of the ligand, then:

when $\alpha = 0°$, $e_\sigma = 4000$, $e_{\sigma x} = 0$, $e_{\sigma \pi} = 0 \text{cm}^{-1}$ and

when $\alpha = 90°$, $e_\sigma = 0$, $e_{\pi x} = 1000$ and $e_{\sigma \pi} = 0 \text{cm}^{-1}$.

For an intermediate α, such as $\alpha = 20°$:

$e_\sigma = 4000\cos^2\alpha = 3532.09$, $e_{\pi x} = 1000\sin^2\alpha = 116.98$ and

$|e_{\sigma\pi}| = \sqrt{(4000 \times 1000)}\sin\alpha\cos\alpha = 642.79 \text{cm}^{-1}$.

The sign of $e_{\sigma\pi}$ is determined in the following way. The bent bond is in the negative xz quadrant, so according to Gerloch and McMeeking[2], this would make $e_{\sigma\pi}$ positive.

The coefficients of the local ligand bonding is given by (with terms for $e_{\sigma\pi}$ added)[3]:

$$
\begin{pmatrix} c_{00} \\ c_{20} \\ c_{21} \\ c_{22} \\ c_{40} \\ c_{41} \\ c_{42} \\ c_{43} \\ c_{44} \end{pmatrix} =
\begin{pmatrix}
\frac{2}{5}\sqrt{\pi}\,(e_{\pi x} + e_{\pi y} + e_{\sigma}) \\
\sqrt{\frac{\pi}{5}}\,(e_{\pi x} + e_{\pi y} + 2\,e_{\sigma}) \\
-\sqrt{\frac{2\pi}{5}}\,e_{\sigma\pi} \\
\sqrt{\frac{3\pi}{10}}\,(e_{\pi x} - e_{\pi y}) \\
\frac{2}{5}\sqrt{\pi}\,(-2\,e_{\pi x} - 2\,e_{\pi y} + 3\,e_{\sigma}) \\
-2\sqrt{\frac{3\pi}{5}}\,e_{\sigma\pi} \\
\sqrt{\frac{2\pi}{5}}\,(e_{\pi x} - e_{\pi y}) \\
0 \\
0
\end{pmatrix} =
\begin{pmatrix}
2587.12 \\
5692.26 \\
-720.566 \\
113.566 \\
7346.69 \\
-1765.02 \\
131.134 \\
0 \\
0
\end{pmatrix}
$$

These are the coefficients in the local ligand frame, and these are the same as the coefficients in the global metal frame.

For a d^1 system, the ligand field matrix in the complex $|m_l\rangle$ is[3]:

	$|{-2}\rangle$	$|{-1}\rangle$	$|0\rangle$	$|{+1}\rangle$	$|{+2}\rangle$
	$\frac{1}{5}(-e_{\pi x} - e_{\pi y} - e_{\sigma})$	0	0	0	0
	0	$\frac{1}{10}(3\,e_{\pi x} + 3\,e_{\pi y} - 2\,e_{\sigma})$	$\frac{e_{\sigma\pi}}{\sqrt{2}}$	$\frac{1}{2}(-e_{\pi x} + e_{\pi y})$	0
	0	$\frac{e_{\sigma\pi}}{\sqrt{2}}$	$\frac{1}{5}(-e_{\pi x} - e_{\pi y} + 4\,e_{\sigma})$	$-\frac{e_{\sigma\pi}}{\sqrt{2}}$	0
	0	$\frac{1}{2}(-e_{\pi x} + e_{\pi y})$	$-\frac{e_{\sigma\pi}}{\sqrt{2}}$	$\frac{1}{10}(3\,e_{\pi x} + 3\,e_{\pi y} - 2\,e_{\sigma})$	0
	0	0	0	0	$\frac{1}{5}(-e_{\pi x} - e_{\pi y} - e_{\sigma})$

Transforming this into the real d-orbital basis[3]:

	$|z^2\rangle$	$|xz\rangle$	$|yz\rangle$	$|xy\rangle$	$|x^2-y^2\rangle$
	$\frac{1}{5}(-e_{\pi x} - e_{\pi y} + 4\,e_{\sigma})$	$e_{\sigma\pi}$	0	0	0
	$e_{\sigma\pi}$	$\frac{1}{5}(4\,e_{\pi x} - e_{\pi y} - e_{\sigma})$	0	0	0
	0	0	$\frac{1}{5}(-e_{\pi x} + 4\,e_{\pi y} - e_{\sigma})$	0	0
	0	0	0	$\frac{1}{5}(-e_{\pi x} - e_{\pi y} - e_{\sigma})$	0
	0	0	0	0	$\frac{1}{5}(-e_{\pi x} - e_{\pi y} - e_{\sigma})$

Eigenvalues: $\{3649.07,\ 0,\ 0,\ 0,\ 0.00134393\}$

Eigenvectors (in columns):
$$
\begin{pmatrix}
0.983841 & 0 & 0 & 0 & -0.179045 \\
0.179045 & 0 & 0 & 0 & 0.983841 \\
0 & 1. & 0 & 0 & 0 \\
0 & 0 & 1. & 0 & 0 \\
0 & 0 & 0 & 1. & 0
\end{pmatrix}
$$

The highest energy orbital is the z^2 type, pointing at the ligand.

From the eigenvector of the highest energy orbital in the calculation above, one gets the situation shown in Figure E2, where a positive $e_{\sigma\pi}$ appears to be a rotation into the positive xz quadrant, rather than the negative quadrant as given by Gerloch et al[3].
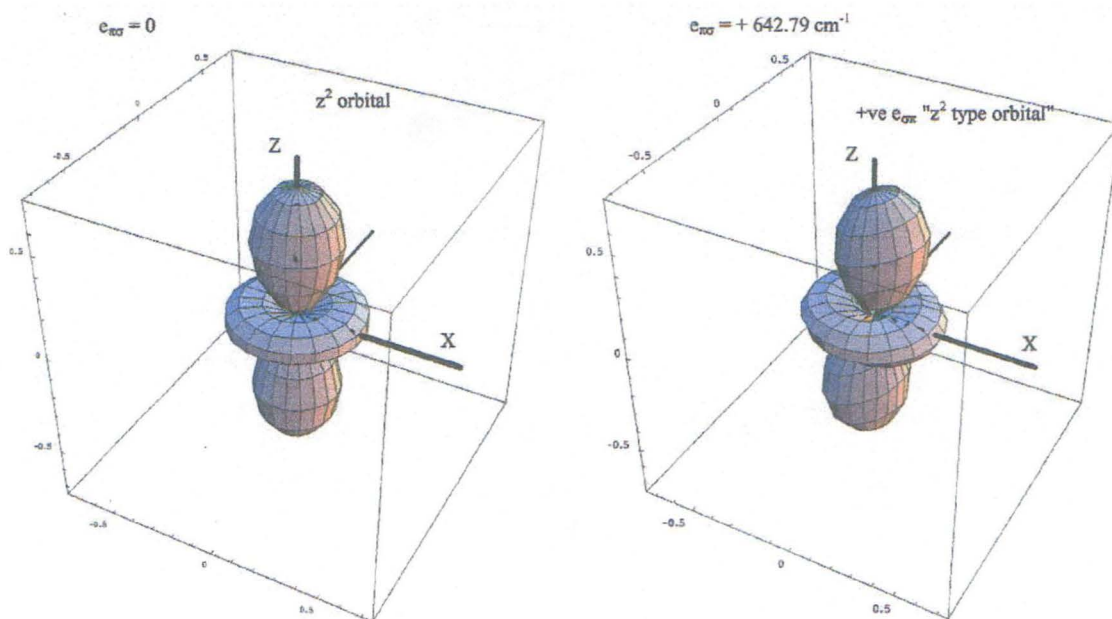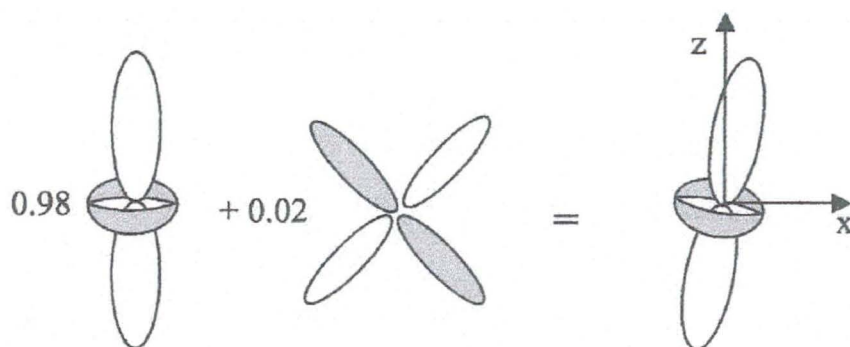

Figure E2: The dz^2 orbital and the "dz^2 type orbital" obtained when $e_{\sigma\pi}$ is positive.

In summary, a positive $e_{\sigma\pi}$ results in a positive off-diagonal element connecting the dz^2 and dxz orbitals. This results in the highest orbital being a mixture of $\Psi = 0.9039z^2 + 0.1790xz$. Adding this mixture:

Therefore, the positive $e_{\sigma\pi}$ corresponds to the rotation shown in Figure E3.
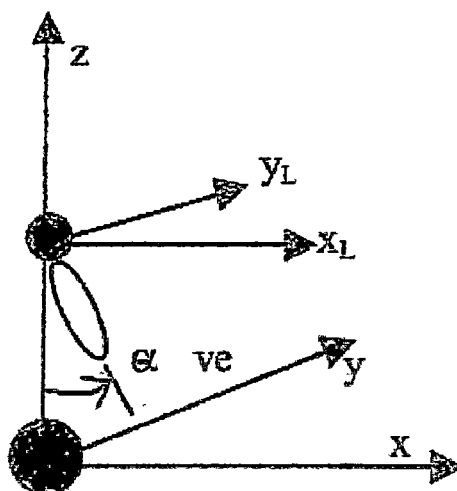
Figure E3: Rotation of the orbital corresponding to a positive $e_{\sigma\pi}$.

With this definition, when the bond is rotated around the y_L axis away from the Ligand-Metal direction (using the right hand for the direction of rotation about y_L), then the sign of $e_{\sigma\pi}$ comes from the sign of Equation E1:

$$e_{\sigma\pi} = -[\sqrt{(e_\sigma \times e_\pi)}]\sin\alpha\cos\alpha \qquad (E1)$$

A positive α gives a negative $e_{\sigma\pi}$ and a negative α gives a positive $e_{\sigma\pi}$.

In the above example, α was negative, so $e_{\sigma\pi} = 642.79\text{cm}^{-1}$, a positive value. If the ligand axes are defined differently (Figure E4), the bent bond is again on the same side, but now α is positive, giving a negative $e_{\sigma\pi}$.
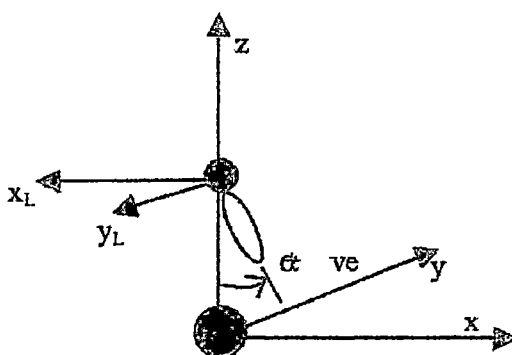

Figure E4: Redefined ligand axes and resulting α sign.

For this example, the ligand field in the local ligand frame, c_{21} and c_{41} are different:

$$
\begin{pmatrix} c_{00} \\ c_{20} \\ c_{21} \\ c_{22} \\ c_{40} \\ c_{41} \\ c_{42} \\ c_{43} \\ c_{44} \end{pmatrix} =
\begin{pmatrix}
\frac{2}{5}\sqrt{\pi}\ (e_{\pi x} + e_{\pi y} + e_{\sigma}) \\
\sqrt{\frac{\pi}{5}}\ (e_{\pi x} + e_{\pi y} + 2\,e_{\sigma}) \\
-\sqrt{\frac{2\pi}{5}}\ e_{\sigma\pi} \\
\sqrt{\frac{3\pi}{10}}\ (e_{\pi x} - e_{\pi y}) \\
\frac{2}{5}\sqrt{\pi}\ (-2\,e_{\pi x} - 2\,e_{\pi y} + 3\,e_{\sigma}) \\
-2\sqrt{\frac{3\pi}{5}}\ e_{\sigma\pi} \\
\sqrt{\frac{2\pi}{5}}\ (e_{\pi x} - e_{\pi y}) \\
0 \\
0
\end{pmatrix} =
\begin{pmatrix} 2587.12 \\ 5692.26 \\ 720.566 \\ 113.566 \\ 7346.69 \\ 1765.02 \\ 131.134 \\ 0 \\ 0 \end{pmatrix}
$$

When this is rotated into the global frame, the result is the same as before:

$$
\begin{pmatrix} c_{00} \\ c_{20} \\ c_{21} \\ c_{22} \\ c_{40} \\ c_{41} \\ c_{42} \\ c_{43} \\ c_{44} \end{pmatrix} =
\begin{pmatrix} 2587.12 \\ 5692.26 \\ -720.566 \\ 113.566 \\ -7346.69 \\ 1765.02 \\ 131.134 \\ 0 \\ 0 \end{pmatrix}
$$

This gives the same ligand field matrix, the same energy levels and wavefunctions. The highest energy wavefunction will be pointing at the direction of the bent bond, as before.

References

1. Adapted from Riley, M., Private Communication, (2001).

2. Gerloch M. and McMeeking R., *J. Chem. Soc. Dalton Trans.*, 2443, (1975).

3. Duer M.J., Fenton N.D. and Gerloch M., *Int. Rev. Phys. Chem.*, **9**, 227, (1990).